KINETICS OF SLAG METAL REACTIONS

DURING SUBMERGED ARC WELDING OF STEEL

by

UDAYANATH MITRA

B. Tech., Indian Institute of Technology, Bombay
(1980)

S.M., Massachusetts Institute of Technology
(1982)

SUBMITTED TO THE DEPARTMENT OF

MATERIALS SCIENCE AND ENGINEERING IN PARTIAL

FULFILLMENT OF THE REQUIREMENTS FOR THE

DEGREE OF

DOCTOR OF SCIENCE

at the

MASSACHUSETTS INSTITUTE OF TECHNOLOGY

February 1984

Signature of Author.. .....
Department of Materials Science and Engineering,
January 13, 1984

Certified by... .....
Thomas W. Eagar,
Thesis Supervisor

Accepted by..... .....
Bernhardt J. Wuensch, Chairman
Departmental Graduate Committee

KINETICS OF SLAG METAL REACTIONS

DURING SUBMERGED ARC WELDING OF STEEL

by

UDAYANATH MITRA

Submitted to the Department of Materials Science and Engineering
on January 13, 1983 in partial fulfillment of the
requirements for the Degree of Doctor of Science in Metallurgy

ABSTRACT

Weld metal chemical composition is shown to be controlled by the direct or indirect interaction between the slag and the metal in three zones: (1) the zone of droplet reactions inside the arc cavity, (2) the zone of dilution and weld pool reactions around the arc, and (3) the zone of the cooling and solidifying weld pool. In the zone of droplet reactions, the oxide constituents of the flux decompose into gaseous suboxides or vapours and oxygen, resulting in plasma-metal reactions which control the oxygen content of the metal. However, chemical kinetics, governed by surface active oxygen, prevents the transfer of alloying elements in this zone. In the zone of dilution and weld pool reactions, direct slag-metal reactions take place and control the transfer of Mn, Si, Cr, S and P. The kinetics of these reactions appear to be controlled by mass transport in the slag phase. The zone of cooling and solidifying weld pool also has a significant influence on weld metal oxygen content, as oxygen is removed in this zone through a mechanism of inclusion growth and separation. Thus the solidification time and the amount of deoxidizers present in the metal also influence oxygen content.

A quantitative kinetic model has been formulated from basic chemical metallurgy principles to predict, for the first time, weld metal chemical composition for any combination of welding consumables and any set of process parameters. This model has been successfully tested with experimental data as well as with numerous data from the literature. In addition, the model identifies errors in the hypotheses of previous investigators and accounts for the many contradictory results reported in literature.

Thesis Supervisor: Thomas W. Eagar

Title: Associate Professor of Materials Engineering

ACKNOWLEDGEMENTS

I wish to express my deep sense of gratitude to Professor Thomas W. Eagar for having suggested the subject of this work and for his guidance and encouragement throughout this investigation. I am also indebted to Mr. Bruce Russell, Mr. Carl Sorensen and Dr. Nunsian Tsai for their help with the experimental equipment and their helpful suggestions. Many thanks are also due to Professor Donald R. Sadoway and Professor Thomas B. King for reviewing this thesis and for their valuable suggestions. Lastly, I would like to thank my family, without whose assistance and encouragement the completion of this work would have been impossible.

This investigation was supported by a grant from the National Science Foundation.

Table of Contents

LIST OF FIGURES

LIST OF TABLES

LIST OF APPENDICES

CHAPTER 1

INTRODUCTION

Arc welding is almost a hundred years old with the first use of an electric arc for welding being reported in 1885 [1]. The use of a flux-shielded process was mentioned in literature as early as 1901 [2]. However, the progress of welding technology has been rather slow and it is only during the last five decades that it has gradually been accepted as a reliable and efficient method for joining metals. Among the different arc welding processes, Submerged Arc Welding is relatively a newcomer, the process being first patented in 1935 [1].

In the process of Submerged Arc Welding (SAW), an arc is maintained between a continuously fed bare wire electrode and the workpiece underneath a blanket of fusible granular flux which shields the weld metal and the arc from the atmosphere (as shown in Figure 1). The high deposition rates obtained in this automated process make it a very economical method of metal joining. However, during SAW as in other flux shielded processes, chemical reactions take place between the molten flux and the metal. This interaction between the slag and the metal results in compositional changes affecting the structure and properties of the weldment. Thus, in order to control the mechanical properties of the weld metal and match them with those of the workpiece, it is necessary to estimate the extent of interaction between the slag and the metal. This need is more acute now since

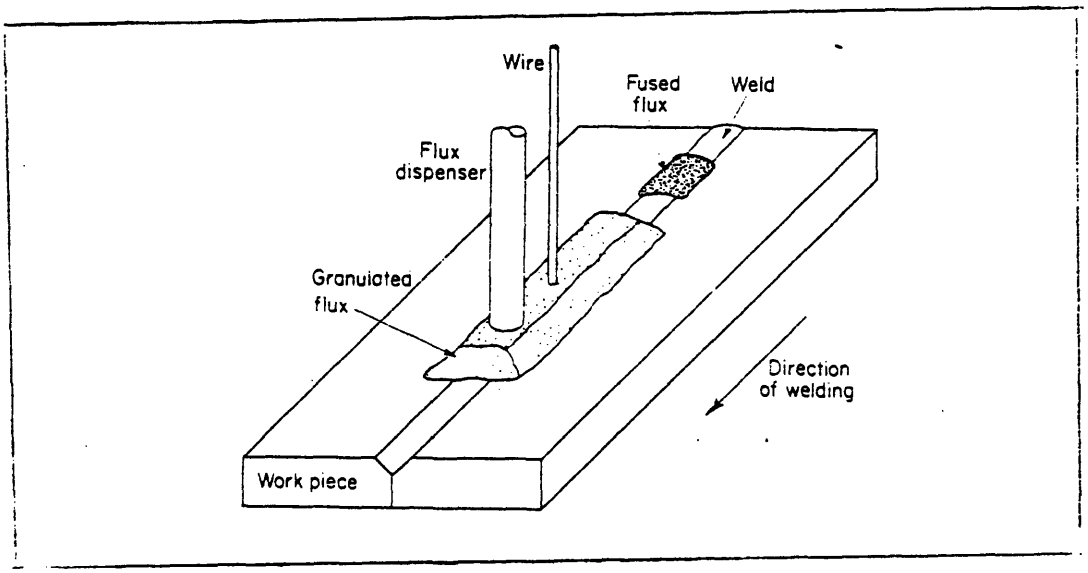

Figure 1: Schematic representation of the submerged arc welding process [3].

major improvements in steelmaking technology have improved base metal properties and have resulted in the creation of entirely new classes of steels, such as the High Strength Low Alloy (HSLA) steels for use in shipbuilding, pipelines, pressure vessels, etc. Thus far there is no general method for determining weld metal composition. Empirical equations have been used to predict weld chemistry only for specific welding consumables under a narrow range of welding conditions, and more scientific approaches have given, at best, only a qualitative explanation of the changes occurring in weld chemistry.

The present work aims at establishing a quantitative relationship between the composition of welding consumables used, the welding parameters employed and weld metal chemistry. The work differs from the many investigations in the past in that it incorporates fundamental principles of chemical metallurgy and solidification processing and at the same time recognizes the physical changes which occur during the submerged arc welding process. This thesis is presented in seven chapters. The sequence of the presentation is mainly based on the chronological order of experiments and on analysis performed during the course of the investigation. The following chapter contains a review of the work done by previous researchers and points out some of the drawbacks and discrepancies in their analyses. The third chapter involves preliminary experiments performed to further test the hypotheses of previous researchers. The major work of this thesis is the fourth chapter where an entirely new theory is presented to explain the changes occurring in weld metal chemistry during SAW. A kinetic model has been formulated

to predict weld metal composition. The fifth chapter presents the methods used for estimating the theoretical parameters introduced in Chapter Four. It also explains the relationship between the welding consumables, the process parameters, and the theoretical parameters. The sixth chapter presents the verification of the theory through several different experiments. The theory is also successfully tested by applying it to the numerous data published by previous investigations. Finally, the last chapter summarizes the important conclusions of this investigation.

The thesis has been deliberately presented in a concise form, so that the main ideas may be easily appreciated at first reading. Frequent references, however, have been made to the appendix which is in two parts. Section A of the appendix deals with detailed explanations, mathematical derivations and some details of experimental procedure which have been omitted from the main body of the thesis. Section B of the appendix contains raw data from the numerous experiments (involving over one hundred welds) performed during the course of this investigation.

CHAPTER 2

PREVIOUS WORK

Several researchers have studied the interaction between the slag and the metal in submerged arc welding of steel. Most of the work done by these researchers was based solely on metallurgical thermochemistry, although lately some other theories incorporating kinetic considerations have also been proposed. Before examining the work by these researchers, it is necessary to give a brief description of some terms used by them and which are also used in this thesis.

2.1. Submerged Arc Welding Fluxes And Their Classification

Welding flux is defined by the American Welding Society to be a material used to dissolve or facilitate removal of oxides and other undesirable substances. Welding slag has no formal definition, but is generally used to describe the fused residue remaining after welding. Submerged arc welding fluxes usually consist of combinations of manganous oxide and silica or lime and silica with additions of various other oxides to produce complex oxide fluxes. Lately, fluxes having titania, magnesia, alumina, and fluorspar as the major constituents have also been produced. Submerged arc welding fluxes may be produced in one of three ways: fused, bonded and agglomerated. Jackson [4] gives a detailed description of this and also lists the advantages and disadvantages of each method of production.

Fluxes are most commonly classified by a basicity index, but many definitions of this index have been suggested [5,6]. The International Institute of Welding (IIW) has defined the basicity index as

$$B.I. = \frac{MgO + CaF_2 + CaO + BaO + SrO + Na_2O + K_2O + Li_2O + 1/2(MnO + FeO)}{SiO_2 + 1/2(Al_2O_3 + TiO_2 + ZrO_2)}$$

Eagar [7] has suggested that CaF_2 acts only as a diluent and should be removed from the formula. Researchers have also found an empirical relationship between the basicity index of the flux [7,8] and oxygen, but others disagree with the use of the basicity index as an indicator of weld metal oxygen content [9].

2.2. Analyses Based on Metallurgical Thermodynamics

Most researchers who have used only thermodynamic considerations in their analysis [10-15] have considered reactions such as

$$x\,\underline{M} + y\,\underline{O} = (M_xO_y) \qquad (1)$$

and

$$x\,\underline{M} + y(FeO) = (M_xO_y) + y\,Fe \qquad (2)$$

The equilibrium constants for the above two reactions are

$$K_1 = \frac{(a_{M_xO_y})}{[a_{\underline{M}}]^x [a_{\underline{O}}]^y} \qquad (3)$$

$$K_2 = \frac{(a_{M_xO_y})}{[a_{\underline{M}}]^x [a_{FeO}]^y} \qquad (4)$$

By determining the chemical composition of the weld metal and slag and by either assuming ideally behaving slags or extrapolating activity data from steelmaking literature researchers have computed values for K_1 and K_2. From these values of K_1 and K_2 an 'effective reaction temperature' (also called 'effective equilibrium temperature' or pseudo equilibrium temperature) may be determined, since the equilibrium constants K_1 and K_2 are functions of temperature. The results obtained by different researchers are shown in Table 1. Based on these results, some researchers [10-14] concluded that equilibrium was attained and others [15-18] maintained that the slag and metal did not reach equilibrium. In addition to the different results obtained by different researchers (Table 1), these purely thermodynamic analyses have two very serious shortcomings:

1. They do not take account of the initial composition of the electrode and the base plate composition, though these are as important as flux chemistry in determining weld metal composition. (The small change in slag composition due to changes in weld metal chemistry cannot explain the strong influence of electrode and base plate composition.)
2. These analyses do not take into account the influence of welding parameters, although the effects of these parameters on weld chemistry is significant as shown in

Table 1: Values of the Effective Reaction Temperature Obtained by Different Investigators.

Investigator (Reference)		Effective Reaction Temperature Range
Christensen	[10]	1800 - 2100°C
Belton	[11]	1930 - 2030°C
Davies	[13]	1600 - 1650°C
Potapov	[14]	1900 - 2400°C
Van Bemst	[15]	1500 - 2400°C
Mitra	[16]	1700 - 2000°C
Chai	[17]	1800 - 2100°C
North	[18]	1700 - 2400°C
Lau	[28]	1680 - 3130°C

Table 2: Weld Metal Chemistry Variations Observed on Changing the Welding Process Parameters for Two Types of Fluxes (from reference 19).

Element	Flux Type	
	Manganese Silicate	Calcium Silicate
C	0.05 - 0.15%	0.07 - 0.16%
Mn	1.03 - 1.28%	0.58 - 1.09%
Si	0.33 - 0.92%	0.11 - 0.44%
O	0.067 - 0.174%	0.021 - 0.058%

Table 2 [19].

Besides the above two factors, most analyses based on metallurgical thermochemistry do not distinguish between the dependent and independent variables [20]. For example, if equation (3) is used, then the amount of alloying element M may be determined only if the oxygen concentration is known. Consequently, in view of these many shortcomings, any analysis based solely on metallurgical thermochemistry cannot result in any successful prediction of weld metal composition.

2.2a. Analyses Based On More Complex Thermodynamic Models

Some researchers have tried to apply the ionic theory of slags [21] to examine slag-metal equilibrium during Submerged Arc Welding [13,22]. However, many welding fluxes are acidic and the silica present in them need not exist only as $(SiO_4)^{4-}$ ions. This makes it difficult to calculate the concentration of oxygen ions (O^{2-}). In order to avoid the problem of computing the concentration of (O^{2-}) ions, Davis and Bailey [22] suggested that the process of deoxidation by silicon may be represented as

$$\underline{Si}^{4+} + 4\ \underline{O}^{2-} = (SiO_4^{4-}) \qquad (5)$$

from which they defined an 'equilibrium ratio'

$$k^{Si}_{SiO_4} = \frac{(SiO_4^{4-})}{[Si][O]^4} \qquad (6)$$

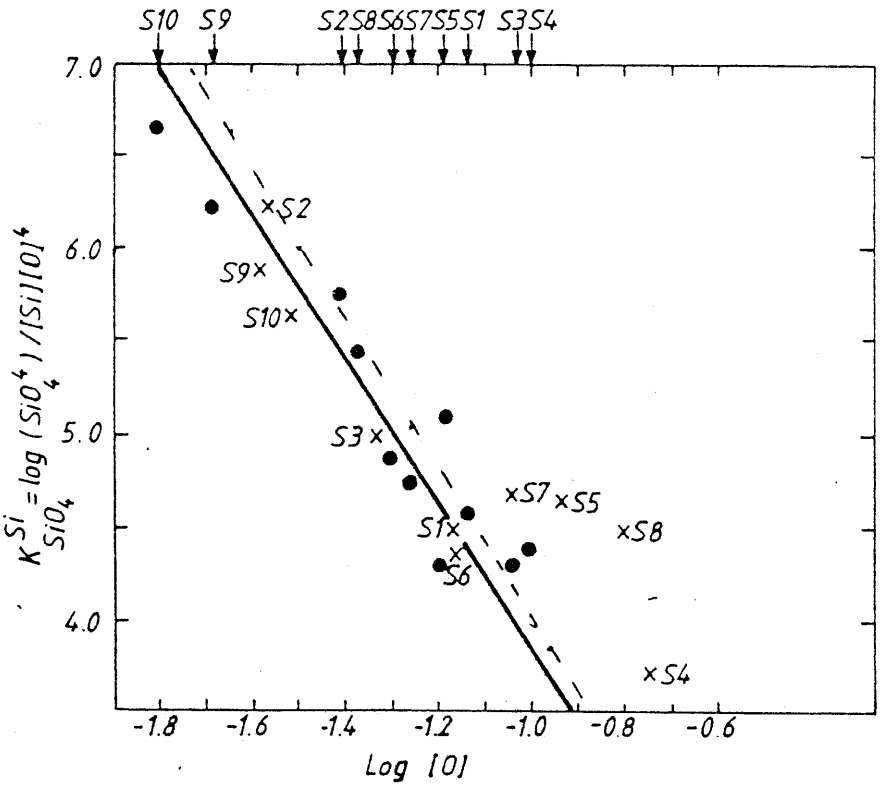

Figure 2: Results of Davies on silicon transfer in weld metal. Solid line (from original figure by Davies) is a plot of $K^{Si}_{SiO_4}$ against log O. Dashed line (not present in original figure) is a plot of $\log \frac{1}{[O]^4}$ against log [O].

This value of log $k^{Si}_{SiO_4}$ was plotted against log [O] and a straight line of gradient-4 was obtained, as shown in Figure 2. From this, they concluded that equilibrium between slag and metal for silicon may be represented by equation (5). However, as shown by the dotted line in Figure 2, a plot of log $\frac{1}{[O]^4}$ against log [O] practically coincides with the line drawn by Davis. This is not surprising since the variation of $[O]^4$ in equation (6) is much more than the variation of (SiO_4^{4-}) or [Si]. Moreover, the mere use of the ionic theory does not eliminate the shortcomings of any analysis based solely on thermochemistry, as mentioned earlier.

Recently [23,24] Kokh has proposed a highly complicated thermodynamic model which considers electrode composition as well as flux composition in determining weld metal chemistry. However, Kokh's model ignores the effect of welding process parameters and is thus unable to make quantitative predictions about weld chemistry. Also the model makes use of empirically introduced 'retardation factors' the values of which are unknown a priori, and the lengthy procedure of the analysis requires either the use of a digital computer or several graphical steps.

2.2b. The Neutral Point Concept

Recently, Chai and Eagar [25] carried out an extensive study of slag-metal reactions during submerged arc welding of steel. They discovered that for each flux there was a neutral point (or effective equilibrium point) at which there was no transfer of alloying element

between the slag and metal. However, this neutral point was not normally reached during the welding process and the deviation from this point was dependent on kinetic (process) factors. The neutral point itself was independent of these process factors. These investigators also formulated a thermodynamic model capable of predicting the neutral point. Their model was based on the following assumptions:

1. The effective temeprature of chemical reactions in the weld pool is 2000°C.
2. An empirical relationship exists between the basicity index of the welding flux and weld metal oxygen content [shown in Figure 3].
3. The activity of the components of welding slags may be determined by extrapolating steelmaking data from 1600 to 2000°C by assuming regular solution behavior.
4. The primary reactions of interest are those involving silicon, manganese and oxygen.

Of these, the second assumption is noteworthy in that it implies that the transfer of oxygen is independent of the transfer of other alloying elements. Eagar had suggested earlier [26] that the high amounts of oxygen obtained in submerged arc weld deposits may be due to the oxygen present in the arc plasma, resulting from the decomposition of the oxides present in the slag to suboxides and oxygen. Results of later work by Chai and Eagar [27] and more recently by Lau [28] appear to support this mechanism of oxygen transfer. Figure 4 illustrates the existence of a neutral point. It also indicates

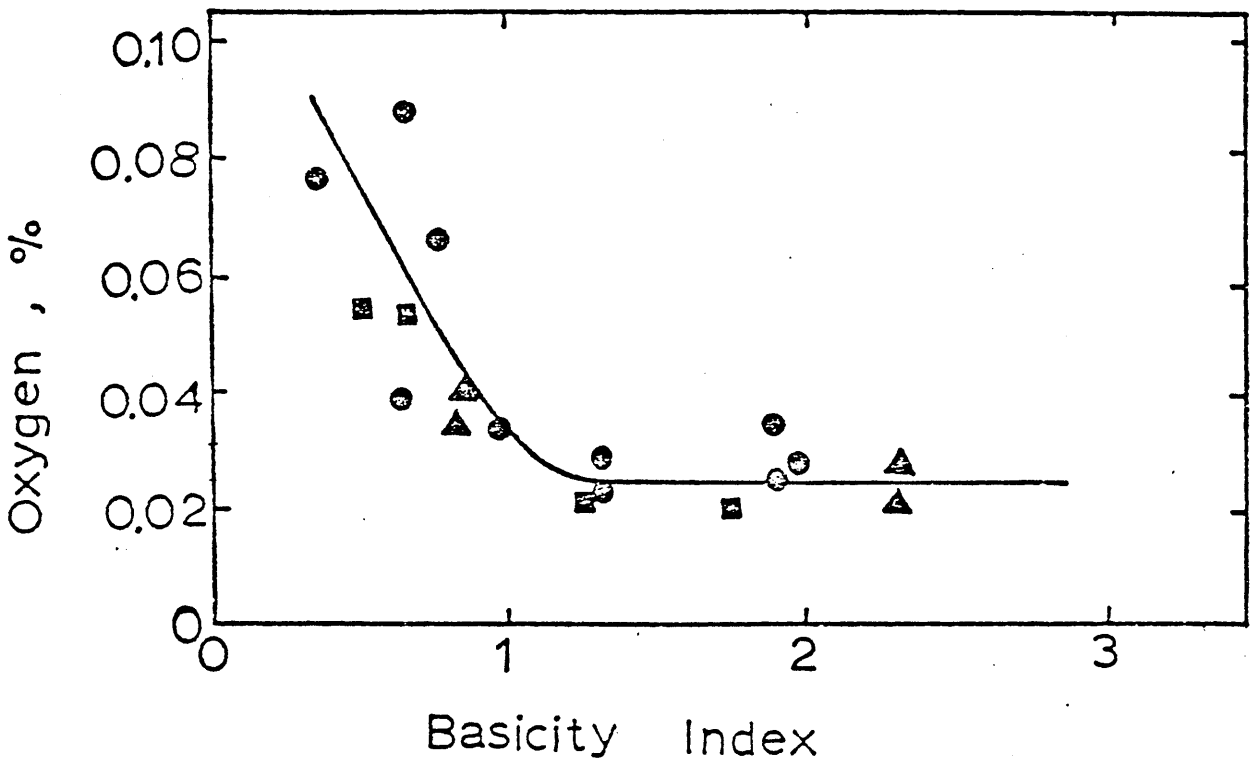

Figure 3: The empirical relationship between the weld metal oxygen and the flux basicity index [7].

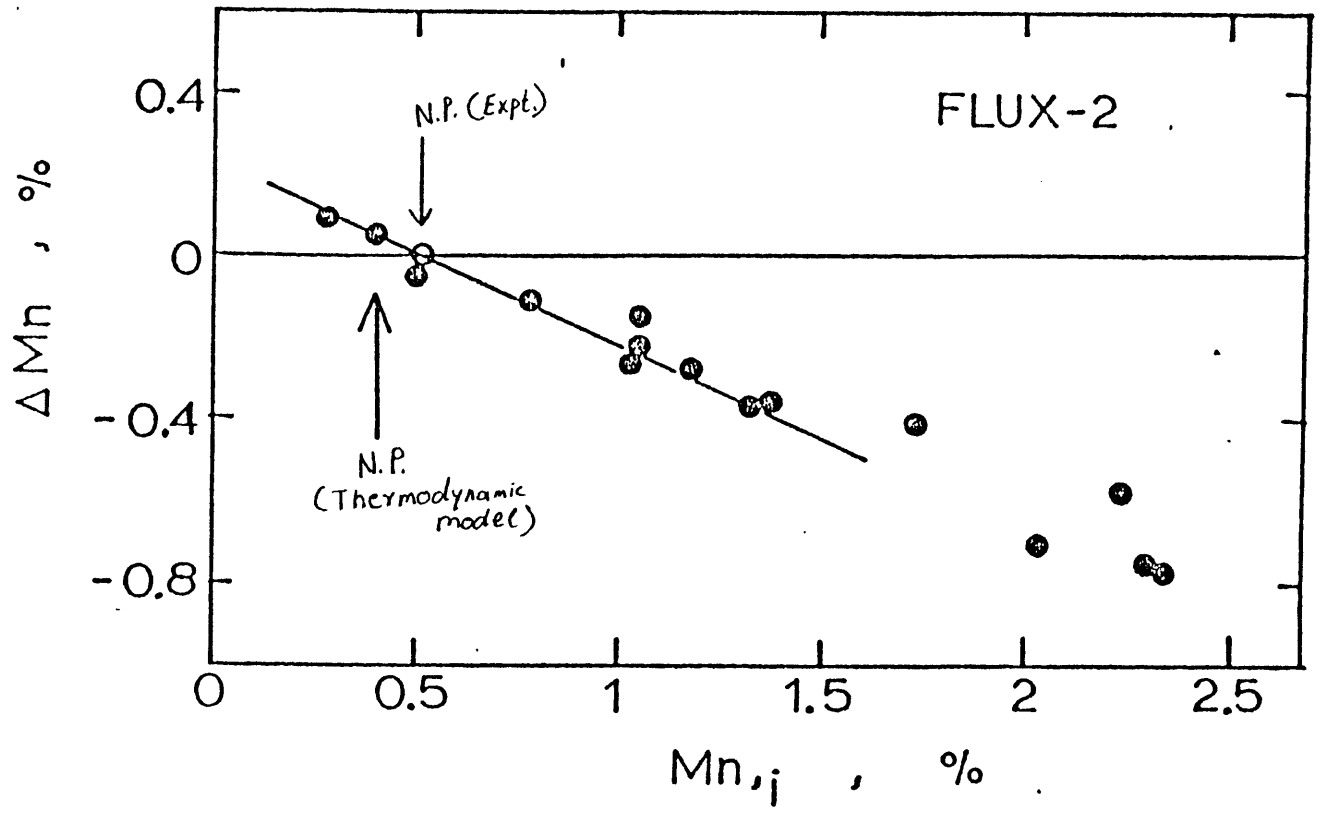

Figure 4: Results from work by Chai and Eagar indicating the existence of a neutral point [25].

very clearly the dependence of final weld metal chemistry on the initial electrode and baseplate composition.

In their analyses, Chai and Eagar did not explain how or why the welding process factors controlled the kinetics of slag-metal reactions, but they recognized that the composition of the welding consumables used exert a thermodynamic control over weld metal chemistry while the welding process parameters have a kinetic control over the extent of the reactions.

2.3. Effect of Welding Process Parameters On Weld Metal Composition

Many investigators have studied the effect of welding parameters on weld metal composition [10,18,19,29-35]; and all of them have concluded that these parameters have a very significant influence on weld metal chemistry. However, as yet, no quantitative theory has been proposed which takes the effect of these parameters into account and successfully predicts weld metal composition.

Frumin [29] was the first researcher to investigate the influence of welding voltage and current on weld metal chemical composition. He found that the transfer of alloying elements between slag and metal increases with increasing voltage and decreases with increasing current. He explained this phenomenon by considering SAW as a process where the electrode melts and the molten droplets pass through a slag layer and settle into the pool as shown schematically in Figure 5 (from reference [29]). On increasing voltage or decreasing

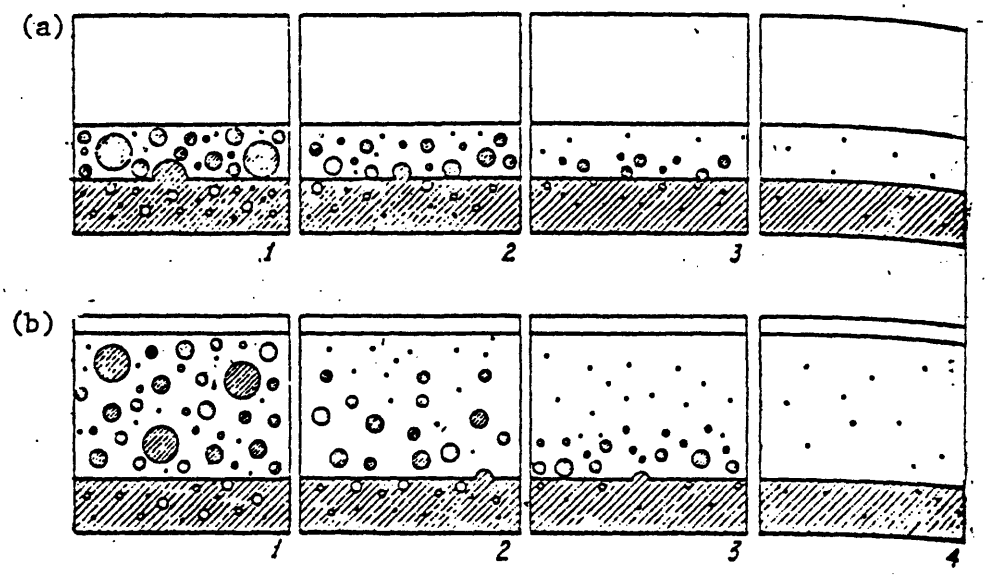

Figure 5: Frumin's representation of the submerged arc weld process (a) at low slag to metal ratio (b) at high slag to metal ratio [28]. (Note: This is a totally incorrect representation of the SAW process.)

current the ratio of molten slag to the amount of deposited metal from the molten electrode increases, thereby increasing the amount of alloy transfer (as shown in Figure 5). However, his analysis ignores the existence of an arc cavity, and the possibility of reactions occurring in the weld pool was not considered. Also, although variations in both voltage and current significantly change the slag to metal ratio, they do not significantly affect the depth of the slag layer (Figure 5 is an incorrect representation of the effect of voltage or current changes on slag depth). However, as will be shown in Chapter 5, not only Frumin's experimental data but that of all the other investigators can be explained with the new theory presented in this thesis (Chapter 4).

Christensen [10] also studied the effect of welding conditions on weld metal chemistry. He concluded that the effect of these parameters on weld metal chemistry was less than that due to variations in welding consumables. He classified fluxes into three types: (1) Manganese silicate, (2) Calcium silicate and (3) Basic. For each flux, he characterized the amount of Mn, Si and O transfer by two variables, (1) the initial or nominal manganese content (the nominal manganese content is the manganese content expected by mere fusion of electrode and baseplate in the absence of chemical reactions) and (2) an operational parameter (n) which is a product of voltage (V), current (I) and travel speed (v), ($n = 0.059\ VIv$; where the units of V, I and v are in units of volts, amps and cm/s, respectively). Figure 6 lists his results. Although the use of the above two variables

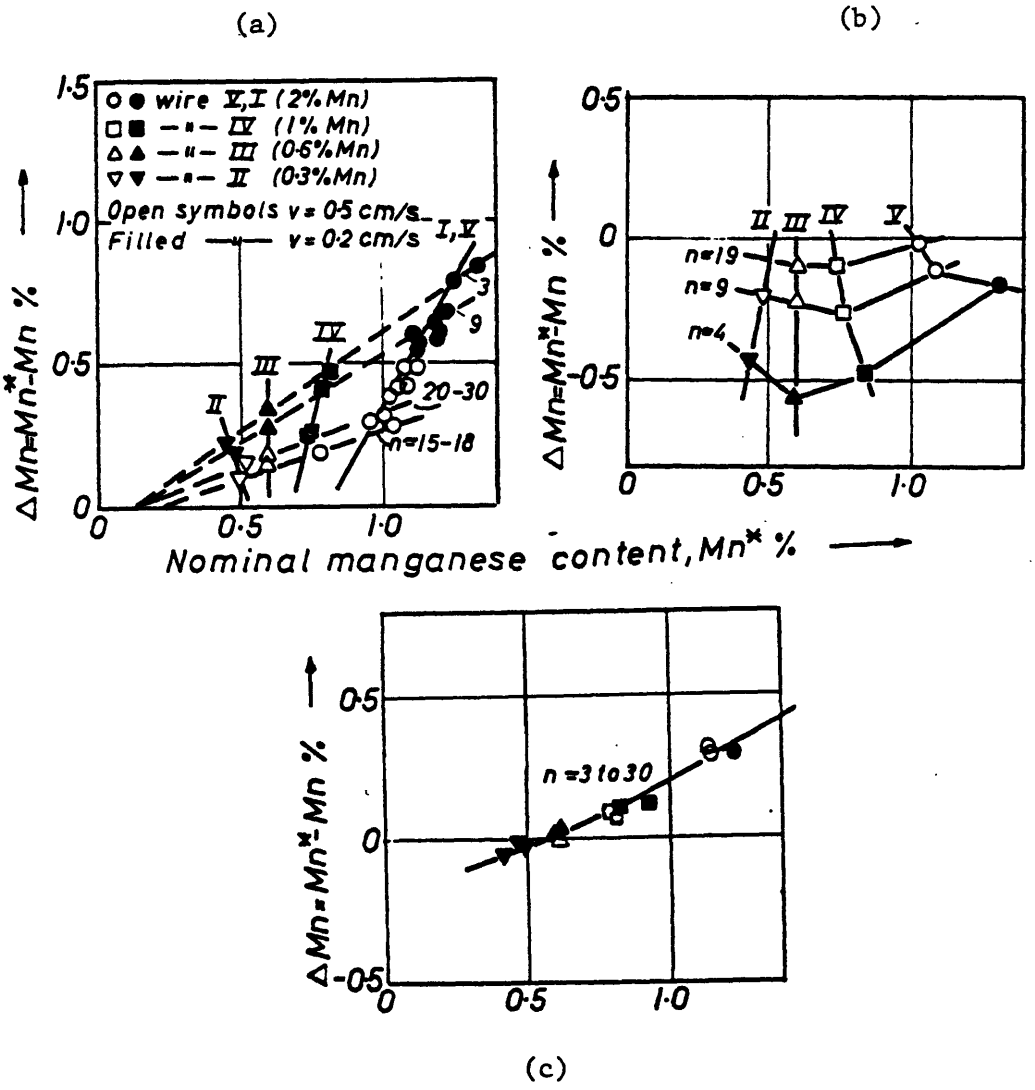

Figure 6a: Christensen's results on the transfer of manganese (a) results for acid calcium silicate fluxes (b) results for manganese silicate flux (c) results for basic calcium silicate flux [10].

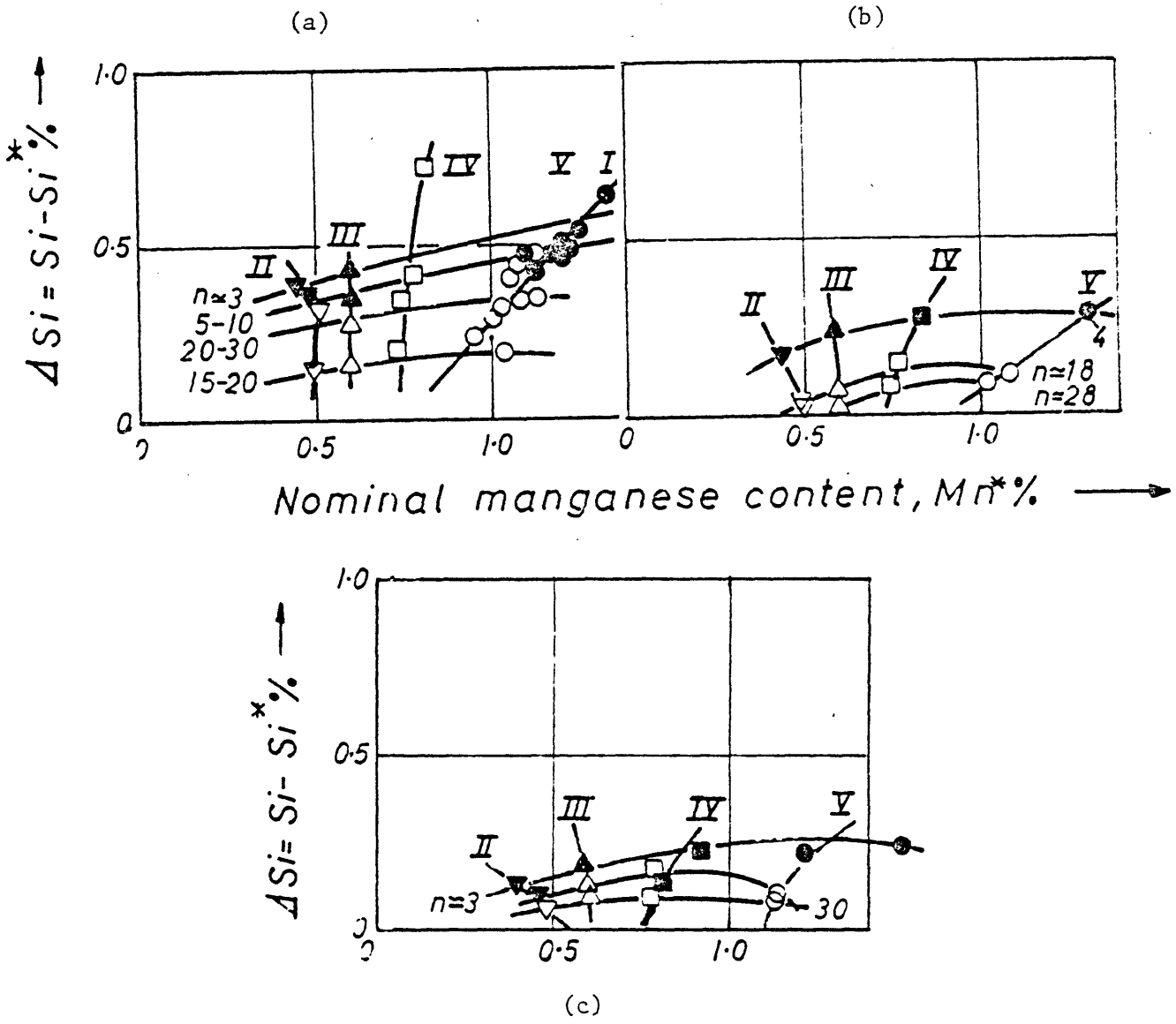

Figure 6b: Christensen's results on the transfer of silicon (a) results for acid calcium silicate fluxes (b) results for manganese silicate flux (c) results for basic calcium silicate flux [10].

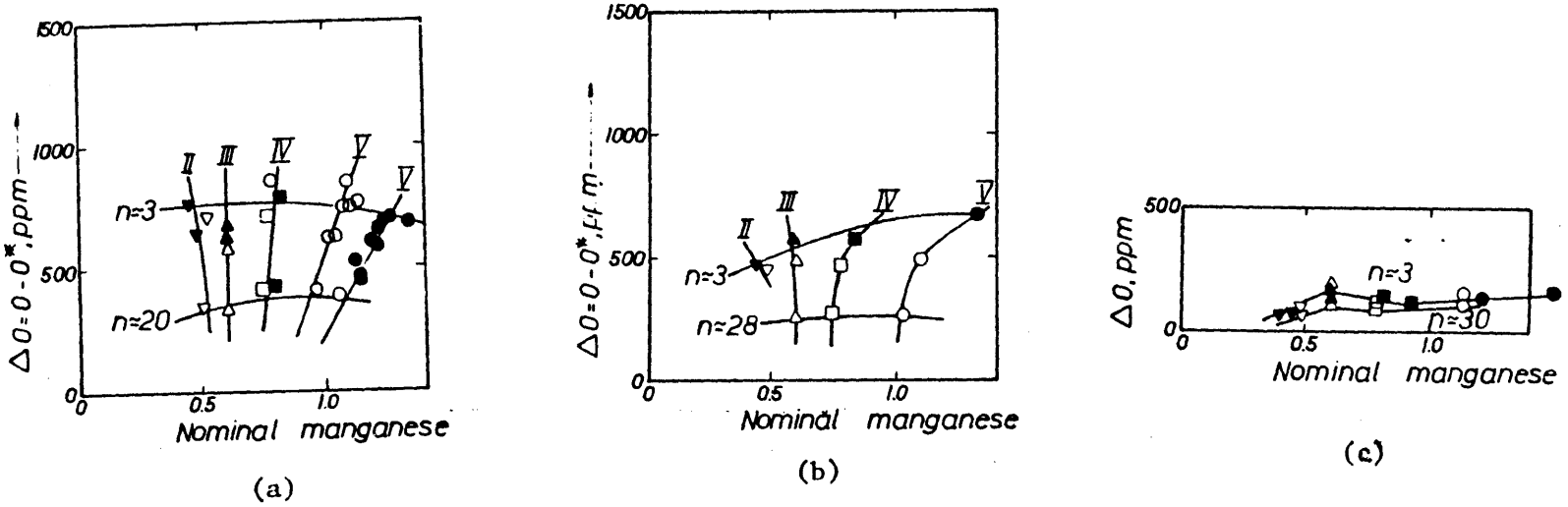

Figure 6c: Christensen's results on the transfer of oxygen (a) results for acid calcium silicate fluxes (b) results for manganese silicate flux (c) results for basic calcium silicate flux [10].

is mainly empirical and there is no quantitative relationship between these variables and weld composition, Christensen's work provides some useful ideas about the extent of alloy transfer in different fluxes.

2.3.1. The Droplet-Reaction Time Theories

Recently some researchers have suggested that slag-metal reactions and the transfer of alloying elements take place inside the arc column [18,30-36]. Pokhodnya et al. [30,31] suggested that the kinetics of these reactions were governed by the 'relative reaction time' of the droplets at the electrode tip. He used x-ray cinematography to determine this time and his results are shown in Figure 7. In his model, current is the main factor controlling 'relative reaction time' and consequently the kinetics of the reactions, whereas voltage has a much smaller effect. Although his results show relationships between relative reaction time and current and voltage, he did not conduct any experiment to determine the direct effect on weld metal chemistry due to changes in the relative reaction time of droplets in the absence of any change in the welding parameters, nor did he actually collect the tips and analyze them. Recent work by Lau [28], who actually collected and analyzed electrode tips and the droplets after they passed through the arc shows that current does not control the chemical composition of droplets either at the electrode tip or after it passes through the arc. Pokhodnya based his results on the chemical composition he obtained from only three multiple pass welds, by considering the top weld bead composition to be the same as the

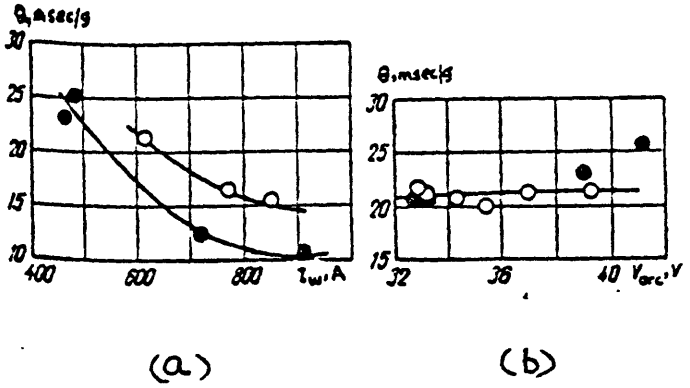

Figure 7: Effects of the welding conditions on the relative time for which droplets react at the electrode tip: (a) V_{arc} = 40V; (b) I_w = 600-620 A with the electrode positive and 470-580 A with the electrode negative, $v_{e.f.}$ = 46 m/hr; (•) electrode negative (o) electrode positive. [from ref. 31]

droplet composition. In his analysis, Pokhadnya also tried to show that the 'relative mass of slag' used by Frumin [29] could not be used to determine the kinetics of slag-metal reactions and also that the time spent by the droplets in flight inside the arc column is unimportant.

The most convincing 'proof' of the droplet theory came from the results of North [18]. He made multilayer welds (ten high pads) using 1.85-1.93% manganese electrode wire and an acid calcium silicate flux (65% SiO_2 - 35% CaO) under different welding conditions. His results indicated that increasing the voltage increased the amount of manganese lost to the slag whereas increases in current had the opposite effect. He explained this by suggesting that these parameters controlled the time of reaction between the electrode droplet and slag either at the electrode tip or as the drop transfers through the arc cavity. In order to prove this mechanism of alloy transfer he collected the droplets by using a rotating water cooled anode and analyzed them with an electron microprobe. The way these results were presented (Appendix A.1) made the droplet theory look convincing. However, as Figure 8 shows, there is a very wide variation between the droplet composition and that of the top weld of the ten high pad made under identical welding conditions. [According to the droplet theory the composition of both droplet and the top multiple-pass weld bead should be the same.]

Other proponents of the droplet theory have argued that it is not possible to have any quantitative theory based on the droplet-reaction time mechanism [32,33] and have suggested the use of empirical equations [32-36].

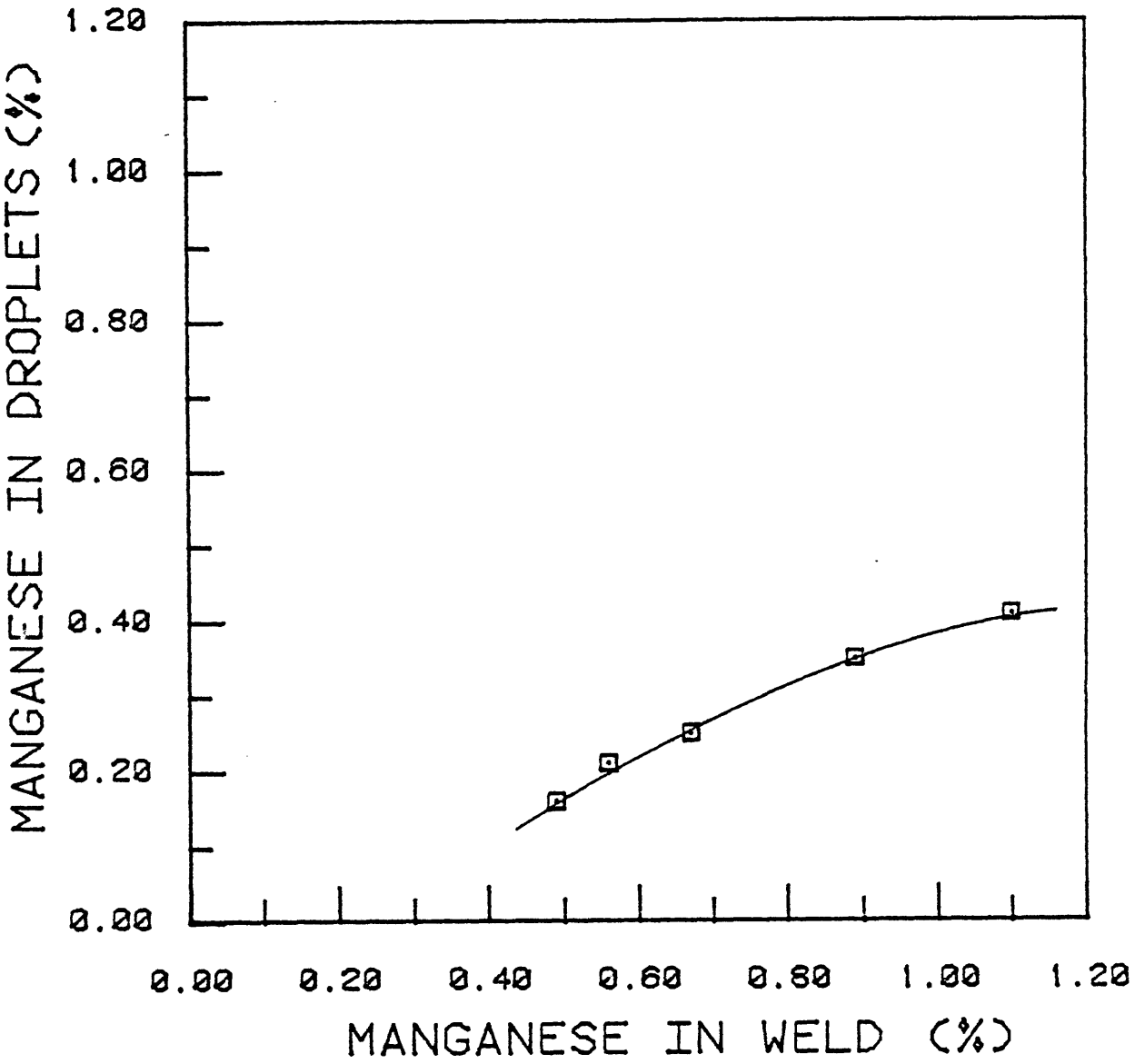

Figure 8: Comparison of droplet composition with actual weld bead composition (multipass welding) from work by North [18].

Potapov et al. [32,33] proposed that for 'chemically active silicate fluxes' (by chemically active fluxes he meant those from which a significant amount of alloying element is transferred to or from the oxides), the change in the amount of alloying element could be given in the form of regression equations based on the chemical composition of the flux, the electrode and the welding current, speed and voltage. For example, he gave the equation of transfer of manganese as

$$\Delta[Mn] = -0.2 + 0.48 \frac{(MnO)_f}{[Mn]_i B} + \frac{24\ V_{arc}}{I_w v_w} \qquad (7)$$

where $\Delta[Mn]$ is the amount of manganese transferred from the slag to the metal, $[MnO]_f$ is the molar fraction of manganese oxide in the flux, B is the flux basicity and V_{arc}, I_w and v_w are the welding voltage (in volts), current (in amps) and travel speed (in mm/s), respectively.

However, if this formula is applied to the 'chemically active' fluxes free of MnO such as those used by North or the acid calcium silicate fluxes used by Christensen the equation yields positive values of $\Delta[Mn]$ for different welding conditions (as high as $\Delta Mn = +1\%$) implying that manganese is transferred to the metal from a flux which does not contain MnO!

Thier [35] has proposed another empirical equation, again based on regression analysis:

$$\Delta X = M_o + a(u-u_o) + b(1/I - 1/I_o) - [K_o + c(u-u_o) + d[1/I - 1/I_o]]X_E \qquad (8)$$

where ΔX = amount of alloying element transferred to the metal

X_E = alloy content of electrode

U_o = 'standard voltage' = 29 V

I_o = 'standard current' = 580 A.

U and I are the welding voltage and current. [Unlike Potapov, Thier considered weld metal composition to be independent of travel speed.] M_o, a, b, K_o, c and d are six empirical constants which vary for different fluxes and which must be determined by a regression analysis for each flux. According to Thier the alloy content of the top layer of a multi-pass weld is given by

$$X = X_E + \Delta X \qquad (9)$$

since he considered all the reactions to be taking place at the droplet stage. However, if equations (8) and (9) are applied to the flux LW 280, used by Thier [34,35] and the values for the six constants M_o, a, b, K_o, c and d as determined by Thier [35] are used, and the welding conditions are assumed to be 29 V DCEP ('standard voltage') and 200 A, some unlikely results are obtained as shown in Table 3. This table shows that according to equations (8) and (9), as electrode manganese content increases the weld metal (multipass) manganese content decreases and even becomes negative under the same welding flux and identical welding conditions!

There are several other drawbacks in using either empirical equation (7) or (8). However, this discussion is not aimed at criticizing

Table 3: Effect of Electrode Composition on Top Weld Bead Composition in a Multirun Weld Pool as Predicted by Thier's Empirical Formula for Flux LW280 [35]. Welding Conditions: 29 V DCEP, 200 A.

Electrode Composition Mn_E (%)	Amount Lost or Gained by droplet, ΔMn (%)	Weld Metal Composition (according to Thier) $Mn = Mn_E + \Delta Mn$
0	1.87	1.87
1	0.53	1.53
2	-0.81	1.19
4	-3.49	0.51
6	-6.17	-0.17
8	-8.85	-0.85

the use of these equations, but rather to demonstrate that empirical equations provide useful information only in the narrow range of flux-electrode combination and under the limitations of the welding conditions from which they were derived. Any claims of generality [32, 33] or scientific basis [32-36] for these equations cannot be accepted.

2.4. Oxygen Transfer in Submerged Arc Welding

Unlike the transfer of other elements during the submerged arc welding process, researchers have not been able to determine successfully which welding process parameters affect the weld metal oxygen content. The effect of flux composition on weld metal oxygen content has been a matter of some controversy. Eagar suggested that a 'basicity index' may be used to predict the oxygen content of weld metal when using silicate fluxes [7]. Others have argued that an 'oxygen potential' concept is more appropriate [9,28]. However, unlike the 'basicity index', no formal definitions or formulae for oxygen potential in welding fluxes have been proposed [7]. Neither the 'basicity index' nor the 'oxygen potential' concepts take into account the account the effect of welding parameters on oxygen content, although these parameters may change the oxygen content in the metal by as much as 300% [19].

Recent work by Lau has provided very useful information on the sources of oxygen contamination during SAW. His work confirms that oxygen enters the metal due to plasma-metal reactions in the arc

column as suggested by Eagar [7,26,27]. North [9] and Potapov [32] also suggested that oxygen is transferred to the metal inside the arc column, although they attributed this to slag-metal reactions rather than to reactions between the arc plasma and the metal. Thus, while several researchers have studied the reactions during submerged arc welding and have tried to predict weld metal composition, their results are at best empirical, and many discrepancies and contradictions exist.

CHAPTER 3

PRELIMINARY EXPERIMENTS

The review of the work by previous investigators showed that the results obtained by them were often contradictory and that general quantitative relationships between consumable composition, process variables and weld chemistry do not exist. At first review, the droplet theory seems to be promising and elaborate experiments have been designed to control the reaction time of droplets, and to collect the droplets [37]. However, on more careful examination two serious shortcomings of the droplet theory were noted:

1. In spite of the fact that several researchers had claimed this mechanism of element transfer, none of them had been able to put forward any quantitative scientific theory.
2. The droplet theory contradicted the results of the classic work by Christensen and Chipman [38] on Manual Metal Arc Welds.

Christensen and Chipman recognized that the chemical reactions could take place in the plasma of the arc as well as in the weld pool and in order to determine the region where the reactions take place they made welds on two plates - one consisting of wrought Swedish charcoal iron which was free of manganese and the other on a slab of 7% manganese steel using the same electrode. They compared the slag composition of these welds to that obtained from multipass welds with the same

covered electrode. Their results (shown in Table 4) indicate that manganese is transferred to the slag while welding the 7% Mn steel, but the slag loses manganese while welding the iron base plate. From this, they concluded that the controlling step for chemical reactions between the slag and the metal takes place in the weld pool, since mixing of the alloying elements from the base plate occurs only in the weld pool itself.

In view of these two observations, it was decided to perform some simple preliminary experiments to test the validity of the droplet theory before proceeding with more elaborate experiments. The composition of the electrodes, base plates and flux used in the preliminary experiments as well as those performed later (Chapter 5) are listed in Tables 5, 6 and 7, respectively. (Tables 8, 9 and 10 lists the electrode, base plate and flux compositions used by other researchers.) Fluxes Fx-1, Fx-2, and Fx-3 are used commercially, Fx-4 was prepared in the laboratory by induction melting. The welding equipment consisted of a Linde VI-800 power supply with an Linde EH-10 electrode feeder and an UCC-8 control.

In the first experiment, a series of welds were made using different combinations of baseplate and electrodes. The welds were made with the same flux and under constant welding conditions [30 V DCEP, 400 A, 40 cm/min]. The results of these experiments are shown in Table 11. The complete chemical analysis of the welds, and the process parameters used in this experiment as well as in the other preliminary experiments is listed in Appendices B.1 and B.2. If reactions

Table 4: Data from Christensen and Chipman's Work [30] Showing that the Transfer of Alloying Elements Occur in the Weld Pool. Data is for MMA Welds with RA6020 Electrode Being Used for all Welds.

% Mn in Base Plate	% Mn in Weld Metal	% MnO in Slag
trace	0.33	16.8
trace	0.37	17.4
multipass welds	0.53	21.0
multipass welds	0.54	21.7
7.0	3.6	38.9
7.0	3.4	37.0

Table 5: Chemical Composition of Electrodes Used in this Study.

Electrode	Si	Mn	O	Other
A-7 (1/8" dia)	0.01	0.18	.04	.04% C, .02% P, .03% S
A-7 (3/32" & 1/16" dia)	0.01	0.10	.04	.04% C, .02% P, .03% S
A-681	0.93	1.64	0.02	
Ax-90	0.46	1.31	.02	1.93% Ni, .016% P, .007% S 0.4% Mo
A-705-3	0.54	1.20	0.02	
Page Med-C	0.15	1.10	0.02	0.6% C
L-70	0.11	0.80	-	
LD-86	0.80	1.60	-	
LD-44	0.02	2.44	0.02	0.44% Mo, 0.66% Ni
LD-40 (1/8" dia)	2.04	2.04	0.02	
LD-80	0.03	0.45	0.04	
LD-40 (3/32" dia)	0.02	2.17	0.02	

Table 6: Chemical Composition of Baseplates Used in This Study

Baseplate	C (%)	Si (%)	Mn (%)	O (%)	S (%)	P (%)	Other
1008	0.02	0.001	0.35	.04	.008	0.010	
1020	0.08	0.14	0.45	-	.020	.015	
EZ20	0.21	0.11	1.21	.01	0.160	.017	
HiSi	0.01	3.23	0.07	.01	.022	.009	
Stainless	0.08	0.47	1.64	.01	.007	.022	18.4% Cr 9.7% Ni
HiP	0.06	0.26	1.57	.01	.005	.098	
HY-80	0.16	0.22	0.26	.01	.012	.011	2.17% Ni 1.35% Cr

Table 7: Chemical Composition of Fluxes Used in This Study

Flux Constituent	Fx-1	Fx-2	Fx-3	Fx-4
SiO_2	50	36	55	40
CaO	3	47	28	-
MgO	-	-	12	-
MnO	40	0.10	0.5	-
$A\ell_2O_3$	-	-	5	-
CaF_2	5	10	-	60
TiO_2	-	5	-	-
FeO	-	-	-	-

Table 8: Composition of Some Electrodes Used by Other Researchers

Researcher (Ref.)	No.	C %	Mn %	Si %	S %	P %	Cu %	N p.p.m.	O %
Christensen [10]	I		1.95	0.03	0.03	0.02	n.d.	41	.030
	V	0.13	1.94	0.08	0.03	0.03	n.d.	n.d.	n.d.
	VI		2.04	0.00	0.03	0.03	n.d.	79	.034
	IV	0.12	1.06	0.08	0.08	0.022	0.14	43	.01
	III	0.13	0.59	0.02	0.024	0.012	n.d.	54	.013
	II	0.03	0.30	0.02	0.011	0.006	n.d.	22	.031
Belton [11]	-	.022	.06	.02	.015	.006	-	18	.10
North [18]	-	-	1.93	-	-	-	-	-	-
North [48]	53	.12	1.59	.29	.012	.012	-	-	.008
Lau [78]	-	.11	1.00	0.27	.003	.017	-	-	.016

Table 9: Chemical Composition of Some Baseplates Used by Other Researchers.

Researcher (Ref.)	BasePlate No.	%C	%Mn	%Si	%S	%P	%O
Christensen [10]	A	.10	0.65	0.26	.032	.030	.011
	B	.09	0.49	0.22	.032	.016	.006
	E	.13	0.60	0.19	.023	.008	.014
Belton [11]	-	.022	.06	.027	.010	.012	.06
	-	.20	.47	.044	.35	.014	.04
Lau [28]	-	.07	1.79	0.23	.03	.08	.004
Christensen and Chipman [38]	Wrought Iron	-	0.0	-	-	-	-
	7% Mn Steel	-	7.0	-	-	-	-

Table 10: Some Flux Compositions Used by Researchers in Previous Work

Researcher/ Flux Name Used	Constituent	SiO_2	CaO	MgO	MnO	Al_2O_3	CaF_2	TiO_2	FeO	Other
Christensen [10]	a	49	32	10	0.2	6	2	-	0.3	-
	c	52.5	24	n.d.	0.2	4	7	-	0.6	-
	d	52.5	29	n.d.	0.2	4.5	3.5	-	0.2	-
	e	38	8	n.d.	35	4	7.2	-	1.11	-
	f	40	40	n.d.	4.3	2	8	-	0.24	-
Mitra [16]	A	42	48	-	0.1	-	-	-	-	10% Cr_2O_3
	B	43	40	-	0.1	-	-	-	-	17% Cr_2O_3
	C	29	40	-	0.1	-	8.7	4.1	-	18% Cr_2O_3
	D	42	2.7	-	29.0	-	4.1	-	1.8	18% Cr_2O_3
Chai [17]	F1	42	41	-	16	-	-	-	-	-
	F2	40	23	-	8	30	-	-	-	-
	F3	50	3	-	40	-	5.0	-	-	-
	F4	36	47	-	0.1	-	10	5.0	-	-
North [18]		65	35	-	-	-	-	-	-	-
Thier [35]	LW280	35	22	11.6	6.7	15.7	5.2	1.0	-	0.7% Fe_2O_3

n.d.: not determined.

Table 11 : Results of preliminary experiments showing alloy transfer is not controlled by droplet reactions.

Weld No.	Electrode	Composition of Base Plate	Weld Metal Composition Nominal*	Actual	Change in Composition due to Chemical Reactions	Welding Conditions
1-1	0.18% Mn	1.21% Mn	0.78% Mn	0.88% Mn	+0.10% Mn	30V DCEP
1-2	1.20% Mn	1.20% Mn	1.20% Mn	1.20% Mn	0.0% Mn	400 A
1-3	2.17% Mn	0.35% Mn	1.08% Mn	1.15% Mn	+0.07% Mn	40 cm/min
1-4	0.18% Mn	0.35% Mn	0.28% Mn	0.64% Mn	+0.36% Mn	Flux Fx-1
2-1	0.93% Si	0.00% Si	0.32% Si	0.70% Si	+0.38% Si	30V DCEP
2-2	0.8% Si	0.8% Si†	0.80% Si	0.85% Si	0.05% Si	400 A 40 cm/min Flux Fx-1

*Nominal Weld Composition = (Baseplate composition)(Dilution) + (Electrode composition)(1-Dilution)

†Artificial baseplate made of electrode wire used.

between the droplets from the electrode and the slag account for the transfer of manganese and silicon then weld 1-1 made with a 0.18% Mn electrode and a 1.21% Mn baseplate in Table 11 should gain a great deal of manganese whereas weld 1-3 made with 2.17% Mn electrode and 0.35% Mn baseplate should lose a great deal of manganese. However, the experimental data (Table 11) show that the gain of manganese was similar for both welds. Also weld 1-4 made with 0.18% Mn electrode, 0.35% Mn baseplate gained much more manganese than either weld 1-1 or 1-3, since its nominal composition was much lower. Similar results can be seen for Si from welds 2-1 and 2-2 indicating that slag-metal reactions occur in the weld pool after the electrode droplets mix with fused metal from the baseplates.

The second experiment was performed with an electrode containing traces of alloying elements (0.01% Si, 0.18% Mn, 0.00% Cr) and baseplates and fluxes of different compositions as shown in Table 12. In this experiment, the experimental parameters were varied. These parameters as well as the complete chemical composition is listed in Appendices B.1 and B.2. The data in Table 12 show clearly that the weld metal loses Mn, Si and Cr even on welding with electrodes essentially free of these elements thus confirming that the controlling reactions occur in the weld pool.

Preliminary experiments were also made to study the effect of consumable composition on oxygen transfer. In one experiment, a series of multiple pass welds were made using different combinations of electrodes and baseplates for two different fluxes Fx-1 and Fx-2. In

Table 12: Alloying Elements Lost to Slag on Welding with A-7 (alloy free) Electrodes

(a) Welds made with EZ20 Baseplate and Fx2 Flux.

Weld No.	Weld Metal Composition		Amount Lost
	Mn nominal (%)	Mn actual (%)	ΔMn(%)
P1	0.87	0.57	-0.30
P2	0.77	0.60	-0.17
P3	0.76	0.53	-0.23
P4	0.83	0.59	-0.24
P5	0.50	0.43	-0.07
P6	0.72	0.57	-0.15
P7	0.67	0.40	-0.27
P8	0.63	0.38	-0.25

(b) Welds made with HiSi Baseplate and Fx-2 Flux.

Weld No.	Weld Metal Composition		
	Si nominal (%)	Si actual (%)	ΔSi(%)
42	2.14	2.00	-0.16
43	2.05	1.78	-0.27
44	2.05	1.74	-0.31
45	2.24	2.02	-0.22
46	2.40	2.33	-0.17

(c) Welds made with Stainless Baseplate and Fx-1 Flux

Weld No.	Weld Metal Composition Cr nominal (%)	Cr actual (%)	Amount Lost ΔCr(%)
S1	11.59	10.30	-1.29
S2	12.42	10.80	-1.62
S3	11.222	7.89	-3.33
S4	14.90	13.10	-1.80
S5	15.46	13.33	-2.16
S6	15.46	13.0	-2.46
S7	10.67	5.84	-4.83
S8	13.06	11.4	-1.66

these experiments, the welding constants were maintained at 30V DCEP, 300 A and 60 cm/min. The results of this experiment are presented in Table 13, and, as in the previous experiment, the full chemical analysis is presented in Appendix B.2. The results of Table 13 show that, although flux composition has the strongest influence in determining weld metal composition, both electrode and baseplate compositions have significant influence. Also the top (sixth) layer contains greater amounts of oxygen than the first layer for all the welds. Also, welds were made with flux F-4 (60% CaF_2 - 40% SiO_2) with a high silicon electrode (0.93% Si) and baseplate (3.23% Si) and it was noted that the metal could lose silicon and gain oxygen. The result of this experiment along with other data from literature is presented in Table 14. The results of both Tables 13 and 14 are discussed in more detail in the next chapter.

The results of the preliminary experiments clearly disprove claims that the alloying elements are transferred in the zone of droplet reactions. Also, Christensen and Chipman's [38] conclusion on the importance of weld pool reactions must be at least partially correct. Thus, a new approach starting from first principles is necessary to investigate and explain the reactions that occur during submerged arc welding.

Table 13: Effect of Electrode and Baseplate Composition on Weld Metal Oxygen Content

Flux	Electrode Composition	Baseplate Composition	Layer 1		Layer 3		Layer 6	
			Weld No.	Oxygen	Weld No.	Oxygen	Weld No.	Oxygen
Fx-1	0.01% Si, 0.1% Mn	.001% Si, 0.35% Mn	601	0.17	603	0.20	606	0.22
Fx-1	0.01% Si, 0.1% Mn	3.23% Si, 0.06% Mn	101	0.12	103	0.22	106	0.20
Fx-1	0.93% Si, 1.67% Mn	3.23% Si, 0.06% Mn	201	0.10	203	0.17	206	0.18
Fx-1	0.93% Si, 1.67% Mn	0.001% Si, 0.35% Mn	501	0.13	503	0.18	506	0.20
Fx-2	0.01% Si, 0.1% Mn	3.23% Si, 0.06% Mn	601	0.04	403	0.06	-	-
Fx-2	0.93% Si, 1.64% Mn	3.23% Si, 0.06% Mn	301	0.02	303	0.03	306	0.03

Table 14: Data Showing Transfer of Oxygen is Independent of Transfer of Silicon and Manganese

Ref	Flux Name	Weld No	Flux Type	ΔMn	ΔSi	ΔO (ppm)
-	Fx-4	Si-1	CaF_2 - SiO_2	-	-0.31	+ 800
-	Fx-4	Si-3	CaF_2 - SiO_2	-	-0.23	+1000
17	F-2	2-6	CaO - MnO - SiO_2 - Al_2O_3	-0.36	-0.10	+ 600
17	F-2	2-3	CaO - MnO - SiO_2 - Al_2O_3	-0.36	-0.04	+ 580
17	F-2	2-16	CaO - MnO - SiO_2 - Al_2O_3	-0.40	-0.05	+ 600
17,19	F-4	8	CaO - SiO_2 - Al_2O_3	-0.50	-0.24	+ 400
17,19	F-4	3	CaO - SiO_2 - Al_2O_3	-0.20	-0.02	+ 360
58	7B	7B	CaO - CaF_2 - Al_2O_3	-0.52	-0.11	+ 180
58	28B	28B	CaO - CaF_2 - Al_2O_3	-0.47	-0.17	+ 180

CHAPTER 4

THEORY

In this chapter, a new theory is presented to explain the chemical interactions which occur between the slag and the metal in submerged arc welding. This theory is completely different from mechanisms suggested by previous investigators [9-15,23,24,28 35] but it will be shown in Chapter 5 that the experimental data of these researchers are not only consistent with but lend strong support to this new theory. It is proposed that chemical interaction between the slag and the metal occurs in the three zones as indicated in Figure 9.

1. The zone of droplet reactions.
2. The zone of dilution and weld pool reactions.
3. The zone of cooling and solidifying weld pool.

4.1. Zone of Droplet Reactions

In this region, the droplet forms at the electrode tip and then travels through the arc column as shown schematically in Figure 9. The entire process occurs in a few milliseconds [30-32] and the temperature of the droplets is very high: in the range 2000-2500°C [39]. Due to the high temperatures it is thermodynamically possible for several chemical reactions to occur as can be seen from the discussion in Appendix A.2. However, the results of the preliminary experiments (Ch.3)

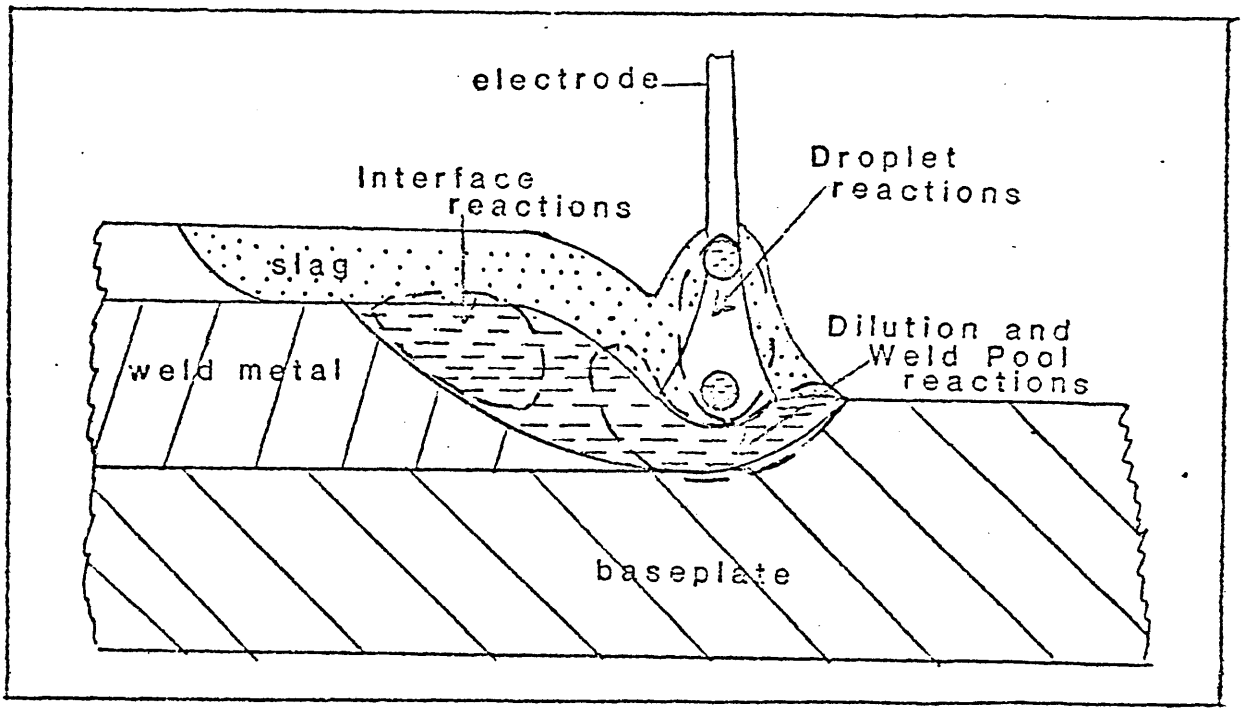

Fig. 9 The three reaction zones which control the chemical composition of the weld metal during submerged arc welding

show that there is a negligible amount of alloy transfer (Si,Mn,Cr) in this region indicating that kinetic considerations are important.

Although the alloying elements Si, Mn and Cr are not transferred in this zone, the results of our investigation as well as data from several other researchers indicate that oxygen is transferred to the metal in this zone [9,26-28,32]. The strongest evidence comes from the results of Lau [28] who determined the oxygen content in the electrode tips, in the droplets after their flight through the arc column, and in the weld pool. He also found that changing the welding parameters did not significantly influence the oxygen content in the droplets. His results are shown in Figure 10. The observation of pores and inclusions in electrode tips and droplets by other researchers [9,31] as well as in the present work (Figure 11) also indicates that oxygen is transferred in this region. Table 13 indicates that, in multiple pass welds, the top weld contains more oxygen than the bottom layer. This observation also supports a mechanism of oxygen transfer in the droplet zone, although the difference in oxygen in the different weld layers is partly due to the difference in the alloy content of the electrode and the baseplate. Table 14 indicates that, for some welds, although the weld metal gains oxygen, it loses silicon and manganese (in addition to iron). If, in addition to manganese and silicon transfer the oxidation of iron is also considered, then an oxidation balance for slag-metal reactions indicates that the total amount of oxygen transferred into

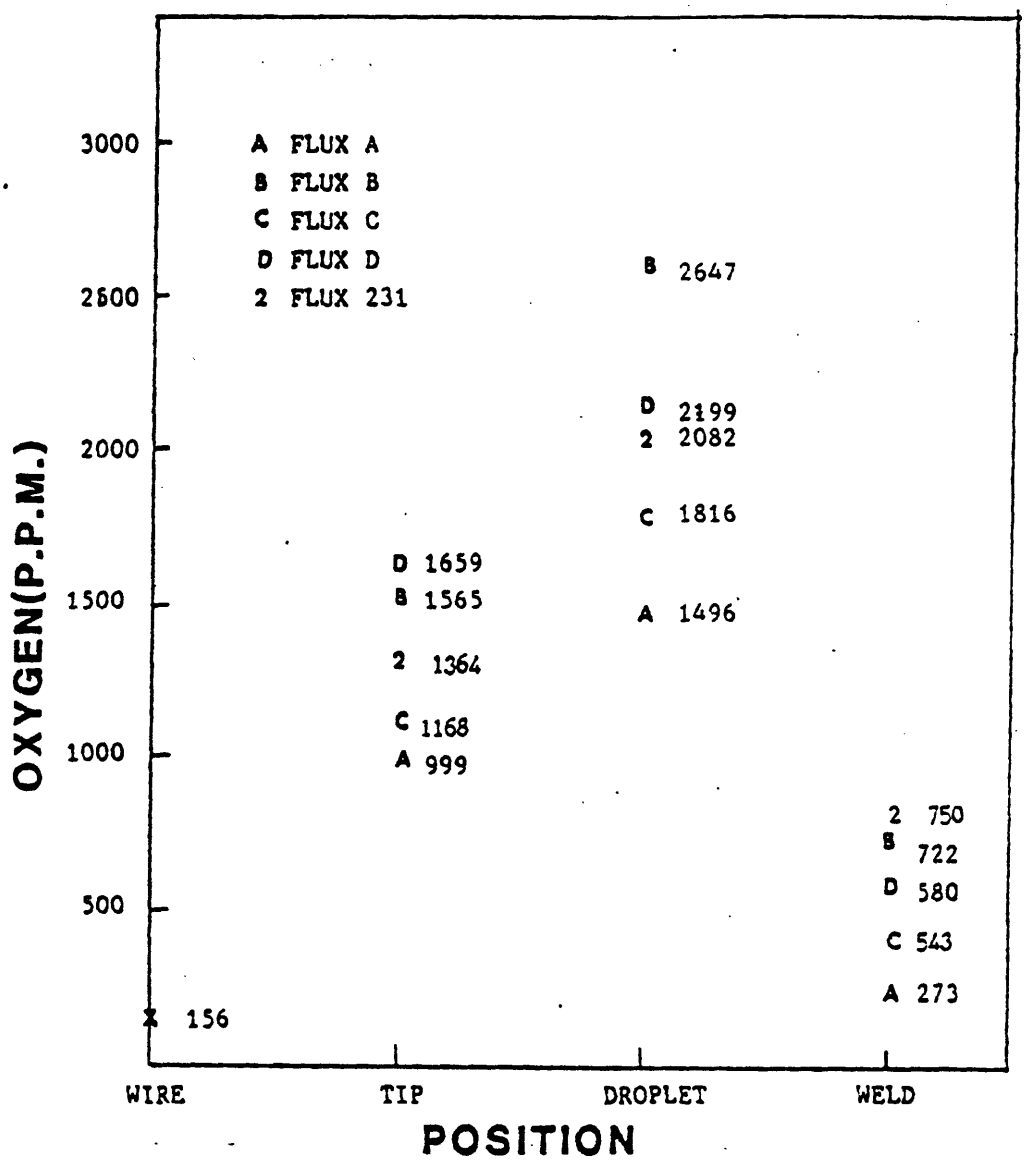

Figure 10a: Oxygen levels at different stages of welding at 600 A [from ref. 28].

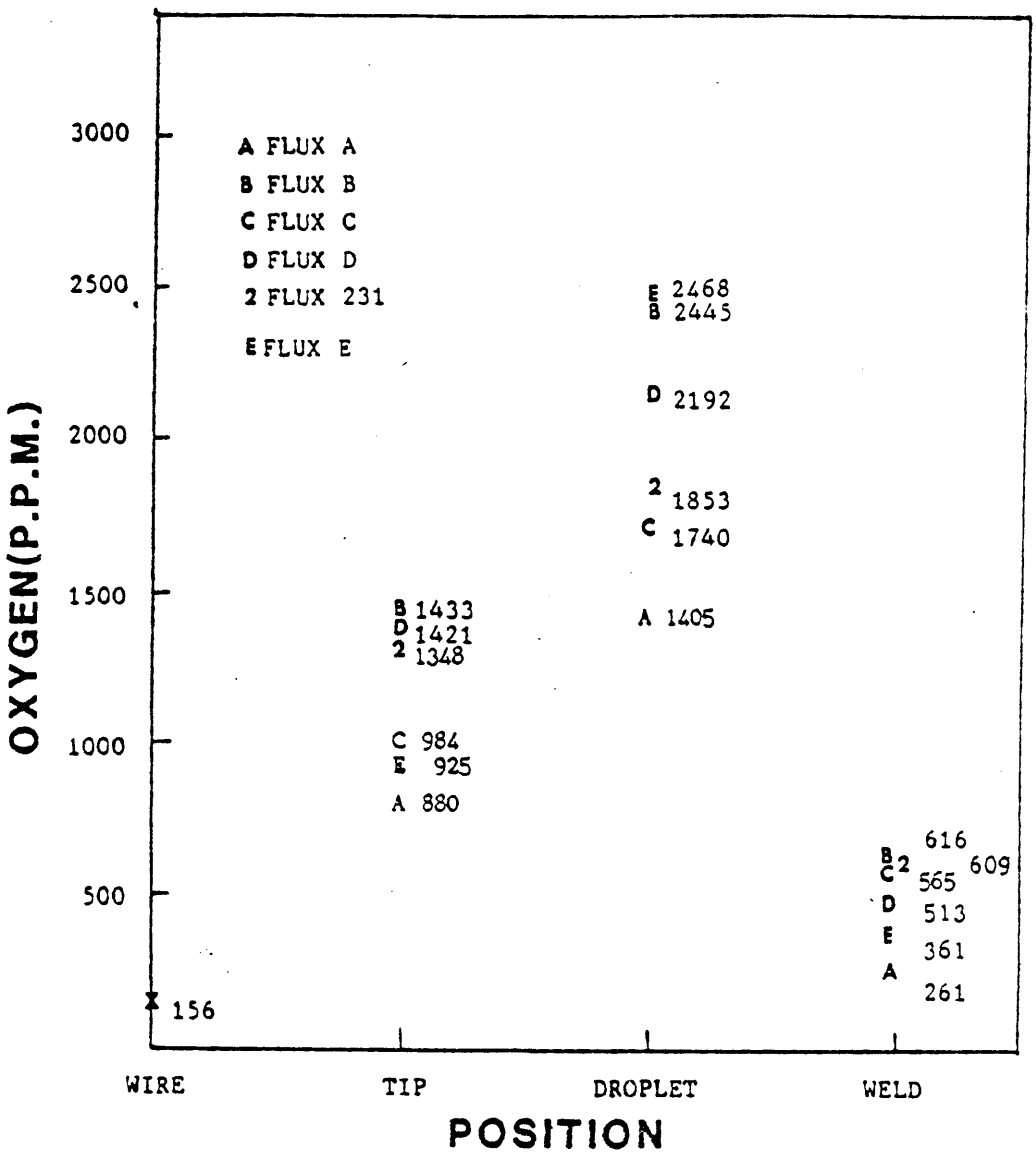

Figure 10b: Oxygen levels at different stages of welding at 300 A [from ref. 28].

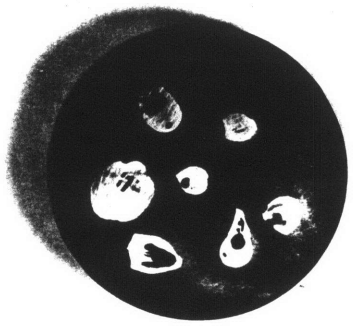

Fig.11: Photograph showing pore formation at elactrode tips.

the weld metal on account of such slag metal reactions is much lower than the actual amount of oxygen transferred to the weld metal. In fact, in many cases, an oxidation balance of slag metal reactions indicates that the weld metal should have a lower oxygen content than the electrode/baseplate used which is contrary to experimental observations. Appendix A.3 gives examples from Christensen and Belton's data [10,11] to illustrate the point. Also, as pointed out earlier by Eagar [7], an excess of oxygen is always found in the final weld metal-slag system as compared to the starting weld metal-flux system for any combination of welding consumables and process parameters. This observation indicates that the transfer of oxygen to the weld metal does not occur simultaneously with the transfer of the other alloying elements, supporting our earlier observations (Tables 11, 12), and rules out direct slag-metal reactions at the droplet stage.

The oxygen present in the arc plasma which is responsible for the plasma-metal reactions in this zone has two possible sources:

1. Decomposition of flux constituents into suboxides and oxygen, and
2. Contamination from the atmosphere.

Both reasons have been considered earlier by Eagar [7,26,27] and more recently by Lau [28]. The decomposition of flux constituents into suboxides and oxygen seems to be the primary source of oxygen since different fluxes produce different oxygen levels in the weld metal, depending on the stability of the flux constituents [7,8,25-28].

The analysis of Chai and Eagar on binary oxide-calcium fluoride fluxes [27] shows that even oxides stable under steel making temperatures (such as MgO) may decompose to gaseous suboxides or vapours and oxygen in the arc-plasma and lead to the transfer of considerable amounts of oxygen into the weld metal (see Figure 12). Contamination by oxygen from the atmosphere plays a much smaller role [7,19,26,27,28] but cannot be totally ruled out as a source of oxygen. Also, atmospheric oxygen may reoxidize the suboxides and vapours generated inside the arc plasma back into their original oxide forms after these gases escape from the arc cavity.

The fact that oxygen is transferred into the droplets in this zone, whereas there is little exchange of the alloying elements, may not be very surprising, if the analysis by Richardson [40] on the decarburization of levitated iron droplets is examined. Richardson showed that in the early stages of decarburization of levitated iron droplets, the reaction

$$[\underline{O}^s] \rightarrow [\underline{O}^b] \qquad (10)$$

does not proceed forward (the superscripts b and s indicate bulk and surface concentration). The oxygen rapidly builds up to the surface and this surface active oxygen prevents the carbon from reaching the interface and reacting. A similar phenomenon may be occurring inside the arc cavity during the process of submerged arc welding, with the surface active oxygen keeping out the other elements during the few

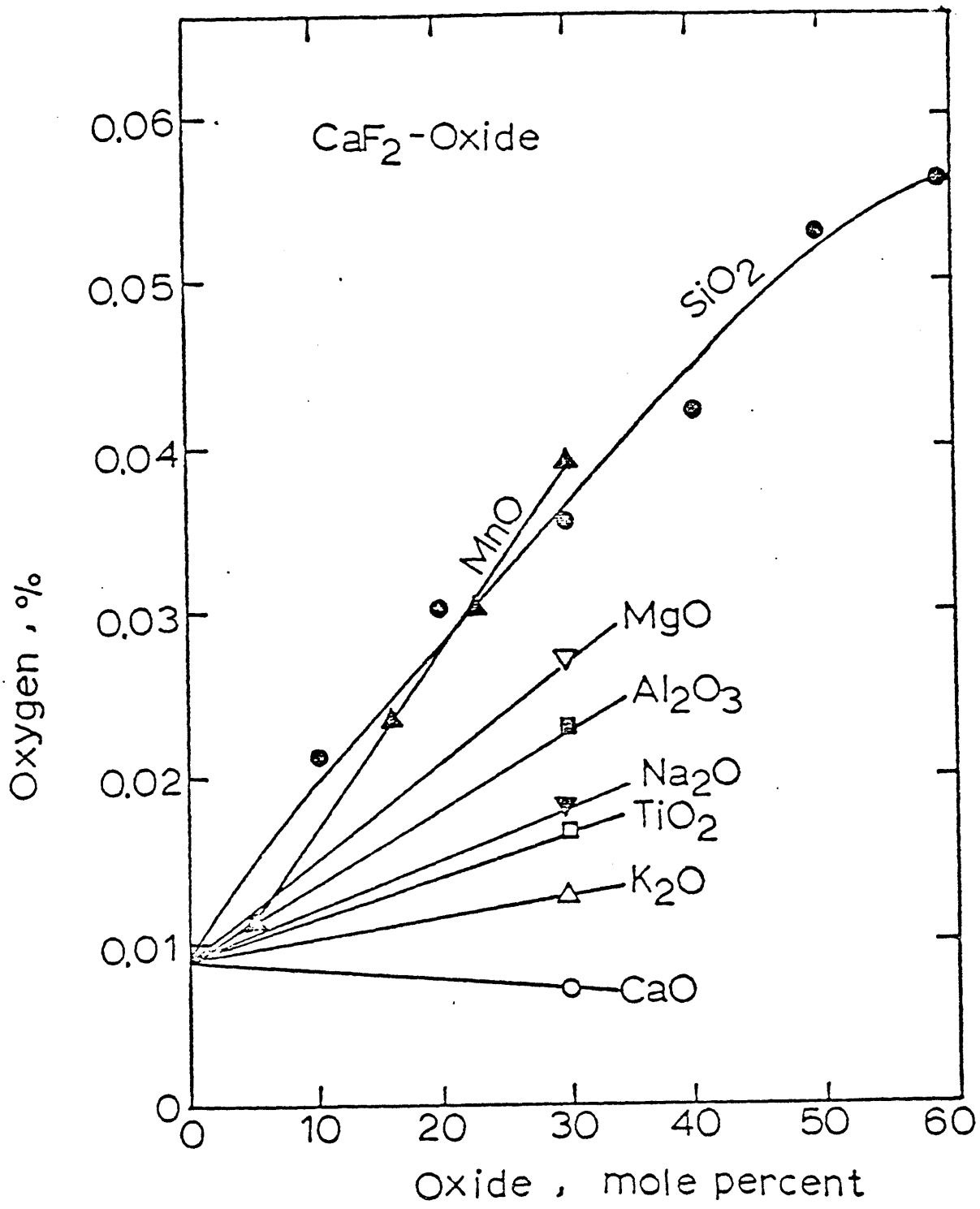

Figure 12: Weld metal oxygen produced with binary CaF_2-oxide flux systems [from ref. 27].

milliseconds in which the drops form at the electrode tip and fall through the arc cavity. This mechanism is consistent with the views of Richardson [40], "There is now little doubt that chemical kinetics may interfere in some high-temperature reactions between gases and metals and it seems likely that adsorption of such surface active elements such as oxygen and sulphur will influence these kinetics."

4.2. Zone of Dilution and Weldpool Reactions

In this zone, the falling droplets becomes 'diluted' with molten metal from the baseplate (Figure 9). The high temperature and the large convective forces in this region lead to intimate mixing in the molten metal and result in vigorous chemical reactions at the slag-metal interface near the arc. The results in Tables 11 and 12 indicate that slag-metal reactions do occur in this region. Previous researchers had found that increases in voltage or decreases in current result in an increase in the amount of alloying elements transferred between the slag and the metal and had suggested different mechanisms of element transfer to explain this phenomenon [28,29,31-33]. The results of our preliminary experiments, when the welding conditions were varied, agree with the experimental observations of these researchers. However, since the electrodes were virtually free of Mn, Si and Cr, the influence of voltage and current on the transfer of these elements is clearly due to their influence on the kinetics of slag-metal reactions in the weld pool. Figures 13, 14 and 15, which are plots of the amount of alloying element transferred between the

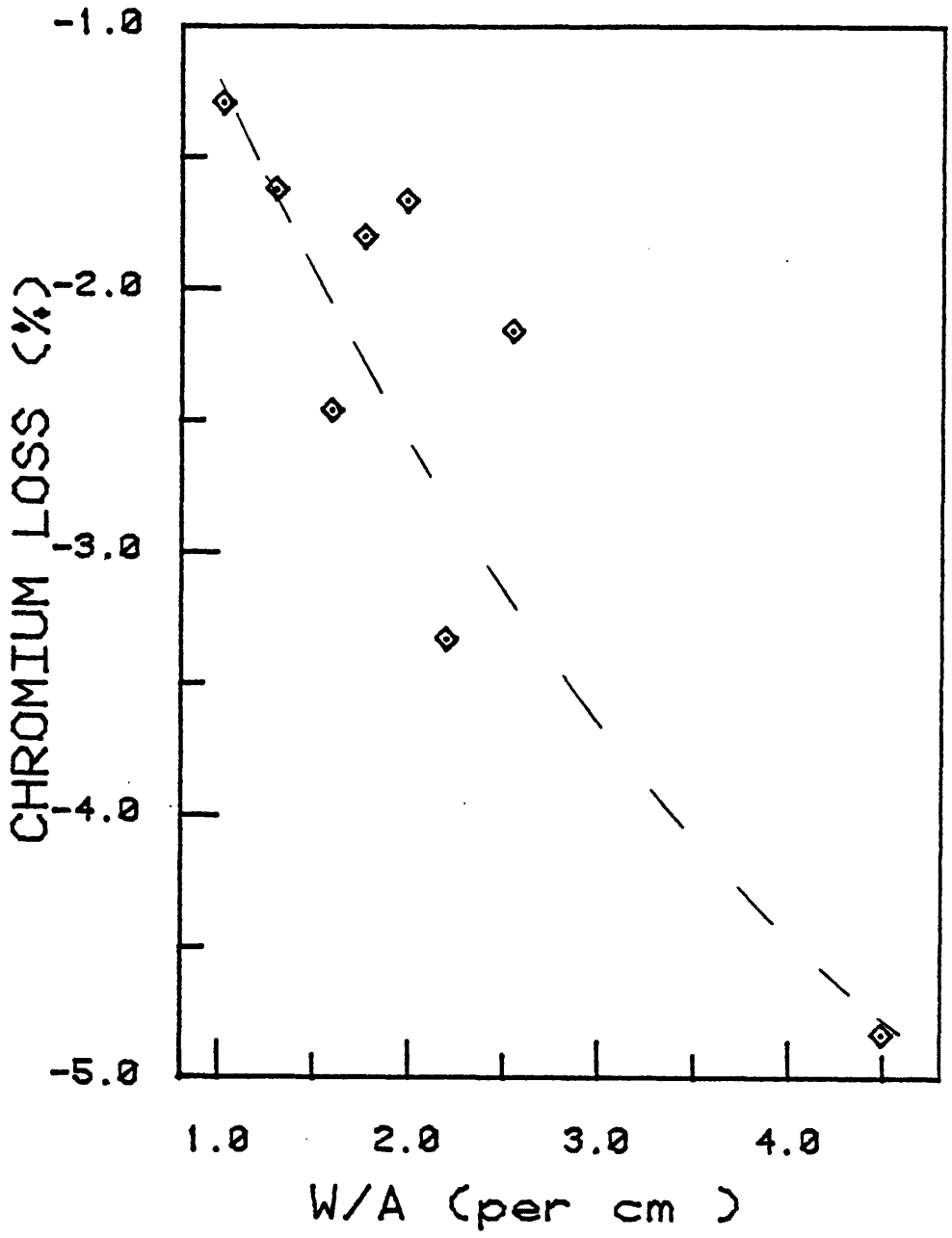

Figure 13: Effect of the ratio of weld width to transverse cross-sectional area (w/a) on the loss of chromium from the metal to the slag. Flux Fx-1, stainless baseplate and A-7 electrodes used for all welds.

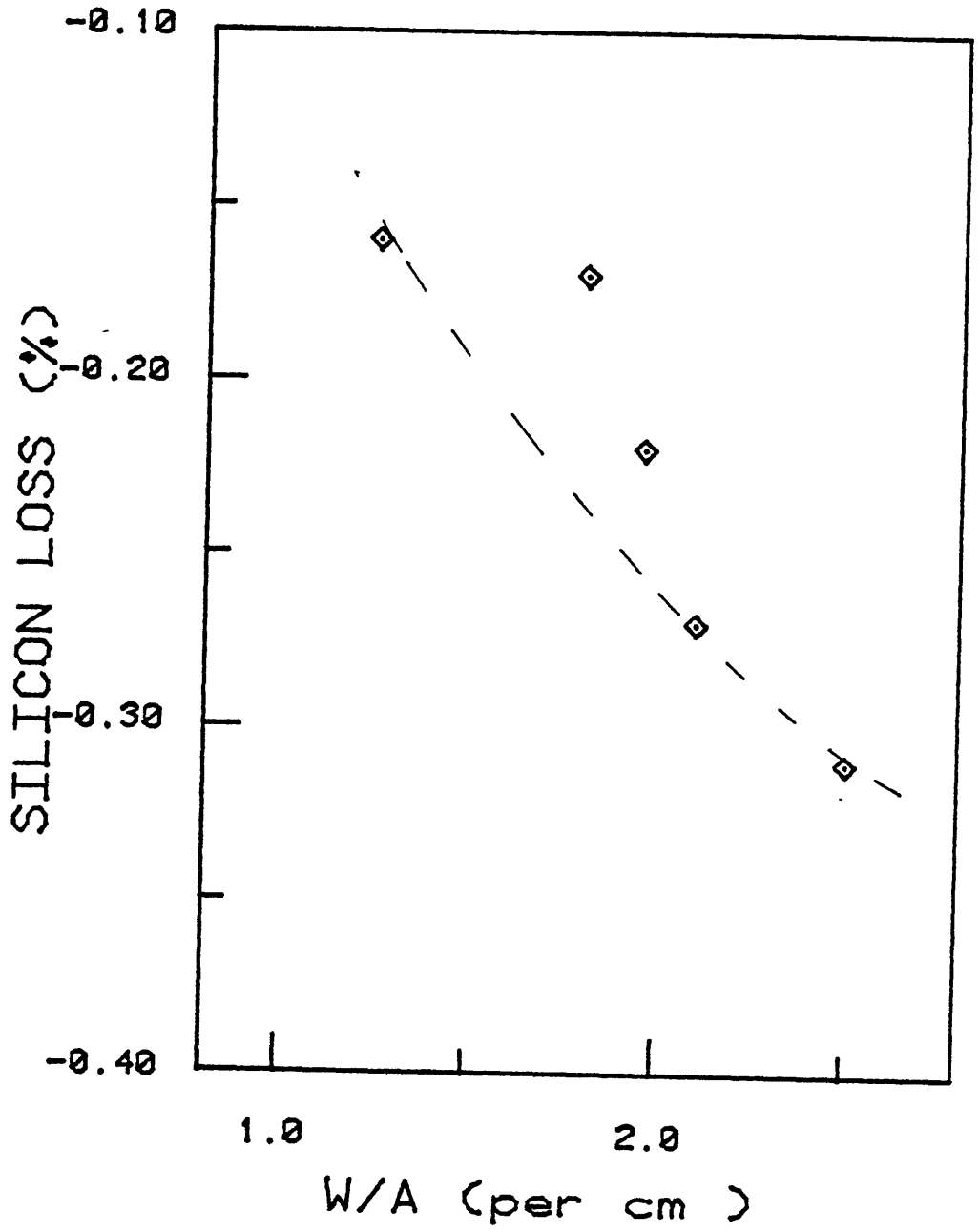

Figure 14: Effect of the parameter (w/a) on the loss of silicon from the metal to the slag. Flux Fx-2, HiSi baseplate and A-7 electrode used for all welds.

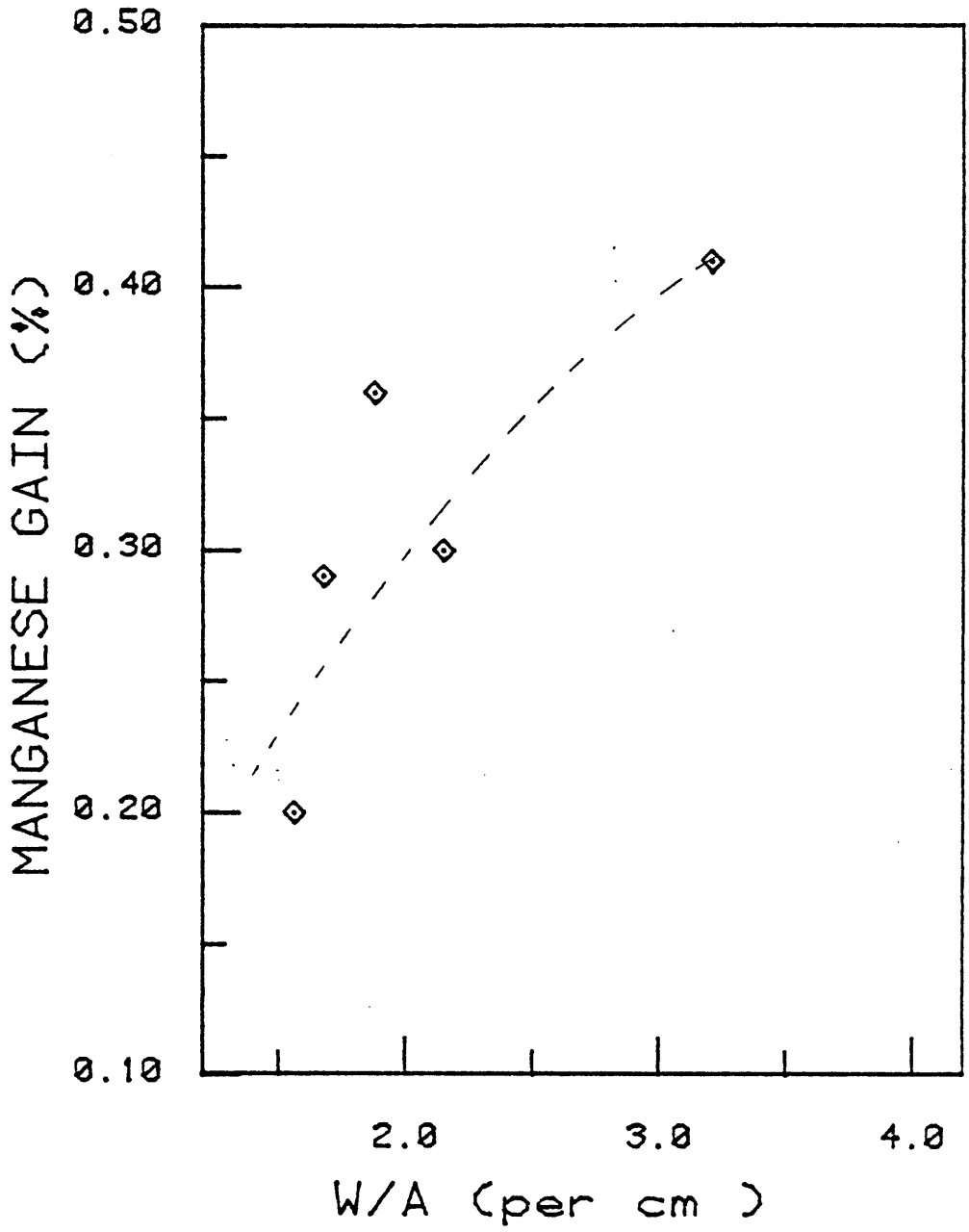

Figure 15: Effect of the parameter (w/a) on the transfer of manganese from the slag to the metal. Flux Fx-1, 1008 baseplate and A-7 electrodes were used.

slag and the metal against the ratio of the width to transverse cross-sectional area of the weld metal, qualitatively explain the effect of voltage and current on the kinetics of slag-metal reactions. As voltage is increased the area of the slag-metal interface is increased or the ratio of the width to cross-sectional area is increased, but, on increasing current, the volume of the weld metal is increased or the ratio of the width to cross-sectional area is decreased and these changes in weld geometry affect the kinetics of metal transfer. Based on these observations a quantitative model was formulated, to predict the amount of alloying elements in the weld metal for any combination of welding consumables and process parameters.

4.2.1. The Kinetic Model

The model considers the slag and the metal to be two immscible stirred liquids with an alloying element M being transferred at the slag metal interface. Then, for an interface reaction, such as

$$\underline{M} + x\underline{O} = (MO_x) \qquad (11)$$

to proceed, three events have to take place [41]:

1. Reaction species (the relevant ions in the oxide MO_x) have to move between the bulk slag and the slag-metal interface.
2. Chemical reaction (11) has to occur at the slag metal interface.

3. The alloying element M has to move from the slag-metal interface to the bulk metal.

The kinetics of slag-metal interactions may therefore be controlled or affected by any of these three steps. The three steps may be represented schematically by an activity-distance diagram (Figure 16).

4.2.1a. Assumption

The model assumes that:

1. A neutral point (N.P.) exists for each welding flux. The slag and metal are at an effective equilibrium only when the nominal composition of the weld (i.e. the total composition due to the simple mixing of metal from the electrode and workpiece in the absence of chemical reactions) is the same as the neutral point. That is, no transfer of the alloying element takes place at the neutral point. Furthermore, the neutral point is not affected by variations in the process parameters. This assumption is based on the results of Chai [17,25] (Ref. Ch. 2.2(b)) and is supported by the experimental data of Thier [34].†

† It should be noted that when the nominal metal alloy content is greater than the neutral point the alloying elements will be transferred from the metal to the slag. This loss of alloying elements will occur even if the weld metal is gaining oxygen, as long as the above condition holds. This explains the results observed earlier in Table 14.

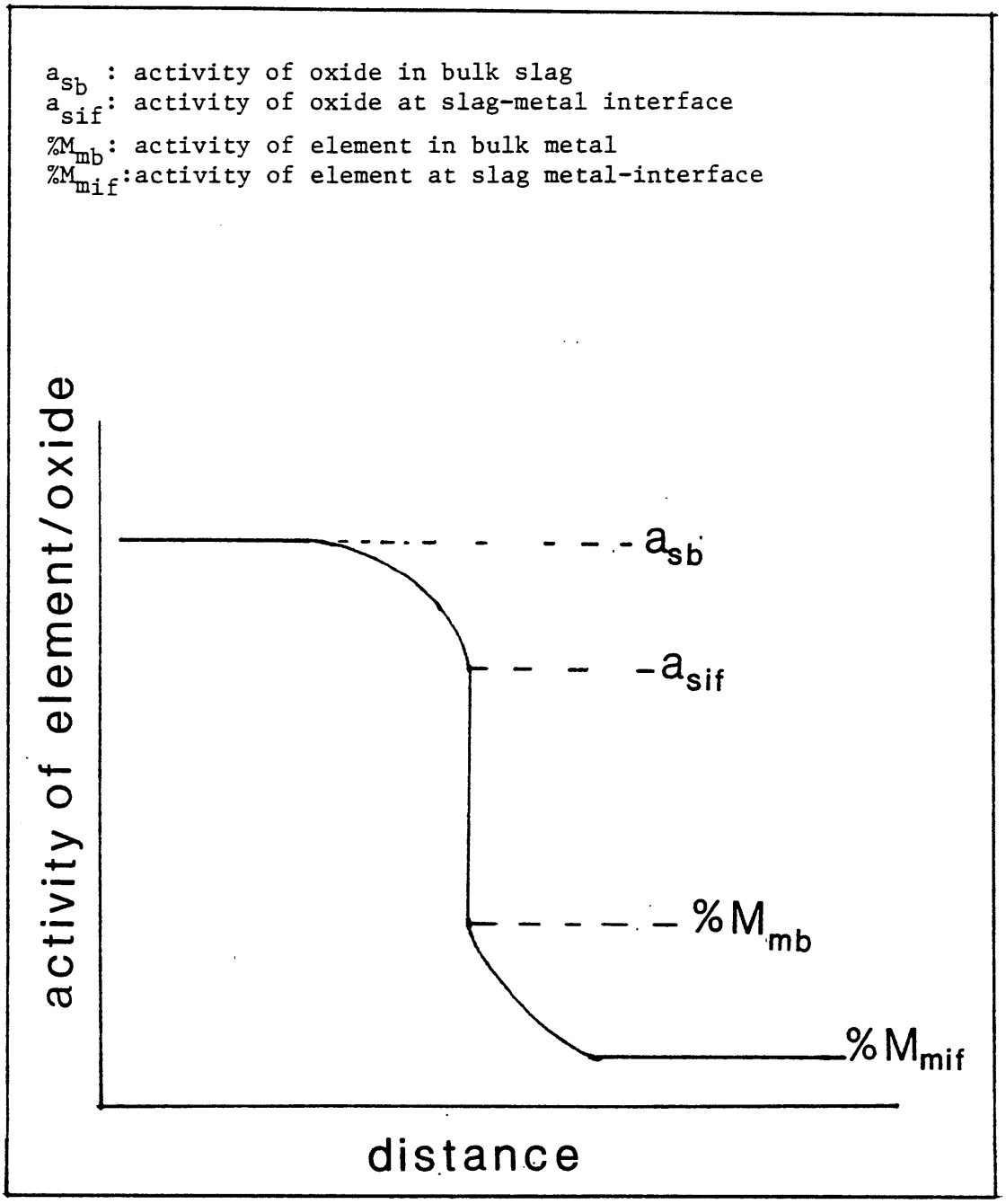

Figure 16: Activity distance diagram for oxide (MO_x) in the slag and alloying element M in the metal at the slag metal interface.

2. The equation of continuity is valid for the transfer of the alloying element. That is, the mass flux (J) of alloying element M which flows from the bulk slag to the slag-metal interface is equal to the mass flux of M passing through the chemical reaction stage and that which is passing from the interface to the bulk metal. The amount of this mass flux (J), however, can and will change with time.

3. The mass transfer coefficients of the alloying element M in the slag (k_s) and the metal (k_m) are independent of one another and of the activities of the reacting species.

4. The initial oxygen concentration in the weld pool (and not the final weld metal oxygen content) is dependent only on flux composition. This assumption may seem surprising considering that the transfer of the alloying element M also involves the simultaneous transfer of oxygen by reaction (11). However, in the weld pool, transfer of several elements takes place simultaneously. The reactions

$$\underline{Si} + \underline{O} = (SiO_2) \qquad (11a)$$

and

$$\underline{Mn} + \underline{O} = (MnO) \qquad (11b)$$

may either proceed forward or backward, but there is always the oxidation of iron (except in fluxes containing

over 40% FeO, which is rare, and in that case reactions (a) and (b) go backwards)

$$Fe + \underline{O} = (FeO) \qquad (11c)$$

Also, as explained in Section 4.1, the oxygen content of the weld metal is controlled by plasma-metal reactions involving the liquid-metal droplets. Thus, in the region of weld pool reactions, although some metal oxygen transfer may occur from the weld metal to the slag, more oxygen introduced in the form of falling droplets and possibly through the region directly under the arc may keep the pool oxygen level almost constant. The existence of a singular neutral point as demonstrated by Chai and Eagar [25] and which also may be observed from Thier's data [34] strongly supports the current assumption. It should be noted though that, unlike the initial weld pool oxygen content, the final amount of oxygen in the weld metal does depend on welding process parameters and electrode/base plate composition, in addition to flux composition. This is due to a mechanism of inclusion formation, growth and separation which will be discussed in Section 4.3.

5. The temperature range over which weld pool reactions occur near the arc is small. The fact that the arc-metal interface is maintained at temperatures up to a maximum of 2500°C [39]

provides some justification for this assumption. The validity of this assumption will be justified later (in Chapter 5) by considering the data of other researchers.

6. The chemical reaction (11) is first order. There is no direct justification for this assumption and it has been used to keep the analysis simple. Elliot [43] has noted that although the idea of reaction order has been used in gas-kinetic studies, it has not been very useful in kinetic studies on slag-metal systems. However, results of later experiments along with data of other researchers (Chapter 5) indicate that this assumption may be justified since the chemical reaction step might not be rate controlling in this system.

4.2.1b. Derivation

If equation (11) is at equilibrium, then the equilibrium constant may be written

$$K = \frac{(a_{MO_x})_{eq}}{[a_M][a_{\underline{O}}]^x_{eq}} \qquad (12)$$

when the subscript eq denotes the equilibrium composition. Neglecting the effect of interaction terms on the activity of the metal [41,42],

$$K = [a_{MO_x}]_{eq}/[\%M][a_O]^x \qquad (13)$$

Since the slag and metal are at equilibrium only at the neutral point [17,25], then

$$K = \frac{(a_{MO_x})_{flux}}{[N.P.][a_O]^x} \qquad (14)$$

or

$$m = \frac{[N.P.]}{(a_{MO_x})_{flux}} = \frac{1}{K[a_O]^x} \qquad (15)$$

where m is the partition coefficient of the alloying element M between the metal and the slag. From assumptions 4 and 5, it follows that m is a constant. Even if assumption 5 is not strictly correct, m may still remain constant since a decrease in temperature increases the value of K, but decreases the value of $[a_O]$.

Let dq be the amount of alloying element M transferred between the metal and the slag. Then

$$dM = \frac{dq}{V_m} = \frac{(A_{s/m})(J)dt}{V_m} \qquad (16)$$

where J is the mass flux of alloying element M (wt% cm/s)

V_m is the volume of the weld metal (cm^3)

$A_{s/m}$ is the area of the slag-metal interface (cm^2)

dM is the differential change in the concentration of the alloying element M in the metal (in wt%)

dt is the differential change in time (s).

Equation (16) may also be written as

$$J = \left[\frac{V_m}{A_{s/m}}\right] \frac{dM}{dt} \tag{17}$$

Since the equation of continuity is valid (Assumption 2), the mass flux J is also given by the following equations [41,44]

$$J = k_s(a_{sb} - a_{sif}) \tag{18}$$

$$J = k_m(M_{if} - M_b) \tag{19}$$

$$J = k_1 a_{sif} - k_2 M_{if} \tag{20}$$

where k_s and k_m are the mass transfer coefficients in the slag and the metal

k_1 and k_2 are the forward and backward reaction rate constants

a_{sb} and a_{sif} are the activities of the chemical oxide MO_x in the bulk slag and at the slag-metal interface at any instant

M_b and M_{if} are the activities of the element M in the bulk metal and at the metal-slag interface.

Also at equilibrium (and only at equilibrium):

$$k_1 a_{sif} = k_2 M_{if}$$

or

$$\frac{k_1}{k_2} = \left(\frac{M_{if}}{a_{sif}}\right)_{eq} = \frac{N.P.}{[a_{MO_x}]_{flux}} = m \qquad (21)$$

that is

$$\frac{k_1}{k_2} = m \qquad (21)$$

During the course of the welding process both the metal and the slag compositions change. The activity of the oxide in the bulk slag is therefore not exactly the same as that in the flux. However, this change is small due to mass balance consideration. For example, a change in metal composition from 0.1% Mn 0.1% Si to 1% Mn 0.5% Si will change a 30% MnO - 30% SiO_2 flux composition to approximately 29% MnO - 29% SiO_2 composition or a change in metal composition from 1.0% Mn, 0.1% Si to 0.5% Mn, 0.5% Si will change a slag composition of 0.1% MnO - 50% SiO_2 to about 1% MnO - 49% SiO_2. Thus the slag can be considered to have a greater "capacity" as a source or sink of alloying elements than can the metal. More will be said about this later.

$$a_{sb} = [a_{MO_x}]_{flux} + (\gamma)(b)[M_i - M_b] \qquad (22)$$

where γ: activity coefficient of the oxide (MO_x) in the flux

b: a mass balance factor $b = [\frac{\text{Mol wt of } MO_x}{\text{At wt of M}}] * \frac{\text{wt of metal}}{\text{wt of slag}}$

M_i: initial or nominal concentration of alloying element M.

$$M_i = M_{e\ell}(1 - d) + M_{B.P.}(d) \tag{23}$$

where $M_{e\ell}$ and M_{BP} are the alloy content of the electrode and baseplate respectively and d is the dilution factor. Combining equation (15) with equation (22) we get

$$a_{sb} = \frac{N.P.}{m} + (\gamma)(b)(M_i - M_b) \tag{24}$$

Combining equations (24) and (18) we get

$$\frac{m}{k_s} J = N.P. + (m)(\gamma)(b)(M_i - M_b) - ma_{sif} \tag{25}$$

or letting a factor

$$\beta = (m)(\gamma)(b) \tag{26}$$

$$\frac{m}{k_s} J = N.P. + \beta(M_i - M_b) - ma_{sif} \tag{27}$$

Equation (19) may be written as

$$\left(\frac{1}{k_m}\right) J = M_{if} - M_b \tag{19a}$$

and equation (21) may be substituted in equation (20) to give

$$\left(\frac{1}{k_2}\right) J = ma_{sif} - M_{if} \tag{28}$$

Adding equations (26), (19a) and (27) we get

$$\left(\frac{m}{k_s} + \frac{1}{k_m} + \frac{1}{k_2}\right) J = N.P. - M_b + \beta(M_i - M_b) \tag{29}$$

Substituting equation (17) for J we get

$$\left(\frac{m}{k_s} + \frac{1}{k_m} + \frac{1}{k_2}\right)\left(\frac{V_m}{A_{s/m}}\right)\frac{dM}{dt} = (N.P. - M_b) + \beta(M_i - M_b) \tag{30}$$

Solving this differential equation from t = 0 to t = t and using the initial condition at t = 0, $M_b = M_i$ (nominal weld composition) gives a solution of the form

$$N.P. + \beta[\%M_i] - [1 + \beta][\%M_f] = [N.P. - M_i] * \exp[-(A_{s/m}/V_m)(1+\beta)(\alpha)] \tag{31}$$

where

$$\alpha = \int_0^t \frac{dt}{1/k_m + m/k_s + 1/k_2} \tag{32}$$

and M_f is the final weld metal composition. For most welding fluxes it can be shown that for transfer of Mn and Si,

$$\beta = m\gamma b \simeq 0 \qquad \text{(ref. Appendix A.4)}$$

and equation (30) reduces to

$$(N.P. - M_f) = (N.P. - M_i) * \exp\left(- \frac{A_{s/m}}{V_m} \alpha\right) \qquad (33)$$

If we consider the approximation

$$a_{sb} \simeq [a_{MO_x}]_{flux} \qquad (34)$$

since as mentioned earlier the flux composition does not change significantly during the welding process, then equation (32) may be directly derived by substituting equation (34) for equation (22).

If the terms in equation (33) are rearranged then an expression is obtained for predicting weld metal composition

$$M_f = N.P. - (N.P. - M_i) * \exp\left(-\alpha \frac{A_{s/m}}{V_m}\right) \qquad (33)$$

In the right hand side of this expression (equation (33)), the first term (N.P.) is the neutral or equilibrium point reached if and only if the slag and metal are at equilibrium. The second term $[(N.P. - M_i) * \exp(-\alpha A_{s/m}/V_m)]$ is the deviation from the neutral point. The term $(N.P. - M_i)$ is the thermodynamic driving force and the term $\exp(-\alpha A_{s/m}/V_m)$ incorporates the kinetic considerations which include the effect of variations in the welding process parameters.† Equation (33) may also be written as

$$\Delta M = M_f - M_i = (N.P. - M_i)(1 - \exp(-\alpha A_{s/m}/V_m)) \qquad (33a)$$

†More is said about this in the next chapter.

where ΔM is the amount of alloying element transferred from the slag to the metal or vice versa. Since the factor $(1 - \exp(-\alpha A_{s/m}/V_m)]$ is always positive the sign of ΔM will depend on the sign of $(N.P. - M_i)$. That is, whether the alloying element M is transferred from the slag to the metal or the reverse depends only on the thermodynamic factor $(N.P. - M_i)$. Kinetic considerations (welding process parameters) may change the magnitude of ΔM but they cannot determine its sign. (This excludes the effect of the welding process parameters on dilution and the consequent effect on $(N.P. - M_i)$). This is consistent with the experimental results of all researchers who have studied the effect of welding process parameters on weld composition [10,18,19,28-32]. In the derivation of equations (31) and (33) factors such as surface renewal were not considered. However, it has been shown that the error caused by neglecting this in models where phase resistances are added (such as the one derived in this section) is low [41,45,46].

4.2.1c. The Electrical Analog

A simple way of looking at the process of element transfer during SAW is by using the electrical analog shown in Figure 17. The slag may be considered as a battery with the potential corresponding to the Neutral Point. The weld metal is equivalent to a capacitor (C_m) charged initially to a potential M_i (initial nominal weld composition) which discharges to M_f (final composition) after welding. The treatment of slag as a battery and the metal as a capacitor may be explained by an example: consider a metal of nominal composition

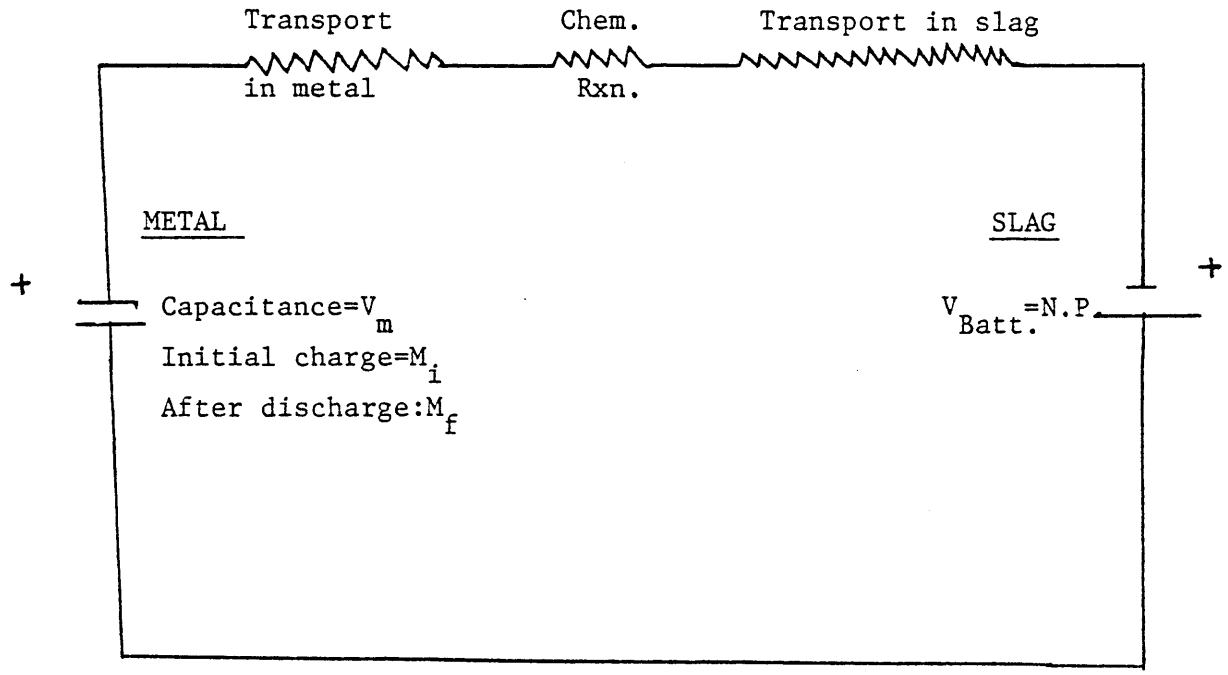

Figure 17: Electrical analog of the kinetic model.

0.1% Si to 1.00% Mn reacting with a flux containing 30% SiO_2, 0% MnO. After welding, let the metal composition change to say 0.8% Si, 0.3% Mn. However, the slag composition would change to about 28.5% SiO_2, 1.5% MnO. (By a simple mass balance.) The small change in slag composition does not significantly change the Neutral Point* so the slag is like a battery at a constant potential, but the metal is like a capacitor of variable potential.

Alternatively, the slag may be considered as another capacitor of capacitance C_s. However, since there is a very small change in slag composition during the welding process, the potential of the slag (N.P.) does not change significantly. Thus, the capacitance of the slag as a source or sink of alloying elements is much greater than that of the metal, i.e. $C_s >> C_m$ (ref. Appendix A.4).

The resistance to the transfer of the element due to mass transport at the slag interface, chemical reaction nonequilibria or mass transport at metal interface may be considered analogous to three electrical resistances in series. As the area of the slag metal interface increases the resistance decreases. Also, as the volume of the metal pool increases, the change in concentration (potential) of the alloying element decreases.

Comparing the solution of the Kinetic Model (equation (33)) to that of the simple RC circuit (equation (35)) many similarities may be observed

---

*This corresponds to $\beta = 0$ in our analysis.

$$(N.P. - M_f) = (N.P. - M_i) * \exp(-\alpha * A/V) \quad (34)$$

$$[V_{battery} - V_{capacitor(after\ discharge)}] = (V_{battery} - V_{capacitor(initial)}) * \exp(-t/RC) \quad (35)$$

R is inversely proportional to A

V is directly proportional to C

4.2.1d. Multipass Welding

Equation (33) applies only to single pass welds. When more than one pass is made, then the composition of the subsequent passes may be calculated by repeated use of equation (33). In such a calculation, the value of M_i to be used for computing the composition of the nth layer is calculated from the value of M_f in the (n-1)th layer, since the (n-1)th layer acts like the baseplate for the nth layer. If the welding conditions are kept constant then the composition of the nth layer (M_{fn}) is given by equation (36). (Derivation in Appendix A.5.)

$$M_{fn} = M_{e\ell} + \left[\frac{(N.P. - M_{e\ell})(1 - F)}{(1 - Fd)}\right][1 - (Fd)^n] + (Fd)^n M_{BP} \quad (36)$$

where

$$F = \exp\left(-\alpha \frac{A_{s/m}}{V_m}\right) \quad (37)$$

and d is the amount of dilution. Since $F < 1$ and $d < 1$, for large n,

$(Fd)^n \rightarrow 0$. So for large n, a steady state solution is obtained

$$M_N = M_{e\ell} + \frac{(N.P. - M_{e\ell})(1 - F)}{(1 - Fd)} \tag{38}$$

This steady state solution indicates that after a large number of passes (typically 6-10) the weld composition will remain constant, providing the welding conditions are not changed. (If the welding parameters are changed, the values of F and d and consequently, M_N will be changed.) During this steady state condition the extra amount of alloying element entering the weld pool as drops from the molten electrode is exactly equal to the amount of alloying elements lost to the slag by weld pool reactions or vice versa. This steady state condition has been observed by different researchers [29-35] but they have incorrectly interpreted the existence of this condition as evidence that the transfer of alloying elements is controlled at the droplet stage. Equation (38) may also be written as

$$\Delta M_N = M_N - M_{e\ell} = (N.P. - M_{e\ell}) \frac{(1 - F)}{(1 - Fd)} \tag{38a}$$

Comparison with equation (33a) indicates that for multipass welding (after 6 or more passes), the thermodynamic driving force for the amount of alloying element M transferred is $(N.P. - M_{e\ell})$ as compared to $(N.P. - M_i)$ for single pass welds. Also, it should be noted that even when $M_i = M_{e\ell}$, ΔM from equation (33a) will be lower than ΔM_N from equation (38a) by a factor of $(1 - Fd)$. This has been observed

in practice [36] but so far researchers could not explain this difference between ΔM and ΔM_N. The greater value of ΔM_N as compared to ΔM is not surprising considering that equilibrium is not normally reached during the SAW process, and in multipass welding, due to the repetitive nature of the process, equilibrium values are more closely approached. However, the steady state condition M_N should not be confused with the equilibrium condition (N.P.). The value of M_N, unlike that of N.P., changes with the welding conditions, as indicated by equations (38) and (37), and as demonstrated by the experimental results of other researchers [29-36]. However, under certain welding conditions (when F is low) the steady state composition may rapidly approach the equilibrium composition.

4.3. Zone of Cooling and Solidifying Weld Pool

In this region, the part of the molten weld pool behind the electrode starts to cool and solidify as the electrode moves away from it (see Figure 9, p. 48). Christensen and Chipman [38] found that there is a small drop in the manganese content near the slag-metal interface in manual metal arc (MMA) welds. This depletion of manganese occurs in a region about 0.05-0.15 mm from the surface of the MMA weld. It exists in weld metal which loses manganese to the slag as well as in metal which gains manganese from the slag. They attributed this interfacial phenomenon to the increasing stability of oxides at lower temperature and the consequent shifting of the equation

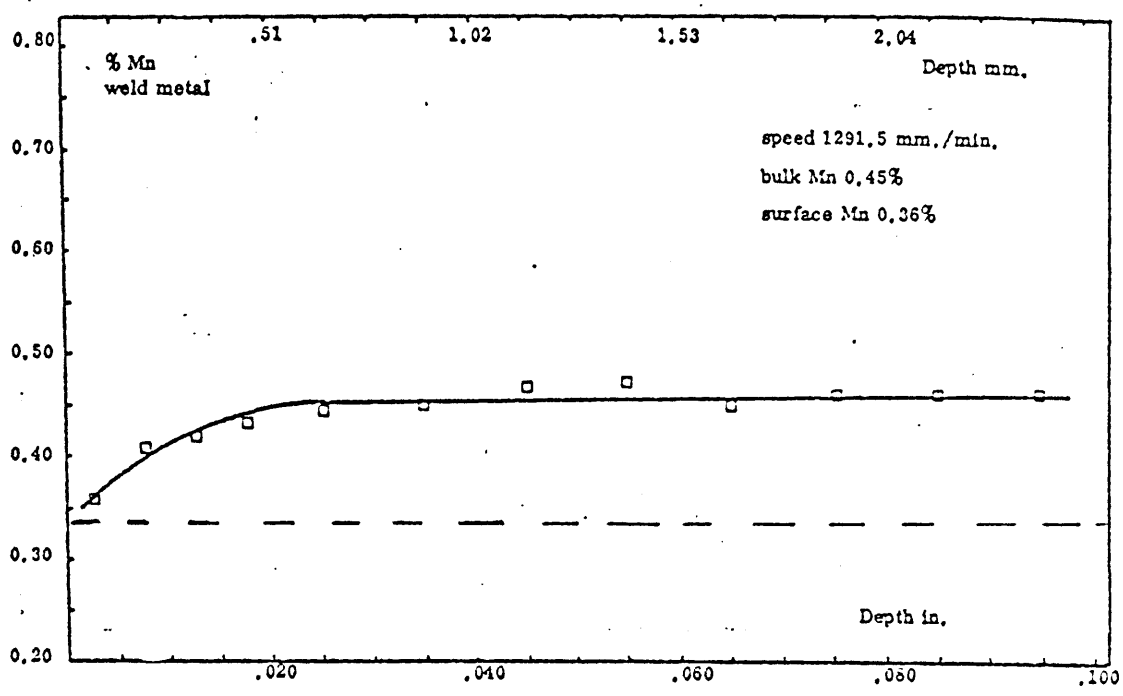

Figure 18: Spatial distribution of manganese in weld metal [from ref. 18]. Dashed line indicates initial manganese content of metal.

$$\underline{Mn} + \underline{O} = (MnO) \qquad (39)$$

to the right.

Later Christensen [10] and North [18] observed similar manganese depletion zones in submerged arc welds [see Figure 18]. Depletion of chromium and silicon in addition to manganese has been observed during submerged arc welding of alloy steels with fluxes containing chromium (111) oxide, but this has been attributed to interfacial reactions resulting in the reduction of trivalent chromium oxide to lower oxide forms [16]. This zone of alloy depletion in submerged arc welds extends only up to a maximum depth of 0.5 mm from the surface and does not affect the overall alloy content of the metal [10,12,18,38]. However, interfacial reactions are not the only reactions which occur in this zone of cooling and solidifying weld pool. More important changes take place within the molten pool itself.

The increased stability of oxides at lower temperatures and the high amounts of oxygen present in the weld pool will result in the formation of inclusions or deoxidation products inside the molten metal [48,49,50]. Furthermore, these inclusions may grow with time by coalescense and the larger ones are more likely to separate from the liquid metal into the slag [51-53]. Even in this zone of cooling weld pool fairly large convective forces may be present, consequently it is unlikely that Stokes' law is applicable. However, the convective forces would help the smaller inclusions to collide and form larger

inclusions. If the time for the weld pool to cool and solidify increases, the inclusions will have a larger amount of time to grow and separate out. Also, if the weld pool contains larger amounts of alloying elements, oxygen supersaturation and consequent inclusion formation will occur earlier, at higher temperatures [48-50] and again these inclusions will have more time to grow and separate. Table 13 shows that deoxidants (Mn and Si) present both in the electrode and the baseplate lower oxygen content in single pass layers and supports the above statement. Furthermore, thermodynamic considerations indicate that deoxidants (Si and Mn) present in the electrode cannot prevent oxidation in the droplet stage. Rather, the deoxidants in both the baseplate and in the electrode reduce the oxygen content of the metal due to inclusion formation and separation during the cooling cycle of the weld pool.

The time taken for a simply shaped casting to solidify is given by Chvorinov's rule [54]

$$t_s = C(V/S)^2 \qquad (40)$$

where t_s = solidification rate

V = volume of the casting

S = surface area of the mold metal interface in the casting.

Figure 19 indicates the experimental results on steel castings of different shapes and sizes, varying from 10 mm thick castings to 65 ton castings [55]. A weld can be considered as a simple casting and equation (40) may be applied to it with V being the volume of the

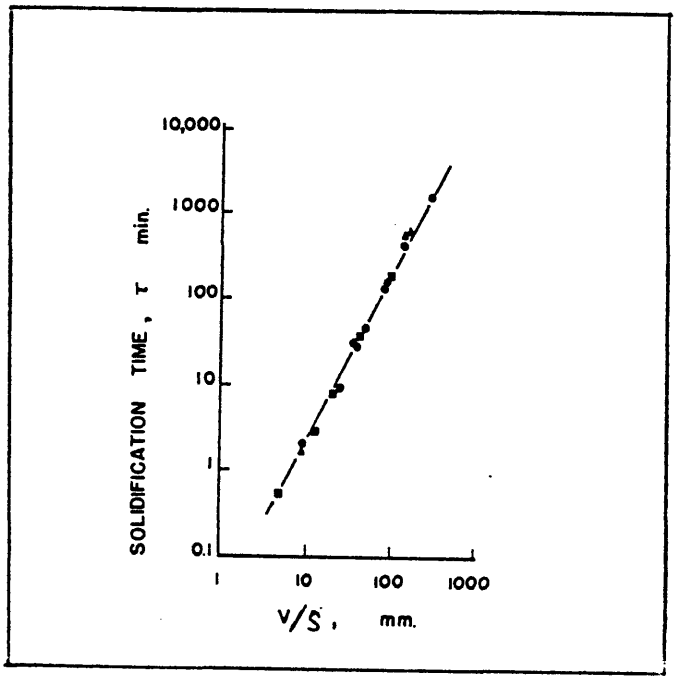

Figure 19: Chrorinov's experimental results on solidification time of castings versus their volume to area ratio [from ref. 54].

weld metal and S the area of contact between the weld metal and the work piece. (Heat loss through the insulating slag layer is neglected.) It should be noted that, due to the presence of a travelling heat source, different points along the same longitudinal line (parallel to the direction of travel of the electrode) will solidify at different times. However, the time for solidification (t_s) for each such point will still be the same. The ratio (V/S) in equation (40) may be substituted by the ratio (a/s), where a is the area of the transverse cross-sectional area of the weld, and s is the length of the fusion line as indicated in Figure 20 so

$$t_s = C(a/s)^2 \qquad (41)$$

As mentioned earlier, a decrease in solidification time will increase oxygen. Thus, if the ratio (s/a) is increased, the oxygen content should increase. Also as (s/a) is increased the average inclusion size should decrease. Both the above predictions may be observed from the experimental results of Chai and Eagar (Figure 21). Later (in Chapter 5), our hypothesis is verified by directly changing the solidification time without varying welding parameters and by applying our analysis to data of other researchers. Before concluding this section, it should be noted again that the main factor controlling weld metal oxygen is flux composition since flux composition controls the oxygen potential in the arc cavity (in the zone of droplet reactions). However, the

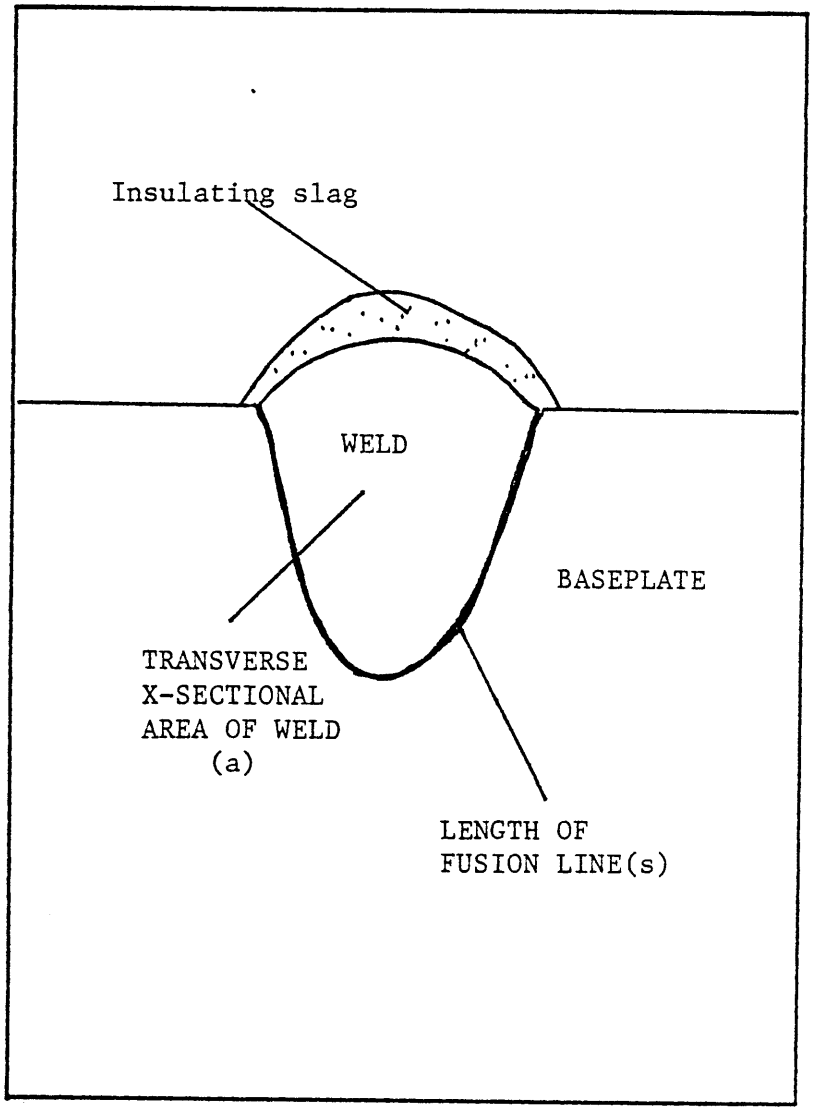

Figure 20: Schematic figure illustrating the parameter (S/a).

SURFACE/VOLUME : 3/cm

SURFACE/VOLUME : 9/cm

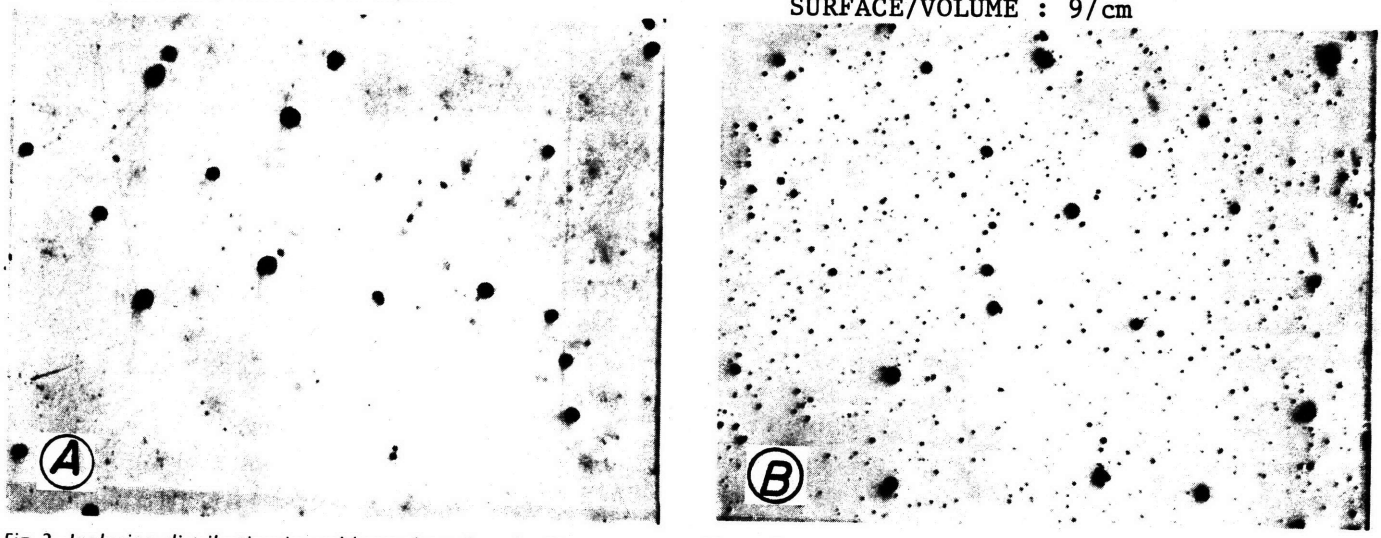

Fig. 3—Inclusion distribution in weld metal produced with manganese silicate flux: A—670 ppm oxygen; B—1740 ppm oxygen

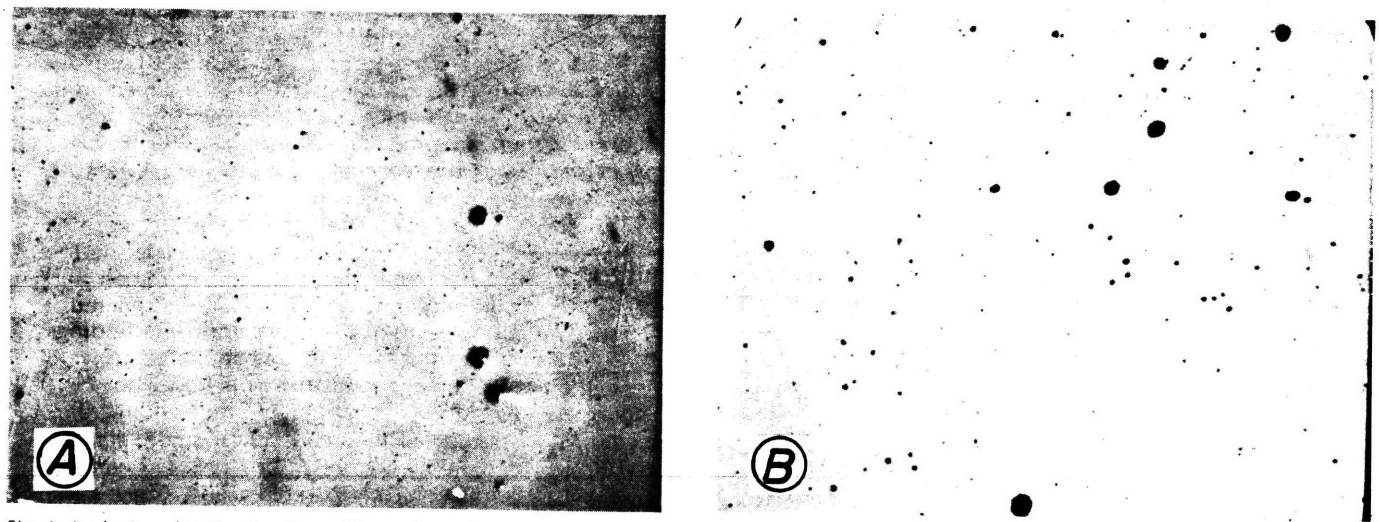

Fig. 4—Inclusion distribution in weld metal produced with calcium silicate flux: A—210 ppm oxygen; B—580 ppm oxygen

SURFACE/VOLUME = 3.5/cm

SURFACE/VOLUME = 7.5/cm

Figure 21 : Micrographs of inclusion distribution in weld metal having different (S/a) ratios (from ref. 19).

welding parameters, and the alloy content of the electrode and base plate also significantly influence final weld metal oxygen content, due to a mechanism of inclusion formation and removal in the cooling weld pool. The effect of the welding parameters on weld metal oxygen is particularly significant on welding with highly oxidizing fluxes. On welding with these fluxes a change in the process parameters may change the oxygen content of the weld metal by as much as 1100 ppm. On welding with the less oxidizing or basic fluxes, changes in the process parameters usually do not change the weld metal oxygen content by more than 400 ppm (see Table 2) [19].

CHAPTER 5

ESTIMATION OF THEORETICAL PARAMETERS

In the previous chapter a new theory was presented to explain and describe the changes that occur in weld metal chemistry during the submerged arc welding process. It was proposed that the oxygen content of the metal is controlled by plasma-metal reactions in the zone of droplet reactions, and deoxidation reactions occuring in the zone of the cooling and solidifying weld pool. The transfer of the other alloying elements is controlled by direct slag metal reactions occuring in the zone of dilution and weld pool reactions. Furthermore, it was proposed that the transfer of an alloying element M may occur by the reaction

$$\underline{M} + \underline{O} = [MO_x] \tag{11}$$

and a kinetic model was formulated to predict weld metal composition.

For single pass welds, the following equation was suggested

$$M_f = N.P. - (N.P. - M_i) * \exp(-\alpha * (A_{s/m}/V_m)) \tag{33}$$

where

M_f: amount of alloy M present in the weld at the end of the welding process

M_i: nominal weld composition or the alloy content of weld metal expected from simple mixing of the electrode and base plate in the absence of chemical reactions. Its values thus depends on both electrode and baseplate composition and the dilution factor (M_{el}, M_{BP} and d, respectively).

N.P.: the neutral point or equilibrium point for the element M in the flux. The value of the neutral point is only determined by flux composition [17].

α: a factor which depends on the mass transfer coefficients, the chemical reaction rate and the partition coefficient. It is related to these variables by equation (32).

$(A_{s/m}/V_m)$: Is the ratio of the area of the slag-metal interface to the volume of the molten metal pool participating in the weld pool reactions.

For multipass welds, when several passes are made without changing the welding consumables or process parameters, equation (33) leads to a steady state value of metal composition:

$$M_N = M_{e\ell} + \frac{(N.P. - M_e)(1 - F)}{(1 - Fd)} \tag{38}$$

where

$$F = \exp(-\alpha\ (A_{s/m}/V_m)) \tag{37}$$

However, before proceeding to verify the model by performing different experiments or by applying it to the data recorded by previous researchers (Chapter 6), it is necessary to indicate how the different theoretical parameters were estimated. Also it is necessary to explain the effect of welding consumables, and welding process parameters (current, voltage, travel speed, polarity, etc.) on each theoretical parameter (N.P., M_i, d, $(A_{s/m}/V_m)$ and α).

5.1 Estimation of the Neutral Point

The neutral point is the chemical composition of the electrode/baseplate combination at which no transfer of alloying elements takes place between the slag and the metal. Thus, for fluxes free of the oxide MO_x the neutral point for the element M is zero. When the flux

contains the oxide MO_x the neutral point may be obtained directly from available experimental data [10,16,17]. Otherwise, it may be estimated by the thermodynamic model developed by Chai and Eagar [17, 25]. In any case, the agreement between predictions by the thermodynamic model and experimental data is good [17,25]. Table 15 lists the values of the neutral points of fluxes used in the present investigation and for those used by previous investigators.

5.1.1 Effect of Welding Consumables on the Neutral Point

The neutral point is only dependent on flux composition. It is independent of the electrode or baseplate composition [17,25].

5.1.2 Effect of Welding Process Parameters on the Neutral Point

The neutral point is independant of the welding process parameters. This follows from the results of Chai [17,25] and is supported by the experimental data of Their [34] (shown later in this chapter as Fig. 27 in Sec. 5.4.2). It should be noted that the kinetic model developed in Section 4.2 and the discussion here is valid only for fluxes which are free of ferroalloys or elemental additions. Later, in Section 6.2.3 the model is modified to explain changes that occur when welding with 'alloy' fluxes (fluxes containing ferralloys or elemental additions).

5.2 Estimation of the Dilution Factor

The dilution factor may be obtained from measurements of the transverse cross-sectional area as shown in Figure 22.

$$d = \frac{B}{B + D} = \frac{B}{a} \tag{44}$$

Table 15: Values of N.P. and α Used in Theoretical Model

Researcher (Ref.)	Flux Name Used in ref.	Neutral Point (N.P.)			$\alpha_{s/m}$		
		Mn	Si	Cr	Mn	Si	Cr
Present Investigation	Fx-1	1.2	0.95	0	1.7	1.7	1.7/3
	Fx-2	0	0.35	-	1.7/3	1.7/3	-
	Fx-3	0	1.20	-	1.7	1.7	-
Christensen [10]	a	0	1.0	-	1.7	1.7	-
	c	0	1.2	-	1.7	1.7	-
	d	0	1.2	-	1.7	1.7	-
	e	0.50	1.50	-	1.7	1.7	-
	f	0.55	0.50	-	1.7/3	1.7/3	-
North [18]	Calcium Silicate	0	-	-	1.7	-	-
Chai [17]	F-1	1.8	0.28	-	1.7/3	1.7/3	-
	F-2	0.5	0.28	-	1.7/3	1.7/3	-
	F-3	1.2	0.95	-	1.7/3	1.7/3	-
	F-4	0	0.35	-	1.7	1.7	-
Frumin [29]	AN-20	0	1.0	0	1.7/3	1.7/3	-
	A-398A	2.5	1.0	-	1.7	1.7	1.7/9
Thier [35]	LW-280	1.25	1.0	-	1.7/3	1.7/3	-
Mitra [16]	A	0	*	19.6	1.7/3	-	1.7/9
	B	0	*	19.9	1.7/3	-	1.7/9
	C	0	*	19.9	1.7/3	-	1.7/9
	D	1.7	*	8.7	1.7	-	1.7/3

- indicates transfer of elements not recorded by the researcher.

* indicates singular N.P. does not exist (see Ref. 16).

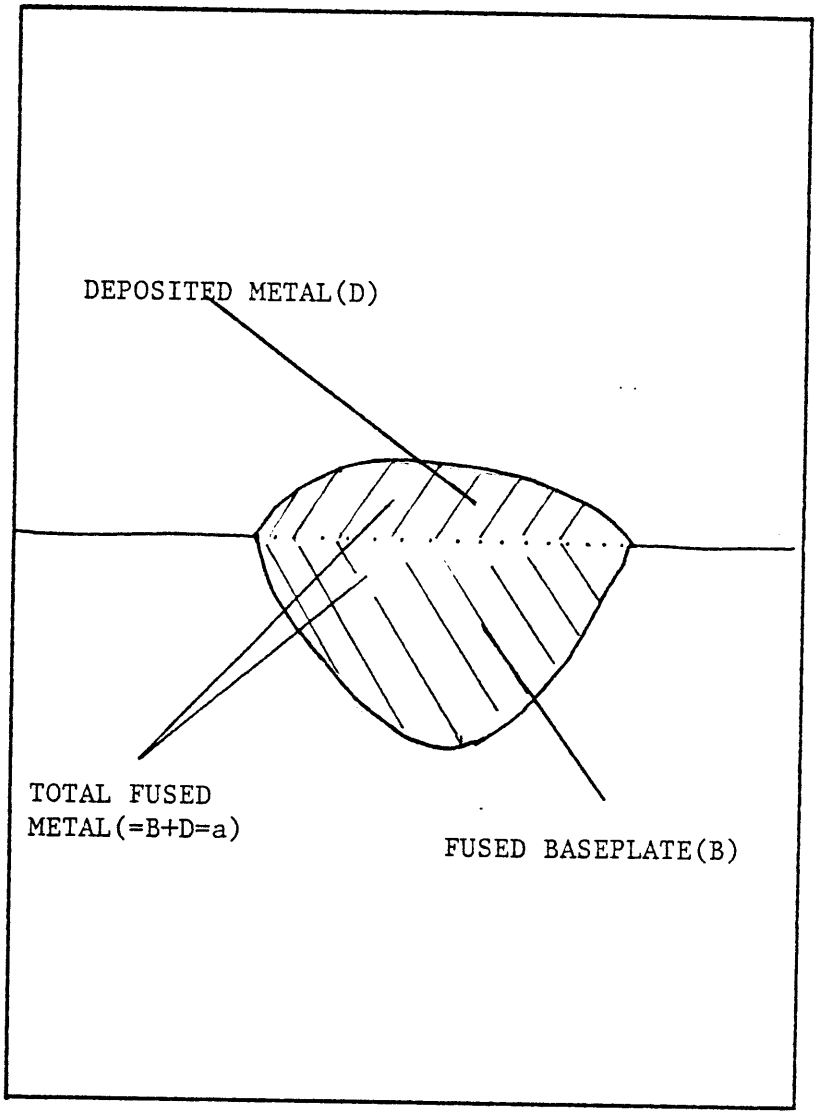

Figure 22 : Schematic figure showing the transverse cross-sectional area of the weld metal and illustrating the parameters B, D and a.

where B: transverse cross-sectional area of fused baseplate

D: transverse cross-sectional are of deposited metal

a: total transverse cross-sectional area

d: dilution factor.

Alternatively dilution may be estimated from the content of relatively noble metals such as Ni, Cu or Mo in weld metal since these elements do not oxidize easily [see Section 5.2.4]. The dilution factor is given by

$$d = \frac{X_{weld} - X_{e\ell}}{X_{BP} - X_{e\ell}} \tag{45}$$

where X_{weld}, $X_{e\ell}$ and X_{BP} are the contents of the Ni, Cu or Mo in the weld, electrode and baseplate, respectively. This method may be applied only when there is a very significant difference in the content of either Ni, Cu, or Mo between the electrode and baseplate compositions. Christensen has formulated charts to predict dilution factors for different fluxes and welding parameters [10]. Normally during the SAW operation dilutions of 0.45-0.70 are obtained although in some specific cases a greater range may be obtained.

5.2.1 Effect of Welding Consumables on the Dilution Factor

The dilution factor 'd' is not affected very much by the choice of welding consumables. It is virtually independent of the electrode and workpiece chosen but is affected slightly by the flux composition. (This may be seen from Belton's data [11]). However, this effect of flux composition is small as compared to changes produced by variations in welding parameters such as current or polarity.

5.2(b) Effect of Welding Parameters on the Dilution Factor

The dilution factor 'd' increases with increasing current resulting in an increase in the amount of metal deposited (D), as well as in amount of baseplate fused (B). However, the increase in B is more than the increase in 'D' so the dilution factor (d = B/B+D) increases with increasing current.[55,56] Polarity also has a significant influence on dilution. DCEP (direct current electrode positive) results in higher dilution than DCEN (direct current electrode negative).[55] The influence of the other welding parameters such as voltage, travel speed and electrode diameter is small. It should be emphasized once again that the dilution normally obtained in submerged arc welds lies in the range 0.45 - 0.70, it changes by less than a factor of two even for large variations in the welding parameters.

5.3 Estimation of Nominal Weld Composition M_i

The nominal metal composition may be estimated from the simple formula:

$$M_i = M_{BP}d + M_{e\ell}(1 - d) \qquad (46)$$

where M_{BP} and $M_{e\ell}$ are the electrode and baseplate composition and d is the dilution factor. It should be noted that it is necessary to estimate the nominal weld composition M_i, only for determining weld metal composition in single pass welds (Eqn. 33). In multipass welds, the metal composition depends only on electrode composition ($M_{e\ell}$) and is independant of the baseplate composition (M_{BP}) as is evident from equation 36.

5.3.1 Effect of Welding Consumables on Nominal Weld Composition

As evident from equation (46), the nominal weld composition is dependant only on electrode and baseplate composition. It is independent of flux composition.

5.3.2 Effect of Welding Parameters on Nominal Weld Composition

The welding parameters control the amount of dilution 'd' (see section 5.2.2) and thus indirectly affect the nominal weld composition.

5.4 Estimation of the Term $(A_{s/m}/V_m)$

It is not possible to directly estimate this term since the actual area of contact between the slag and metal in the zone of weld pool reactions is not known. However, it may be related to parameters which may be measured experimentally. There are three possible parameters which may be related to $(A_{s/m}/V_m)$:

1. The ratio of the length of the slag-metal interface (ℓ) to the transverse cross-sectional area (a) as indicated in Figure 23.
2. The ratio of weld width (w) to transverse cross-sectional area (a) (see Figure 23).
3. The ratio of slag weight (W_S) to metal weight (W_M).

It is likely that there is a surface depression near the arc as indicated in Figure 9 [57], so the parameter ℓ/a may not be the best representation of $[A_{s/m}/V_m]$. Of the other two parameters (w/a) and (W_S/W_M), the first has the advantage of having the same units as $(A_{s/m}/V_m)$. However, in case of a high degree of convection and

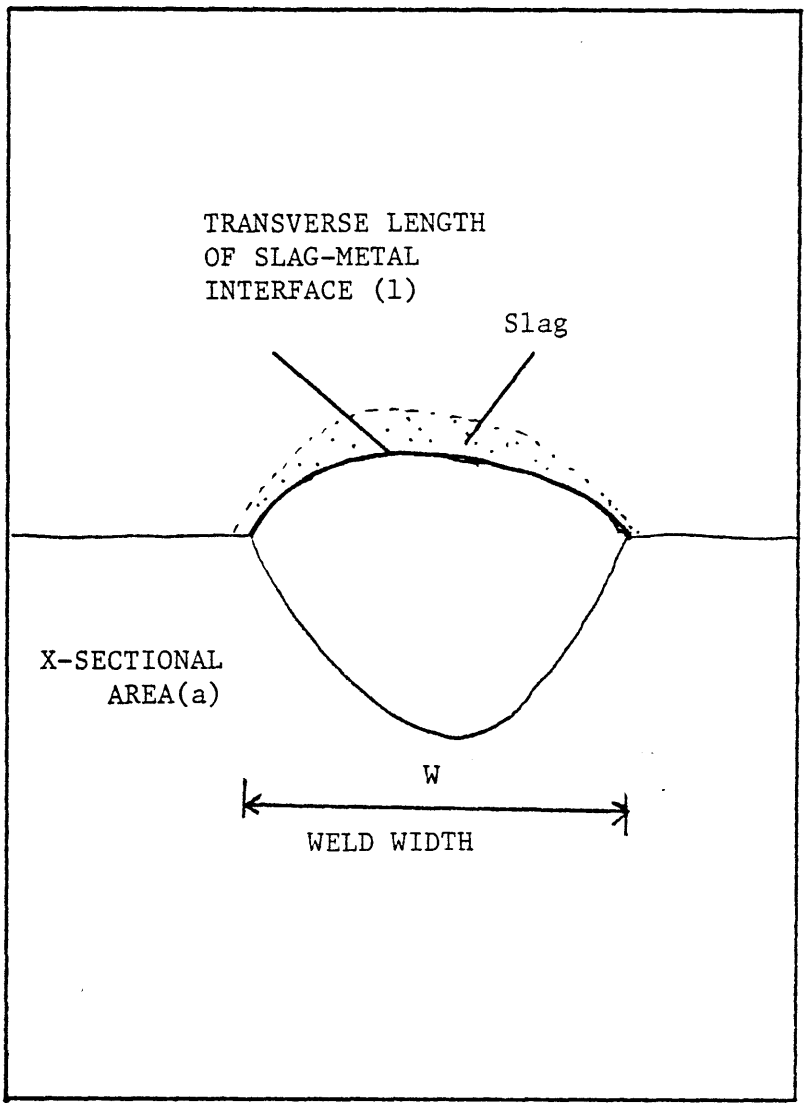

Figure 23: Schematic of the transverse cross-sectional area of a weld, illustrating the parameters (w/a) and (ℓ/a.

turbulence as is likely the case in a weld pool, the parameter (W_S/W_M) may give a better representation of $A_{s/m}/V_m$. Use of (W_S/W_M) does not necessarily imply that all parts of the slag come into direct contact with the metal, rather it implies the fraction of slag which come into direct contact with the metal remains approximately constant. The relation between $(A_{s/m}/V_m)$ and (W_S/W_M) may be expressed by

$$(A_{s/m}/V_m) = C(W_S/W_M) \tag{47}$$

where C is a constant and has the same dimension as $(A_{s/m}/V_m)$,[†] $[(W_S/W_M)$ is dimensionless].

Most previous researchers have recorded the values of (W_s/W_m) in their investigation [10,12,18,28,42]. Some of them have recorded values of W_s/W_E [18,28] where W_S is slag weight and W_E is the weight of deposited electrode metal only, but W_s/W_M may be related to (W_S/W_E) by the simple formula

$$\frac{W_S}{W_M} = \frac{W_S}{W_E}\frac{W_E}{W_M} = \frac{W_S}{W_E}(1 - d) \tag{48}$$

where d is the dilution factor.

In most of the verification plots presented later, values of W_S/W_M have been used since these values were recorded by previous researchers. However, in the experiments performed to directly verify the model both (W_S/W_M) and (w/a) were recorded and when applied gave nearly identical results. This is not surprising considering that all three parameters

---

[†]The constant C may be incorporated in equation (32), so that α is dimensionless when (W_S/W_M) is used as a measure of $A_{s/m}/V_m$. When w/a is used as a measure of $A_{s/m}/V_m$, α is expressed in units of length (cm).

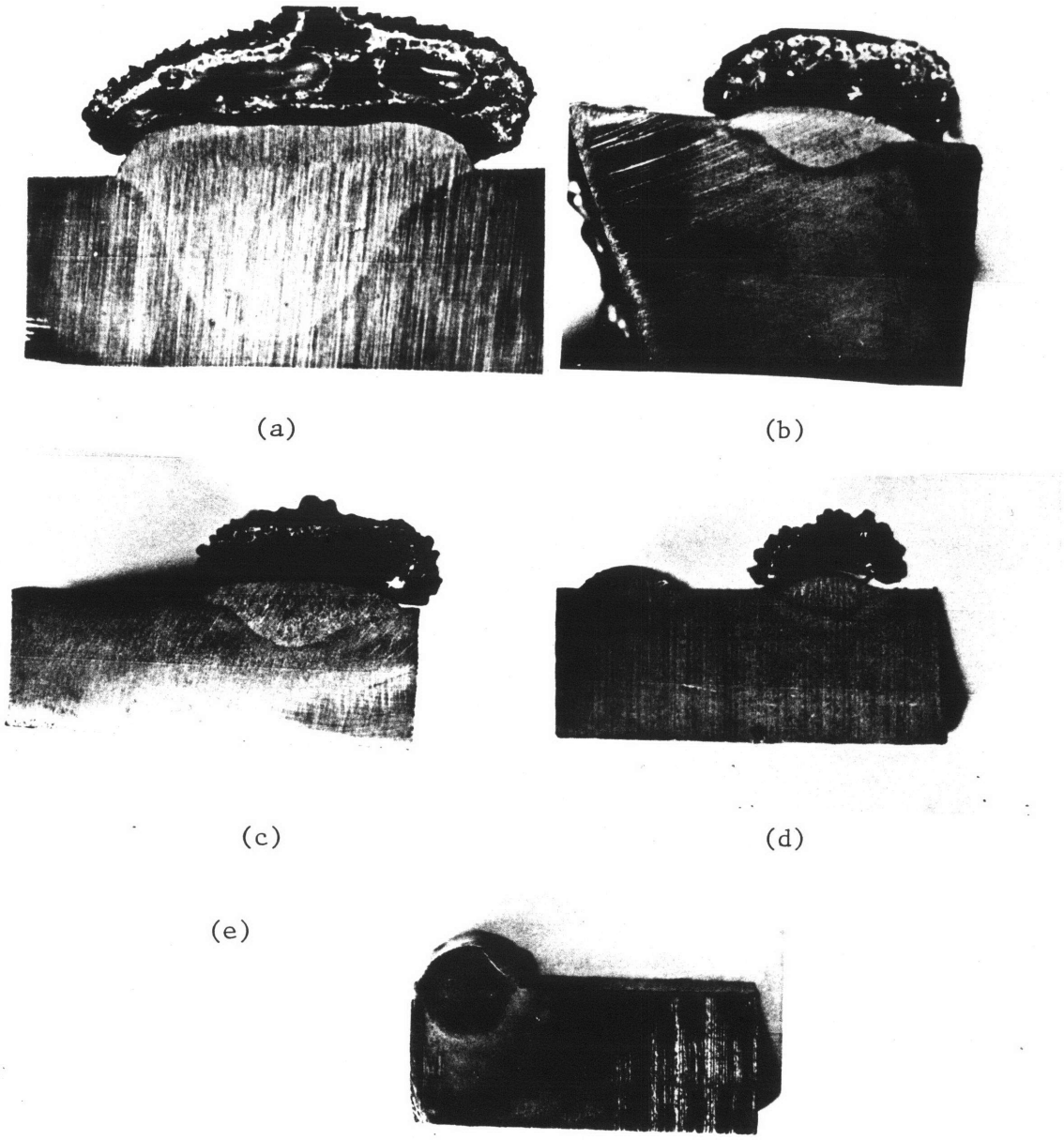

Figure 24 : Transverse cross-sectional areas of weld metal and slag under diffrent welding conditions. Flux Fx-1 used for all welds. (a) Weld No. 800(33V,800A,12cm/min)
(b) Weld No. 1-1(30V,400A,40cm/min)
(c) Weld No. 6B (24V,200A,40cm/min)
(d) Weld No. 26 (32V,300A,40cm/min)
(e) Weld No. 21 (20V,400A,40cm/min)

(ℓ/a), (w/a) and (W_S/W_M) are highly correlated as is evident from the photographs of different welds in Figure 24 and which may be further seen from Appendix A.7.

5.4.1. Effect of Welding Consumables on ($A_{s/m}/V_m$)

The composition of the electrode and baseplate have little influence on ($A_{s/m}/V_m$). Flux composition however, has a strong influence on the viscosity of the slag at temperatures below 1600°C (see Figures 25a, b and c). Since the viscosity of the cooler outer slag layer (not in direct contact with the arc or the pool region beneath the arc) affects weld pool shape, flux composition may play a significant role in determining $A_{s/m}/V_m$. An example of this is shown later in section 6.2.2 while considering Belton's data on the transfer of silicon [11].

5.4.2. Effect of Welding Parameters on $A_{s/m}/V_m$

The effect of the welding parameters current, voltage and travel speed on weld metal geometry and consequently on $A_{s/m}/V_m$ is shown in Figure 26. It shows that on increasing current the volume of the weld pool increases, thus lowering the value of $A_{s/m}/V_m$. However, on increasing voltage, the weld becomes more wider and shallower so the ratio ($A_{s/m}/V_m$) increases. An increase in travel speed decreases both $A_{s/m}$ and V_m, consequently it has little effect on ($A_{s/m}/V_m$). It is interesting to compare the effect of the welding parameters on weld geometry to the effect of these parameters on weld metal composition. Figure 27 shows the effect of changes in current, voltage and travel speed on the amount of alloying element

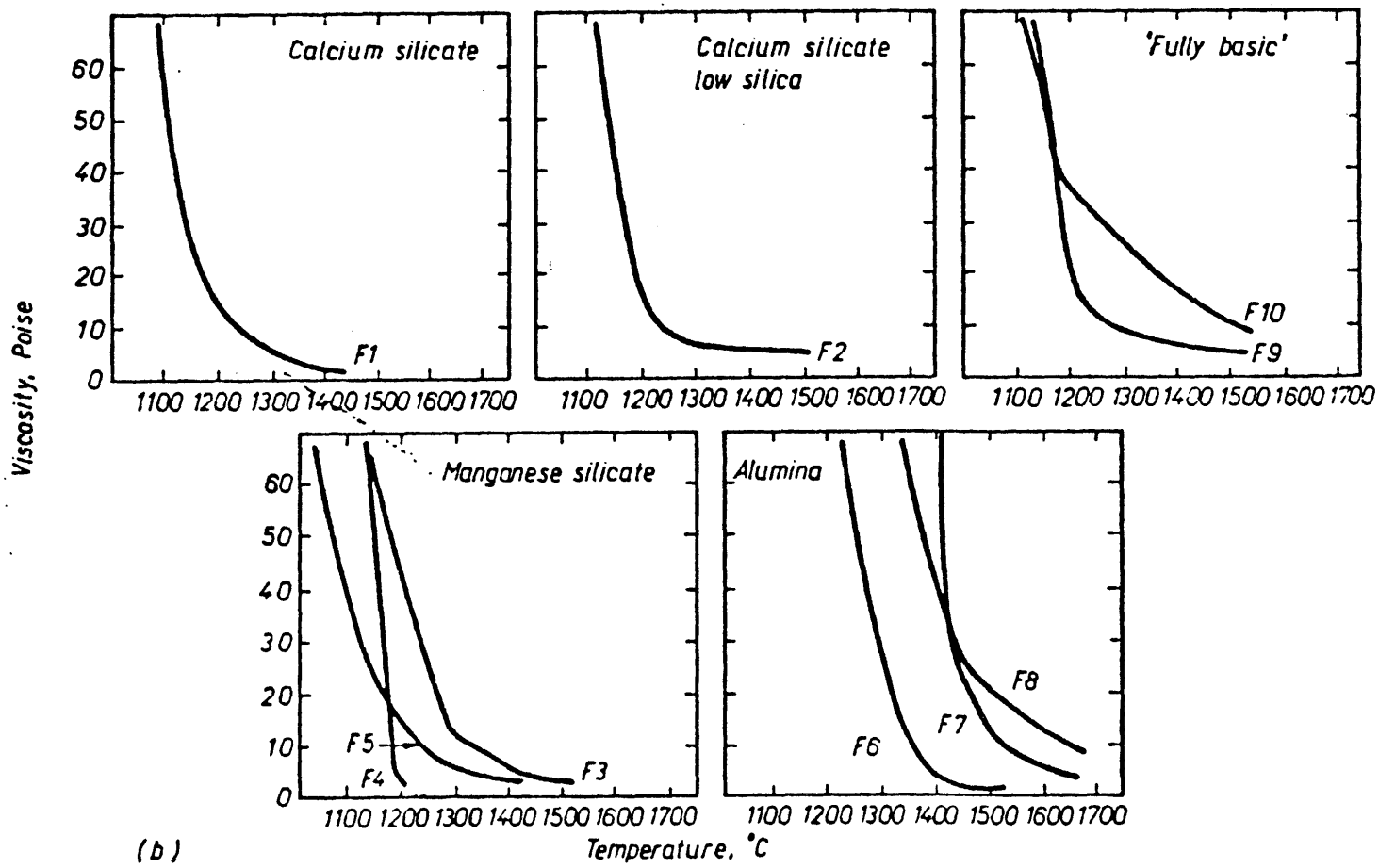

Fig.25(a).: Effect of Temperature on the viscosities of welding slags.[22]

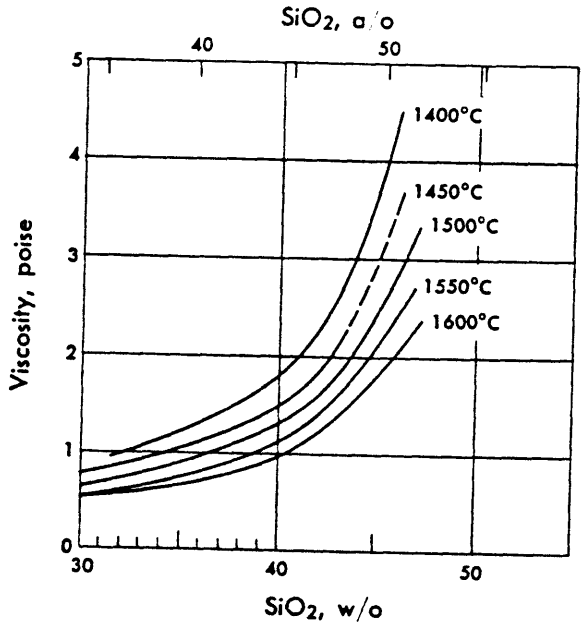

Fig 25(b): Viscosity of $MnO-SiO_2$ slags.[43]

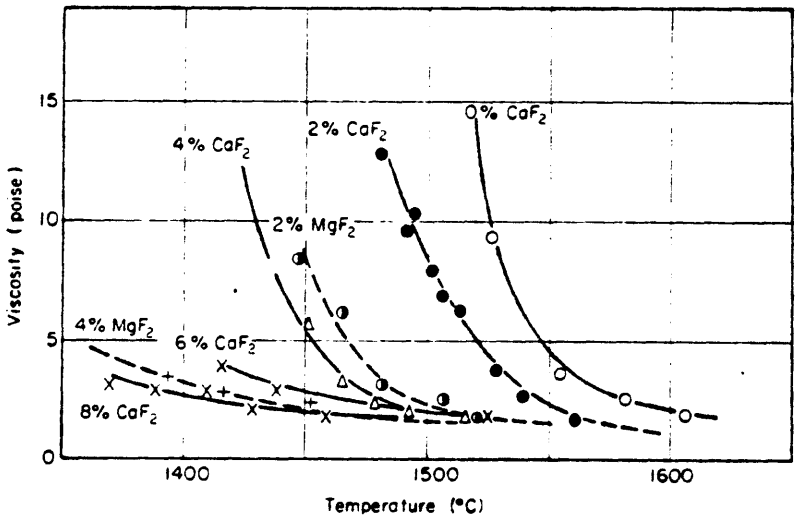

Fig 25(c): Effect of fluoride additions on the viscosity of a $CaO-SiO_2-Al_2O_3-MgO$ slag.[41]

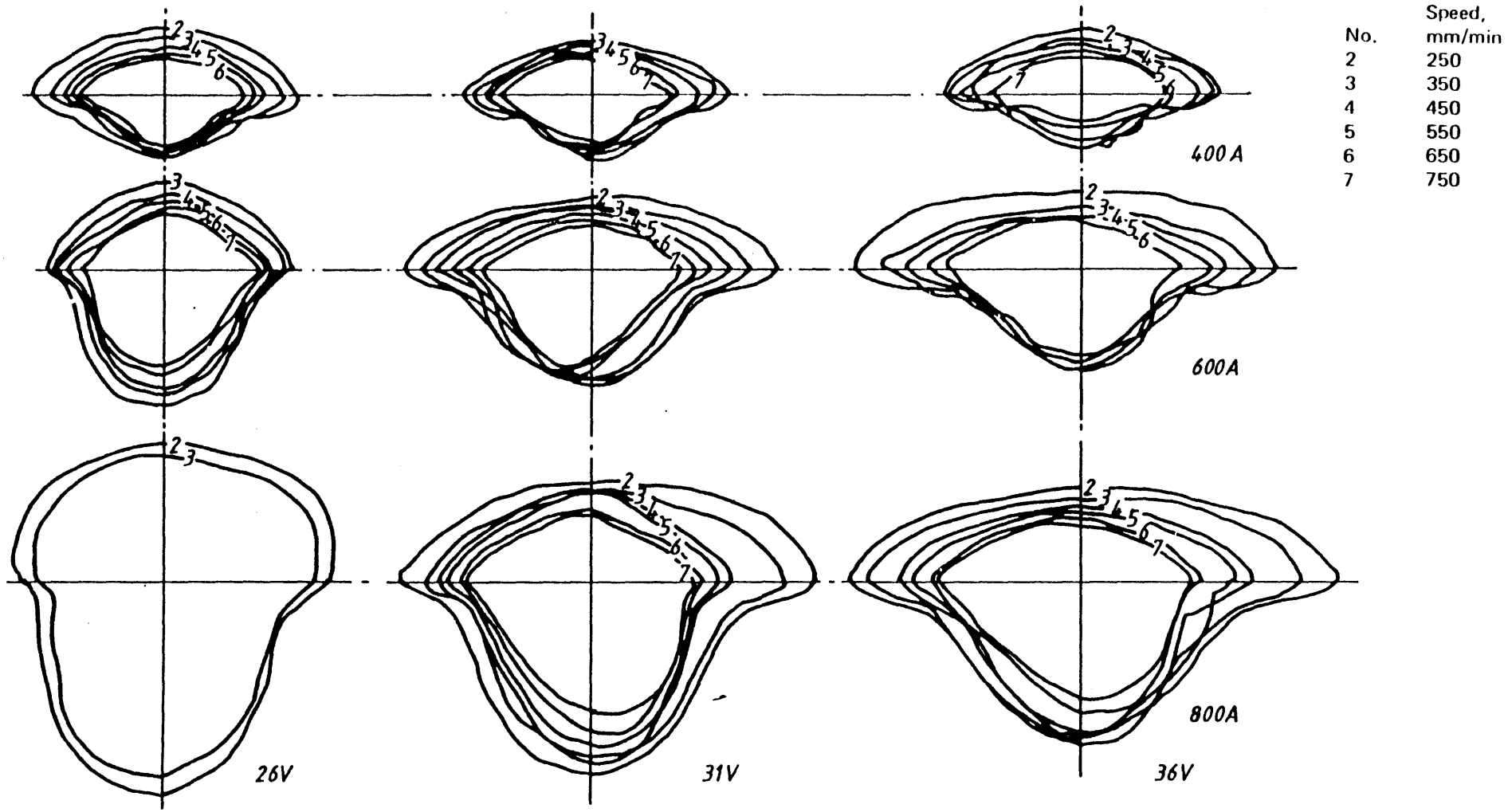

Fig.26: Effect of welding parameters on weld metal geometry. [56]

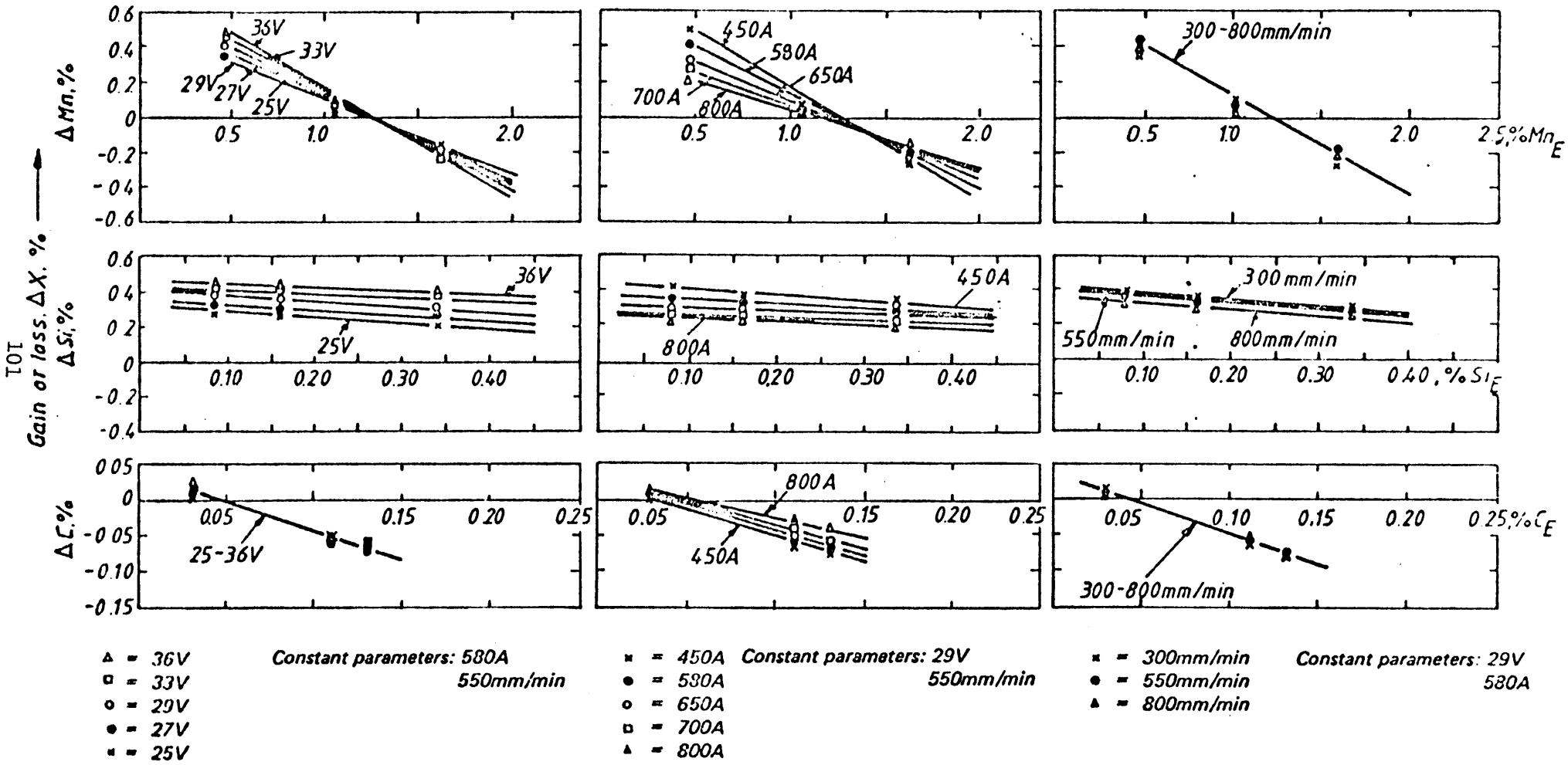

Figure 27 : Influence of (a) voltage, (b) current and (c) welding speed, on reactions of Mn, Si, and C for multipass welding with flux LW280 [from ref. 34].

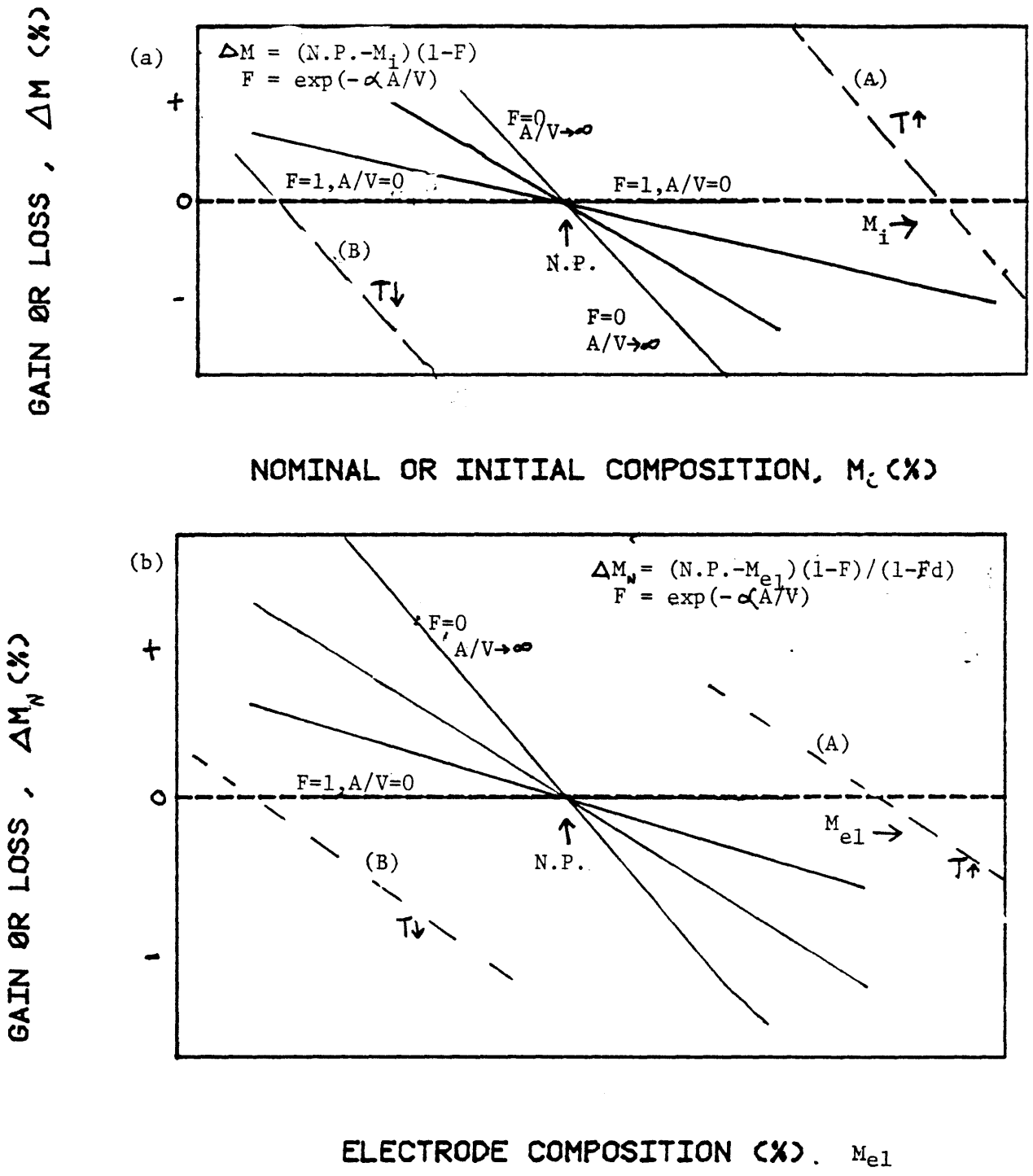

Figure 28: Schematic figure illustrating the transfer of alloying elements on welding with fluxes free of ferro alloys in (a) single pass welds, (b) multipass welds.

transferred between slag and metal in multipass welding [34]. It was stated earlier in Chapter 4, that the amount of alloying element transferred during multipass welding may be given by

$$M_N = (NP - M_{e\ell})\left(\frac{1 - F}{1 - Fd}\right) \tag{37}$$

where

$$F = \exp(-\alpha A_{s/m}/V_m) \tag{38}$$

Figure 27 shows that at the neutral point there is little effect of welding parameters on the amount of alloying element transferred. It also shows that the larger the deviation from the neutral point, or the greater the thermodynamic driving force $(N.P. - M_{e\ell})$,† the greater the amount of alloying element transferred in accordance with equation (38). If the alloy content of the electrode $M_{e\ell}$ is lower than the neutral point (N.P.) then the alloying element is transferred from the slag to the metal, if it is greater, then the metal loses the alloying element to the slag. Figure 27 shows that an increase in voltage increases the amount of alloying element transferred but an increase in current has the opposite effect. Changes in welding speed however have little effect on the amount of alloying element transferred. Comparison of Figure 25 with Figure 27 shows that the effect of welding parameters on the parameter $(A_{s/m}/V_m)$ and on the amount of alloying element transferred ΔM_N, is similar. Thus, an increase in voltage increases both $(A_{s/m}/V_m)$ and $|\Delta M_N|$, an increase in current decreases $(A_{s/m}/V_m)$ and $|\Delta M_N|$, but a change in welding speed has little effect on both $(A_{s/m}/V_m)$ and ΔM_N.

The effect of $(A_{s/m}/V_m)$ on the amount of alloying element transferred in single pass and multipass welding is schematically represented

†Note this is the thermodynamic driving force in multipass welding. In single pass it is $(N.P. - M_i)$.

by Figures 28(a) and (b), respectively. (Compare with Figure 27.) The effect of changes in temperature on the amount of alloying element transferred is also shown schematically in Figures 28(a) and (b). For example, if a change in the welding parameters produces an increase in the temperature then the amount of alloying element transferred at this higher temperature would be represented by the dashed line (A). (At higher temperatures, the oxides are unstable and so more alloying element would be transferred from the metal to the slag.) However if a change in the welding parameters decreases the temperature then the amount of alloying element transferred will be represented by line (B). (See Figure 9.) Either way there would not be a singular neutral point and this would contradict the results of Chai [17,25] and the experimental data of Thier [34] (Figure 27) and others [10,18,31,32].

The similar effect of the welding parameters on $(A_{s/m}/V_m)$ and on weld metal chemistry may also be established by examining North's data [18] (see Appendix B.5). North made multipass welds using electrodes containing 1.85 - 1.93%Mn and a calcium silicate silicate flux (65%SiO_2 - 35%CaO) using different combinations of welding parameters. Figure 29 shows the effect of the welding parameters current, voltage and travel speed on the slag to metal ratio W_S/W_M (which is a measure of $A_{s/m}/V_m$). Figure 30 shows the effect of these parameters on the weld metal composition. Comparison of the two figures again clearly illustrates the similarities between the effect of welding parameters on $(A_{s/m}/V_m)$ and on weld metal chemistry. It should be noted that in the flux used by North, Mn was transferred from this metal to the slag. Thus, as current is increased $(A_{s/m}/V_m)$ decreases, so the amount of manganese lost to the slag decreases and the manganese content

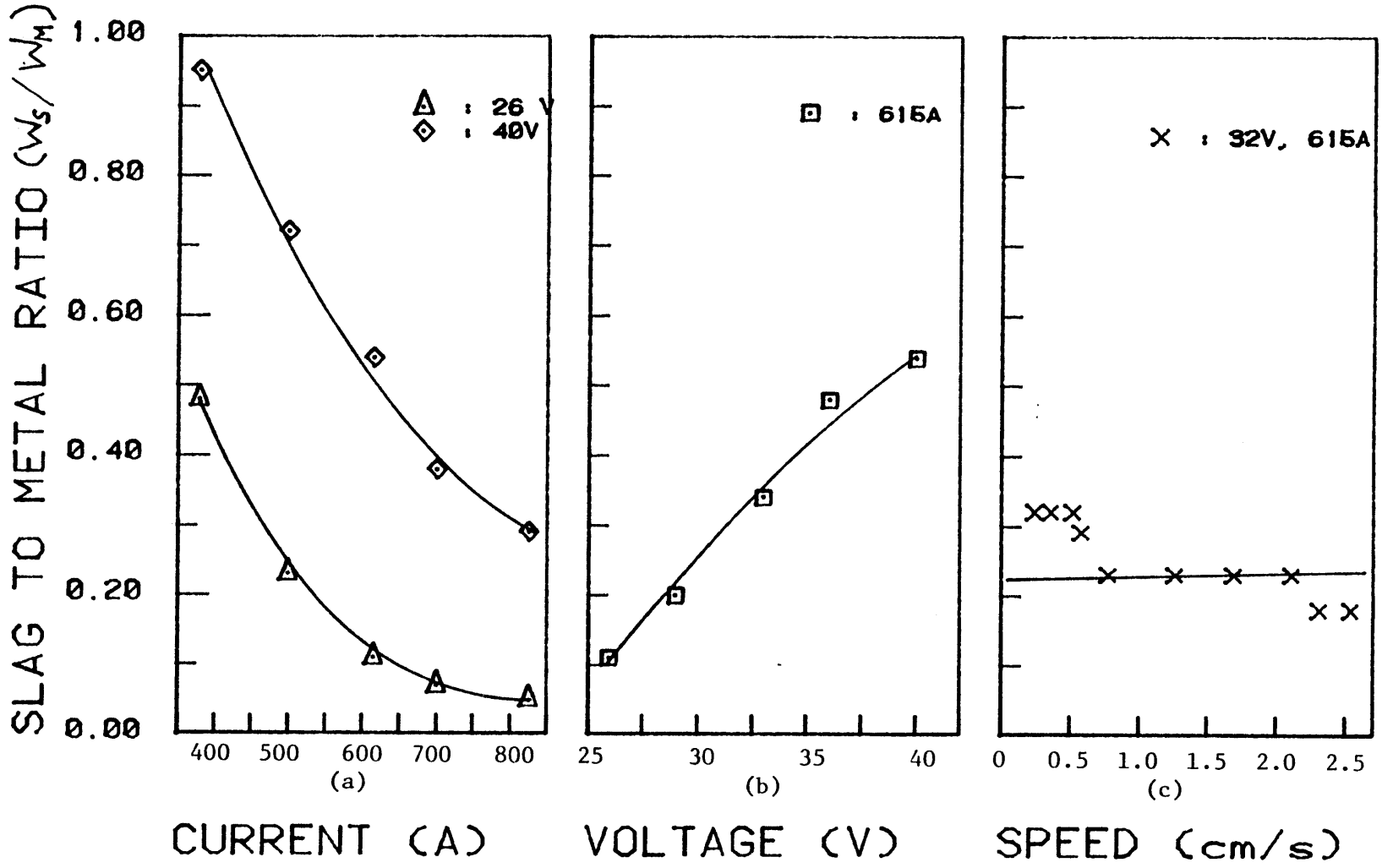

Fig.29: Effect of welding parameters on the ratio of slag weight to metal weight (W_S/W_M). Data from work by North [18].

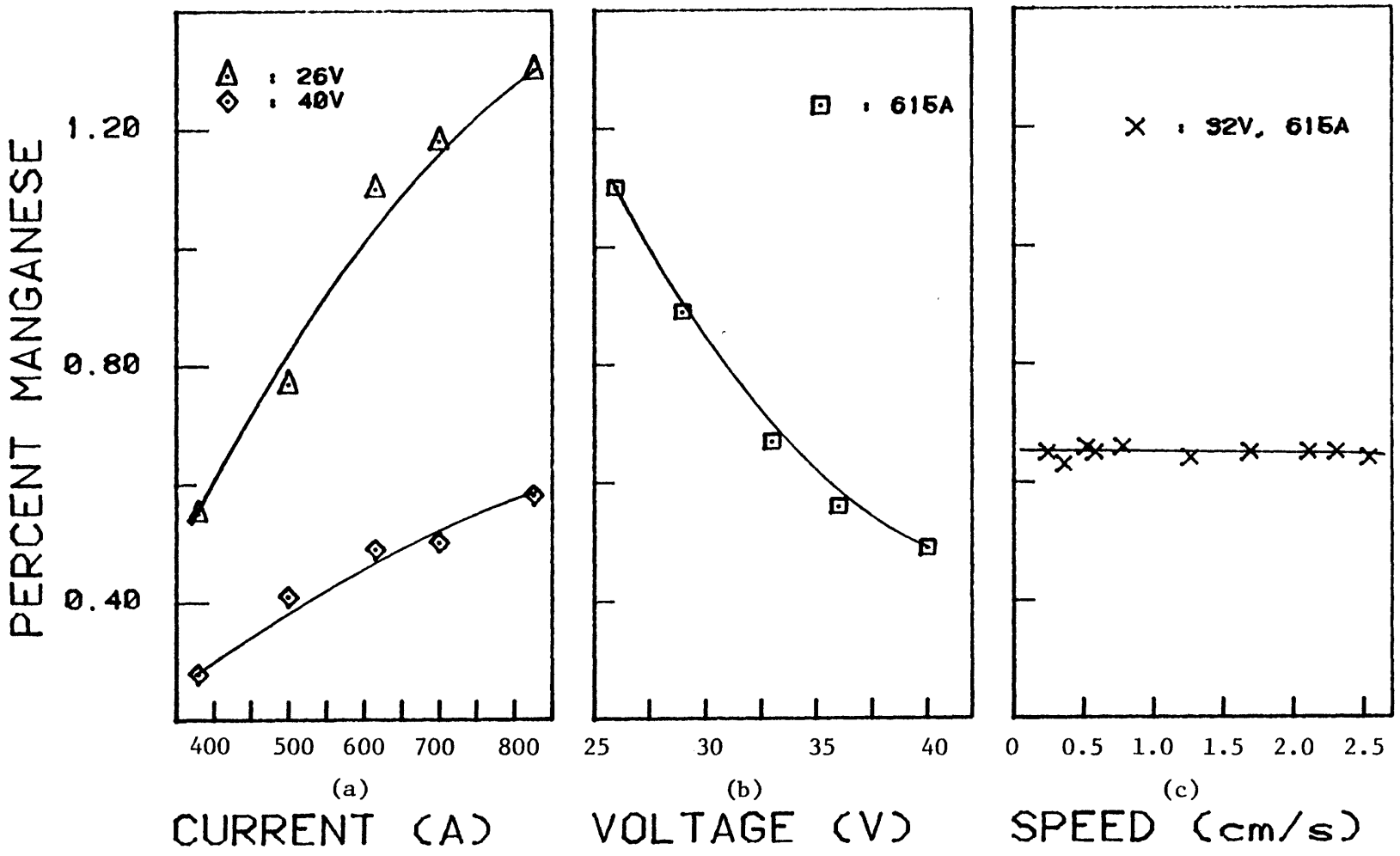

Fig.30: Effect of welding parameters on the manganese content of weld metal. Data are from work by North.[18] (Multipass welds made with 1.9%Mn electodes and 65%SiO_2-35%CaO flux.)

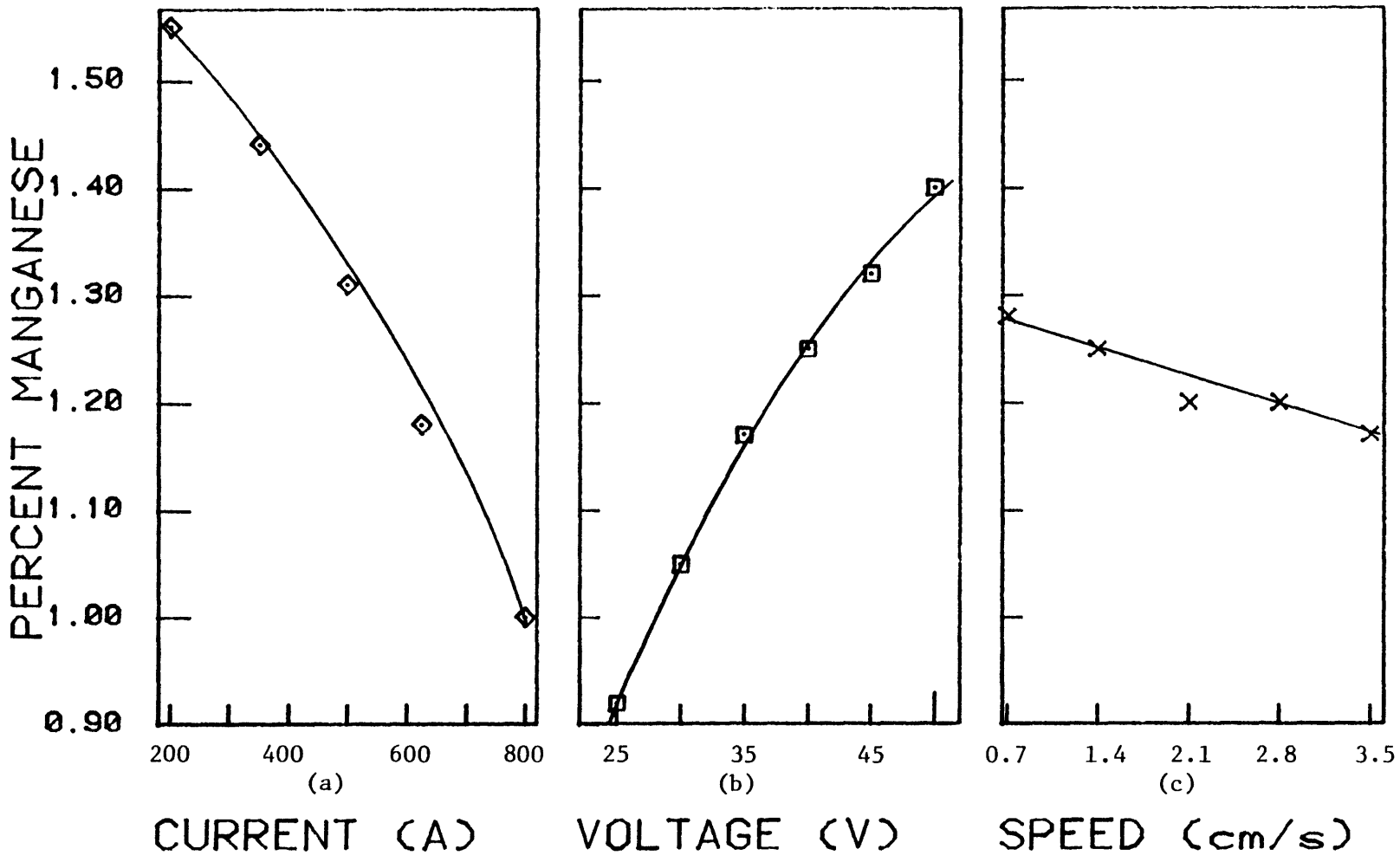

Fig. 31: Effect of welding parameters on the manganese content of weld metal. Data are from work by Potapov [31]. (Multipass welds made with 0.65%Mn electrode and a manganese silicate flux.)
(a): V=36V,v=2.1cm/s; (b) I=600A,v=2.1cm/s; (c) V=36V,I=600A.

of the weld metal increases. An increase in voltage produces the opposite effect since a voltage increase broadens the arc and increases ($A_{s/m}/V_m$). Changes in welding speed however have little effect on $A_{s/m}/V_m$ and consequently on metal chemistry. North's data also indicate that variations in current at a high voltage (40 V) produces a much smaller change in metal chemistry as compared to the effect of current at lower voltage (26 V). (See Figure 30(a)). This is not surprising if the exponential relationship between $A_{s/m}$ and ΔM_N is considered (equations (37) and (38)) since the values of W_S/W_M (and consequently $A_{s/m}/V_m$) are smaller at low voltages. (See Figures 29 and 30(a)). In contrast to North who found that an increase in current or decrease in voltage increases weld metal manganese Potapov [31] found that an increase in current or decrease in voltage decreases the manganese content of the metal (Figure 31). This result is not surprising considering that Potopov used a silicate flux so manganese was transferred from the slag to the metal whereas North used a calcium silicate flux so manganese was transferred from the metal to the slag. The influence of the different welding parameters on ($A_{s/m}/V_m$) and consequently on the extent of alloy transfer in both cases is similár. (Compare Figures 29, 30 and 31.) In addition to the examples given above several more may be presented by using data recorded by other researchers [10,11,29-33] or from the results of the preliminary experiments in the present investigation (see Figures 13-15). However, this section is only intended to make the reader familiar with some of the basic concepts. Later, in Chapter 6, quantitative verification of the theory is presented by performing different experiments where the welding parameters are fixed and $A_{s/m}/V_m$ is varied independently, and also by using the experimental data of several different investigators.

It should be noted that the values of W_S/W_M or w/a may be directly estimated from the values of the welding parameters by using empirical relationships presented by Jackson [58] or Christensen [10]. (Figs. 32 and 33 are examples). The values of W_S/W_M for hundreds of different welding conditions have also been recorded by different researchers [10,16-18,29]. However values of W_S/W_M which are estimated by interpolation of data recorded by these researchers [10,16-18,29], or values estimated from the empirical relationships [10,58] may not be accurate. For precise estimates it is best to make a small weld on a piece of scrap steel and measure w/a or W_S/W_M. This procedure takes only a few minutes and is considerably simpler than the 'tests' currently used for comparing weld metal composition (Appendix A.13 gives an example). In Chapter 6, where the theory is verified by performing different experiments the values W_S/W_M and w/a were those obtained by measurement. Also only the data of those researchers who have recorded the values of W_S/W_M or w/a are used for quantitative verification of the theory in order to minimize error. The data of all other researchers nonetheless been shown to be atleast qualitatively consistent with the new theory.

5.5 Estimation of Alpha (α)

The equations formulated from the kinetic model involve a kinetic factor α, the value of which depends on the values of the mass transfer coefficients (k_m,k_s), the chemical reaction rate constant (k_2) and the partition coefficient m.

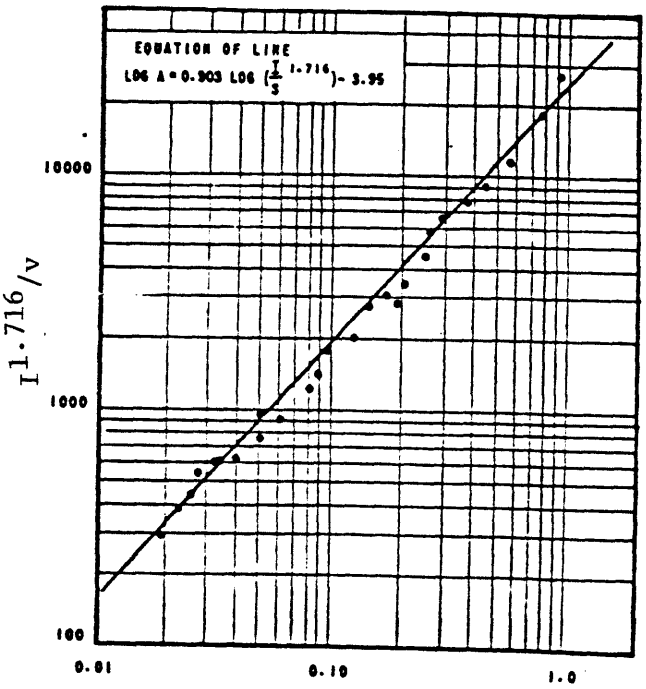

Fig. 32: Effect of current(I) and speed of travel (v) on weld metal cross sectional area.[58]

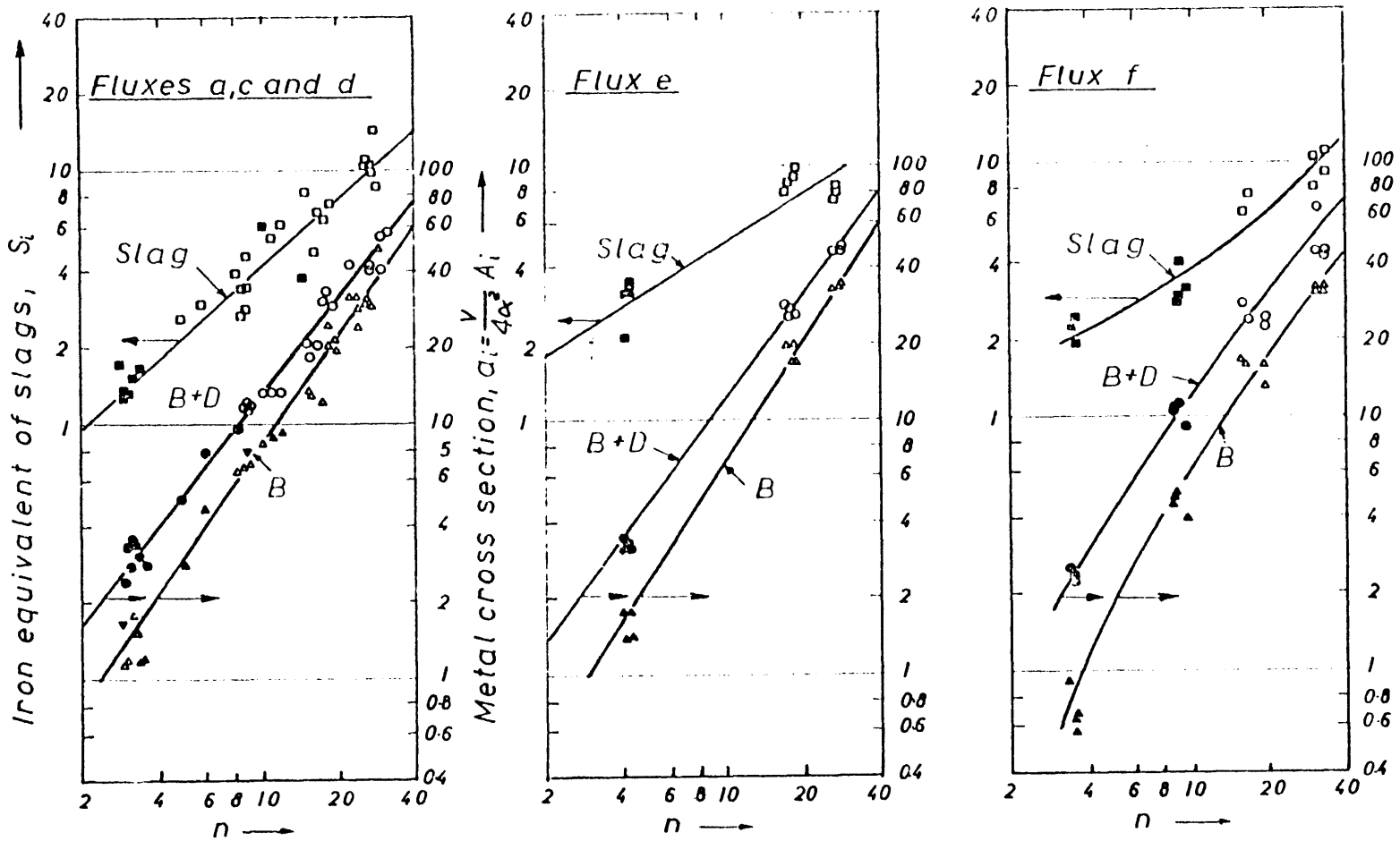

Fig.33: Dimensionless metal and slag cross sections.[10] n:operating parameter(n=.059VIv)

$$\alpha = \int_{o}^{t} \frac{1}{k_m} + \frac{m}{k_s} + \frac{1}{k_2} \, dt \qquad (32)$$

It is not possible to compute the individual mass transfer coefficients or the chemical reaction rate constant or α from first principles since adequate information is not available on the transport processes occurring in the weld pool region inside the arc. Thus, α may be regarded as a 'lumped' or 'grouped' parameter used to characterize the system. (The use of such parameters for studying metallurgical systems at high temperatures was first suggested by Richardson in 1962. [59]). It should be noted that the transport processes occurring inside the weld pool are extremely complex due to the turbulent nature of the pool and due to the simultaneous transfer of mass, heat and momentum between the slag and metal phases. Though these complex phenomena prevent the computation of the individual phase resistances ($1/k_m$ m/k_s and $1/k_2$ it is worthwhile to briefly examine the transport processes occuring in the weld pool. Fluid flow inside the metal pool has been studied by several researchers [60 - 64] . However, there is no universal agreement among these researchers on the nature of the flow or the mechanism responsible for it. Fluid flow may be controlled by four mechanisms: drag on the pool surface due to impingement by the arc plasma, density variations due to thermal gradients, variation in surface tension, and by Lorentz forces. Of these the first two have been shown to have a negligible effect as compared to the others [73,74]. There has been some controversy over whether surface tension variations or Lorentz forces control fluid flow [61-64] but recent work by Oreper,

Eagar and Szekely [65,66] has shown that variation in surface tension is the dominant mechanism. These researchers have also estimated the velocity of the metal in the pool to be of the order of one meter per second. Unlike fluid flow in the metal, the fluid flow in the slag has not been studied. However, since only a small amount of current passes through the slag during arc welding, Lorentz forces will not be a dominant mechanism in the slag. Also, since the slag is more viscous and the variation of surface tension with temperature $(\frac{d\sigma}{dT})$ is lower in slags as compared to the metal [43], fluid flow in the slag, at least near the slag metal interface is likely to be controlled by momentum transfer from the metal.

The value of the Reynolds number and Schmidt number for the slag and metal phases may be estimated by using the velocity (v) estimated by Oreper [78,79] and values of the materal properties of metal and slag recorded in literature [41,43,67].

In the metal

$$Re = \frac{\rho v d}{\mu} = \frac{7.8\ gcm^{-3} \times 100\ cms^{-1} \times 1\ cm}{4 \times 10^{-2}\ gcm^{-1}s^{-1}} \simeq 20000$$

$$Sc = \frac{\mu}{\rho D} = \frac{4 \times 10^{-2} gcm^{-1}s^{-1}}{7.8\ gcm^{-3} \times 10^{-4}\ cm^{2}s^{-1}} \simeq 50$$

In the slag

$$Re = \frac{\rho v d}{\mu} = \frac{3.3\ gcm^{-3} \times 100\ cms^{-1} \times 1\ cm}{1\ gcm^{-1}s^{-1}} = 330$$

$$Sc = \frac{\mu}{\rho D} = \frac{1\ gcm^{-1}s^{1}}{3.3\ gcm^{-3} \times 10^{-6} cm^{2}s^{-1}} = 300000$$

Researchers have shown that at high values of Reynolds numbers and Schmidt number the laminar sublayer in the boundary layer region becomes extremely thin, and the velocity profile in this sublayer becomes independent of the Reynolds number [68,69]. Thus changes in bulk fluid flow brought about by changes in welding parameters[†] should not significantly affect the mass transfer coefficient.

At this point it is again useful to examine the parameter α. The fact that it cannot be estimated from first principles due to the complexity of the process does not make it an empirical constant used to correlate experimental data with theory.[††] This is illustrated by applying equations (37) and (38) to the experimental data recorded by North and allowing α to vary by two orders of magnitude from 0.1 to 10.0 (Here α is dimensionless since the dimensionless parameter W_S/W_M was used as a measure of $A_{s/m}/V_m$). Table 16 shows clearly that the values of the linear correlation coefficient between theory and experiment is hardly affected by α. The results shown graphically in Figure 34 indicates that changes in the value of α may lead to deviations from the actual value but the trend remains the same.[†††]

It should be noted that while the rate controlling step (transport in metal phase, transport in slag phase or chemical kinetics) may not be determined from the little information available on the transport and

---

[†]According to the analysis by Oreper et al [65] changes in the welding parameters should not change flow velocity by more than an order of magnitude.

[††]Wei has presented an interesting discussion on the use of constants for correlating data [70].

[†††]At α = 1.7 there is minimum deviation and the line goes through the origin.

Table 16: Effect of the value of α on the linear correlation between theory and experiment. (Experimental data is from work by North [18]).

Value of Alpha (α)	0.1	0.5	1.0	2.0	3.0	5.0	10.0
No. of data points†	23	23	23	23	23	23	23
Linear Correlation Coefficient	0.92	0.93	0.94	0.96	0.96	0.95	0.91

†Each data point corresponds to a different combination of welding parameters. The consumables used were the same.

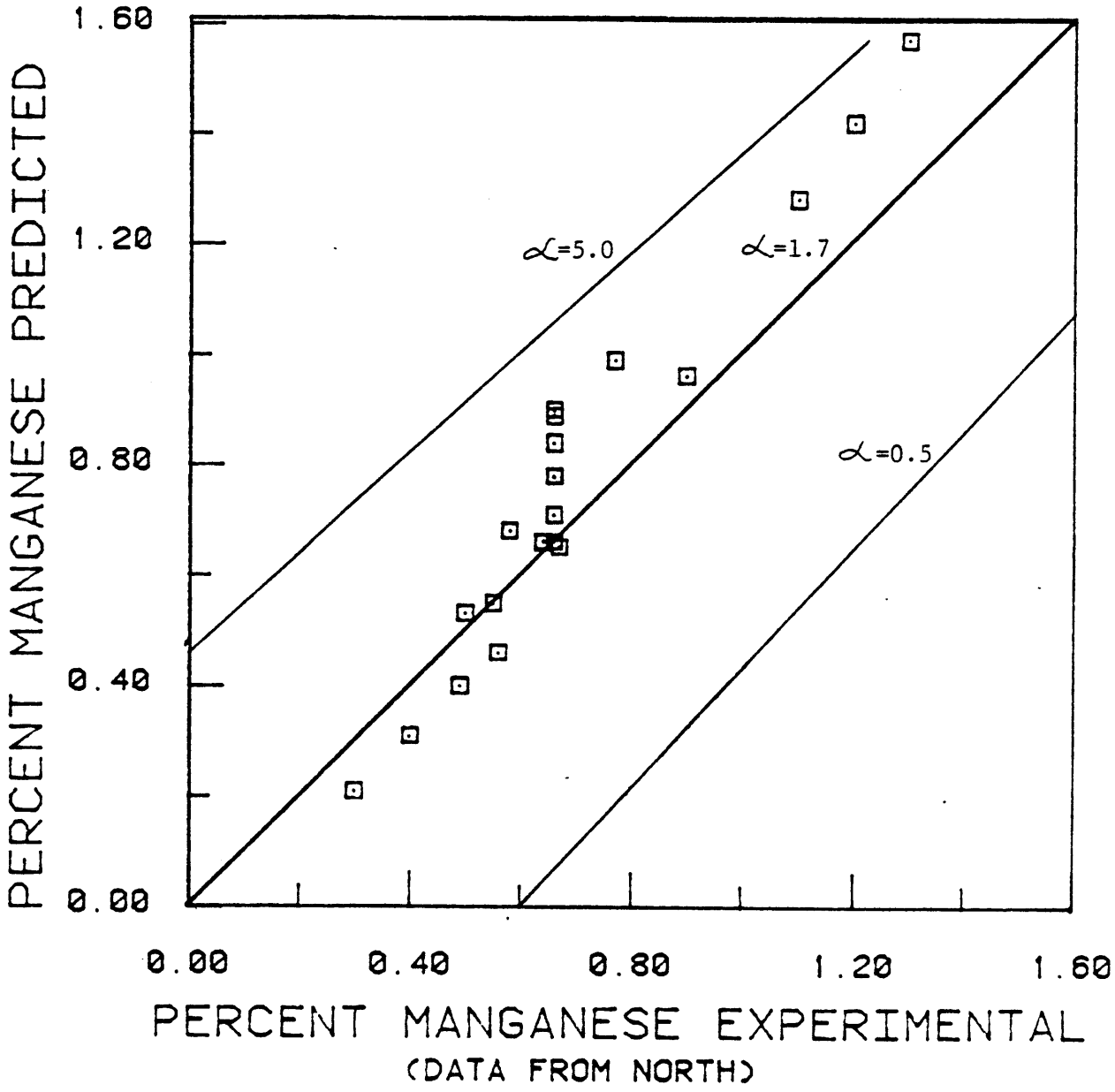

Fig 34: Effect of the value of α on the relationship between theoretical predictions and experimental results. Only data points corresponding to α=1.7 shown.

kinetic mechanisms occuring inside the weld pool, application of the theory to experimental data may provide some valuable information about the rate controlling process. The value of α depends not only on the mass transfer coefficients, k_m,k_s and the chemical reaction rate constant k_2, but also on the partition coefficient m.

The value of m is given by equation (15)

$$m = \frac{[N.P.]}{(a_{MO_x})flux} = \frac{1}{K[a_o]^x} \qquad (15)$$

that is m depends on the value of the equilibrium constant 'K' of the reaction being considered, as well as on the initial oxygen content of the pool. As oxygen content in the weld pool increases, the value of m, the partition coefficient, decreases. Thus, the value of m for highly oxidizing fluxes, such as the acid silicate fluxes, should be lower than for the less oxidizing fluxes such as the basic silicate or the fluoride-alumina based fluxes. Since

$$\alpha = \int_o^t \frac{dt}{\frac{1}{k_m} + \frac{m}{k_s} + \frac{1}{k_2}}$$

if the transfer of an alloying element is controlled in the slag phase, then a significant difference should be observed in the rate at which the alloying element is transferred between the slag and the metal when using highly oxidizing fluxes as compared to less oxidizing fluxes. Furthermore, this should apply whether the alloying element is being transferred from the slag to the metal or the reverse. Examination of data available in literature shows this is indeed the case [10,17,29]. For example, Christensen [10] reported that a change in welding

parameters had a very small effect on the manganese content in basic fluxes, but a much larger effect on acid fluxes (see Figure 6). This point is further illustrated if the catalogs of the leading flux-manufacturers are examined [71,72]. The less oxidizing fluxes are often termed 'neutral' or 'passive' fluxes and in the product description the manufacturers claim that a change in welding variables only has a small effect on metal composition when welding with these fluxes. The acid fluxes are often called 'active' fluxes and in the manufacturer's description the user is informed that large changes in chemical composition of weld metal may be observed, depending on the welding conditions used. The suggestion that transport in the slag phase becomes rate controlling, at least when welding with the less oxidizing fluxes (high 'm'), should not be very surprising considering that at the high temperatures in the weld pool, chemical kinetics is unlikely to be the rate controlling step, and the high values of m in these fluxes should make the term (k_s/m) much smaller than either the metal mass transfer coefficient k_m or the chemical reaction rate constant, k_2.

The value of α may be obtained by applying equations (33) and (38) to experimental data. Table 15 lists the values of α obtained for different fluxes and elements. (More is said about this in Chapter 6.) For the transfer of manganese on welding with highly oxidizing fluxes, α = 1.7 or 0.2 cm depending on whether the ratio (W_S/W_M) or (w/a) is used as a measure of ($A_{s/m}/V_m$). For less oxidizing fluxes, α drops to a third of its value for oxidizing fluxes that is to .067 cm. If the time for the weld pool reactions is of the order of a second, then the overall mass transfer coefficient for highly oxidizing fluxes is 0.2 cm/s and

for the less oxidizing fluxes it is 0.067 cm/s. Kawai et al [73] obtained a overall mass transfer coefficient of about 0.010 cm/s for the transfer of manganese between metal and slag at 1600°C (which is considerably lower than the weld pool temperature) and with the oxygen content of the metal comparable to that obtained on welding with the less oxidizing fluxes. Sherwood and Wei [74] have shown that large scale convection resulting from surface tension driven flows may make the value of the overall mass transfer coefficient several times greater than the value of the mass transfer coefficients when no convection is present. This has been confirmed by the work of others [75]. Thus the value of 0.067 cm/s seems reasonable in view of the higher temperature and the rapid convection in the weld pool. Examination of the spatial distribution of rapidly solidified slags obtained by Chai [17] (Figure 35) indicates values of the overall mass transfer coefficient between 0.032-0.090 cm/s for less oxidizing fluxes. The value of the overall mass transfer coefficient was estimated from values of the mass flux (J) recorded by Chai and is shown in Table 17. Appendix A-9 gives an example of the calculations. It should be noted though that the mass flux (J) obtained by Chai was probably the instantaneous flux just before the metal was quenched. Consequently the values obtained for the overall mass transfer coefficients are not necessarily the average values.

5.5.1 Effect of Welding Consumables on α

The value of the mass transfer coefficients k_m and k_s depends on the density and viscosity of the slag and metal phases [41]. The density of

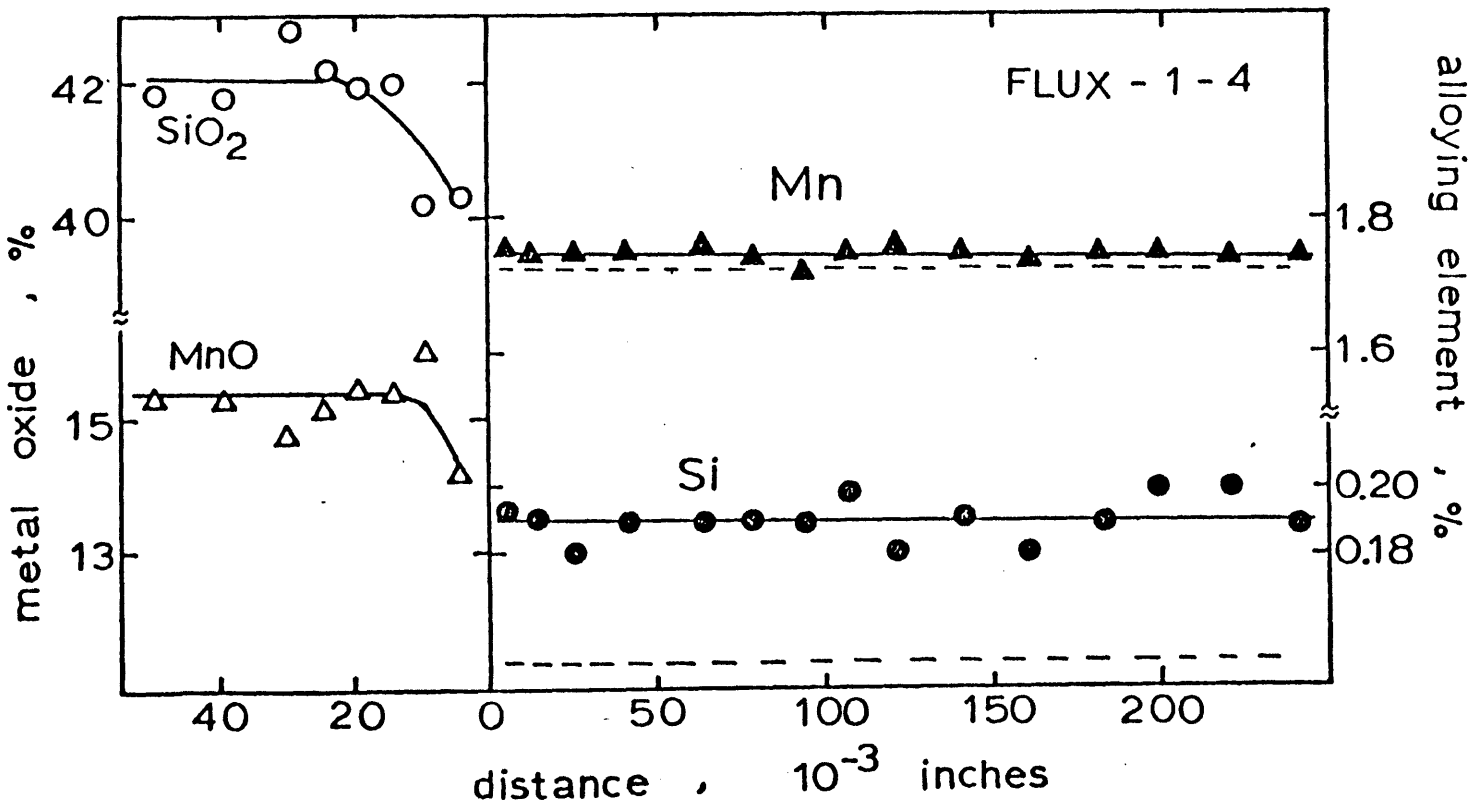

Figure 35: Spatial distribution of manganese and silicon in rapidly cooled weld metal and slag (from ref. 17).

Table 17: Estimation of Overall Mass Transfer Coefficients of Manganese for Low Oxidizing Fluxes as Estimated from the Spatial Distribution Data of Chai [17]. Flux F-1 Used for All Welds. Welds were Rapidly Quenched in a Water Cooled Copper Mold.

Weld No.	Metal J^*(cm%/s)	Phase ΔC(%)	Slag J^*(cm%/s)	Phase ΔC(%)	k_m	m/k_s	$k_{overall} = \frac{1}{\frac{1}{k_m} + \frac{m}{k_s}}$
1-1	-	-	9×10^{-3}	0.77	-	.042	.042
1-2	2.44×10^{-2}	0.35	2.6×10^{-2}	1.54	.070	.060	.032
1-4	-	-	2.2×10^{-2}	1.93	-	.040	.040
1-5	1.76×10^{-2}	0.28	-	-	.063	-	.063
1-11	-	-	2.2×10^{-2}	0.92	-	.09	.090

*These are twice the values recorded by Chai [17]. Chai assumed a reaction time of two seconds in contrast to the assumption of 1 second in the present investigation, for estimating overall mass transfer coefficients.

slag is approximately 3.3 g/cm^3 at 1600^{o}C and there is no significant difference between the densities of different welding slags [41,68]. The density of steel is about 7.8 g/cm^3 at 1600^{o}C. There is little information available on the densities of slag and metal phases at higher temperatures, but both slag and metal densities decrease with increasing temperature [67]. However, as a change in the welding consumables has little effect on metal and slag densities, the effect of density variations, due to changes in welding consumables, on the value of α may be neglected.

Figures 25(a), (b) and (c) shows the effect of flux compositon on viscosity. Although the viscosity of welding slags may vary greatly at lower temperatures, the effect of flux composition on viscosity diminishes rapidly with increasing temperature (see Figures 25(a), (b), and (c)). The viscosity of welding slags at 2000^{o}C is about 1 poise whereas that of liquid steel is about 4 centipoise [43]. At the high temperature at which slag-metal reactions occur inside the pool (around 2000^{o}C) viscosity is unlikely to be affected significantly by the choice of welding consumables. Thus the effect of welding consumables on the value of the mass transfer coefficients is not important.

As mentioned earlier, the value of α depends not only on the value of the mass transfer coefficients k_m,k_s, and the chemical reaction rate constant k_2 but also on the partition coefficient m. The value of m depends on the oxidizing potential of the flux. Thus the main effect of welding consumables on the value of α is due to the effect of flux composition on the partition coefficient.

5.5.2. Effect of Welding Parameters on α

The effect of welding parameters on the values of α may be best illustrated by examining Table 16 and Figure 34. Table 16 clearly shows that the correlation between theory and experiment is independent of the value of α chosen. It should also be noted that the results of Table 16 and Figure 34 are based on 23 data points, each point representing a weld made using the same consumables but different welding parameters. Since the value of α is constant for each set of 23 data points it is clearly not affected by the welding parameters. Furthermore, earlier in Section 5.4.2 the effect of the independent welding parameters, current, voltage and travel speed on weld metal chemistry was presented. These effects certainly cannot be explained by any variations in α due to changes in the fluid flow. Researchers [68,69] have shown that the laminar sublayer in the boundary region which controls mass transfer is extremely thin for systems having high Reynolds or Schmidt numbers (such as the metal and slag in the weld pool), and the velocity profile in this sublayer is independent of the Reynolds number. Other researchers have shown that the Marangoni number (which controls the surface tension driven flows) in the weld pool is of the order of 10^5. Changes in welding parameters have little effect on the order of magnitude of this number and consequently do not have a very significant effect (an order of magnitude effect) on flow velocities [65,66]. The fact that a change in the welding parameters has little effect on α should not be therefore very surprising. The effect of welding parameters on the value of α is not important, at least in comparison with the effect of these parameters on $A_{s/m}/V_m$ (shown in Section 5.4.2).

CHAPTER 6

VERIFICATION AND APPLICATION

In Chapter Four, a new theory was presented to explain the changes that occur in weld metal chemistry during the submerged arc welding process. Verification of this new theory is presented in this chapter by describing different experiments. Also the theory is tested with the numerous data available from work done by previous researchers. This chapter is split into four main sections. The first section deals with the transfer of oxygen which is controlled mainly by plasma metal reactions in the zone of droplet reactions and by deoxidation reactions inside the molten pool in the zone of cooling and solidifying weld pool. In the second section, the transfer of other alloying elements is discussed and the quantitative kinetic model formulated in the previous chapter is verified. The third section contains a brief discussion on the application of the new theory for flux classification and development. In the last section some suggestions for further work has been made.

5.1. Transfer of Oxygen

5.1.1. Transfer in the Zone of Droplet Reactions

The weld metal gains oxygen mainly in this zone. It has been suggested that this is mainly due to decomposition of the oxide constituent of the slag into suboxides or vapour and oxygen and the subsequent reaction of this oxygen with the metal droplets [26,27].

The experimental results of Lau [28] (see Figure 10) who collected the droplets both at the electrode tip and after flight through the arc, the results of Chai and Eagar (see Figure 12) [27] and the results presented in Table 14 and Appendix A.3 support this mechanism. However, at the present stage, it is still not possible to obtain precise quantitative estimates of the amount of oxygen transferred due to the complexity of the possible reactions inside the arc. (Welding slags usually contain several different oxides which may decompose to several other suboxides or vapour and oxygen inside the arc cavity. Furthermore, some of these oxides or suboxides may react with each other.) Eagar's basicity index gives a rough guideline for estimating the amount of weld metal oxygen for silicate fluxes [7], but for alumina or fluoride based fluxes a qualitative analysis of the stability of the oxide constituents may be more suitable [28]. However, much more work needs to be done in this area before any scientific model may be formulated. The possibility of using levitation melting data or techniques, and the possible application of results of kinetic studies in plasma and electric arc furnaces to the arc welding process should also be examined.

Some researchers [76,77] have suggested that additions of calcium fluoride to the flux reduces the weld metal oxygen content by reducing the partial pressure of oxygen inside the arc cavity by generating 'fluoric gases' such as SiF_4 by reactions such as

$$2\ CaF_2 + SiO_2 = 2\ CaO + SiF_4(g) \qquad (42)$$

Eagar [27] however has suggested that CaF_2 acts only as a dilutant in the slag thereby lowering oxygen content. Recent work by Kuzmenko [78] also shows that there is negligible interaction between CaF_2 and SiO_2 and these reachers have claimed that "CaF_2 in fluxes has no very useful effect." [78]

In the present study, an attempt was made to resolve this controversy by using anhydrous iron (II) fluoride (FeF_2) additions to the flux. FeF_2 is less stable than CaF_2 and should also have less effect on the activity of SiO_2 than CaF_2. Thus, additions of FeF_2 to welding fluxes should yield more 'fluoric gases' by a reaction similar to (42) above and also by decomposition and vaporization of FeF_2 itself (BP 1900°C). Table 18 indicates the results of blending 4-20% FeF_2 to flux Fx-1 ($MnO-SiO_2$). Unfortunately the results obtained are contradictory. In some cases, there is a significant difference in oxygen content whereas in others there is little difference. The results of this experiment again illustrates the complex nature of interactions inside the arc cavity and indicates the need for further work in this area. Experiments were also performed by using high carbon electrodes (0.5-0.7% carbon) to examine whether oxygen content may be significantly reduced by using such wires, since carbon unlike Si and Mn is a good deoxidizer at high temperatures in the zone of droplet reactions (see Appendix A.2). The results, shown in Table 19 indicate that there is little difference in weld metal oxygen content, confirming our explanation of control by chemical kinetics in the droplet region (ref. 4.1) and illustrating the similarity in the

Table 18: Effect of FeF_2 Additions in Weld Metal Oxygen Content. All Welds Made with A-7 Electrodes.

Weld No.	Baseplate	% FeF_2 (addition to Flux Fx-1)	% Oxygen	Welding Conditions
26	1008	0	0.21	300 A, 32 V, 40 cm/min
F-4	1008	4%	0.18	300 A, 32 V, 40 cm/min
F-8	1008	8%	0.15	300 A, 32 V, 40 cm/min
600	HY-80	0%	0.057	600 A, 30 V, 12 cm/min
F-600	HY-80	20%	0.066	600 A, 30 V, 12 cm/min
400	HY-80	0%	0.072	400 A, 28 V, 12 cm/min
F-400	HY-800	20%	0.079	400 A, 28 V, 12 cm/min
800	HY-80	0%	0.072	800 A, 33 V, 12 cm/min
F-800	HY-80	20%	0.074	800 A, 31 V, 1 cm/min

Table 19: Effect of Carbon in Electrode on Oxygen in Weld Metal.

All Welds with Flux Fx-1 on HY-80 Baseplates.

Welds with A-7 Electrode (0.04% C)		Welds with Med-C Electrode (0.6% C)		Welding Conditions
Weld No.	% Oxygen	Weld No.	% Oxygen	
400	0.072	C-400	0.059	400 A, 20V, 12 cm/min
600	0.066	C-600	0.057	600 A, 30V, 12 cm/min
800	0.072	C-800	0.063	800 A, 33V, 12 cm/min

kinetics between decarburization during levitation melting and the droplet-plasma reactions in the SAW process. It should be noted though that weld metal may and does lose carbon but this is due to interfacial reactions involving carbon and oxygen in the weld pool (zone of dilution and weld pool reactions) and is probably responsible for the large pores often found inside the slag. These pores are found under the slag even if the weld metal is sound, indicating that the slag-pores are due to interfacial reactions with carbon rather than nucleation of CO bubbles inside the melt at lower temperatures. (This confirms the analysis by Eagar [7] showing that deoxidizer such as silicon supresses the formation of CO gas bubbles inside the metal.) North [79] used aluminum powder additions to $CaO-Al_2O_3-CaF_2$ fluxes and found these additions to lower oxygen content both at the electrode tip and in the weld metal. This is not surprising since aluminum is a good deoxidizer even at the high temperatures in the droplet region (see Appendix A.2). Since the aluminum was introduced as fine powder blended, with the flux and was not alloyed with the electrode wire, chemical kinetics at the droplet surface [ref. Sec. 4.1] did not necessarily affect the reactions.

6.1.2. Oxygen Transfer in the Zone of Cooling and Solidifying Weld Pool

In Section 4.3, it was proposed that oxygen is removed by a mechanism of inclusion growth and separation in the zone of the cooling weld pool. To verify this hypothesis, experiments were conducted to directly change the solidification time without changing the welding

process parameters. Welds were made on 1 inch thick Hy-80 plates using E-705-3 electrodes, and flux Fx-1. Welds were then made on a bundle of E-705-3 electrodes inside a massive water cooled copper mold using identical welding parameters and flux Fx-1. Table 20 gives the results of this experiment. It distinctly shows that the oxygen content of rapidly cooling weld metal is over twice as great as the unquenched metal. Figure 36 shows the micrographs of the quenched and unquenched metal. The inclusions in the quenched metal are smaller than those in the unquenched metal, and this again supports the hypothesis of oxygen removal by inclusion growth and separation. Our hypothesis of inclusion growth and separation has also been applied to the results of Christensen [10] and Chai [19] for bead on plate welds. In Section 4.3, it was mentioned that solidification time (t_s) may be related to weld geometry by using Chvorinov's eqn. (equation (41)). Since oxygen content increases with decreasing solidification time, and solidification time decreases with increasing s/a (the ratio of the fusion line length to the transverse cross-sectional area of the weld) weld metal oxygen content should increase with increasing (s/a) on using the same welding consumables. Figures 37a to 37c show the results for fluxes used by Christensen and Figures 38a and 38b for those used by Chai [17]. There is large scatter in the figures but they do confirm our hypothesis of inclusion formation and separation in this region. A part of the scatter in Figures 37a - 37c may be due to the method of determining (s/a) from Christensen's data. Since in the available literature [10] only the transverse area of the metal

Table 20: Effect of Solidification Rate and Current Polarity on Oxygen Content of Weld Metal. Flux Fx-1 and A-7 Electrodes Used for All Welds.

Rapidly Quenched Weld (artificial baseplate made with 70S-3 electrodes used)		Normal Weld Metal (HY80 baseplate)		Welding Conditions
Weld No.	% Oxygen	Weld No.	% Oxygen	
Cu 500	0.163	500	0.091	500 A, 30 V, 24 cm/min
Cu 600	0.210	600	0.066	600 A, 30 V, 12 cm/min
Cu 601	0.176	H-600	0.064	600 A, 30 V, 12 cm/min
Cu 700	0.190	H-700	0.077	700 A, 30 V, 12 cm/min
Cu 800	0.143	800	0.072	800 A, 33 V, 12 cm/min
AC-5	0.178	AC-4	0.056	780 A, 32 V, 12 cm/min
		AC-3	0.090	540 A, 34 V, 12 cm/min
		AC-2	0.065	560 A, 30 V, 12 cm/min

(a) weld #Cu 600

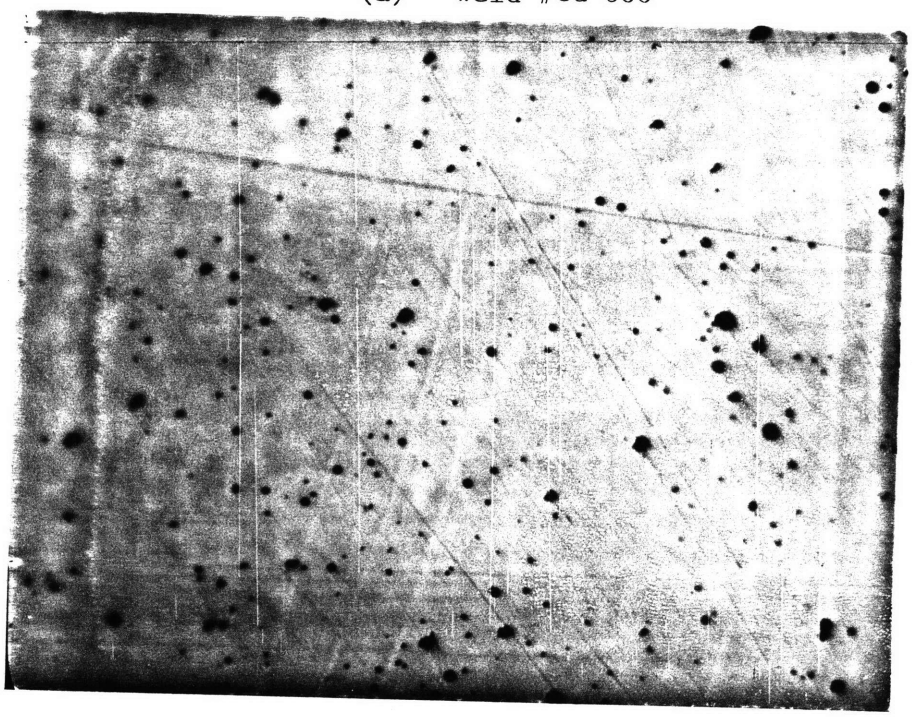

(b) weld #600

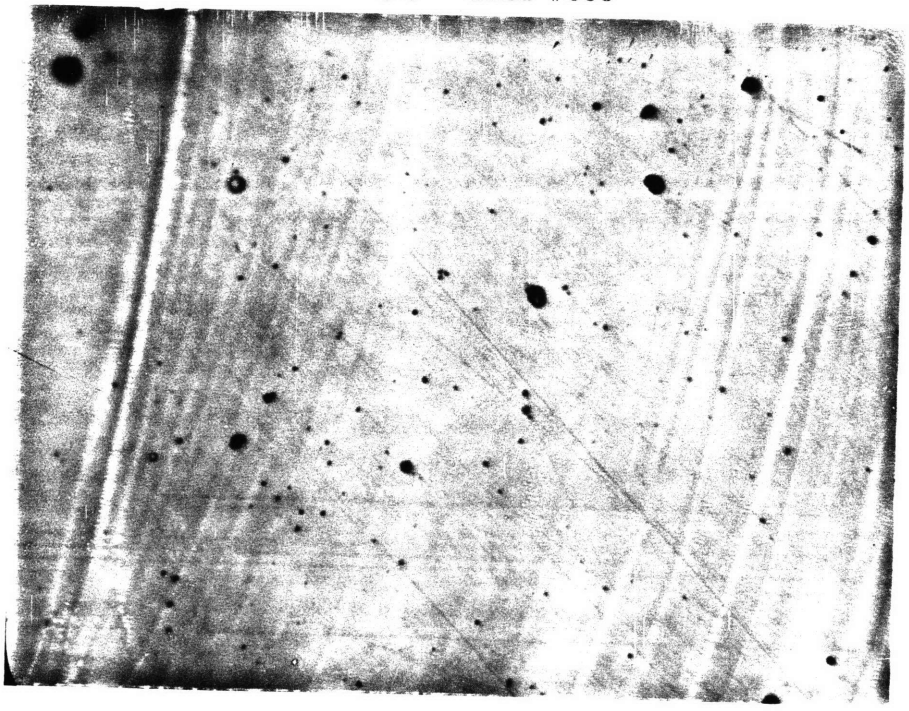

Figure 36 : Comparison of the inclusion distribution in rapidly cooled weld metal using a water-cooled copper mold (a), to that in normal bead on plate welds (b) [Magnification :400X]

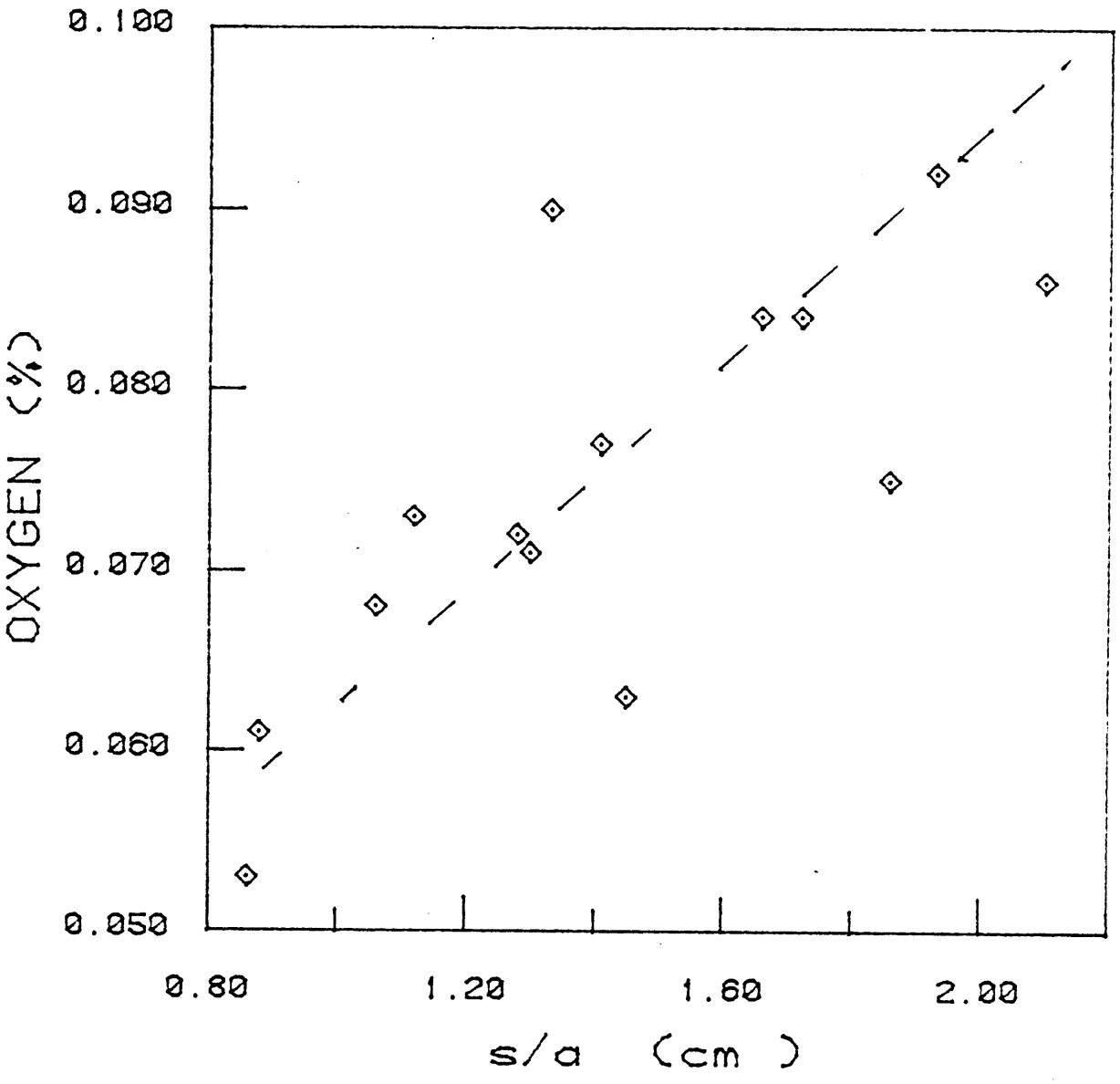

Figure 37a: Variation of oxygen content of the weld metal with the parameter (S/a). Data is for 'flux a' used by Christensen [10].

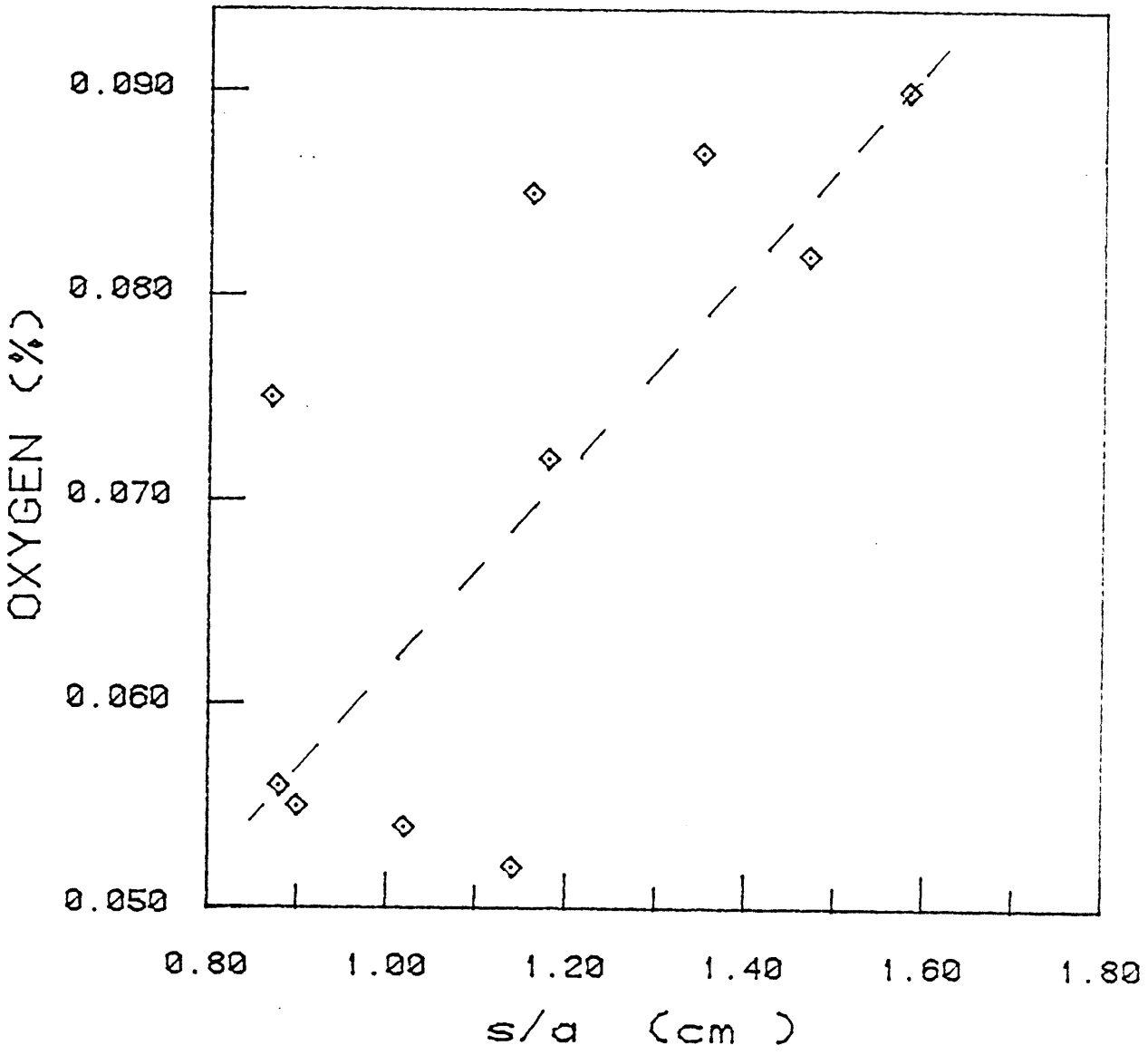

Figure 37b: Variation of oxygen content of the weld metal with the parameter (S/a). Data is for 'flux d' used by Christensen [10].

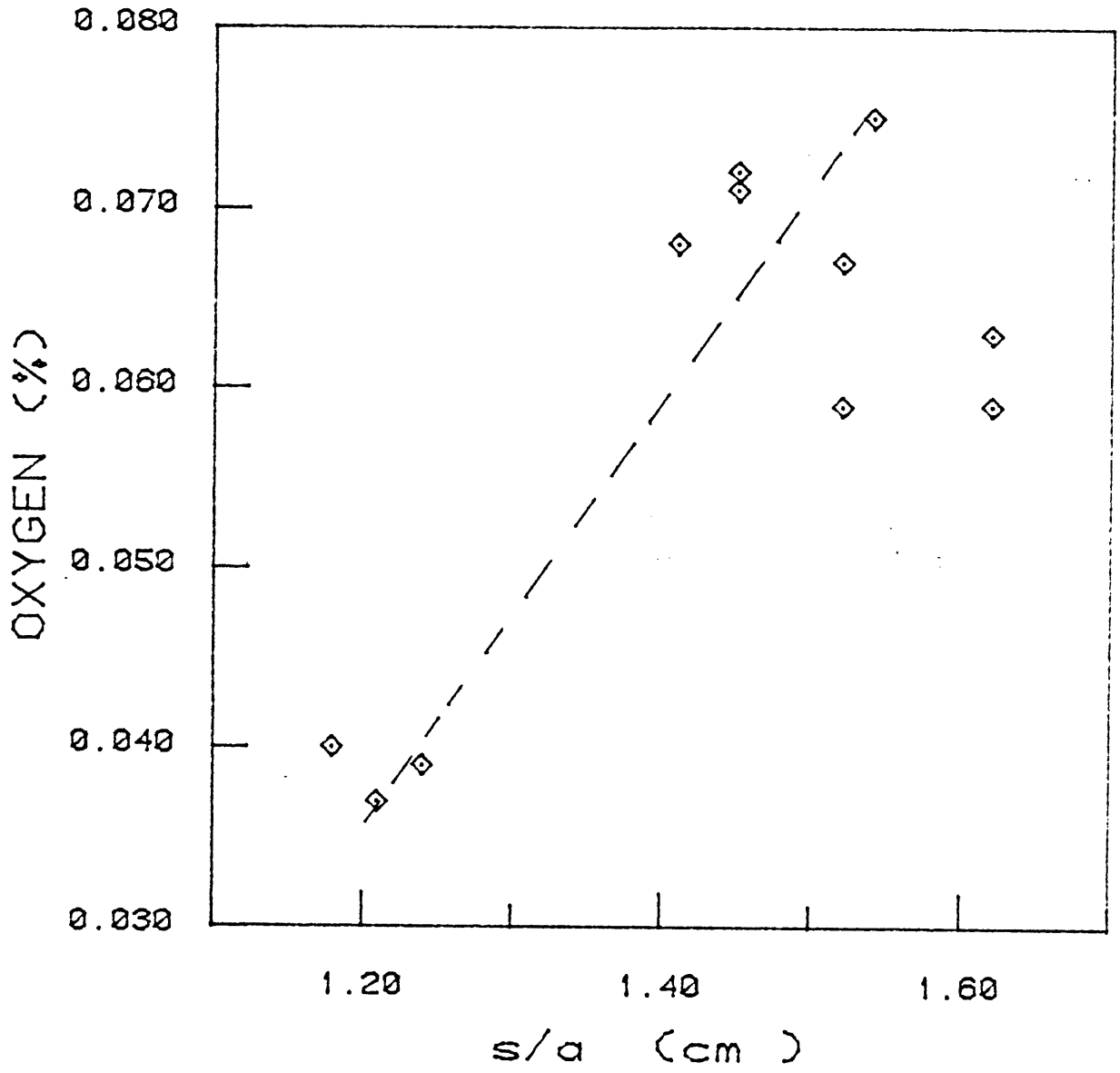

Figure 37c: Variation of oxygen content of the weld metal with the parameter (S/a). Data is for 'flux e' used by Christensen [10].

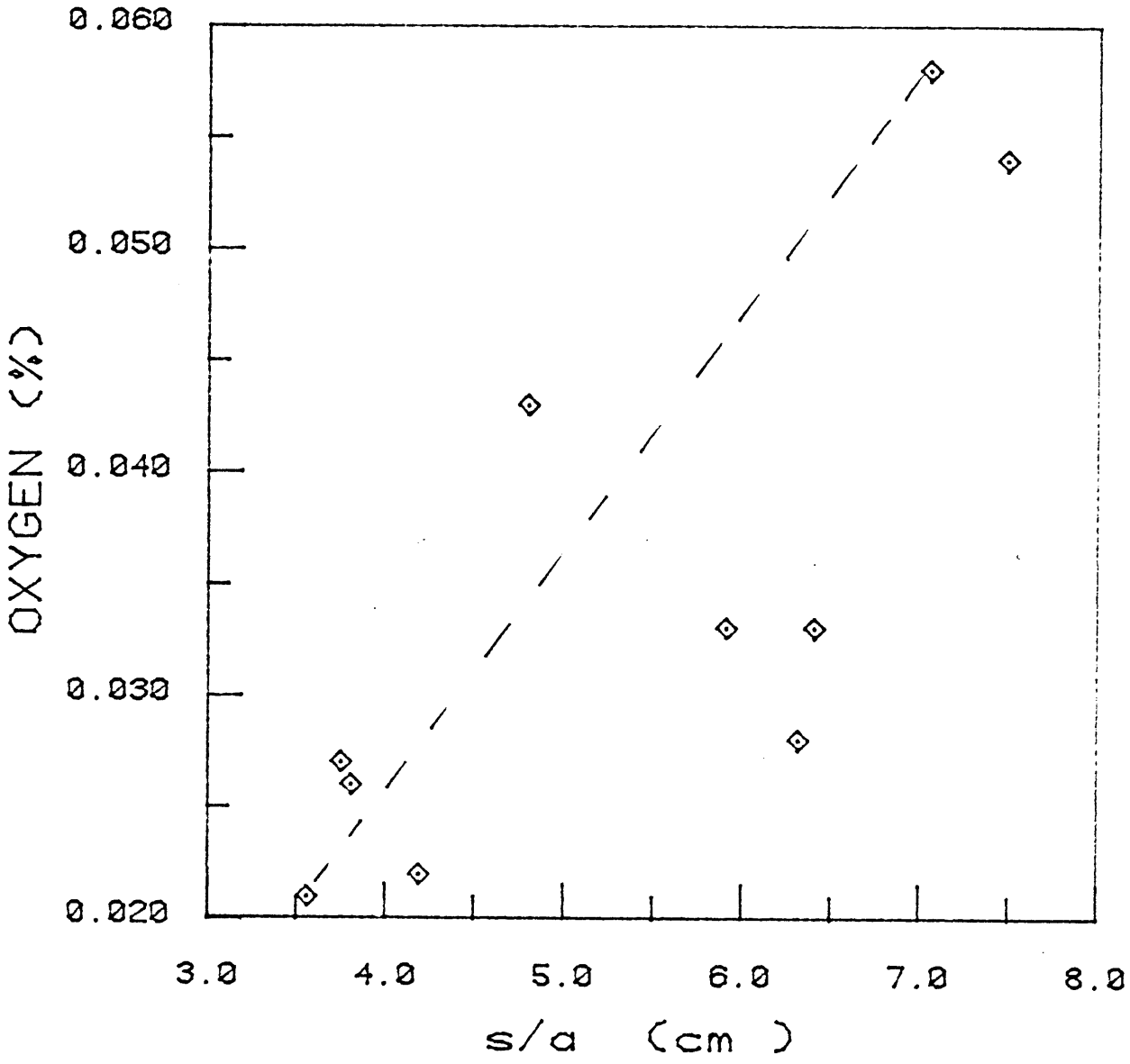

Figure 38a: Variation of oxygen content of the weld metal with the parameter (S/a). Data is for 'flux F-4' used by Chai [17,19].

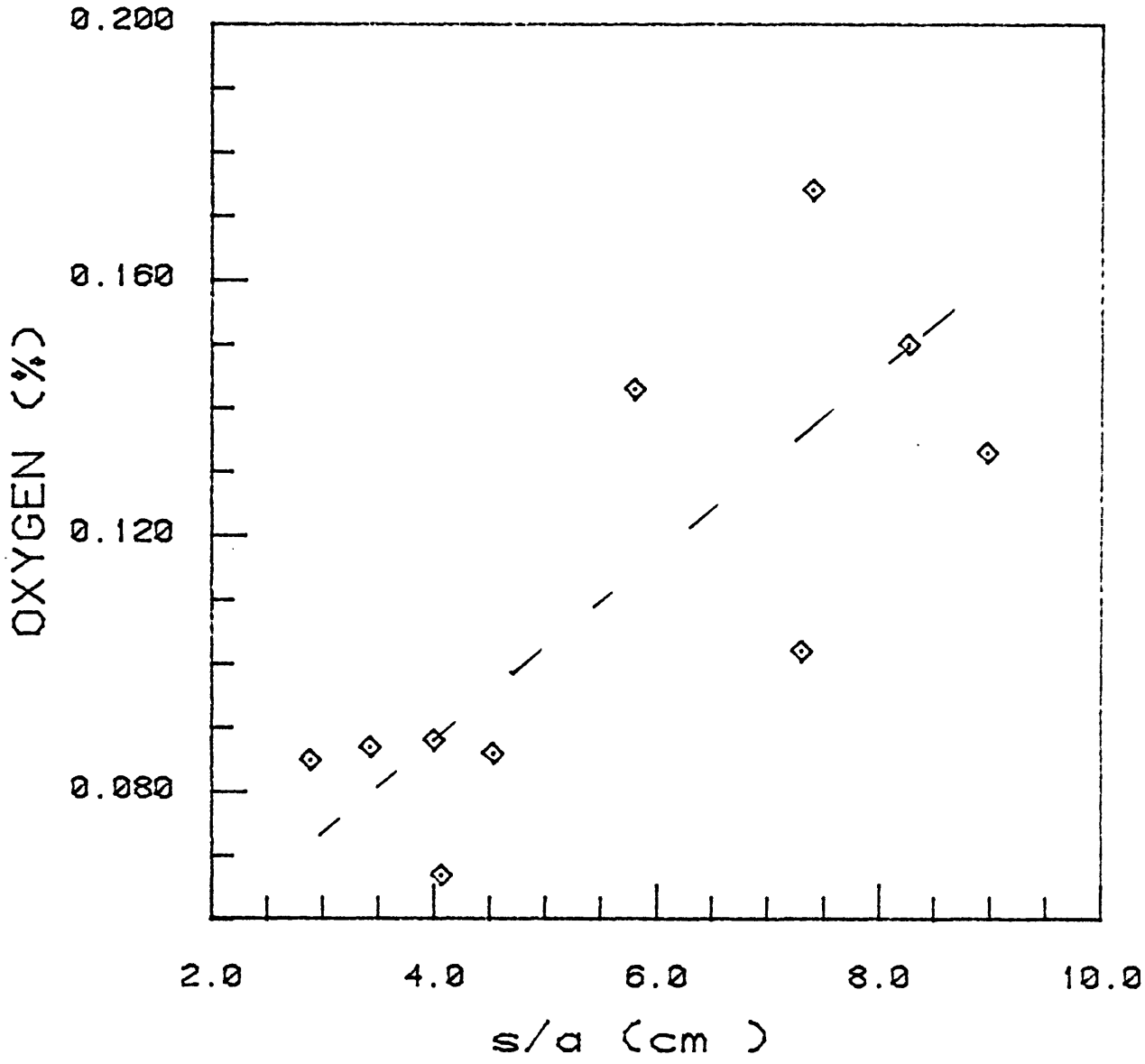

Figure 38b: Variation of oxygen content of the weld metal with the parameter (S/a). Data is for 'flux F-3' used by Chai [17,19].

deposited (B), and total transverse cross-sectional area (a) is recorded, (s/a) was computed by the approximation

$$s/a \approx \frac{3\sqrt{B}}{a} \tag{43}$$

The two parameters B and a are shown schematically in Figure 22. In practice, s/a ranges from $\frac{2.5\sqrt{B}}{a}$ to $\frac{3.5\sqrt{B}}{a}$ for the shapes obtained in submerged arc welds (see Appendix A.6), but the 20% error which may be introduced by the approximation is small when compared to the large changes in the values of (s/a) on changing welding parameters. Figure 39 which shows a plot of weld metal oxygen against (s/a) for welds made in the present investigation, shows less scatter. Here both (s) and (a) were determined by actual measurement of polished and etched welds. Also the micrographs of the results of Chai and Eagar [19] (Figure 21) confirm our hypothesis.

Potapov et al. found that oxygen content of weld metal increases with increasing wire diameter [80] as shown in Figure 40(a). They suggested that as wire diameter is increased, the flux becomes more 'passive' in relation to the weld metal. However, in this experiment the current density was kept constant in the range 35-40 A/mm^2 so there was a 600% increase in the values of the current when a 5 mm wire was used instead of a 2 mm wire. Figure 40b presents the results of Potapov showing the effect of welding current on oxygen content. This result is not surprising since an increase in current makes the s/a ratio of the weld smaller, thus increasing the

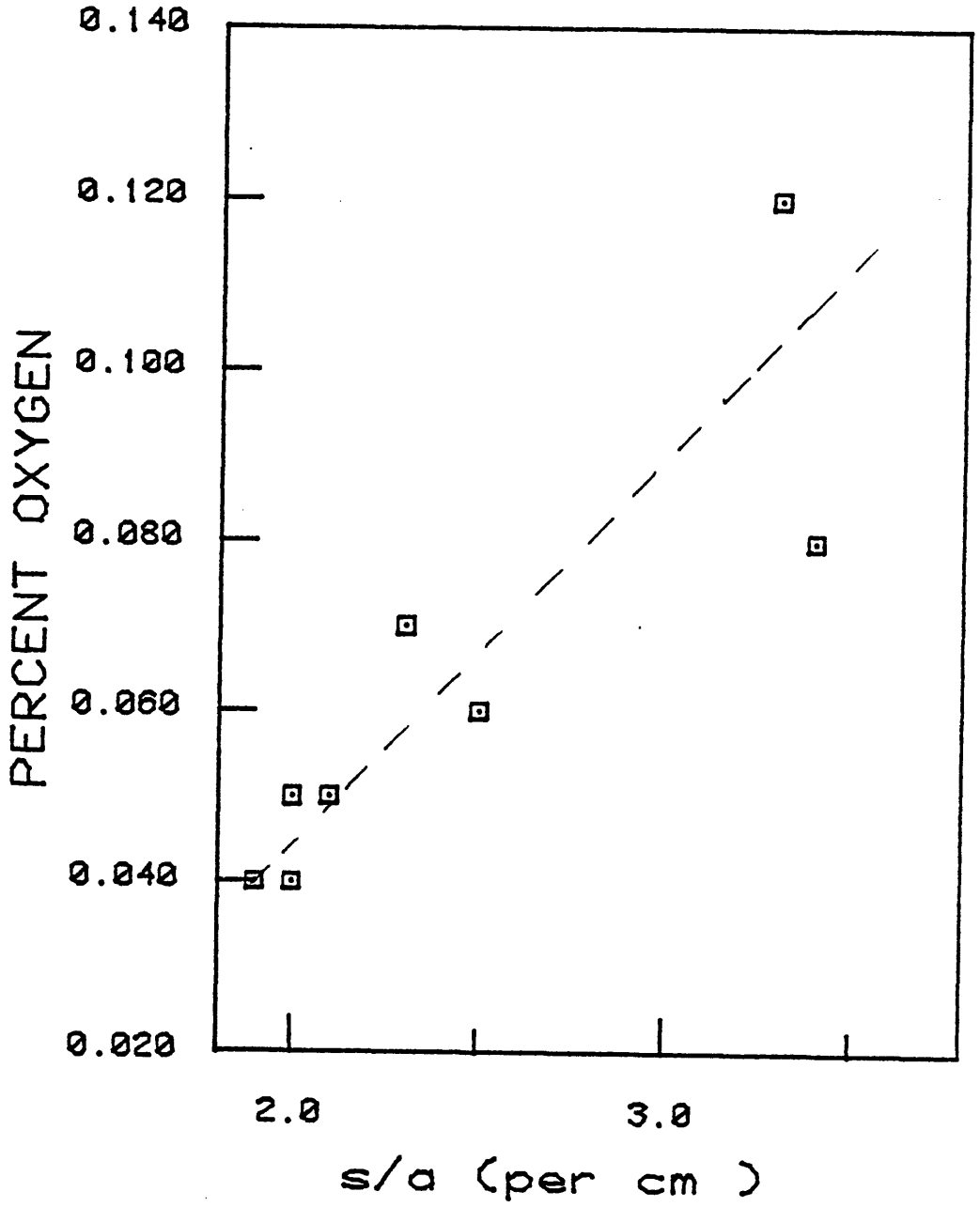

Figure 39: Variation of the oxygen content of the weld metal with the parameter (S/a). Welds made with flux Fx-2, EZ-20 base-plate and A-7 electrodes.

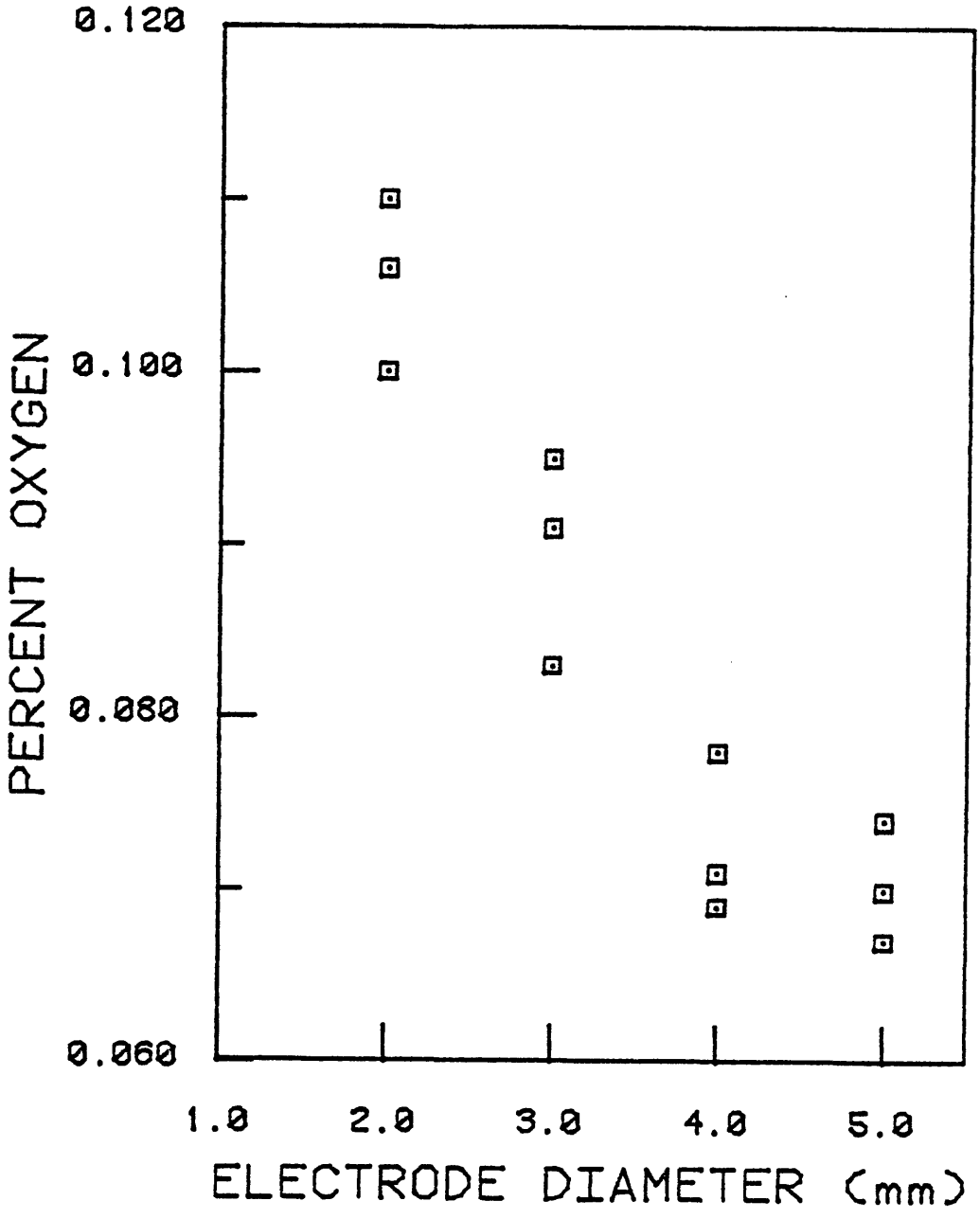

Figure 40a : Relationship between oxygen content of the weld metal to electrode diameter [from ref. 59]. (Note the same current density was used with all electrodes.)

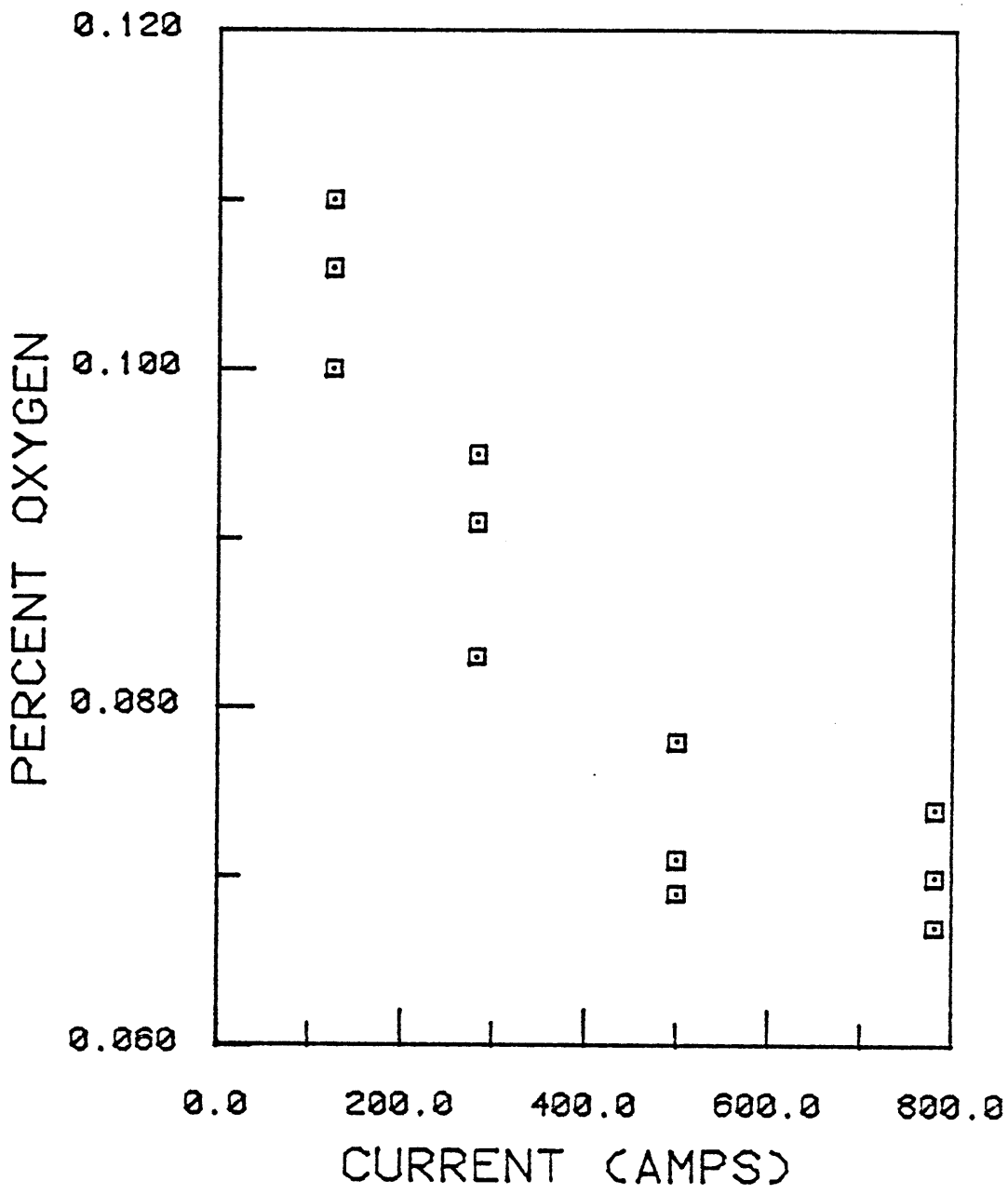

Figure 40b : Relationship between oxygen content of the weld metal to the welding current. Data from ref. 59 (see Figure 26).

solidification time and consequent time for inclusions to grow and separate out.

Recently, there has been some discussion on improving weld metal toughness by using A.C. current, and it has been suggested that the use of A.C. lowers oxygen content [81]. To test this hypothesis a Miller - 1000 A.C. square wave machine was connected to a UEC-8 controller and bead on plate welds made. A rapidly quenched weld was also made using the water cooled copper mold. The results, shown in Table 20, indicate the oxygen content of the rapidly quenched A.C. weld is in the same range as that obtained by D.C. welds, thus eliminating effects of A.C. inside the arc column. The slightly lower oxygen content in weld metal on uxing A.C. SAW may be due to smaller (s/a) ratio of the A.C. weld metals. However, the difference in the oxygen content between the A.C. and D.C. welds (see Table 20) is within limits of experimental error, and more work is necessary, to determine whether oxygen content in A.C. welds is significantly lower. A statistical analysis may be employed in order to overcome the problem of large scatter in the weld metal oxygen content.

6.2. Transfer of Other Alloying Elements

In the previous chapter (in Section 4.2), it was proposed that the transfer of an alloying element M may occur by the reaction

$$\underline{M} + \underline{O} = [MO_x] \qquad (11)$$

and a kinectic mode was formulated to predict weld metal composition.

For single pass welds, the following equation was suggested

$$M_f = N.P. - (N.P. - M_i) * \exp(-\alpha * (A_{s/m}/V_m)) \quad (33)$$

For multipass welds, when several passes are made without changing the welding consumables or process parameters, equation (33) leads to a steady state value of metal composition:

$$M_N = M_{e\ell} + \frac{(N.P. - M_{e\ell})(1 - F)}{(1 - Fd)} \quad (38)$$

where

$$F = \exp(-\alpha(A_{s/m}/V_m)) \quad (37)$$

6.2.2. Transfer of Manganese

The transfer of manganese between the slag and metal in SAW has been studied by many researchers [10,12,14-18,28-36]. However, so far none of them have been able to develop a general model for predicting weld metal manganese content. The transfer of manganese may be reprsented by an equation similar to equation (11)

$$\underline{Mn} + \underline{O} = (MnO) \quad (49)$$

Equation (33) was applied to the results of our preliminary experiments and the following equations were obtained on welding with a highly oxidizing flux

$$M_f = N.P. - (N.P. - M_i) * \exp(-1.7 * W_S/W_M) \qquad (52a)$$

or

$$M_f = N.P. - (N.P. - M_i) * \exp(-0.2 * w/A) \qquad (52b)$$

In equation (52a), $\alpha = 1.7$ if the slag to metal ratio (W_S/W_M) is used as a measure of ($A_{s/m}/V_m$). In equation (52b), $\alpha = 0.2$ cm when the ratio of width to transverse cross-sectional area (w/A) is used as a measure of ($A_{s/m}/V_m$). [See Section 5.2.1e.] As may be seen from Figures 41a and b the use of the two equations give nearly identical results. Also, as Figure 41 shows, a change in the value of α leads to a deviation from the actual composition, but the trend remains the same.

For the less oxidizing fluxes, α is one-third the value for highly oxidizing fluxes and the corresponding equations are

$$M_f = N.P. - (N.P. - M_i) * \exp\left(-\frac{1.7}{3} * W_S/W_M\right) \qquad (53a)$$

or

$$M_f = N.P. - (N.P. - M_i) * \exp\left(-\frac{0.2}{3} * w/A\right) \qquad (53b)$$

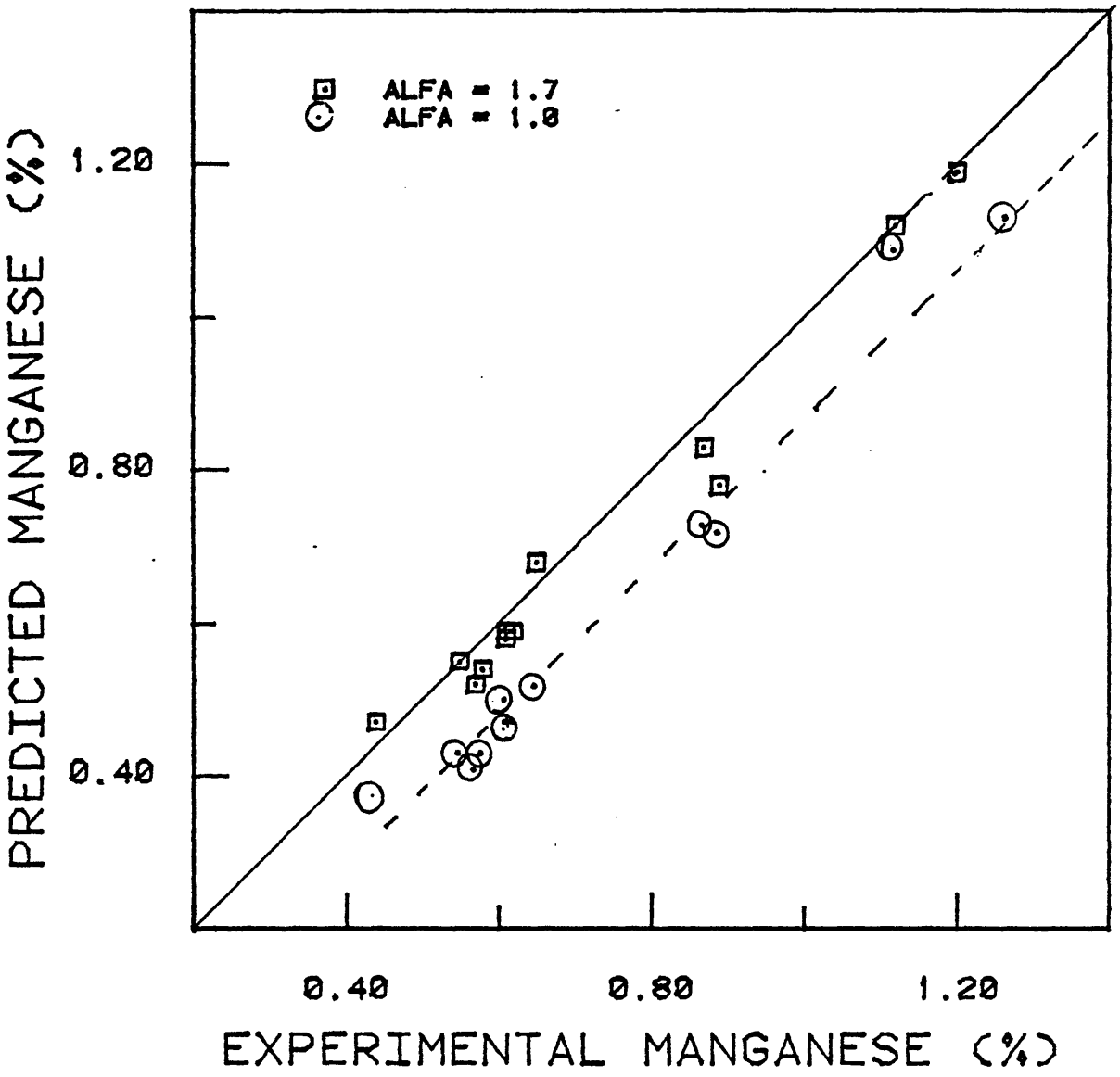

Figure 41 (a). Comparision of manganese content in single pass weld as predicted by theory to that obtained experimentally. Data from results of preliminary experiments. Fx-1 flux used. (N.P.:1.2%Mn, =1.7). Dashed line indicates results if α =1.0 was used instead of =1.7.

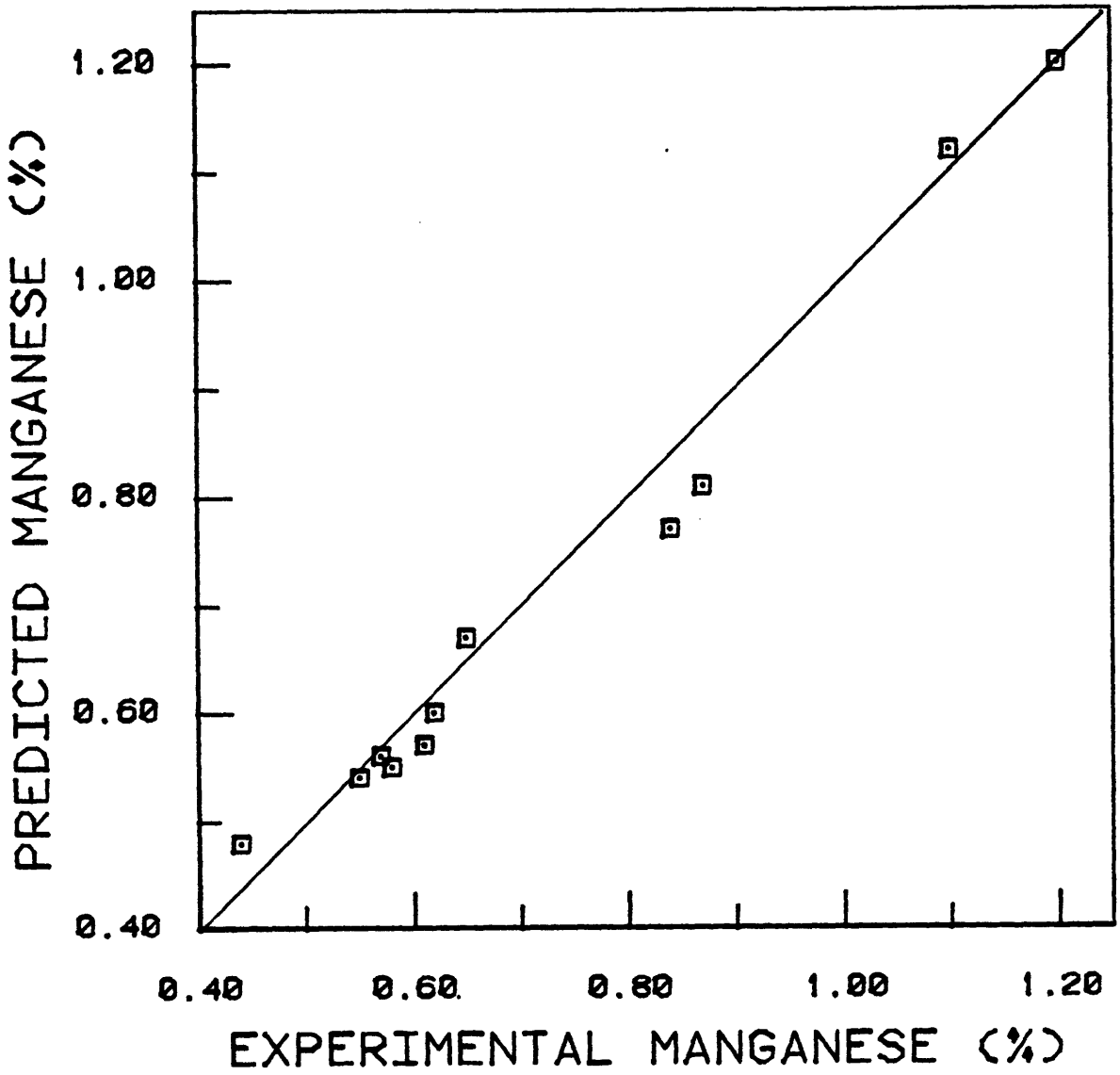

Figure 41b : Comparison of manganese content in single pass weld metal as predicted by theory to that obtained experimentally. Data from results of preliminary experiments. Flux Fx-1 with N.P. = 1.20 and α = 0.2 cm used for all welds. w/A was used as a measure of $A_{S/M}/V_M$.

For multiple pass welding, the corresponding equations are

$$M_f = M_{e\ell} + (N.P. - M_{e\ell})\frac{(1 - F)}{(1 - Fd)} \quad (54)$$

where

$$F = \exp(-1.7\ W_S/W_M) \text{ for highly oxidizing fluxes} \quad (55)$$

or

$$F = \exp(-1.7/3\ W_S/W_M) \text{ for less oxidizing fluxes} \quad (56)$$

Application of equations (52)-(56) to data recorded by previous researchers [10,17,18,29] confirms these conclusions. Figure 42 and Figure 43 show some of the results, the rest are shown in Appendix 8.

Table 21 summarizes these results for manganese transfer. Inspite of the excellent agreement between theory and experiment as shown in Table 19, it was felt that direct confirmation of the model was needed. In order to do this the value of $(A_{s/m}/V_m)$ (or the corresponding (W_S/W_M) or (w/A) ratios) had to be directly changed without changing the welding parameters. This was done by two different experiments. The first experiment involved the use of a massive water-cooled copper mold which had slots of different dimensions. By depositing metal in these slots which contained an 'artificial baseplate' made of electrode wires, the values of (W_S/W_M) could be controlled without changing the welding parameters. Figure 44a schematically illustrates the arrangement used. Figures 44b and c are photographs of the actual apparatus. The results are shown in Figure 45 and the

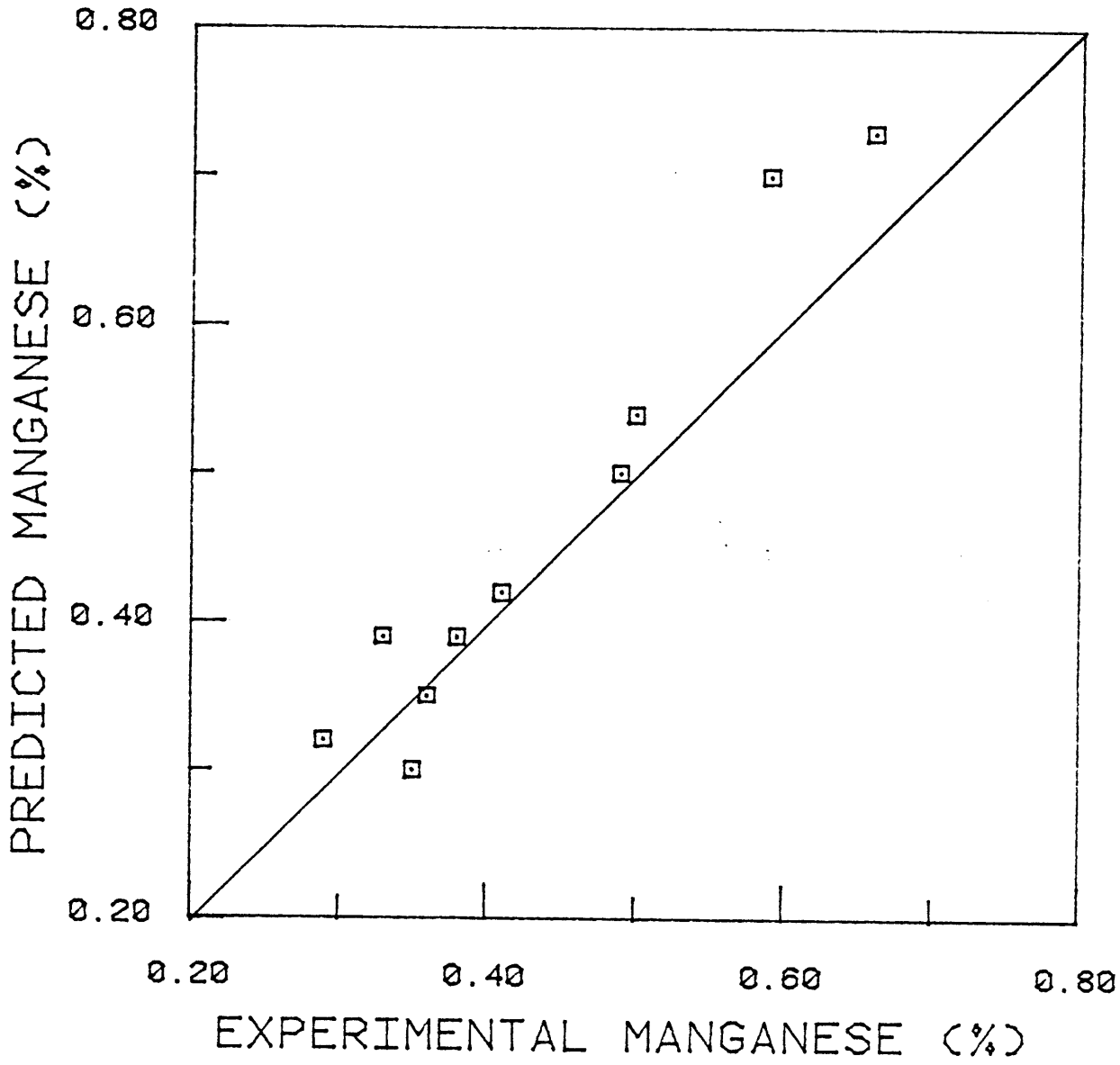

Figure 42a: Comparison of manganese content in single pass weld metal as predicted by theory to that obtained experimentally. Data from experimental work by Christensen [10]. Results are for flux d (α = 1.7, N.P. = 0.00).

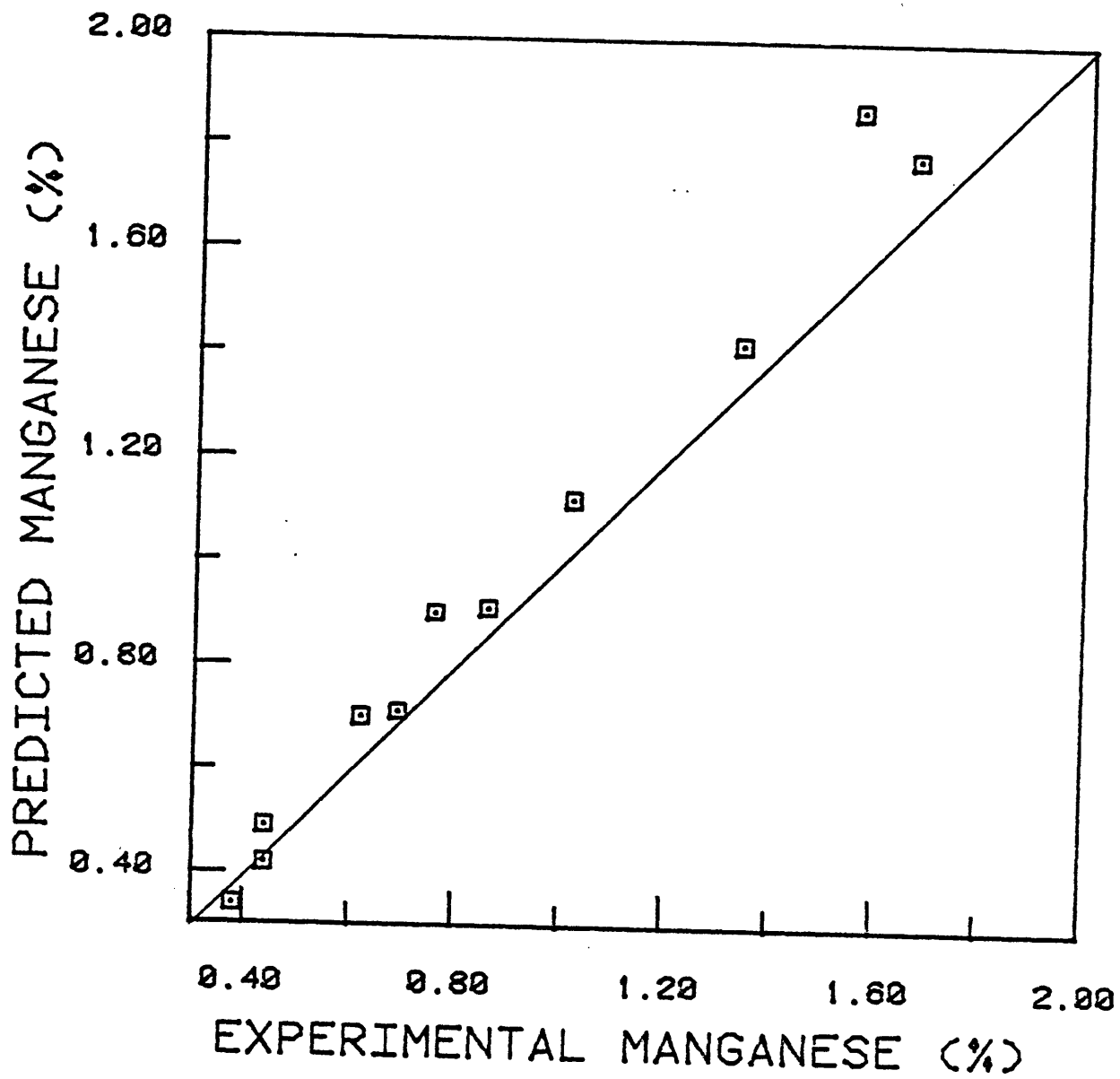

Figure 42b: Comparison of manganese content in single pass weld metal as predicted by theory to that obtained experimentally. Data from experimental work by Chai [17]. Results are for flux F-2 (α = 1.7/3, N.P. = 1.8% Mn).

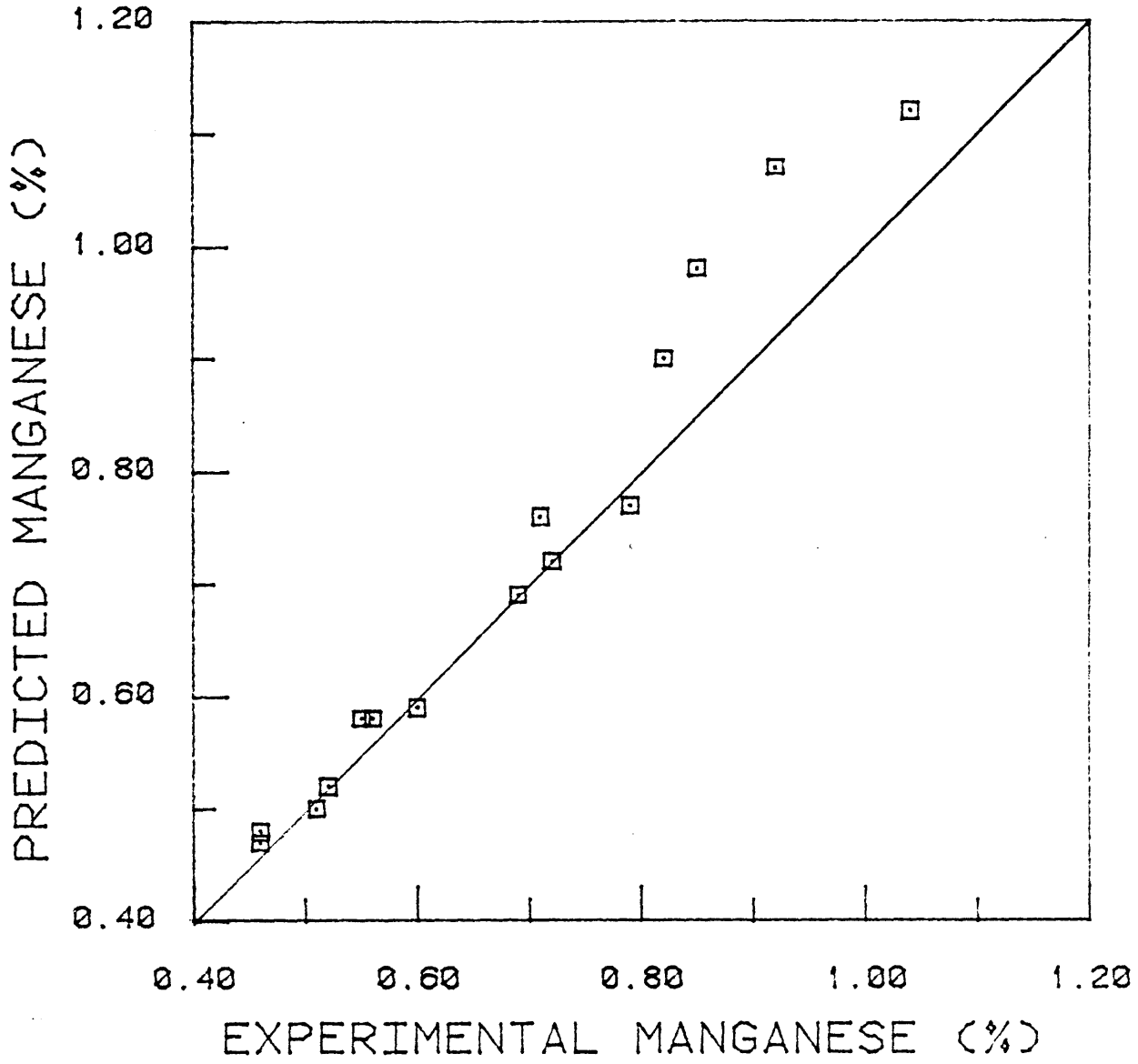

Figure 42c: Comparison of manganese content in single pass weld metal as predicted by theory to that obtained experimentally. Data from experimental work by Christensen [10]. Results are for flux f (α = 1.7/3, N.P. = 0.55% Mn).

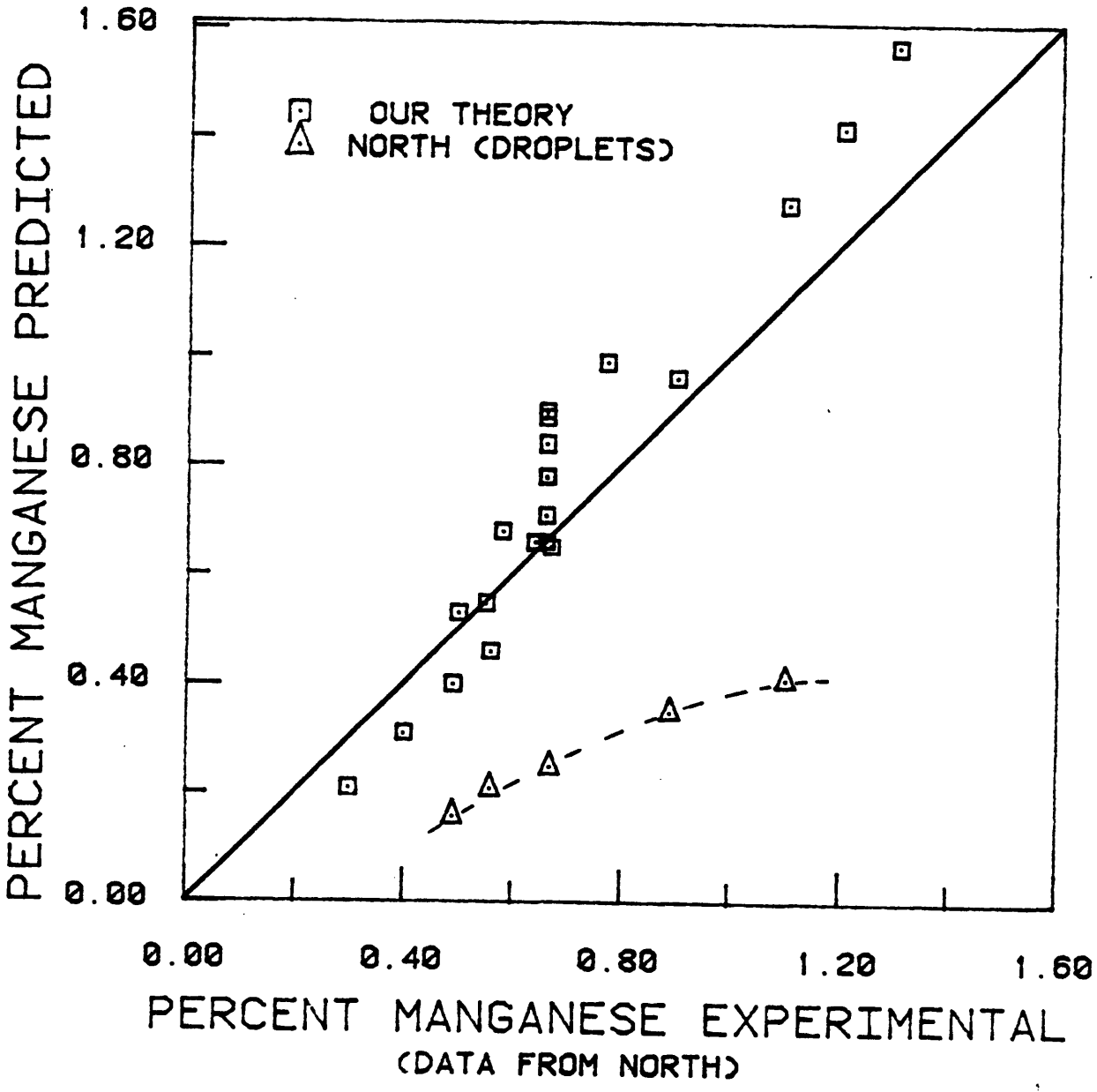

Figure 43a: Comparison of manganese content in multipass weld metal as predicted by theory to that obtained experimentally. Data from experimental work by North with a 65% SiO_2 - 35% CaO flux (N.P. = 0.00% Mn, α = 1.7). Dashed line shows composition of 'droplets' collected by North.

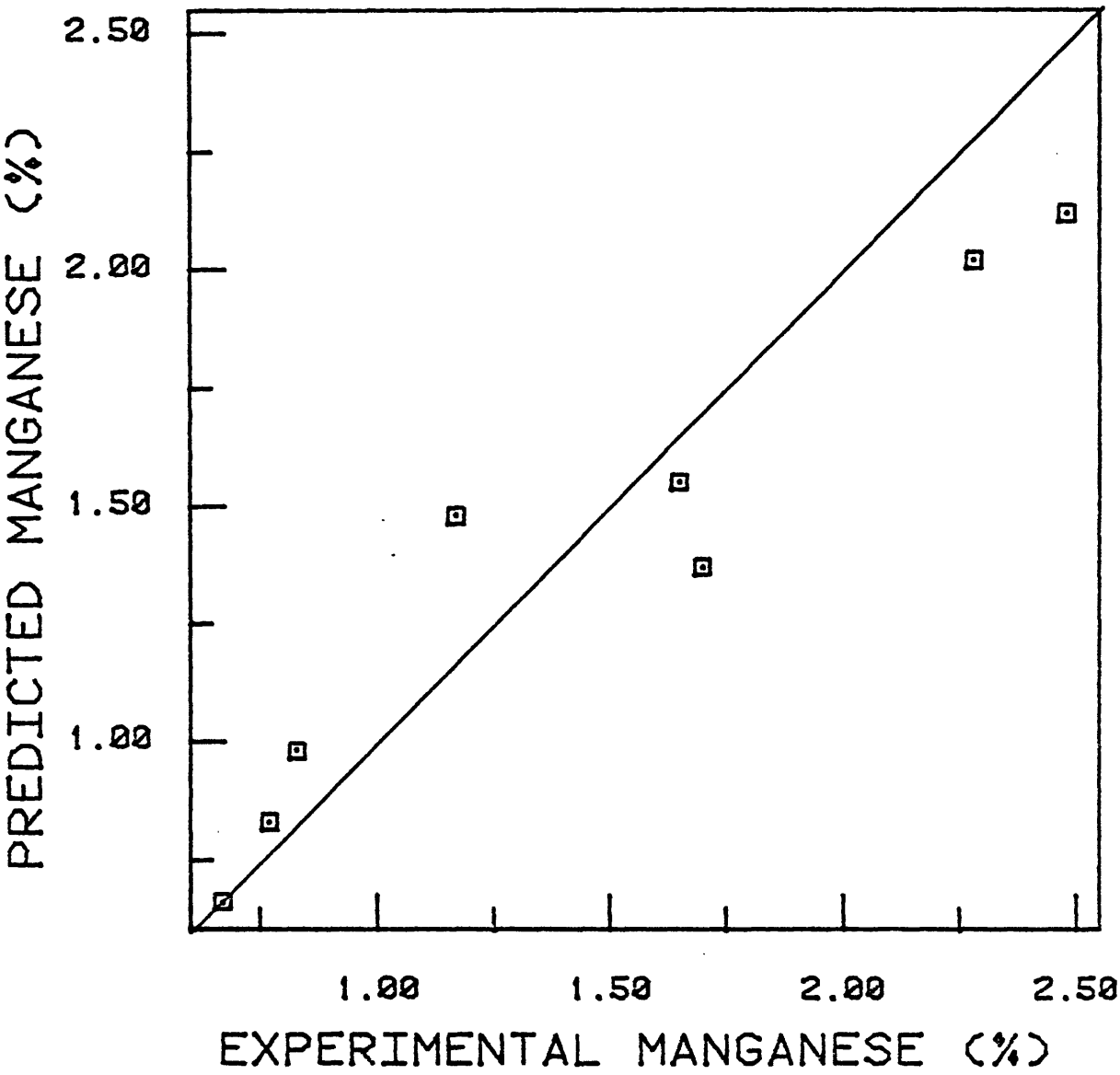

Figure 43b: Comparison of manganese content in multipass weld metal as predicted by theory to that obtained experimentally. Data for flux A-348A used by Frumin [28] (N.P. = 2.5% Mn, α = 1.7).

Table 21: Correlation Between Theoretical Prediction and Experimental Results for the Transfer of Manganese

Researcher (Ref.)	Flux Name	Weld Type	No. of Welds	Linear Correlation Coefficient between Theory & Experiment
Present Investigation (Preliminary Experiments)	Fx-1	Single	12	0.96
	Fx-2	Single	8	0.91
	Fx-3	Single	8	0.83
Christensen [10]	a	Single	14	0.72
	c	Single	6	0.99
	d	Single	10	0.96
	e	Single	11	0.97
	f	Single	16	0.98
North [18]	Calcium Silicate	Multipass	23	0.95
Chai [17]	F-1	Single	10	0.94
	F-2	Single	11	0.96
	F-3	Single	10	0.70
	F-4	Single	10	0.81
Frumin [29]	AN-20	Multipass	7	0.96
	A-348	Multipass	7	0.91
Mitra [16]	A	Single	3	0.90
	B	Single	7	0.92
	C	Single	7	0.91
	D	Single	7	0.93

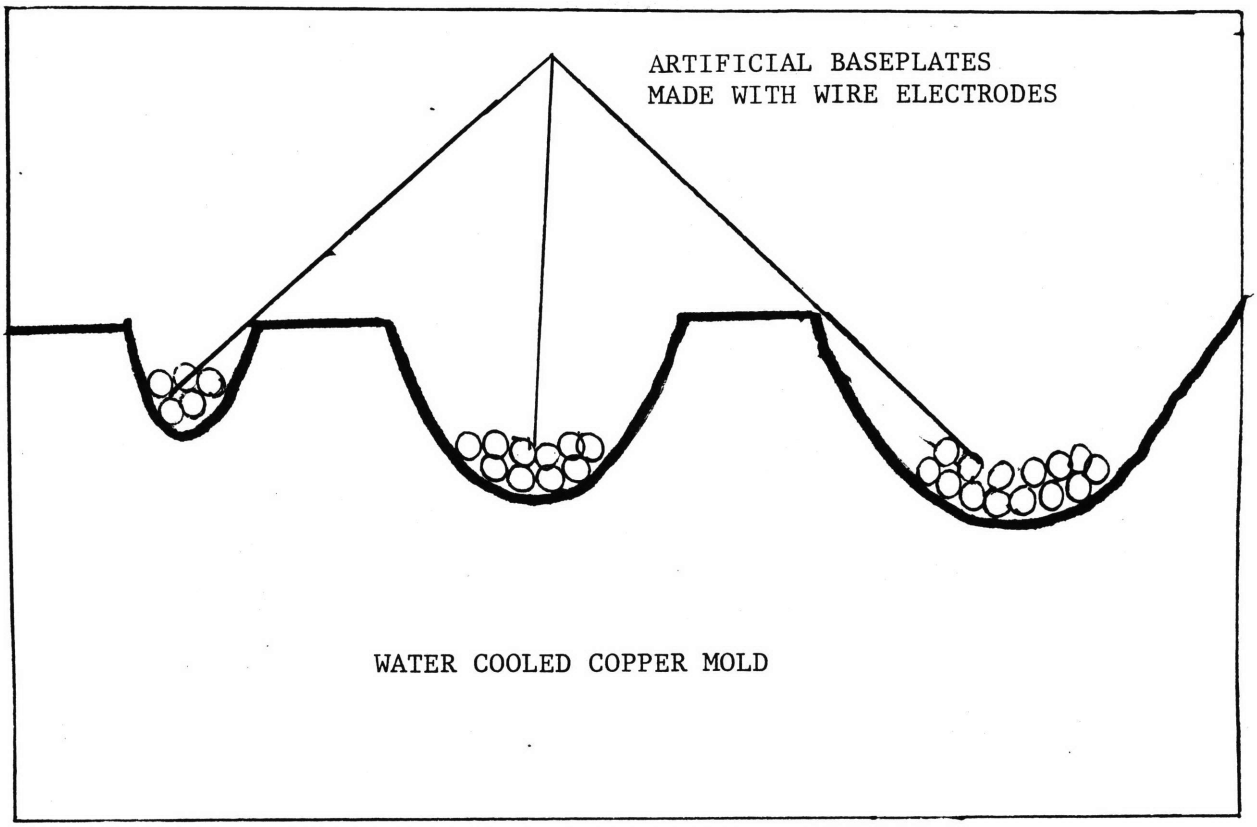

Fig. 44(a) : Schematic reprentation of the copper mold experiment.

Fig. 44 (b) Photograph of the copper mold.

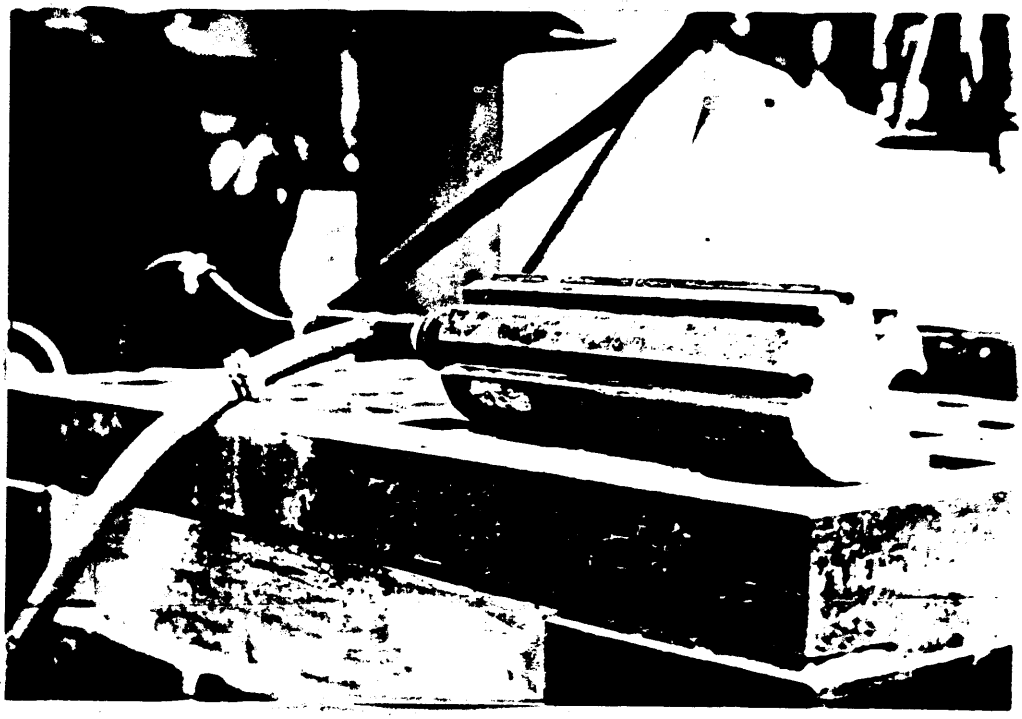

Fig. 44(c) : Photograph of the copper mold

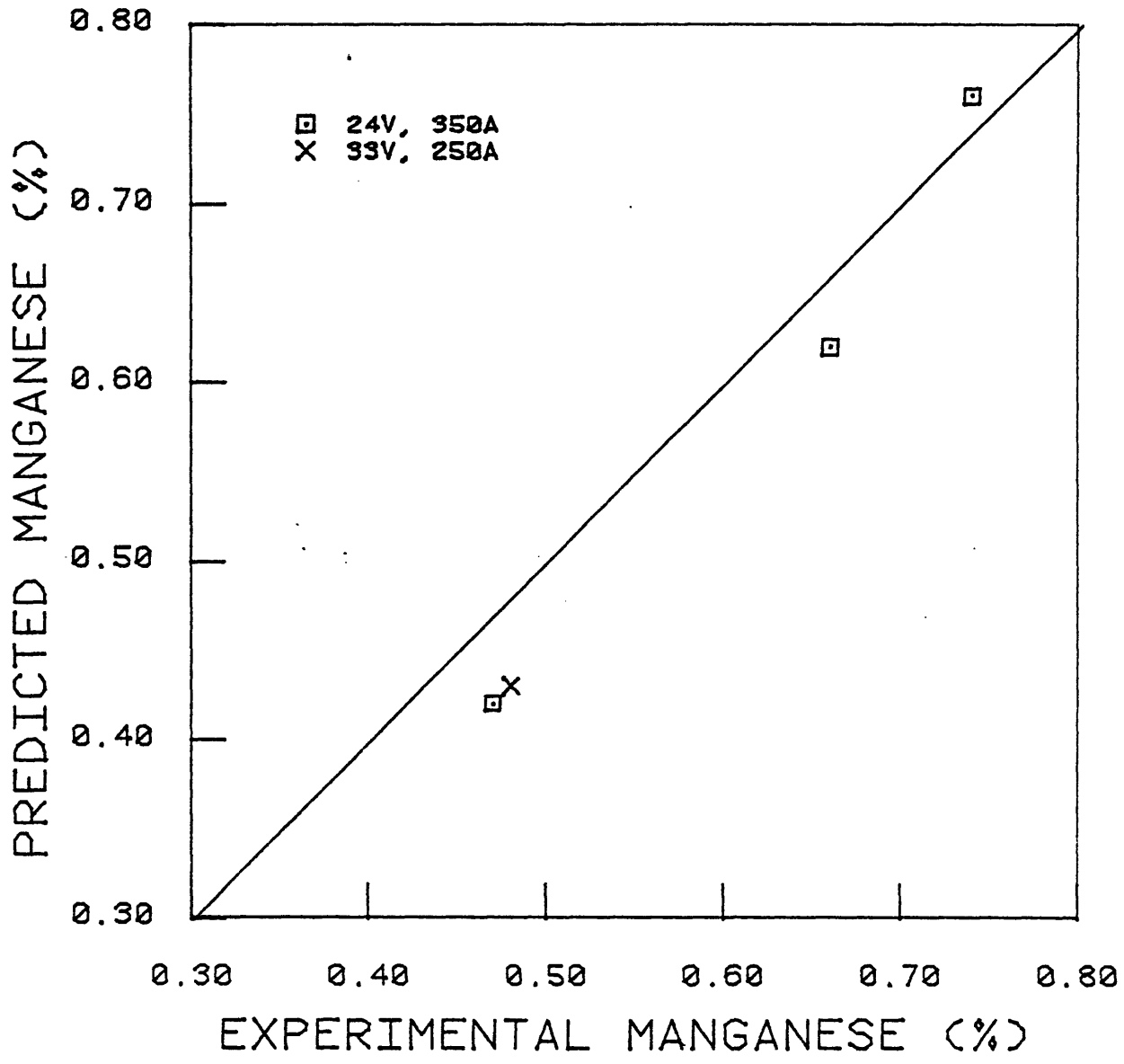

Figure 45: Results of the experiment with the water-cooled copper mold. Flux Fx-1 and electrode A-7 used for all welds. Artificial baseplates made by placing bundles of A-7 electrodes on the mold.

Table 22: Welding Conditions and Chemical Composition of Welds Deposited in Water-Cooled Copper Mold. Flux Fx-1 and A.7 electrodes were used.

Weld No.	Voltage (Volts)	Current (amps)	Slag To Metal Ratio W_S/W_M	Mn (%)	Si (%)
Cu 1	24	350	.16	.47	.21
Cu 2	33	250	.17	.48	.24
Cu 3	24	350	.34	.66	.36
Cu 4	24	350	.50	.74	.54

complete experimental details are listed in Table 22. The results confirm the model and also indicates that changes in the voltage and current have little effect on weld metal composition if the (W_S/W_M) ratio is kept constant and the same welding consumables are used. (According to the proponents of the droplet-reaction time theory an increase in voltage and decrease in current leads to larger reaction times and consequently to larger amounts of alloy transfer.)

The second experiment consisted of changing the (W_S/W_M) or (w/A) ratio by using an arc oscillator. A cyclomatic magnetic arc oscillator was used and the welding parameters were kept constant at 200 A, 24V DCEP and 40 cm/min when welding with the highly oxidizing manganese silicate flux Fx-1. Figure 46 shows a photograph of the arrangements used. The (W_S/W_M) or (w/A) ratio was varied by varying the amplitude of the oscillations. The details of the oscillator settings and the manganese content of the metal is recorded in Table 23. The complete chemical composition of the metal is given in Appendix B-3. Figures 47a and b shows the results of their experiment. The results again confirm our results, however there is some scatter in these experiments. This was due to the problem of reproducibility on welding with the arc oscillator in Table 23 shows welds made under the same welding conditions and on using identical oscillator settings did not have identical chemical composition, the difference being as high as 0.08% Mn in a few cases. Similar experiments were performed using the basic calcium silicate flux Fx-2. The experimental details are given in Table 24 and the results, shown in Figure 48 again confirm the validity of the kinetic model.

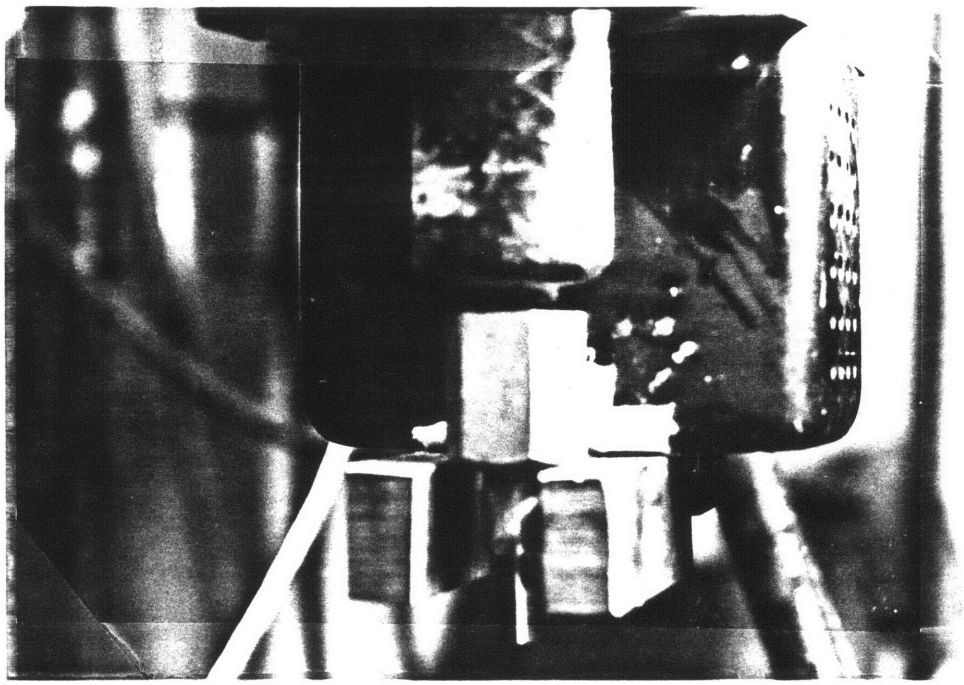

Fig 46. Photograph of the magnetic arc oscillator.

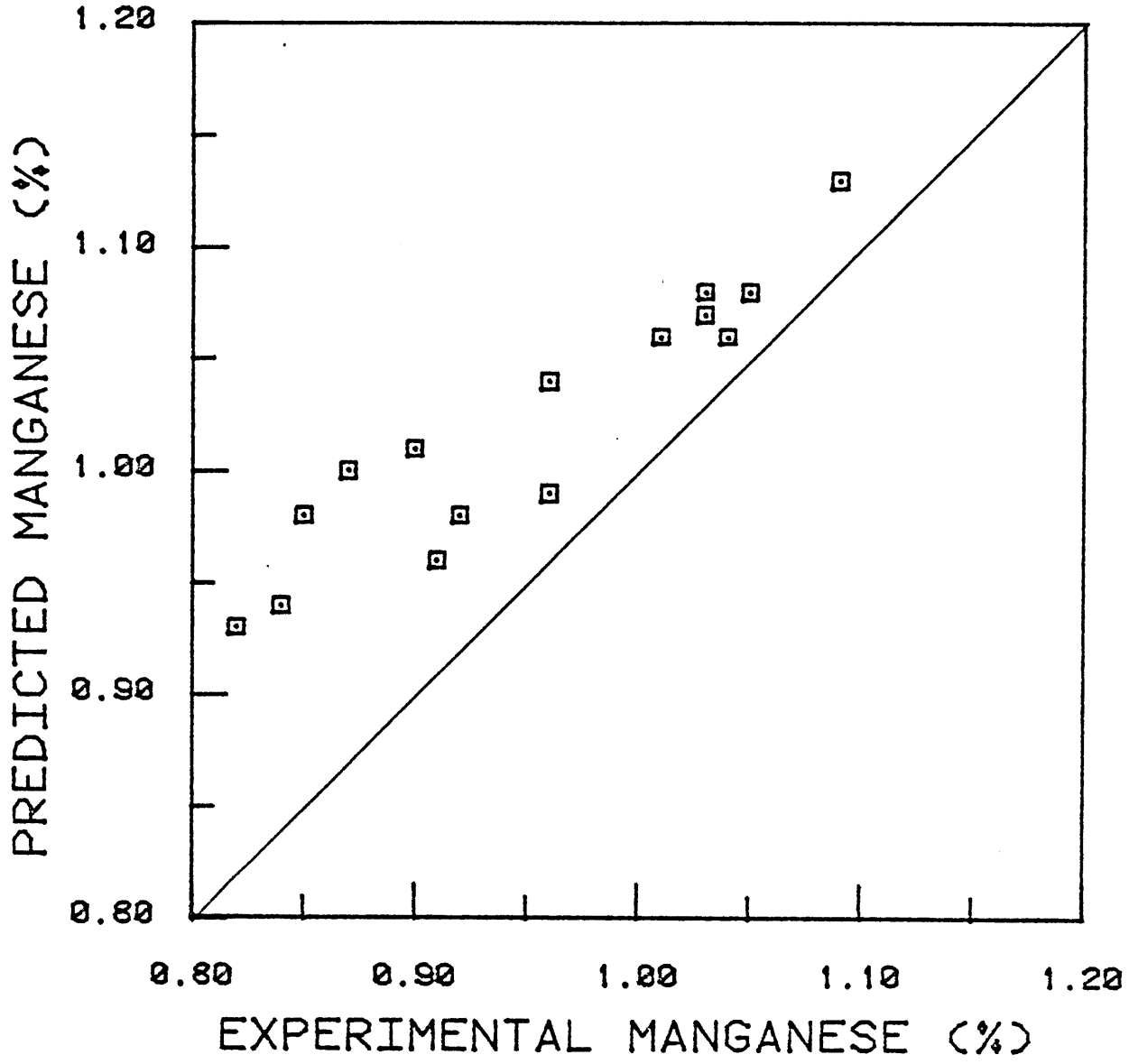

Figure 47a : Results of experiments with the magnetic arc oscillator. Flux Fx-1 (N.P. = 1.2% Mn, α = 1.7), Ax-90 electrode and 1008 baseplate used for all welds. W_s/W_m used as a measure of $A_{S/M}/V_M$.

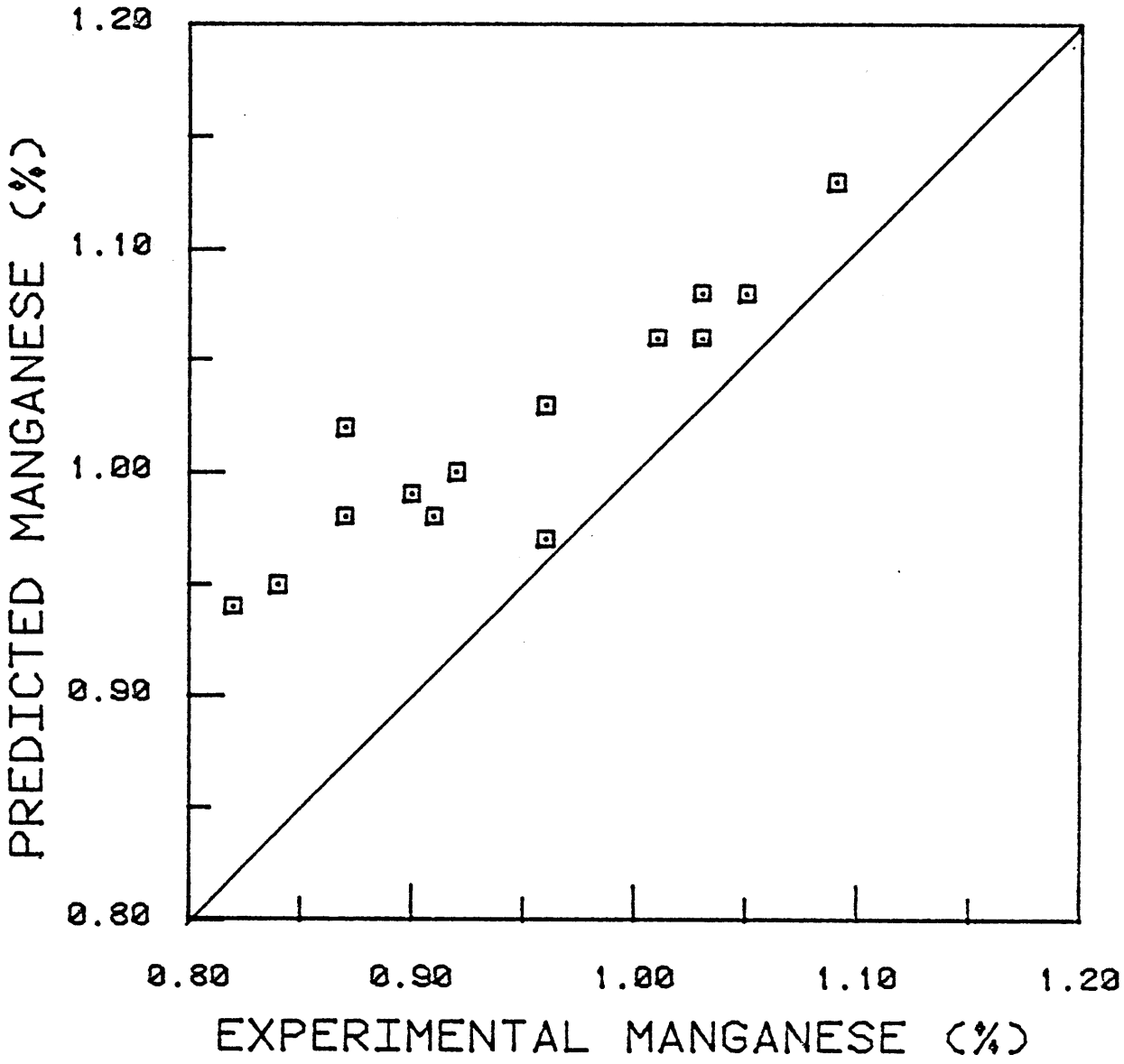

Figure 47b: Results of experiment with the magnetic arc oscillator. Same data as in Figure 36a except w/A used as a measure of $A_{S/M}/V_M$ and α = 0.2 cm.

Table 23: Results of the Experiment with the Magnetic Arc Oscillator. Electrode Ax-90, Baseplate 1008 and Flux Fx-1 Used in All Welds. Welding Conditions Held Constant at 200 A, 24 V DCEP and 40 cm/min Travel Speed.

Weld No.	Oscillator Amplitude	Oscillator Frequency (Hz)	Dilution	w/A	W_S/W_M	Mn	Si
1B	15	7	.57	3.62	0.38	0.91	.50
2A	10	7	.55	3.0	0.42	0.96	.55
3B	700	7	.58	5.91	0.73	0.92	.62
4A	300	7	.63	4.63	0.48	1.03	.56
4B	500	7	.65	5.52	0.58	0.87	.53
5A	300	25	.48	4.0	0.52	0.96	.55
5B	990	7	.40	7.20	0.85	1.09	.69
5C	990	7	.57	6.70	0.81	1.05	.67
6A	700	10	.53	5.95	0.73	1.03	.62
6B	0	0	.56	3.62	0.49	0.90	.55
6C	300	7	.61	4.40	0.46	0.85	.52
7A	100	7	.66	3.75	0.40	0.82	.47
7B	100	7	.66	3.80	0.41	0.84	.51
7C	800	7	.58	5.79	0.72	1.01	.59

Table 24: Results of Experiments with the Magnetic Arc Oscillator Electrode Ax-90, Baseplate HiP and Flux Fx-2 Used for All Welds. Welding Conditions: 200 A, 24V, 40 cm/min Travel Speed, Polarity as Indicated in Table. Oscillator Frequency Held Constant at 7 Hz.

Weld No.	Amplitude	DECP/DCEN (+) (-)	Dilution	w/A	W_S/W_M	Mn	P
11 H	100	+	.38	3.23	.38	1.23	.049
11 K	600	+	.46	4.77	.50	1.20	.053
11 E	600	+	.33	4.7	.55	1.07	.098
11 N	800	+	.44	5.0	0.60	1.05	.057
12 H	4.1	+	.55	4.1	.42	1.31	.071
13 K	300	+	.37	3.85	.40	1.25	.053
13 E		+	.27	4.12	.48	1.13	.042
13 N	200	+	.34	3.48	.41	1.17	.031
15 E	15	-	.23	4.27	.43	.78	.037
15 K	10	-	.22	4.8	.49	.75	.038
15 N	300	-	.21	5.48	.63	.98	.031
15 O	300	-	.21	5.50	.65	.98	.028

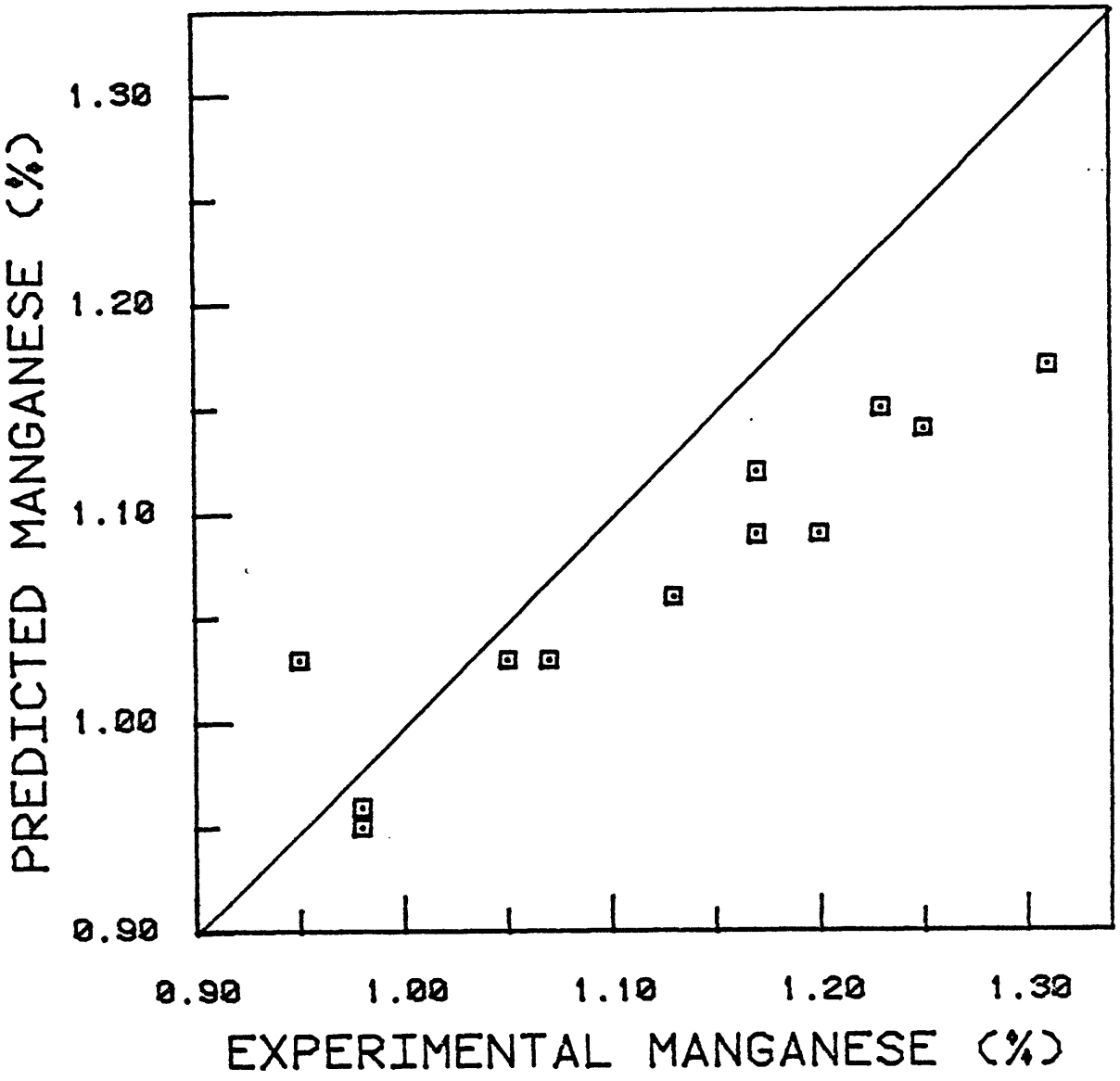

Figure 48a: Results of experiment with the magnetic arc oscillator. Flux Fx-2 (N.P. 0% Mn, α = 1.7/3), electrode Ax-90 and Hi-P baseplate used for all welds. W_s/W_m used to measure $A_{S/M}/V_M$.

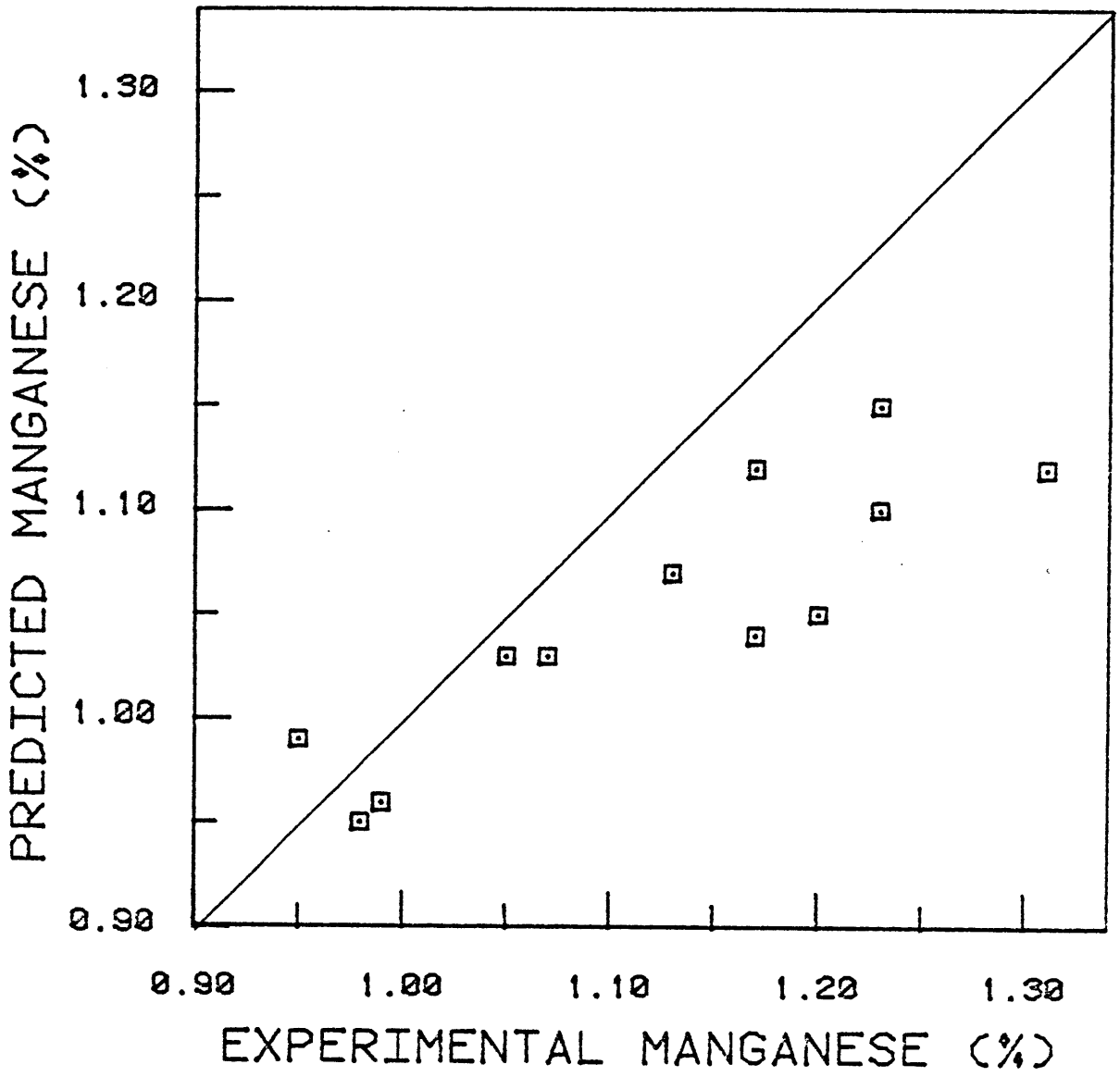

Figure 48b : Same data as Figure 37a except w/a used to measure $A_{S/M}/V_M$, α = 0.2/3 cm.

Lau [28] found that a change in welding parameters had a much larger effect on the chemical composition of welds which were made using fluxes containing large amounts of either MnO or SiO_2 as opposed to fluxes containing CaF_2 and Al_2O_3. This is not surprising considering that the former set of fluxes are highly oxidizing. Lau also found that on welding with a flux of 25% CaO-75% CaF_2, there was more loss of manganese from the weld metal than on welding with $CaO-Al_2O_3-CaF_2$ fluxes. He attributed this to oxidation by the atmosphere but his data indicate that use of the two different flux types resulted in comparable oxygen levels in the weld metal. A more likely explanation is that the larger manganese loss on using the 25% CaO-75% CaF_2 flux was due to the wider weld bead and consequently larger value of $(A_{s/m}/V_m)$ obtained on using this fluid slag ($CaO-CaF_2$) as compared to the narrower weld beads obtained by using more viscous $CaO-Al_2O_3-CaF_2$ slags. Lau [28] has also suggested that a significant loss of manganese may be occurring by vaporization inside the arc cavity as the droplets pass through the arc. However, Kim and Mclean [82] have shown that the amount of manganese lost by vaporization may be determined by the expression

$$\ln \frac{(\%Mn)_t}{(\%Mn)_o} = -2.7 \exp\left(-\frac{31870}{1.987\ T}\right) (A/V)t$$

where $(\%Mn)_o$ and $(\%Mn)_t$ are the initial and final manganese content, t the time for reaction (in s), and A and V are the surface and volume of the metal droplet. Substitution of the appropriate values for the

various terms (as indicated in Appendix A.10) shows that the manganese loss from the electrode by evaporation is expected to be less than 0.005% Mn. Lau has suggested that enhancement [40,41] due to the formation of an oxide fog may lead to greater loss. However, an enhancement factor of 20 still leads to a maximum of 0.1% Mn loss from the electrode by evaporation. The overall manganese content of the weld metal would be even less affected since metal from the electrode usually makes up less than 50% of the overall weld metal. Also, it is unlikely that an oxide fog will be present in the hotter inner part of the arc. Lau's conclusion was derived from the droplets he collected by striking an arc on a massive copper substrate under a bed of flux with the electrode travelling at a high speed. The droplets had a radius of approximately 2 mm and application of solidification theory [54] indicates that the solidification time would be about 0.25 sec (see Apendix A.7). During this time slag-metal reactions can take place and due to the high surface to volume ratio of the droplets, considerable manganese transfer can take place. This also explains the low values of manganese obtained by North in his droplets (see Appendix A.7).

6.2.3. Transfer of Silicon

The transfer of silicon may be represented by the equation

$$\underline{Si} + 2\ \underline{O} = (SiO_2) \qquad (57)$$

At the neutral point

$$K = \frac{(a_{SiO_2})_{flux}}{[N.P.]\,[a_o]_{eq}} \tag{58}$$

$$m = \frac{N.P.}{a_{SiO_2}} = \frac{1}{K[a_o]^2_{eq}} \tag{59}$$

On applying equations (33) and (38) to the results of the preliminary experiments and to the work by previous researchers [10,17,29] it is found that the equations for the transfer of silicon are identical to those for the transfer of manganese. That is equations (52a) and (b) may be used for single pass welds with highly oxidizing fluxes, equations (53a) and (b) for less oxidizing fluxes, and equations (54)-(56) for multipass welds. Figure 49 shows some of the results obtained for silicon. Other results are recorded in Appendix 12. Table 25 summarizes the results. The values of α for the transfer of silicon are the same as for manganese. This may appear surprising, however, it should be noted that in welding fluxes the partition coefficients for silicon or manganese are of the same order since

$$m_{Si} = \frac{1}{K_{Si}[a_o]^2} \tag{59}$$

$$m_{Mn} = \frac{1}{K_{Mn}[a_o]} \tag{60}$$

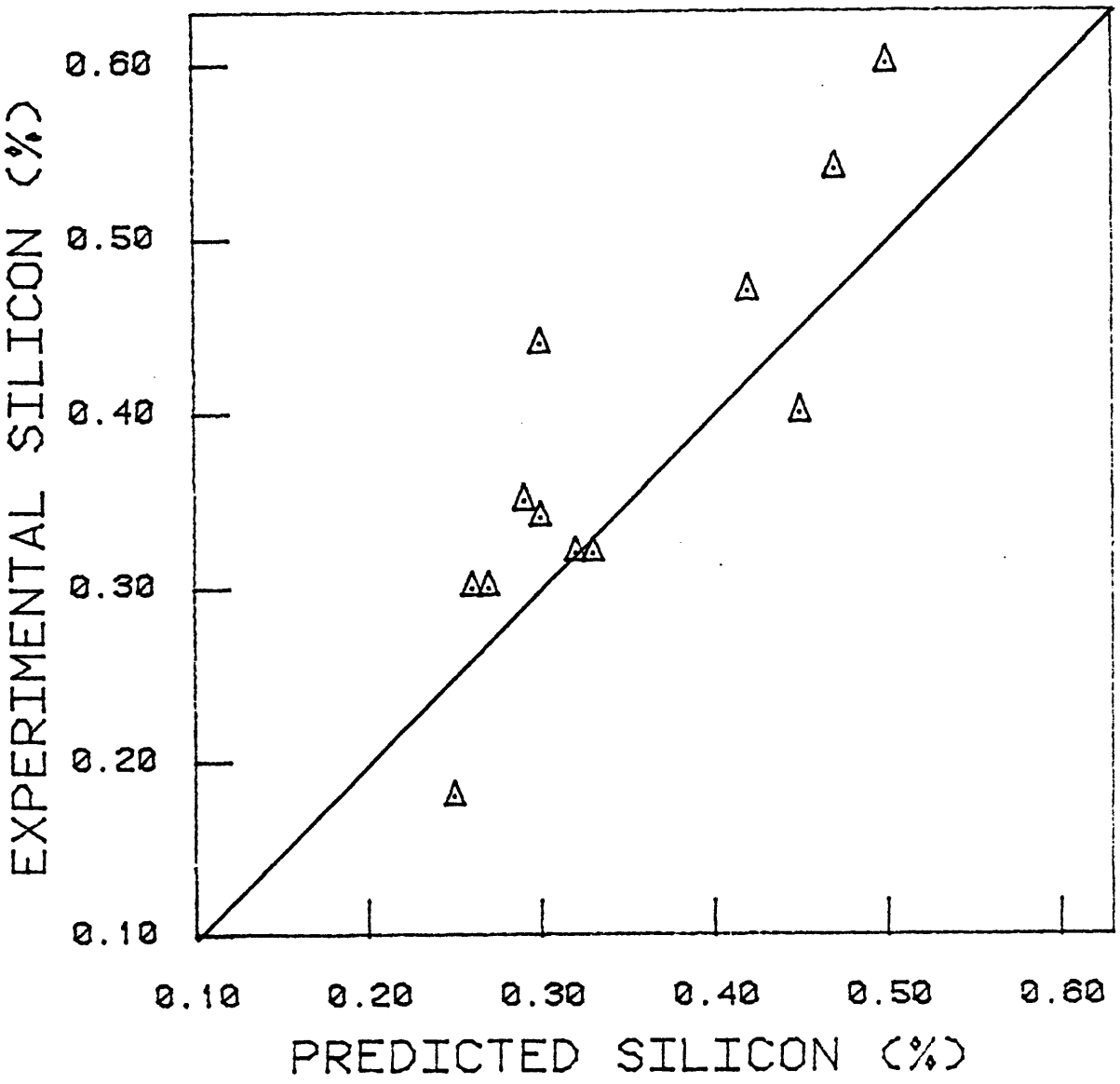

Figure 49a: Comparison of silicon content on single pass welds as predicted by theory to that obtained experimentally. Data from results of preliminary experiment. Flux Fx-1 (N.P. = 0.95% Si, α = 1.7) used for all welds.

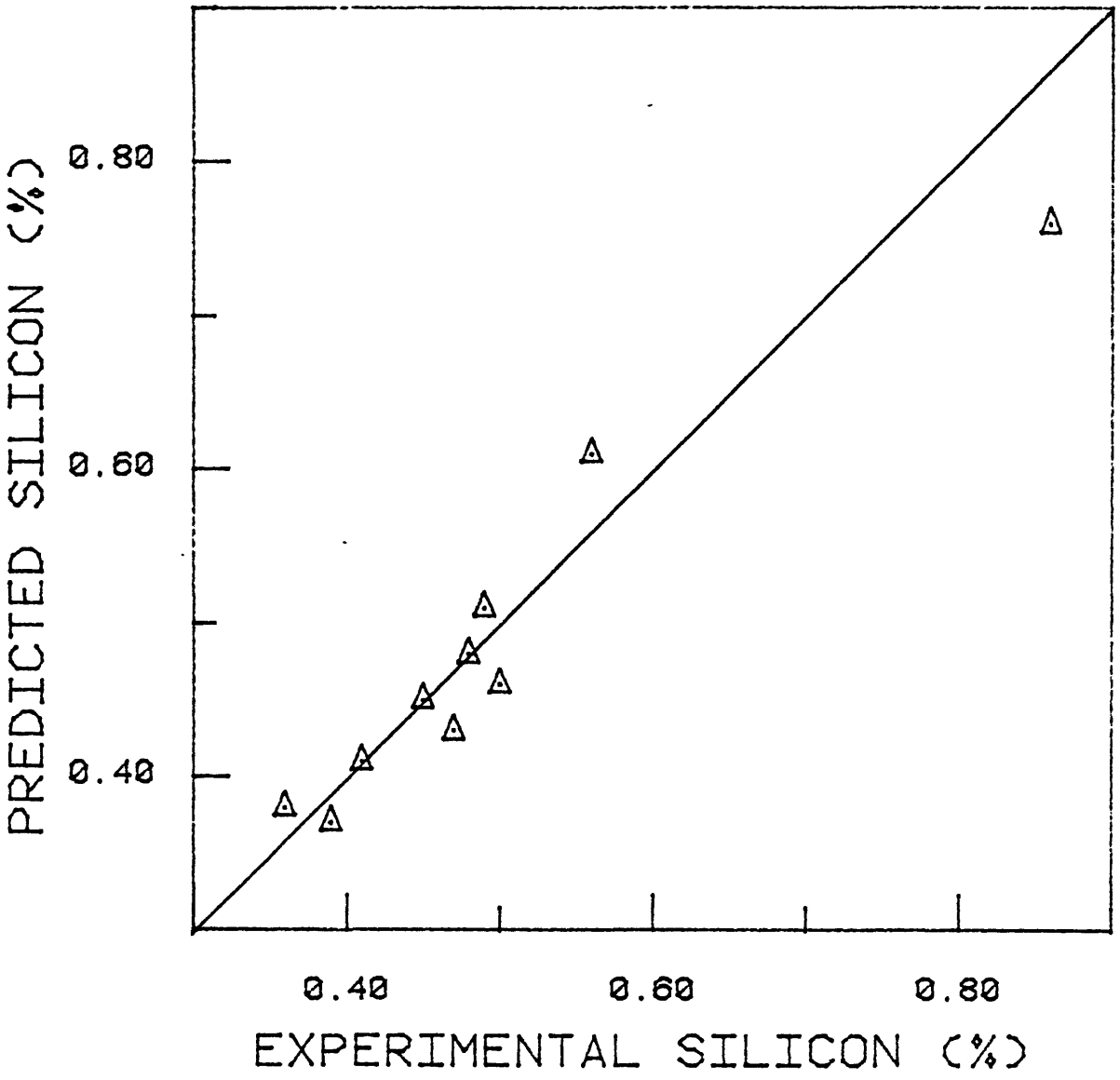

Figure 49b: Comparison of silicon content in single pass welds as predicted by theory to that obtained experimentally. Data from experimental work by Christensen using flux d (N.P. 1.2% Si, α = 1.7) [10].

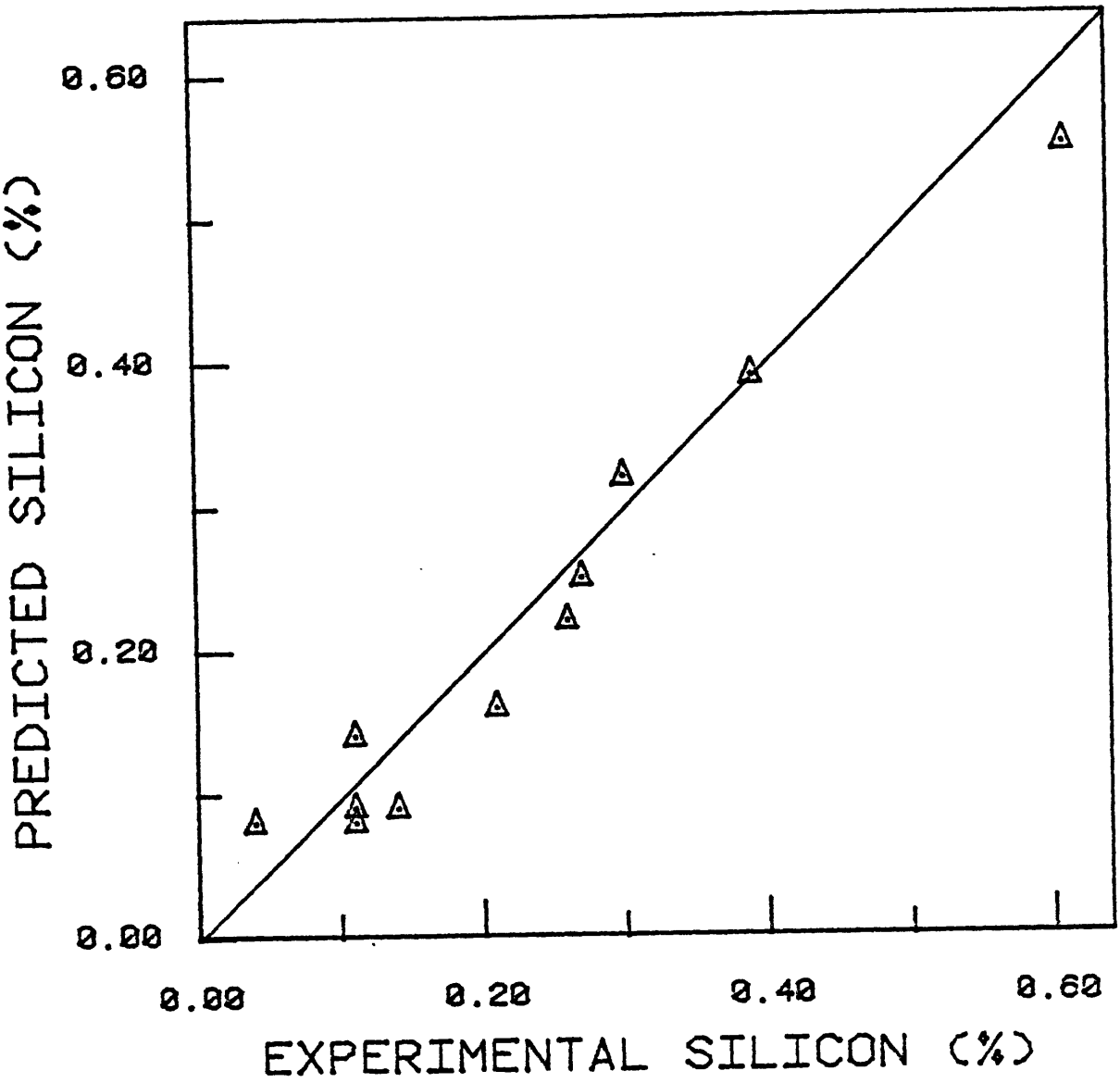

Figure 49c: Comparison of silicon content in single pass welds as predicted by theory to that obtained experimentally. Data from experimental work by Chai using flux F-2 (N.P. 0.28% Si, α = 1.7/3) [17].

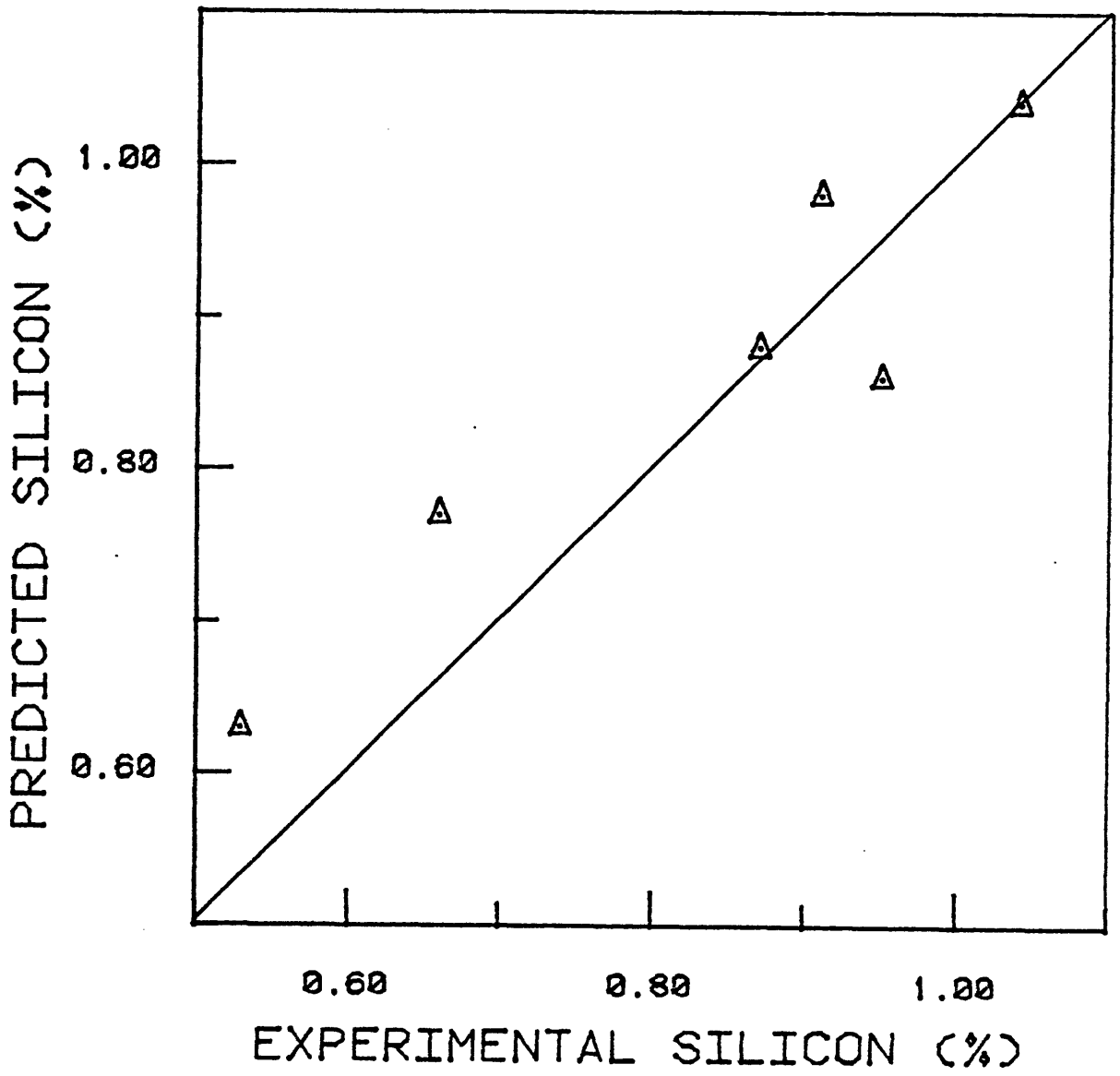

Figure 49d: Comparison of silicon content in multipass weld metal as predicted by theory to that obtained experimentally. Data from experimental work by Frumin using AN-20 flux (N.P. = 1.0% Si, α = 1.7/3) [28].

Table 25: Correlation Between Theoretical Predictions and Experimental Results for Transfer of Silicon

Researcher (Ref.)	Flux Name	Weld Type	No. of Welds	Linear Correlation Coefficient between Theory & Experiment
Present Investiga. (Preliminary Experiments)	Fx-1	Single	12	0.92
	Fx-2	Single	8	0.88
	Fx-3	Single	8	0.83
Christensen [10]	a	Single	14	0.86
	c	Single	6	0.96
	d	Single	10	0.96
	e	Single	11	0.88
	f	Single	16	0.82
Chai [17]	F-1	Single	10	0.94
	F-2	Single	11	0.97
	F-3	Single	10	0.73
	F-4	Single	10	0.68
Frumin [29]	AN-20	Multipass	7	0.96
	A-348A	Multipass	7	0.92

K_{Si} the equilibrium constant for reaction (57) is an order of magnitude greater than K_{Mn} the equilibrium constant for reaction (49). However, in equation (59), the K_{Si} is multiplied by $[a_o]^2$ and in equation (60), K_{Mn} is multiplied by $[a_o]$; so the two partition coefficients m_{Mn} and m_{Si} are comparable. The value of m_{Si} may be somewhat lower than m_{Mn}, but the value of k_s the mass transfer coefficient of silicon in the slag will be lower than that for manganese [43] so the ratio (k_s/m) should not change very much. If mass transfer in the slag is the rate controlling step then the similarity between manganese and silicon transfer should not be very surprising. Chai's data on the spatial distribution of silicon (see Figure 35) indicates that silicon transfer is controlled by mass transport in the slag. However the technique that he used has an estimated error of ±5% [17], and the concentration gradient observed for silicon lies in this error band.

Experiments were also conducted to directly verify the kinetic model by performing experiments to change the $(A_{s/m}/V_m)$ ratio directly without changing the welding parameters. The experiments were performed using a water-cooled copper mold and an arc oscillator. The details of the experiments are listed in Tables 22 and 23 and the results are shown in Figures 50 and 51, respectively. The results again confirm our theory.

Belton [11] studied the transfer of silicon on welding with calcium silicate fluxes. He used fluxes containing ferrosilicon as well as simple $CaO-SiO_2$ fluxes. In this section, only his results with the simple $CaO-SiO_2$ fluxes will be discussed, the results with

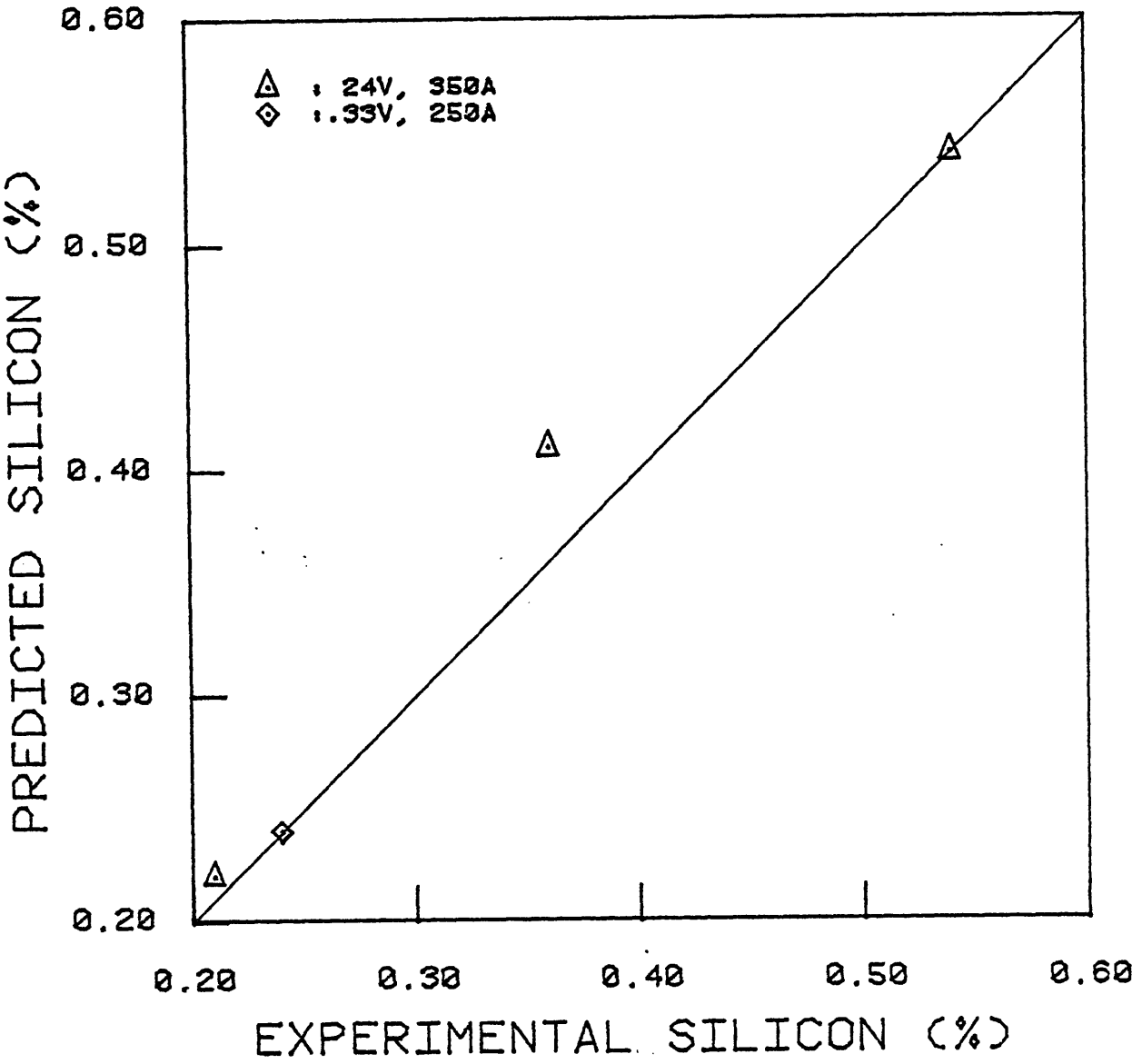

Figure 50 : Results of experiment with the water-cooled copper mold. Flux Fx-1 (N.P. 0.95% Si, α = 1.7) and A-7 electrode used for all welds.

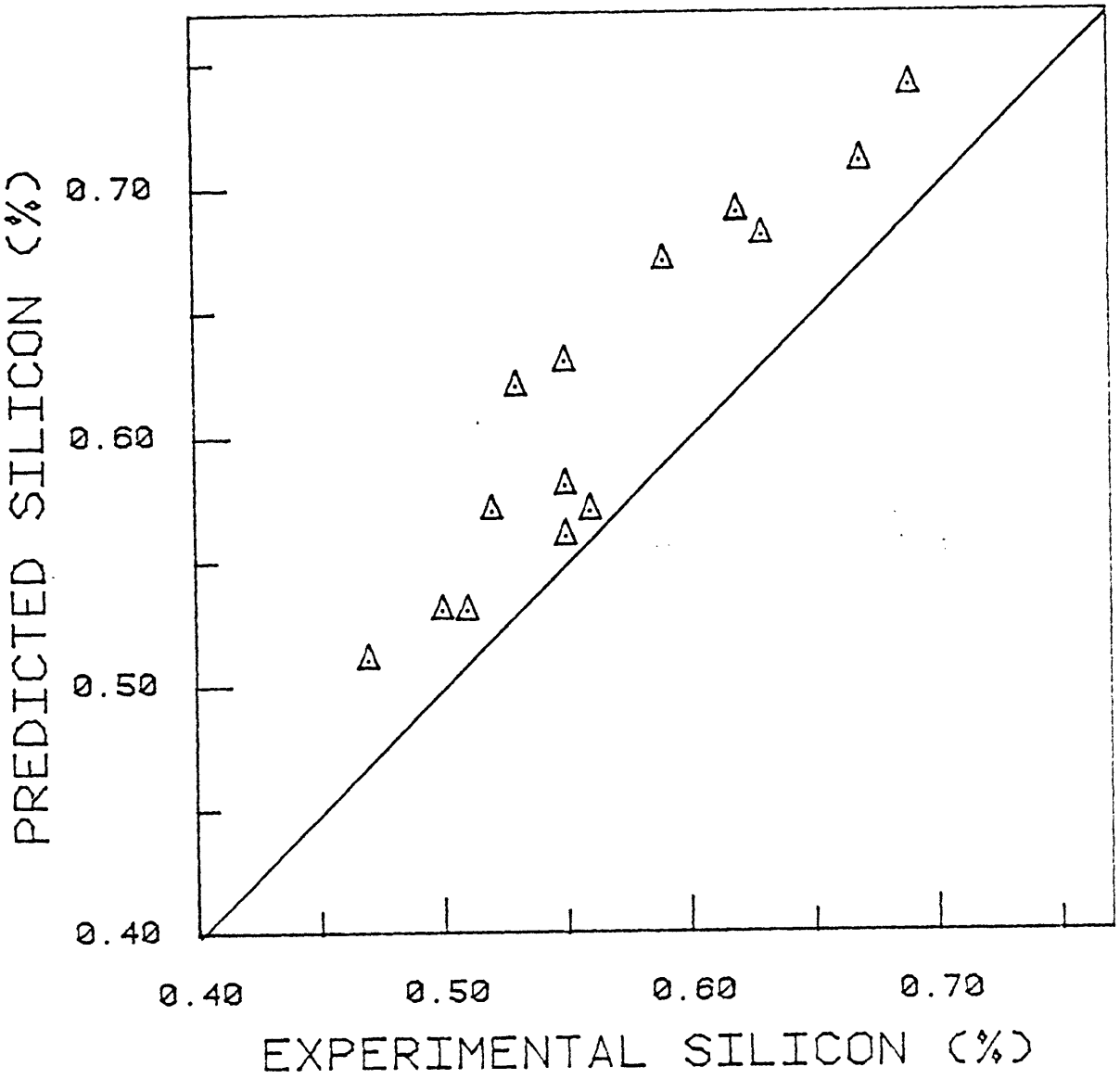

Figure 51a: Results of experiment with the magnetic arc oscillator. Flux Fx-1 (N.P. 0.95% Si, α = 1.7), Ax-90 electrode and 1008 baseplates used for all welds W_s/W_m used as a measure of $A_{S/M}/V_M$.

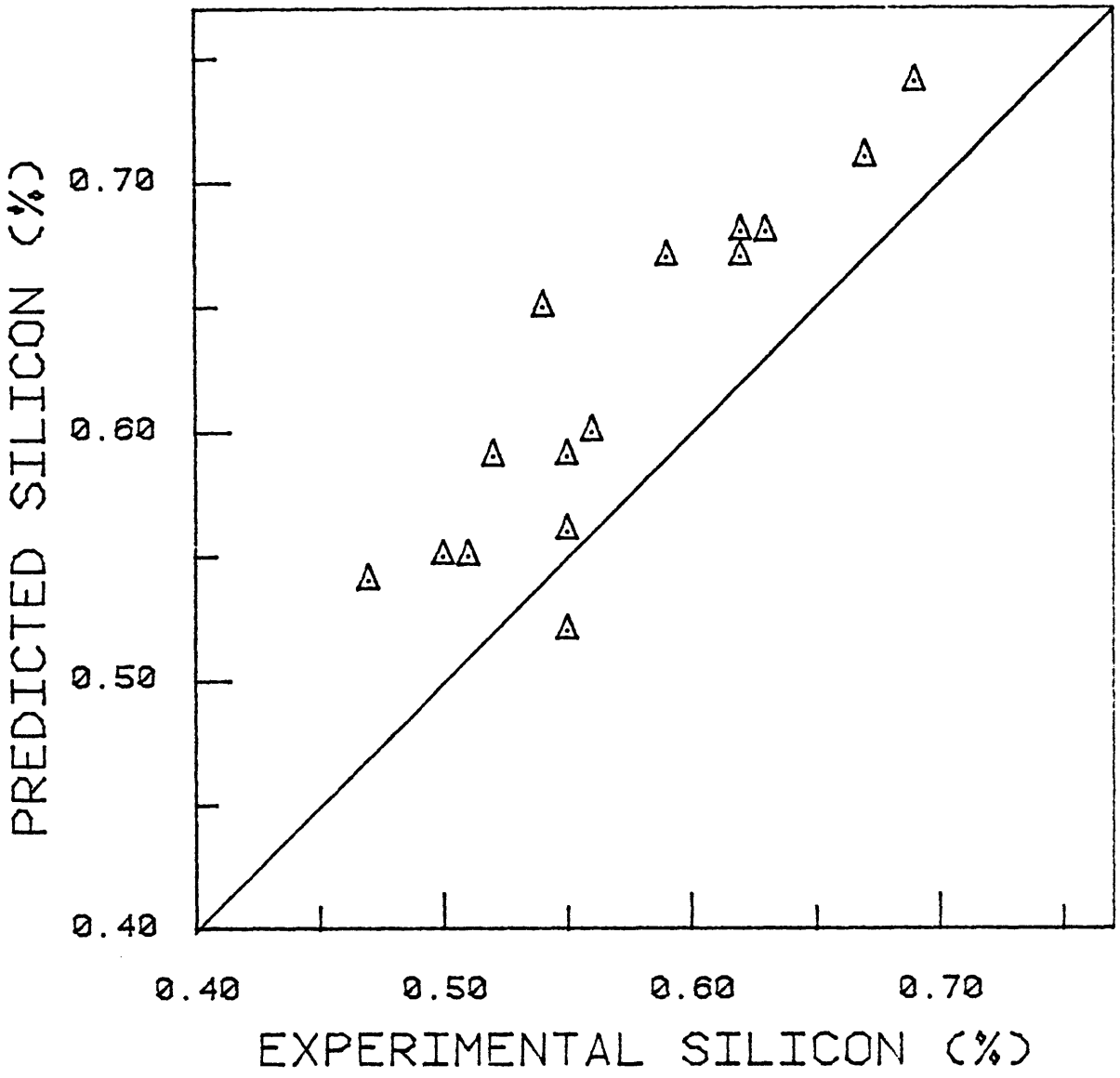

Figure 51b: Results of experiment with the magnetic arc oscillator. Same data as in Figure 43a except w/A used as a measure of $A_{S/M}/V_M$, α = 0.2 cm.

fluxes containing ferro-silicon are dealt with in a later section (Section 5.2.9). The simple $CaO-SiO_2$ fluxes used by Belton contained less than 1% FeO and only 2-3% Na_2O. The balance (96-98%) was made up of either CaO or SiO_2 with the SiO_2/CaO ratio being varied from 1 to 7.5. The welding electrode and base plate, contained less than 0.04% silicon, and the welding parameters were kept constant. Belton considered the slag and metal to be at equilibrium in the range 1930-2030°C. This was indicated by his experimental data, as shown in Table 26. It shows that when the activity of SiO_2 increases from 0.18 to 0.30, the amount of silicon increases from 0.10 to 0.31%. However, when the activity of SiO_2 increases from 0.3 to 0.80 the amount of silicon increases from 0.31% to 0.36% and then drops off to 0.29%. The concentration of oxygen, however, keeps on increasing from 0.10% when a_{SiO_2} = 0.18 to 0.22 when a_{SiO_2} = 0.80. Also the amount of FeO in the slag increases from 4.91% to 10.3% when a_{SiO_2} changes from 0.18 to 0.80. (The fluxes contained less than 1% FeO initially.) This clearly indicates that

1. The transfer of silicon and oxygen is not simultaneous, that is, SiO_2 is not decompossing by a one-step process.
2. Kinetic factors are involved in the transfer of silicon.

Neither the droplet time theory or the effective equilibrium theory can explain the result seen in Table 26. Examination of the data presented by Belton in the same paper on the influence of flux composition on weld geometry explains the results. Figure 52a shows macrophotographs of weld beads made with different slags. Also

Table 26: Results of Belton on Silicon and Oxygen Transfer in Simple $CaO - SiO_2$ Fluxes [11]

% SiO_2	a_{SiO_2} (as computed by Belton)	% Si	% O	K	T(°C)
47.6	0.18	.10	.10	180	1931
49.2	0.19	.12	.12	106	1969
50.5	0.20	.23	.09	107	1970
54.6	0.30	.31	.12	67	2007
55.7	0.32	.27	.13	70	2003
58.0	0.40	.36	.13	66	2009
67.2	0.71	.31	.17	79	1994
70.2	0.74	.29	.26	38	2054
74.1	0.80	.29	.22	57	2020

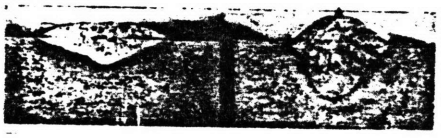

Figure 52a: Macrophotographs showing the influence of slag composition on the contours of the weld bead. Left - run no. 1 (47.6% silica); right - run no. 6 (74.1% silica) [from ref. 11].

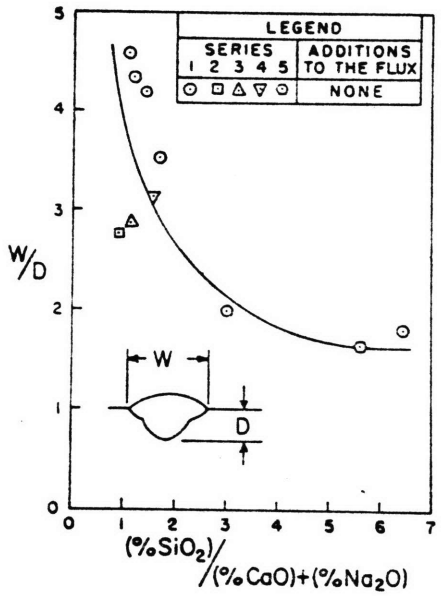

Figure 52b: The influence of the acidity ratio on the width to depth-of-penentration ratio of the weld bead. Data are taken from the experiments with simple fluxes [from ref. 11].

Figure 52b shows the influence of the ratio of $\%SiO_2$ to ($\%CaO + \%Na_2O$) on the depth to pentration ratio for the different fluxes used. Thus when a more acid flux was used, that is when the SiO_2 content was increased, the more viscous flux gave a lower ($A_{s/m}/V_m$) ratio thus lowering the amount of silicon transferred, although the thermodynamic driving force for the silicon transfer was larger due to the larger value of a_{SiO_2}. The oxygen, however, did keep on increasing with increasing a_{SiO_2} sainces it is transferred mainly in the droplet stage. Thus, a close examination of Belton's data confirms the new theory. Belton's data are also important because they indicate that in addition to flux composition and the welding parameters, flux viscosity may also play an important role in determining weld geometry which consequently influences alloy transfer.

6.2.3. Transfer of Chromium

The transfer of chromium is more difficult to study than the transfer of manganese or silicon, since chromium exhibits several oxidation states in the slag [16,83]. If the equation

$$\underline{Cr} + x\underline{O} = (CrO_x) \qquad (61)$$

is used to represent the transfer of chromium then the equilibrium constant

$$K = \frac{(a_{CrO_x})}{[a_{Cr}]\,[a_{\underline{O}}]^x_{eq}} \qquad 62$$

where x is a number in the range $1 \leq x \leq 1.5$ [83]. In earlier work, it was shown that a singular neutral point existed for chromium transfer [16]. Also from data recorded in previous work [16] the partition coefficient m is determined to be about 20 for calcium-silicate-chromate fluxes ($m = N.P./a_{Cr_2O_3} \simeq 20/1$). This is several times greater than the partition coefficient for manganese or silicon. If the kinetics of chromium are controlled by transport in the slag phase then the transfer of chromium between the metal and the slag should be much lower than the transfer of manganese or silicon. Furthermore, the lower rate of transfer should occur when chromium is being transferred from the metal to the slag or the reverse. Application of equations (33) and (38) to the results of previous work [16,29] confirms that transport in the slag phase is rate controlling. The equations used for single pass welds are

$$M_f = N.P. - (N.P. - M_i) \exp\left(-\frac{1.7}{9} (W_S/W_M)\right) \tag{63}$$

for less oxidizing fluxes, and

$$M_f = N.P. - (N.P. - M_i) \exp\left(-\frac{1.7}{3} (W_S/W_M)\right) \tag{64}$$

for highly oxidizing fluxes. For the multipass welds made by Frumin with a less oxidizing flux, the equation is

$$M_f = M_{e\ell} + \frac{(N.P. - M_{e\ell})(1 - F)}{1 - Fd} \tag{38}$$

with

$$F = \exp\left(- \frac{1.7}{9} (W_S/W_M)\right) \tag{65}$$

The results are shown in Figures 53 and 54. Table 27 from work by Frümin, shows that the transfer of chromium is much lower than that of manganese with a flux free of both chromium and manganese and justifies the earlier arguments that transport in the slag phase is rate controlling.

6.2.4. Transfer of Nickel, Molybdenum, Copper and Other 'Noble' Elements

In previous work, it had been shown that there is negligible loss of relatively 'noble' elements such as nickel, molybdenum and copper [16]. However, the theory developed in Chapter 4 must also be able to rationalize the transfer of these elements. It should be noted that equation (33) was derived from the more general equation (31), by letting the factor $\beta \simeq 0$. However, this approximation $\beta = 0$ is no longer valid for the transfer of nickel, molybdenum, copper or other 'noble' elements.

The value of β is given by the equation

$$\beta = m\gamma b \tag{26}$$

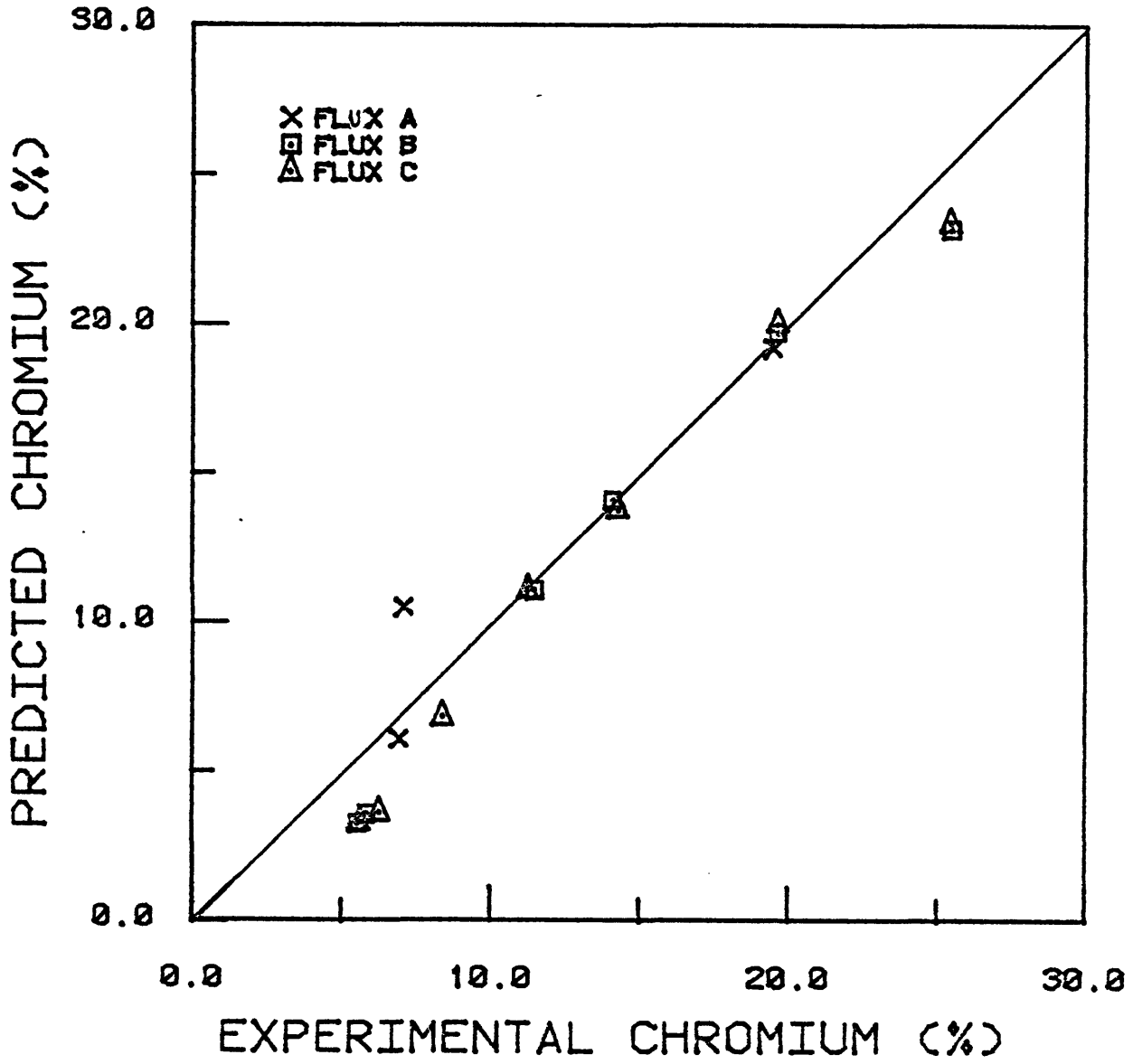

Figure 53a: Comparison of chromium content in single pass weld metal as predicted by theory to that obtained experimentally. Data is for $CaO-Cr_2O_3-SiO_2$ fluxes [N.P. 19.6% Cr, α = 1.7/9] [from ref. 16].

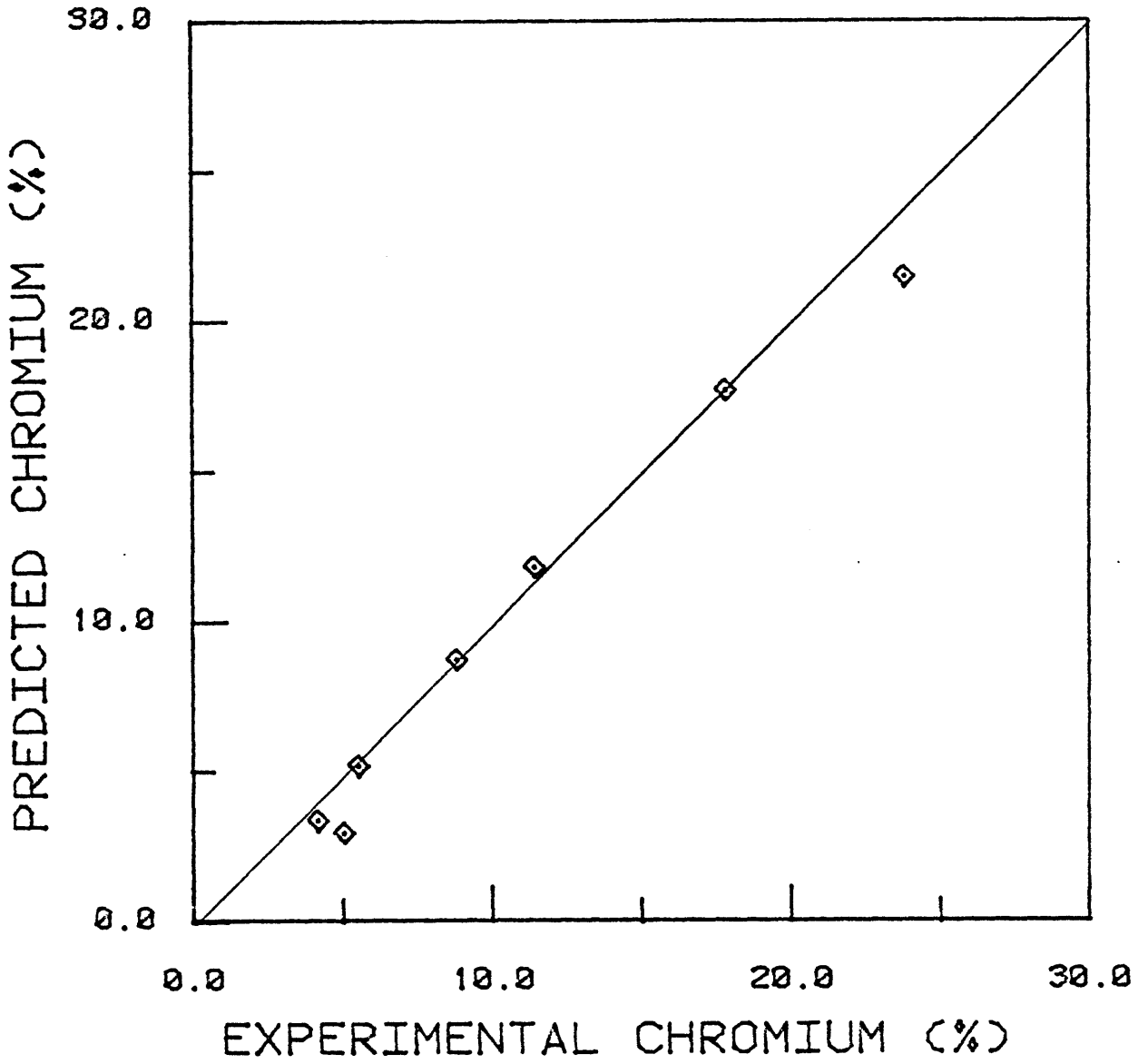

Figure 53b : Comparison of chromium content in single pass weld metal as predicted by theory to that obtained experimentally. Data is for $MnO-Cr_2O_3-SiO_2$ fluxes [N.P. 8.7% Cr, α = 1.7/3] [from ref. 16].

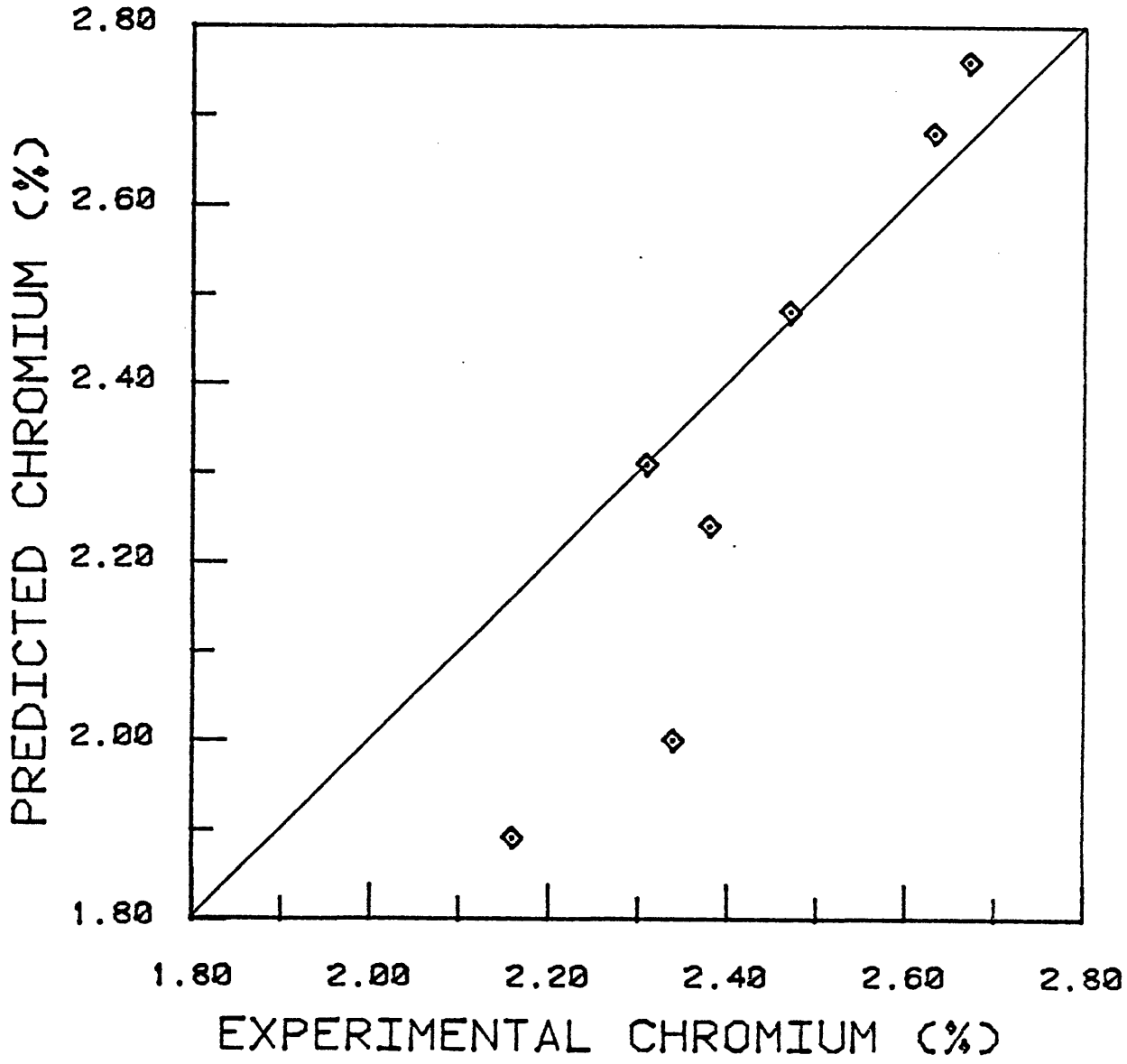

Figure 54: Comparison of chromium content in multipass weld metal as predicted by theory to that obtained experimentally. Data is for flux AN-20 used by Frumin [28], N.P. = 0.00% Cr, α = 1.7/9.

Table 27: Comparison of Manganese and Chromium Transfer in Multipass Weld with a 1.55% Mn, 2.92% Cr Electrode and AN-20 Flux (N.P. 0% Mn, 0% Cr) [Data from Ref. 28.]

Weld No.	Amount of Alloying Elements Transferred to Slag		Normalized Amount of Alloy Transferred	
			$\Delta Mn^* = \Delta Mn/1.55$	$\Delta Cr^* = \Delta Cr/2.92$
	ΔMn	ΔCr	ΔMn^*	ΔCr^*
I	-0.82	-0.61	-0.53	-0.20
II	-0.98	-0.76	-0.63	-0.26
III	-0.92	-0.58	-0.64	-0.20
IV	-0.49	-0.45	-0.32	-0.15
V	-0.70	-0.54	-0.45	-0.18
VI	-0.17	-0.25	-0.11	-0.08
VII	-0.45	-0.29	-0.29	-0.09

*normalized by dividing by the thermodynamic force (N.P. - M_{el})

where m is the partition coefficient, γ the activity coefficient of the oxide and b is a mass balance factor. For the elements such as Ni, Mo, or Cu the partition coefficient 'm' is at least 4 or 5 orders of magnitude greater than the partition coefficient for Si, Mn or Cr. [This is because m is inversely proportional to the equilibrium constant K.] The values for the equilibrium constant for equations leading to the formation of the unstable oxides NiO, MoO_2 or Cu_2O are much lower than those for the more stable oxides SiO_2, MnO or Cr_2O_3.] Thus now $\beta >> 1$ (typically $\beta > 10$) for the transfer of Ni, Mo or Cu. Equation (31) may also be written as

$$M_f = \frac{N.P.}{1 + \beta} + \frac{\beta}{1 + \beta} [M_i] - \frac{[N.P. - M_i]}{1 + \beta} * \exp[-(A/V)(1 + \beta)\alpha] \quad (31a)$$

If the flux is initially free of the oxides of these 'noble' alloying elements as is generally the case, then N.P. = 0 and since $\beta >> 1$

$$M_f \simeq M_i \quad (66)$$

Thus, as observed experimentally, the amount of noble alloying elements such as Ni, Mo or Cu in the weld metal will be that expected from a simple mixture of electrode and baseplate compositions.

6.2.5. Transfer of Phosphorus

The transfer of phosphorus may be represented by the reaction [67]:

$$2\underline{P} + 5\underline{O} = (P_2O_5) \qquad (67)$$

This reaction is highly exothermic so the transfer of phosphorous should be highly temperature sensitive. Kawai et al. [64] have noted that the mass transfer coefficient of phosphorous in slag is of the same order as that of manganese in the slag. Equation (52) was used to study the transfer of phosphorous between a calcium silicate flux and a 0.1% P, rephosphorized steel baseplate supplied by Bethlehem Steel Corp. An arc oscillator was used to change the slag to metal ratio. Also welds were made using both electrode negative and electrode positive. The experimental conditions are listed in Table 24 and the results shown in Figure 55. The figure indicates good agreement between theory and experiment and justifies our hypothesis that the temperature of the weld pool around the arc over which the chemical reactions take place does not change very much when the welding parameters are changed. Our results contradict the claims of Thier [34,35] that electrode positive results in a higher weld pool temperature and an increase in current results in a drop of the pool temperature. Thier's conclusions were based on his experimental results [Figure 56] but these may be explained by the theory from

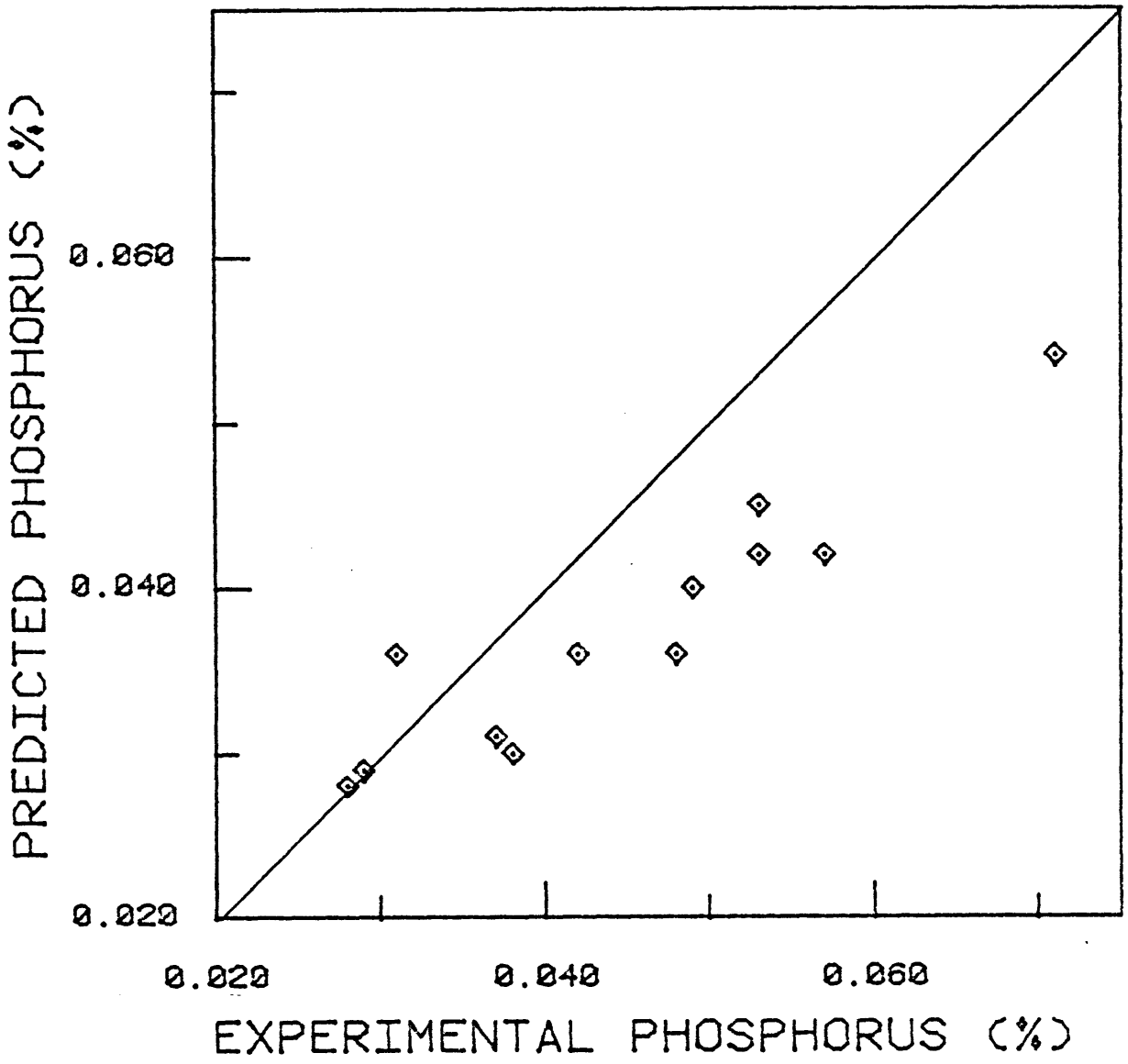

Figure 55 : Results of experiment with the magnetic arc oscillator comparing phosphorous transfer as predicted by theory to that obtained experimentally. Flux Fx-2 [N.P. 0.016% P (assumed), α = 1.7/3].

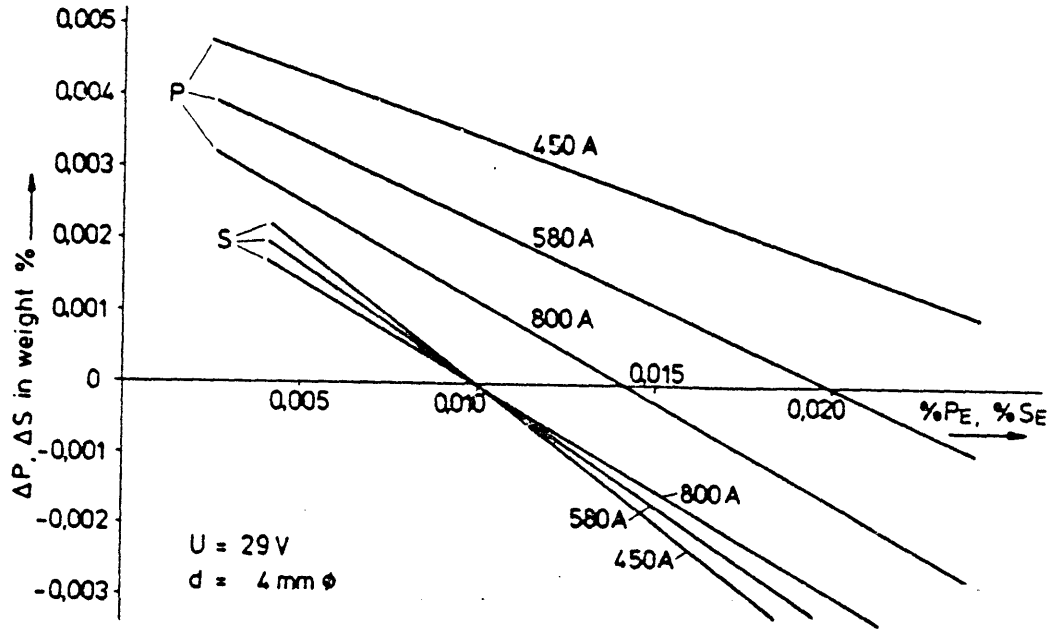

Figure 56: Thier's results on effect of welding current on the transfer of sulphur and phosphorous using flux LW280 [from ref. 35].

presented here. It should be noted that when phosphorous is being transferred from the slag to the metal, in addition to reaction (67), there may be some direct dissolution of phosphorous into the metal. For example, the flux may contain phosphorous as phosphides such as iron phosphide and some of it can directly dissolve into the metal before being converted to phosphate ions. This phenomenon will be considered in detail later and Thier's results are explained in the later section on alloy fluxes [see Section 5.2.9].

6.2.6. Transfer of Sulphur

Unlike the other elements, sulphur in the metal phase is removed by the reduction reaction

$$\underline{S} + (O^{2-}) = (S^{2-}) + \underline{O} \qquad (68)$$

and not by oxidation. This reduction reaction has been shown to occur in steel making, and it is likely that it is responsible for transfer of sulfur during submerged arc welding, since at the higher temperatures encountered in submerged arc welding, sulfur removal by oxidation would be even more difficult. It is necessary to clarify this point since in standard welding literature [55] it is noted that sulfur is removed by an oxidation mechanism. In earlier work, it was shown that a neutral point exists for sulfur for both highly oxidizing manganese silicate fluxes and for less oxidizing calcium silicate fluxes [16]. Since equation (68) is a reducing reaction and not

a oxidizing reaction (eq. 11), the rate of transfer of sulphur in highly oxidizing fluxes should be equal to or less than that obtained on using the less oxidizing fluxes, if mass transfer in slag phase is rate controlling (unlike the transfer of the other elements Si, Mn, Cr and P). Examination of previously recorded data shows this to be the case. Equation (52) was applied to the data for sulfur and Figure 57 shows the results. However, it should be noted that variation in sulfur content may occur in different batches of the same flux, so too much emphasis cannot be placed on the quantitative values obtained. (The values of the neutral point for sulfur were taken from earlier experimental data on the same flux batches [16]. If the sulfur content of the flux is changed, the neutral point changes.)

6.2.7. Transfer of Carbon

During submerged arc welding, carbon is usually oxidized by the reaction

$$\underline{C} + \underline{O} = CO(g) \qquad (69)$$

and the metal thus loses some carbon. However, in exceptional cases, such as on welding very low austenitic steel with fluxes prepared in carbon lined vessels, the metal can gain carbon [16]. Usually the carbon contents of the electrode and work piece are kept low to minimize cracking, and the transfer of carbon is not as great

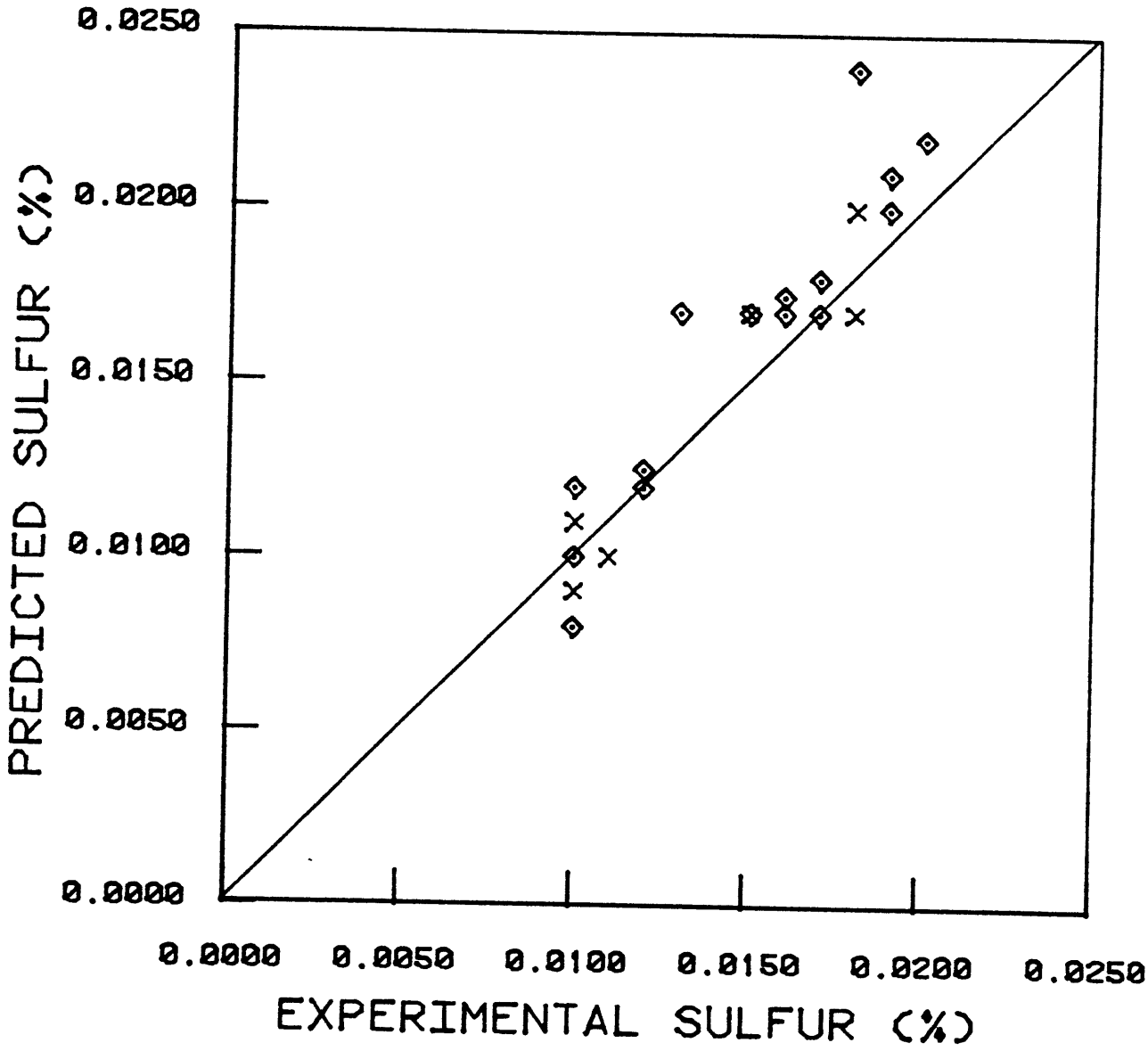

Figure 57: Comparison of sulfur content in single pass weld metal as predicted by theory to that obtained experimentally. Data is for welds made with fluxes A, B, C and D (from ref. 16).

as the transfer of other alloying elements. There are very few data available and in many cases the accuracy of chemical analysis is of the same order as the changes in carbon level during the welding process. As expected, oxidizing fluxes produce lower carbon in the weld metal [16]. Thier's data [34](Figure 35) indicate that the transfer of carbon is similar to the transfer of other alloying elements in that it is influenced in the same manner by current. This is probably due to a change in the $A_{s/m}/V_m$ ratio. His data indicate that voltage has little effect but this observation cannot be explained either by his droplet theory or by direct application of our theory. However, closer examination of his data indicates that the carbon content remains constant at the neutral point on using different voltages and this may indicate that reaction (69) is fairly rapid at the slag metal interface. Once again it should be emphasized that the magnitude of the carbon transferred is small so errors in chemical analysis can also be responsible for the data.

6.2.8. Oxidation of Iron

Most welding fluxes in use today contain less than 1% iron oxide. However, during the welding process part of the iron is oxidized so that the iron content of slags is usually in the range 1-6% FeO [10,11,16,58].

The oxidation of iron may be represented by the reaction

$$Fe + \underline{O} = (FeO) \qquad (70)$$

It should be noted that since the flux usually contains less than 1% iron oxide, the oxygen potential of the flux is certainly not controlled by the iron oxide. Rather the oxygen potential of the flux is controlled by the decomposition reactions of various other oxides such as SiO_2, MnO and Al_2O_3 which are present in large quantities, into suboxides and oxygen. In the zone of weld pool reactions, part of the iron reacts with the oxygen to form the additional iron oxide in the slag.

6.2.9. Element Transfer on Using Alloy Fluxes

The discussion so far has been on fluxes free of either ferro-alloys or elemental additions (such as nickel or chromium powder additions). The theory as developed in Chapter 4 does not take into account such additions. Consequently the equations (31) and (33) have to be modified if the welds are made with such alloy fluxes. To analyze the effect of these alloy additions, different steps may be considered:

1. Part of the 'alloy' present in the slag goes directly into the weld pool in the zone of weld pool reactions, thus changing the initial or 'nominal' metal composition

$$M_i' = M_i + \eta M_{F\ell} (W_S/W_M) \tag{71}$$

or

$$M_i' = M_{e\ell}(1 - d) + M_{BP} d + \eta^* M_{F\ell} * (W_S/W_M) \tag{72}$$

where η is an efficiency factor; it indicates the fraction of the alloying element present in the slag which enters the weld pool and $M_{F\ell}$ is the weight percent of alloying element M present in the flux either as elemental or as ferroalloy.

2. Chemical reactions occur in the zone of dilution and weld pool reactions. The amount of the alloying elements present after these reactions occur may be determined by using equation (33) for elements such as Si, Mn and Cr. However, M_i' is now substituted instead of M_i in equation (33) to give the new equation

$$M_f = N.P. - (N.P. - M_i') \exp(-\alpha A_{s/m}/V_m) \tag{73}$$

or

$$\Delta M = M_f - M_i = (N.P. - M_i')(1 - \exp(-\alpha A_{s/m}/V_m)) + \eta(W_S/W_M)M_{F\ell} \tag{74}$$

For multiple pass welding using a procedure similar to that in Appendix A.5 and using equations (73) and (72) as the starting equations, again a steady state composition M_N is obtained:

$$M_N = M_{e\ell} + (N.P. - M_{e\ell}) \frac{(1 - F)}{(1 - Fd)} + \frac{\eta M_{Fe}(W_S/W_M)}{1 - Fd} \tag{74}$$

or

$$M_N = M_N - M_{e\ell} = (N.P. - M_{e\ell}) \frac{(1 - F)}{(1 - Fd)} + \frac{\eta M_{F\ell} (W_S/W_M)}{1 - Fd} \quad (74a)$$

For the transfer of more noble elements, such as Ni, Mo, or Cu (see Section 5.2.4)

$$M_f = M_i' \quad (75)$$

for single pass welds. For multiple pass welds

$$M_N = M_{e\ell} + \frac{\eta M_{F\ell} (W_S/W_M)}{1 - d} \quad (76)$$

3. In the analysis presented in Chapter 4 on unalloyed fluxes the amount of alloy transferred in the zone of cooling and solidifying weld pool was considered to be negligible. This assumption is no longer valid when the fluxes contain large amounts of ferroalloys. However, Belton's data on the spatial distribution of silicon in the weld metal as influenced by addition of ferrosilicon to the flux (Figure 58) indicate that transfer of alloying elements on this zone becomes important only when there is more than 4% ferroalloy in the flux.

There are very few data available in the literature on element transfer on using alloy fluxes. Comparison of the data recorded by Bagryanski [84] on fluxes with addition of 4% nickel

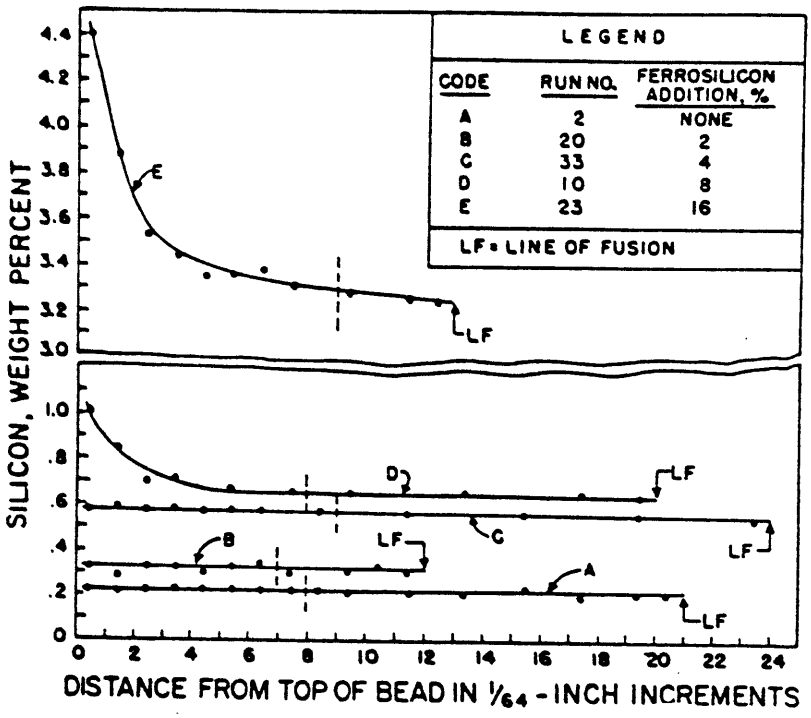

Figure 58: The spatial distribution of silicon in the weld metal as influenced by the addition of ferrosilicon to the flux. The vertical dashed lines represent the level of the plate surface.

powder to the data of other researchers using similar fluxes free of nickel [29] indicates that η is about 50%.

Due to the lack of data it is difficult to make quantitative comparisons, however a qualitative assessment of the effect of the alloying elements can be made by using equations (33a) and (38a). Earlier using equations (33a) and 38a), the transfer of alloying elements in oxide or 'unalloyed' fluxes was presented schematically in Figure 28. On using equations (73a) and (74a), the transfer of the alloying elements is represented by Figure 59. From the figure, it can be seen that for alloy fluxes a change in welding parameters can change the 'direction' of transfer, that is on changing the welding parameters the metal can gain alloying elements instead of losing or the reverse. Thus in Figure 59, at point A, the metal gains alloying element but at point B it loses alloying element. Comparison of data presented by Thier on alloy flux 10.80 (Figure 60) shows similar results. On increasing current the $(A_{s/m}/V_m)$ or the (W_S/W_M) ratio is decreased so the lines are shifted to the left. An opposite effect is expected for increases in voltage.

In Section 5.2.5, Their's results for phosphorus transfer were discussed (Figure 48). Since the phosphorus present in the flux need not have existed initially only as phosphate but could also exist as phosphide (such as iron phosphide Fe_3P) which is analogous to ferroalloys, and the results should be similar to Figure 59. Comparison of Figures 56 and 59 make this quite evident.

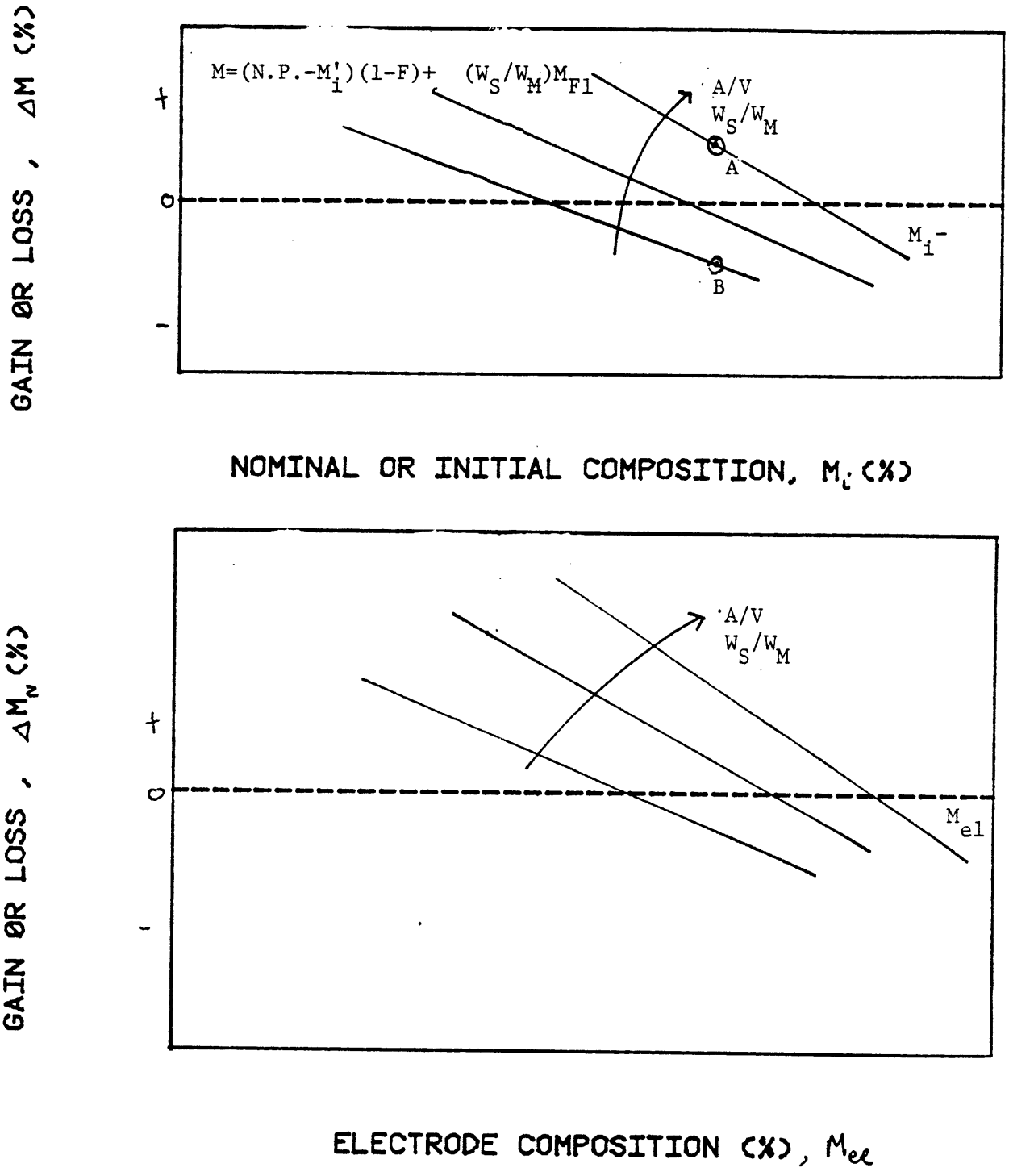

Figure 59 : Schematic figure illustrating the transfer of alloying elements on welding with 'alloy' fluxes in (a) single pass welds, (b) in multipass welds.

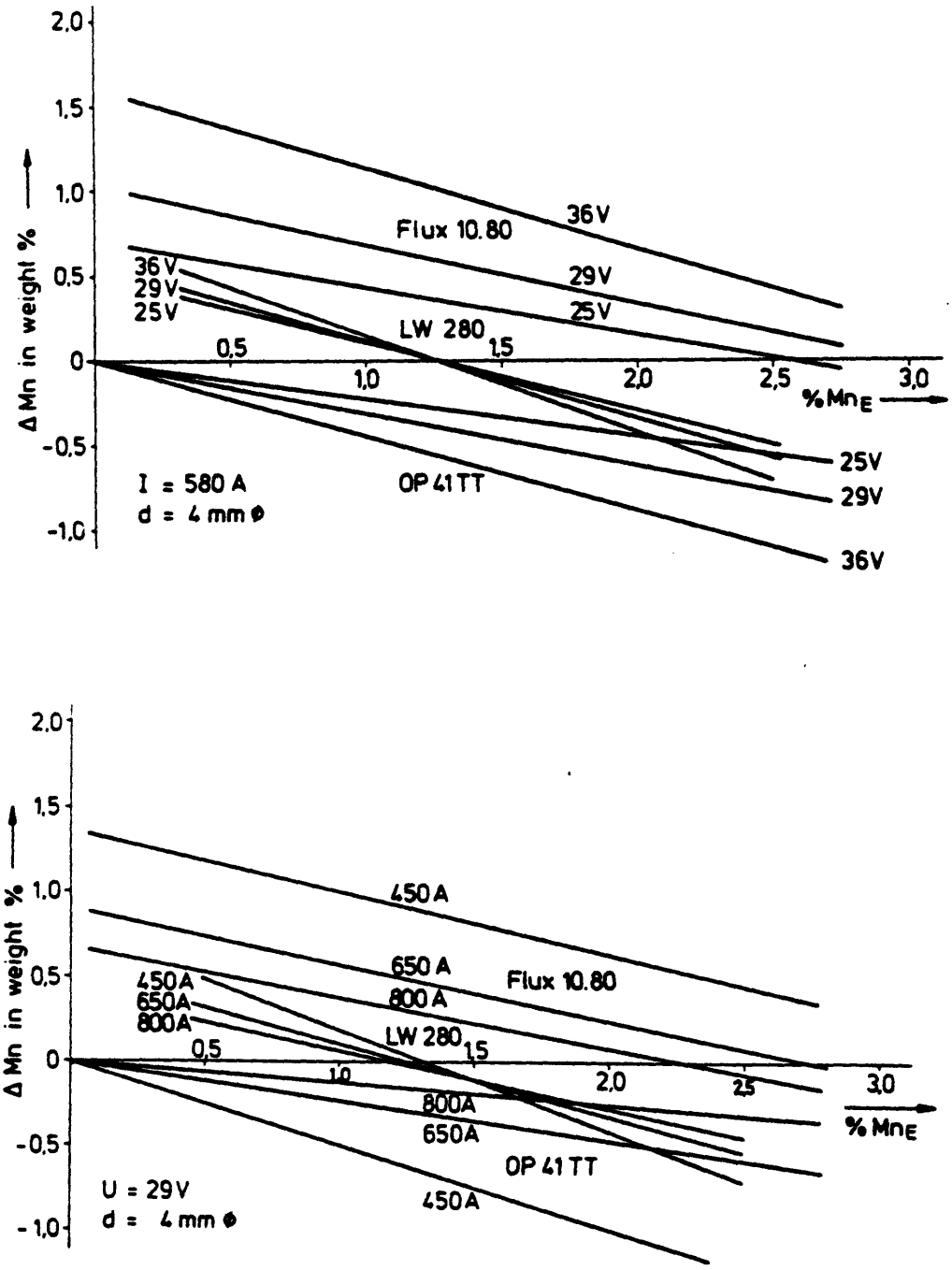

Figure 60: Gain or loss of manganese in multipass welding when using different fluxes, under different welding conditions. Fluxes 10.80 contains ferro manganese (a) effect of changes in voltage, (b) effect of changes in current [from ref. 35].

More experimental work is necessary before quantitative relationships can be found but the approach presented in this section seems a promising way for analyzing element transfer on using 'alloy' fluxes during submerged arc welding operations. In practice, there will be some contribution from the ferroalloys in the zone of cooling and solidifying weld pool, and also the mixing of the alloying elements in the weld pool and the chemical reactions will occur simultaneously rather than sequentially. Any quantitative formulation must take these factors into account.

6.3. Flux Classification and Development

In Chapter 2, Section 2.1, it was briefly mentioned that several systems of flux classification are used. Fluxes are classified by their type (e.g. manganese silicate, calcium silicate, etc.), by their basicity index or by specific welding codes (e.g. the German DIN code). Current systems of flux classification however just act as a rough guide to the user on the amount of alloying element which will be transferred. The product literature supplied by flux manufacturers also gives the range of 'typical' compositions of weld metal expected on using a particular flux. However, these 'typical' compositions are not guaranteed and the user has to determine by trial and error the parameters which give a specific composition. The kinetic model developed in this study now provides a basis from which weld metal chemistry may be determined. Its inherent simplicity makes it suitable

for use even by a relatively unsophisticated user, and though desirable, it is not necessary for the user to understand the specific mechanisms of element transfer. It is strongly suggested that in the future, the neutral points of the fluxes be either supplied by the manufacturer or be incorporated in the welding codes. The flux type or the basicity index gives an idea of the oxidizing potential of the flux and may be used to determine alpha (α). The kinetic model should also help manufacturers of welding consumables to develop better fluxes and cover a wide range of baseplate compositions by suitable flux formulation and by matching it with a limited number of electrodes. It should be noted though that besides weld metal chemistry, several other factors, such as arc stability, bead shape, and slag detachability determine the composition of commercial fluxes. Nevertheless the results of the present investigation should considerably shorten the empirical approaches to flux development currently in use.

In the present investigation, slag-metal interactions in the submerged arc welding process were investigated. This process (SAW) was selected because it is more reproducible than manual processes , and due to the considerable data available in literature. However, the results of the current investigation may be easily extended to other flux shielded welding processes.

Before concluding this section, it is necessary to comment on some very recent developments in flux classification [23,36]. There is some controversy as to whether the amount of alloying elements

transferred during single pass welds (ΔM), should be used as a standard for establishing welding flux codes, or whether the amount transferred during multipass weld (ΔM_N) should be used instead [36]. The controversy is easily resolved, if the difference between the two terms ΔM, and ΔM_N is considered (ref. Section 4.2.1d). Both these parameters may be related to each other by equations (33a) and (38a) and either may be used to develop welding codes, as long as the difference between the two terms is realized. (Any attempts to equate the two terms will result in confusion, as in ref. 36). From a practical viewpoint, it is better to use results of single pass welds since considerably less effort is involved in this process as compared to multipass welding.

6.4 Suggestions for Further Work

In the current investigation a kinetic model has been formulated to predict weld metal chemistry. The results for the transfer of alloying elements such as silicon,manganese and chromium indicate that the diffrence between theoretical prediction and experimental observation is usually less than 10%. It will be difficult to further minimize this error since the initial chemical composition of diffrent batches of the same welding consumables usually vary by 5-10%.

Much more work needs to be done , however, on the transfer of oxygen. At present it is not possible to accurately predict the oxygen content of the weld metal. Levitation melting techniques may be used to study the thermodynamics and kinetics of oxygen transfer in the zone of

droplet reactions. Although in these technique the droplet cannot fall through an arc, an arc 'atmosphere' may be artificially generated or introduced inside the levitation melting chamber. The removal of oxygen through inclusion growth and seperation may also be studied further. Experiments may be designed to control the solidification time of the weld pool.(Conical 'concentrator' type induction coils may be used to vary solidification time through controlled preheating and postheating of the baseplate.) Attempts may also be made to determine whether quantitative models on inclusion growth and removal during steelmaking operations can be extended to predict the extent of inclusion removal during arc welding operations.

In the present investigation slag-metal reactions during submerged arc welding was studied. The results may be extended to other flux shielded arc welding processes such as manual metal arc welding and flux cored arc welding. One important diffrence between submerged arc and the other processes is that in the latter the arc is not shielded by slag but by inert gas or gaseous products generated from additives such as cellulose. Consequently there is more nitrogen contamination (from the atmosphere) and sometimes more hydrogen contamination (from additives). It may be intersting to study the kinetics of reactions involving these impurities,particularly the effect of oxygen on the reaction mechanisms.

CHAPTER 7

CONCLUSION

During the process of submerged arc welding chemical interactions occur between the slag and the metal. In the present investigation, this interaction has been extensively studied and has resulted in the following conclusions:

1. Direct or indirect chemical interaction between the slag and the metal occurs in three zones. These are (i) the zone of droplet reactions, (ii) the zone of dilution and weld pool reactions and (iii) the zone of cooling and solidifying weld pool.
2. In the zone of droplet reactions, the oxide components of the flux decompose to gaseous suboxides or vapours and oxygen. Plasma-metal reactions result in a large increase in metal oxygen content in this zone. However, chemical kinetics, which appears to be controlled by the surface active oxygen, prevents the transfer of the alloying elements, such as Mn, Si and Cr in this zone.
3. The zone of dilution and weld pool reactions controls the amount of alloying elements exchanged between the metal and the slag. A quantitative kinetic model has been formulated which can predict the extent of the reactions occurring in the weld pool. This model considers the

effect of electrode and work piece compositions and the effect of welding parameters in addition to the effect of flux composition, for predicting weld metal chemistry. It has been successful for the first time in making quantitative predictions on weld metal composition. It is also in excellent agreement with the experimental data recorded by previous researchers. From the results of the kinetic model, it appear that mass transport in the slag phase is the rate controlling step for the transfer of elements between the slag and the metal. Thus, the partition coefficient of an alloying element between the metal and the slag, appears to have a very significant influence on the kinetics of the reactions. The amount of alloying elements transferred depends to a great extent on the ratio of the area of the slag-metal interface to metal volume ($A_{s/m}/V_m$). Changes in the welding process parameters results in large variations in ($A_{s/m}/V_m$) and strongly influence weld metal chemistry. The amount of alloying elements transferred also depends on the neutral point of the flux used. The greater the difference between the nominal metal composition and the neutral point, the greater the thermodynamic driving force, and the greater the amount of alloying elements transferred.

4. As the weld pool starts to cool, oxygen supersaturation results in the nucleation of oxide inclusions. In this zone of cooling and solidifying weld pool oxygen is removed by a mechanism of

inclusion growth and separation. An increase in the solidification time results in lower oxygen content of the pool.

Apart from the fundamental results noted above, the present investigation explains several other phenomena observed during the submerged arc welding process. These include observations of steady state compositions during multipass welding, effects of flux viscosity on metal chemistry, and the differences in the kinetics of alloy transfer between 'active' and 'non active' fluxes. The study addresses successfully all major issues raised by different researchers in this field during the last three decades. It also shows conclusively that fundamental principles of chemical metallurgy, kinetics, and solidification processing may be applied to explain and describe quantitatively the changes that occur in metal composition during an apparently complex process such as submerged arc welding.

REFERENCES

1. Mercer, J.F., "Trends in Welding Consumables: A Preliminary Assessment," Proc. Intl. Conf. on Trends in Steel and Consumables for Welding. The Welding Institute, London, Nov. 1978, p. 69.

2. Braune, J., "Electric Welding," J. Iron and Steel Inst., Vol. 60, No. 2, 1901, p. 484.

3. Lancaster, J.F., The Metallurgy of Welding Brazing and Soldering, George Allen and Urwin Ltd., London, 1970.

4. Jackson, C.E., "Fluxes and Slags in Welding," WRC Bulletin, No. 190, December 1973.

5. Wagner, C., "The Concept of the Basicity of Slags," Metall. Trans B., Vol. 6B, September 1975, p. 405.

6. Popatov, N.N. and Kurlanoc, S.A., "A Quantitative Evaluation of the Basicity of Welding Fluxes," Welding Production, No. 9, 1978, p. 6.

7. Eagar, T.W., "Sources of Weld Metal Oxygen Contamination During Submerged Arc Welding," Welding J., Vol. 57, No. 3, 1976, p. 76-s.

8. Tuliani, S.S., Boniszewski, T. and Eaton, N.F., "Notch Toughness of Commercial Submerged Arc Weld Metal," Welding and Metal Fabrication, Vol. 42, No. 8, 1969, p. 327.

9. Noor, C., North, T.W. and Bell, H.K., "Characteristic Properties of Flux Formulations Used in Submerged Arc Welding," Weld Res. Abroad, 1977.

10. Belton, G.R., Moore, T.J., Tankins, E.S., "Slag-Metal Reactions in Submerged Arc Welding," Welding Journal, Vol. 42, No. 7, 1963, p. 289-s.

11. Christensen, N., "Spatial Distribution of Manganese, Silicon, Chromium and Oxygen in Submerged Arc Weld Deposits," Contract DA-91-591 EVC 3455, U.S. Dept. of Army, European Research Office, November 1965.

12. Palm, J.H., "How Fluxes Determine the Metallurgical Properties of Submerged Arc Welds," Welding J., Vol. 51, No. 7, 1972, p. 358-s.

13. Davis, M.L.E. and Bailey, N., "How Submerged Arc Welding Flux Composition Influences Element Transfer," Proceedings of the International Conference on Weld Pool Chemistry and Metallurgy, London, April 1980, p. 289.

14. Potapov, N.N. et al, "On the Oxidation of Chromium and Niobium in the Welding of Austenitic Steels," Svar. Proiz, 1980, No. 7, p. 1.

15. Van Bemst, A., "Contribution a l'etude des reactions metal-laiter loss du soudage a l'arc des aciers inoxydables austenitiques," Revue de la Soudure, Vol. 30, No. 1, 1974, p. 38.

16. Mitra, U., "Slag-Metal Reactions During Submerged Arc Welding of Low Alloy and Stainless Steels," S.M. Thesis, Dept. of Materials Science and Engineering, February, 1982.

17. Chai, C.S., "Slag Metal Reactions During Flux Shielded Arc Welding," Ph.D. Thesis, Dept. of Materials Science and Engineering, MIT, 1980.

18. North, T.H., "The Distribution of Manganese Between Slag and Metal During Submerged Arc Welding," Welding Research Abroad, Vol. 23, No. 1, January 1977, p. 2.

19. Chai, C.S. and Eagar, T.W., "The Effect of SAW Parameters on Weld Metal Chemistry," Welding J., Vol. 59, No. 3, 1980, p. 93-s.

20. Widjery, D.J., "New Ideas in Submerged Arc Welding," Proc. Intl. Conf. on Trends in Steel and Consumables for Welding. The Welding Institute, London, Nov. 1978, p. 217.

21. Herasymenko, P. and Speight, G.E., "Ionic Theory of Slag-Metal Equilibrium," J. Iron Steel Inst., Nov, 1950, p. 169.

22. Davis, M.L.E. and Bailey, N., "Have We the Right Idea About Fluxes?," Proceedings of the International Conference on Trends in Steel and Consumables for Welding, London, November, 1978, p. 231.

23. Kokh, B.A., "Thermodynamic Calculation of Alloying From the Slag and Deoxidization of the Metal During Welding," Automatic Welding, Vol. 30, No. 7, 1977, p. 16.

24. Kokh, B.A., "A Graphical Analysis Method of Determining the Alloying and Deoxidization of Welds," Avt. Svarka, Vol. 34, No. 4, 1982, p.18.

25. Chai, C.S. and Eagar, T.W., "Slag-Metal Equilibrium During Submerged Arc Welding," Metall. Trans., Vol. 12B, Sept. 1981, p. 539.

26. Eagar, T.W., "Oxygen and Nitrogen Contamination During Arc Welding," in Weldments: Physical Metallurgy and Failure Phenomenon, Christoffel, R.J., Nippes, E.F., Solomon, H.D., eds., General Electric Corporation, Schenectedy, NY 1979, p. 31.

27. Chai, C.S. and Eagar, T.W., "Slag Metal Reactions in Binary CaF_2-Metal Oxide Welding Fluxes," Weld. J., Vol. 61, No. 7, July 1982, p. 229-s.

28. Lau, T., "Oxygen Contamination in Submerged Arc Welding," Ph.D. Thesis, Dept. of Metallurgy and Materials Science, University of Toronto, Canada, May 1983.

29. Frumin, J.I., "The Kinetics of Interaction Between Metal and Slag in Submerged Arc Welding," Avt. Svarka, 1957, No. 6, p. 1.

30. Pokhodnya, I.K., "A Method of Investigating the Process of Melting and Transfer of Electrode Metal During Welding," Avt. Svarka, Vol. 17, No. 2, 1964, p. 10.

31. Pokhodnya, I.K. and Kostenko, B.A., "Fusion of Electrode Metal and Its Interaction with the Slag During Submerged Arc Welding," Avt. Svarka, Vol. 18, No. 10, 1965, p. 16.

32. Potapov, N.N. and Lyubavski, K.V., "Oxygen Content of Weld Metal Deposited by Automatic Submerged Arc Welding," Svar. Proiz, 1971, No. 1, p. 11.

33. Potapov, N.N. and Lyubavski, K.V., "Interaction Between the Metal and Slag in the Reaction Zone During Submerged Arc Welding," Svar. Proiz, 1971, No. 7, p. 9.

34. Thier, H., "Metallurgical Reactions in Submerged Arc Welding," Proceedings of the Conference on Weld Pool Chemistry and Metallurgy, The Welding Institute, London, April 1980, p. 271.

35. Thier, H., "Precalculation of Weld Metal Composition in Submerged Arc Welding," IIW Doc, XII-802-83, 1983.

36. Thier, H., "Determining Pickup and Burn-Out Characteristics During Submerged-Arc Welding From Single-Pass Welds." Schweissen Schneiden, September 1982, p. E174.

37. Mitra, U. and Eagar, T., Unpublished research.

38. Christensen, N. and Chipman, J., "Slag-Metal Interaction in Submerged Arc Welding," WRC Bulletin, No. 15, January 1958.

39. Block-Bolten, A. and Eagar, T., "Selective Evaporation of Metals from the Weld Pool," Trends in Welding Research in the United States, ASM, Metals Park, Ohio, 1982, p. 214.

40. Richardson, F.D., "Kinetics of Reactions Between Gases and Liquid Metal," Proc. Intl. Symp. Metall. Chem., Iron & Steel Inst., London, 1971, p. 82.

41. Richardson, F.D., Physical Chemistry of Melts in Metallurgy. Vol. 2, Academic Press, NY, 1974.

42. Sigworth and Elliot, "The Thermodynamics of Liquid Dilute Iron Alloys," Metal Sci., Vol. 8, No. 9, p. 298.

43. Elliott, J.F., Gleiser, M. and Ramakrisna, V., Thermochemistry for Steelmaking. Vol. II, Addison Wesley Publishing Co., Reading, MA 1963.

44. Kawai, Y. and Mori, K., "Equilibrium and Kinetics of Slag-Metal Reactions," Trans. Iron Steel Inst. Japan, Vol. 13, No. 5, September 1983, p. 303.

45. King, C.J., "The Additivity of Individual Phase Resistance in Mass Transfer Operations." A.I.Ch.E. Journal, Vol. 10, No. 5, 1964, p. 671.

46. Szekely, J., "On the Addition of Phase Resistances," Chem. Eng. Sci., Vol. 20, 1965, p. 141.

47. Elliot, J.F. and Wright, J.K., "Equilibrium Phase Relationships During Solidification of Fe-O-C-X Alloys," Can. Metall. Q., Vol. 11, No. (4), 1972, p. 573.

48. Turkdogan, E.T., "Deoxidation of Steel," J. Iron and Steel Inst., Vol. 210, Jan. 1972, p. 573.

49. Turpin, M.L. and Elliot, J.F., "Nucleation of Oxide Inclusions in Iron Melts," J. Iron and Steel Inst., Vol. 199, March 1966, p. 217.

50. Philbrook, W.O., "Oxygen Reactions with Liquid Steel," Intl. Metals Reviews, Vol. 22, Sept. 1977, p. 187.

51. Lindborg, U. and Torssell, K., "A Collision Model for the Growth and Separation of Deoxidation Products," Trans AIME, Vol. 242, Jan. 1968, p. 94.

52. Linder, S., "Hydrodynamics and Collisions of Small Particles in a Turbulent Metallic Melt with Special Reference to Deoxidation of Steel," Scand. J. Metall., Vol. 3, No. 4, p. 137.

53. Flemings, M.C., "Formation of Oxide Inclusions During Solidification," Intl. Metals Reviews, Vol. 22, Sept. 1977, p. 201.

54. Flemings, M.C., Solidification Processing, McGraw-Hill, 1974.

55. Weisman, C., ed., Welding Handbook, Volume 1, 7th Edition, American Welding Society, Miami, FL, 1976.

56. Weisman, C., ed., Welding Handbook, Volume 2, 7th Edition, American Welding Society, Miami, FL, 1976.

57. Lin, M.L. and Eagar, T.W., "Influence of Surface Depression and Convection on Arc Weld Pool Geometry," to be presented at the Symp. Transport Phenom. Matls. Processing, ASME, Boston, MA, November 13-18, 1983.

58. Jackson, C.E., "The Science of Arc Welding," Weld J., Vol. 40, June 1960, p. 225-s.

59. Richardson, F.D., "The Properties and Structures of Phases and Their Relevance to Processes," Steelmaking: The Chipman Conference, Elliot J.F. ed., M.I.T. Press, Cambridge, MA, 1965, p. 65.

60. Ishizaki, K., "Interfacial Tension Theory of the Phenomenon of Arc Welding - Mechanism of Penetration." 'Physics of the Welding Arc Symposium, Institute of Welding, London, 1965, p. 195.

61. Woods, R.A. and Milner, D.R., "Motion in the Weld Pool in Arc Welding, Vol. 50, No. 3, 1971, p. 163-s.

62. Bradstreet, B.J., "Effect of Surface Tension and Metal Flow on Weld Bead Formation," Weld. J., Vol. 47, July 1968, p. 314-s.

63. Ishizaki, K., "A New Approach to the Mechanism of Penetration," Intl. Conf. on Weld Pool Chem. Met., The Welding Institute, London, 1980.

64. Heiple, C.R. and Roper, J.R., "Effect of Minor Elements on GTAW Fusion Zone Shape," Rockwell International Preprint RFP-3224, Colorado, 1981.

65. Oreper, G.M., Eagar, T.W. and Szekely, J., "Convection in Arc Weld Pools," to be published by the Weld. J., 1983.

66. Oreper, G.M. and Szekely, J., Unpublished research.

67. McGannon, H.E., ed., The Making, Shaping and Treating of Steel, 9th Edition, U.S. Steel, 1971.

68. Fowles, P.E., "The Velocity and Turbulence Distribution in the Laminar Sublayer," Sc.D. Thesis, Dept. of Chem. Eng., Massachusetts Institute of Technology, Cambridge, MA, 1966.

69. Sherwood, T.K., Smith, K.A. and Fowles, P.E., "The Velocity and Eddy Viscosity Distribution in the Wall Region of Turbulent Pipe Flow," Ind. Eng. Chem., Vol. 23, 1968, p. 1225.

70. Wei, J., "Least Square Fitting of an Elephant," Chemtech, Vol. 5, Feb. 1975, p. 128.

71. Products Catalog, Linde Gases and Welding Products, Union Carbide Corporation, New York, NY, 1980.

72. Products Catalog, Lincoln Electric Company, Cleveland, Ohio, 1981.

73. Kawaii, Y., Shinozaki, N., and Mori, K., "Rate of Transfer of Manganese Across Metal-Slag Interface and Interfacial Phenomenon," Can. Metall. Q., Vol. 21, No. 4, 1982.

74. Sherwood, T.K. and Wei, J., "Interfacial Phenomenon in Liquid Extraction," Ind. Eng. Chem., Vol. 49, No. 6, p. 1030.

75. Mayr, S.T., "Mass Transfer Enhancement in Gas-Liquid Systems Due to the Marangoni Effect," Sc.D. Thesis, Dept. of Chem. Eng., M.I.T., Cambridge, MA, 1970.

76. Ito, Y., Nakanishi, M. and Katsumoto, N., "Effect of CaF_2 in Flux on Toughness of Weld Metal Relation Between CaF_2 Content in Welding Flux and Impure Gas Content in Weld Metal," The Sumitomo Search, Vol. 16, No. 1976, p. 78.

77. Tullioni, S.S., Ceram, A.L., Bowszewski, T. and Eaton, W.F., "Notch Toughness of Commercial Submerged Arc Weld Metal," Weld. Met. Fab., Vol. 45, No. 7, 1972, p. 247.

78. Kuzmenko, V.G., "Special Features of the Interaction Between Calcium Fluoride and Silicon Dioxide at 800-1900°C," USSR Academy of Sciences, IIW Doc XIIA-051/83, 1983.

79. North, T.H., Bell, H.B., Nowicki, A. and Craig, I., "Slag/Metal Interaction, Oxygen and Toughness in Submerged Arc Welding," Welding J., Vol. 57, No. 3, 1978, p. 63.

80. Potapov, N.N., "The Effect of the Diameter of the Electrode Wire in Submerged Arc Welding, on the Mechanical Properties of the Deposited Metal," Avt. Svarka., Vol. 30, No. 7, 1977, p. 46.

81. Sutton, R.D., Private Communication, Union Carbide Corporation.

82. Kim, C.K. and Mclean, A., University of Toronto, unpublished research.

83. Rankin, W.J. and Biswas, A.K., "Oxidation States of Chromium in Slag and Chromium Distribution in Slag-Metal Systems at 1600°C," Trans. Inst. Min and Met., March 1978, p. C60.

84. Bagryanski, K.V., "Indicator Elements Used for Assessing the Physical Conditions under which Metal and Slag React During Welding," Automatic Welding, Vol. 22, No. 1, 1969, p. 24.

85. Lyman, T., ed., Metals Handbook, Volume 6: Welding and Brazing, 8th Edition, American Society for Metals, Ohio, 1981.

APPENDIX A.1

DATA AS PRESENTED BY NORTH [18]

In Figure A.1(i) the manganese lost by the metal to the slag during multipass welding is plotted against voltage. In Figure A.1(ii) the relative manganese index of the droplets is plotted against voltage. However, it is left to the reader to determine the actual manganese content of the droplets from the calibration curve A.1(iii).

If the actual manganese content of the droplet is determined from Figure A.1(iii) then a much better illustration of North's results is obtained by comparing the amount of manganese lost by the droplets, as compared to the loss during multipass welding as shown in Figure A.1(iv). According to the droplet reaction time theory put forth by North [18] and others [29-36], the amount of alloying elements lost by the droplets is the same as that lost by the weld metal during multipass welding. It is likely that the large loss of manganese from the droplets was due to slag-metal reactions which occur when the droplets are collected [see Appendix A.11]. The high surface area to volume ratio of the droplets is likely to enhance the kinetics of this reaction and account for the large amounts of manganese lost.

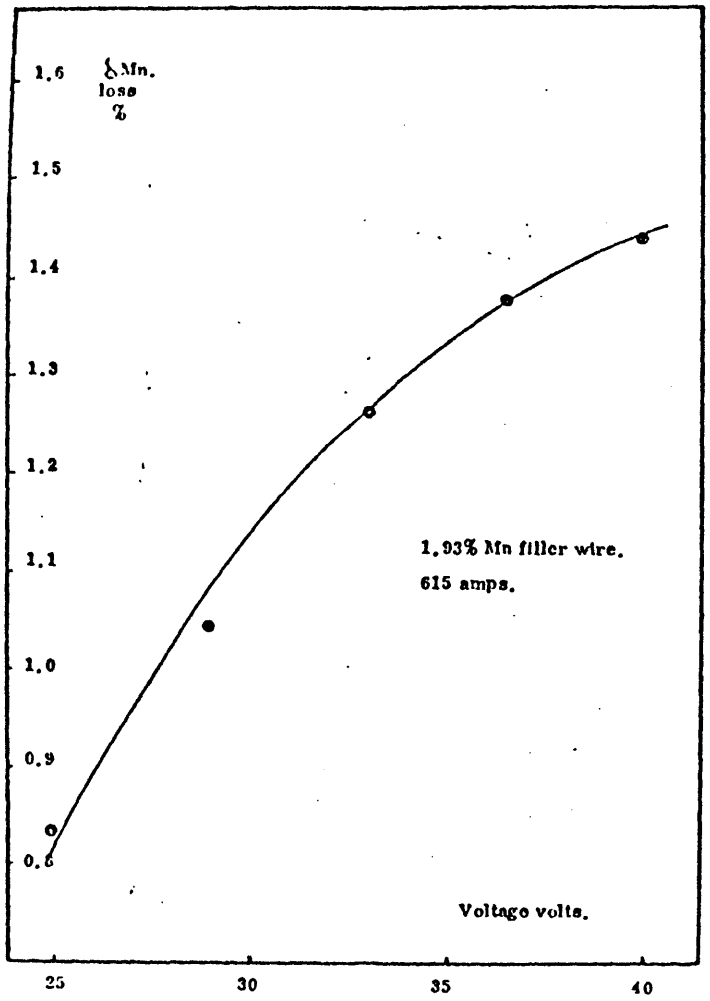

Fig. A (i) Relation between manganese loss and arc voltage. 1.93% Mn filler wire with (65 wt.% SiO_2. 35 wt.% CaO) flux.

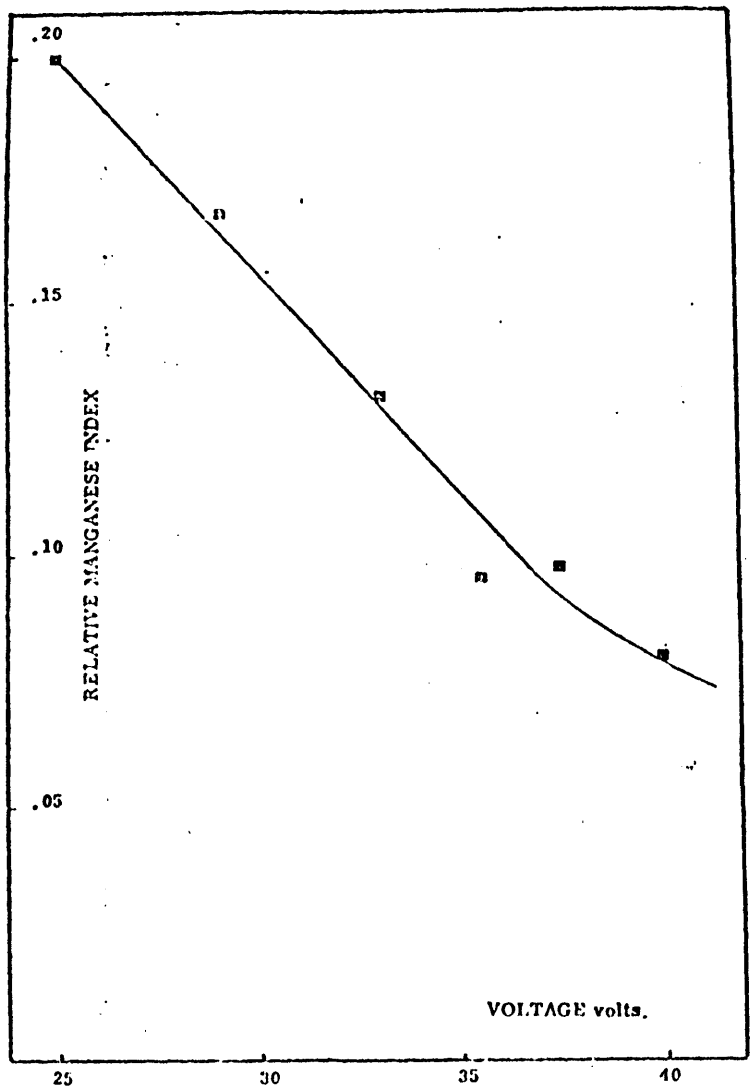

Fig. A (ii) Relation between arc voltage and the relative manganese index of droplets.

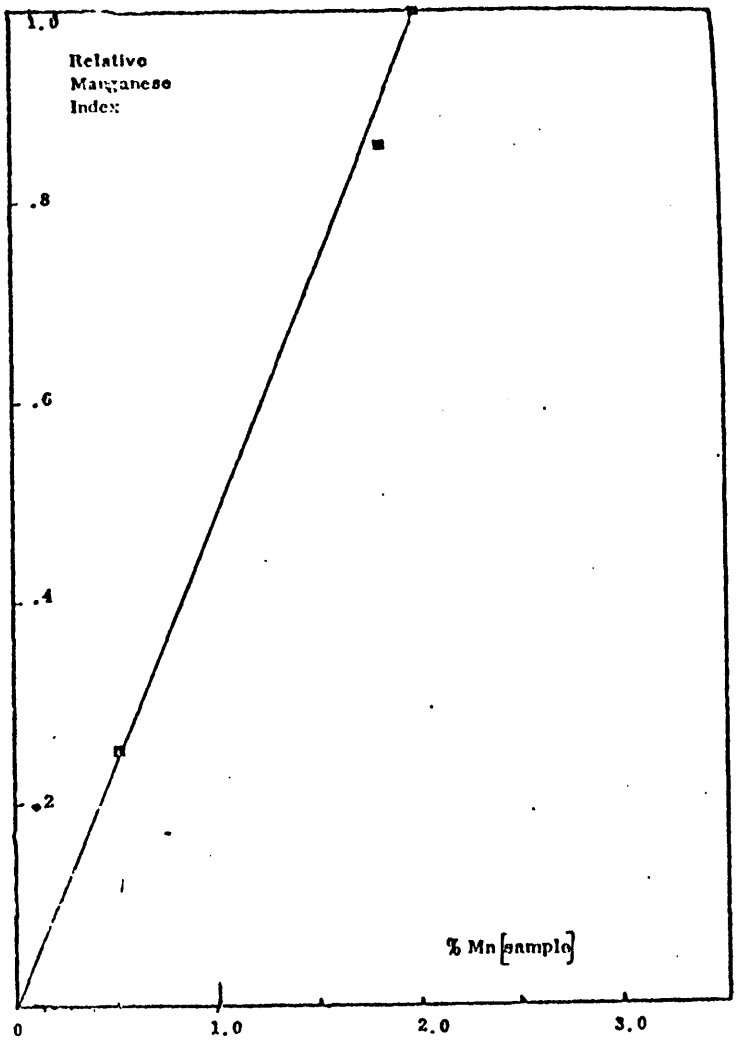

Fig.A(iii): Calibration curve of relative manganese index and manganese content.

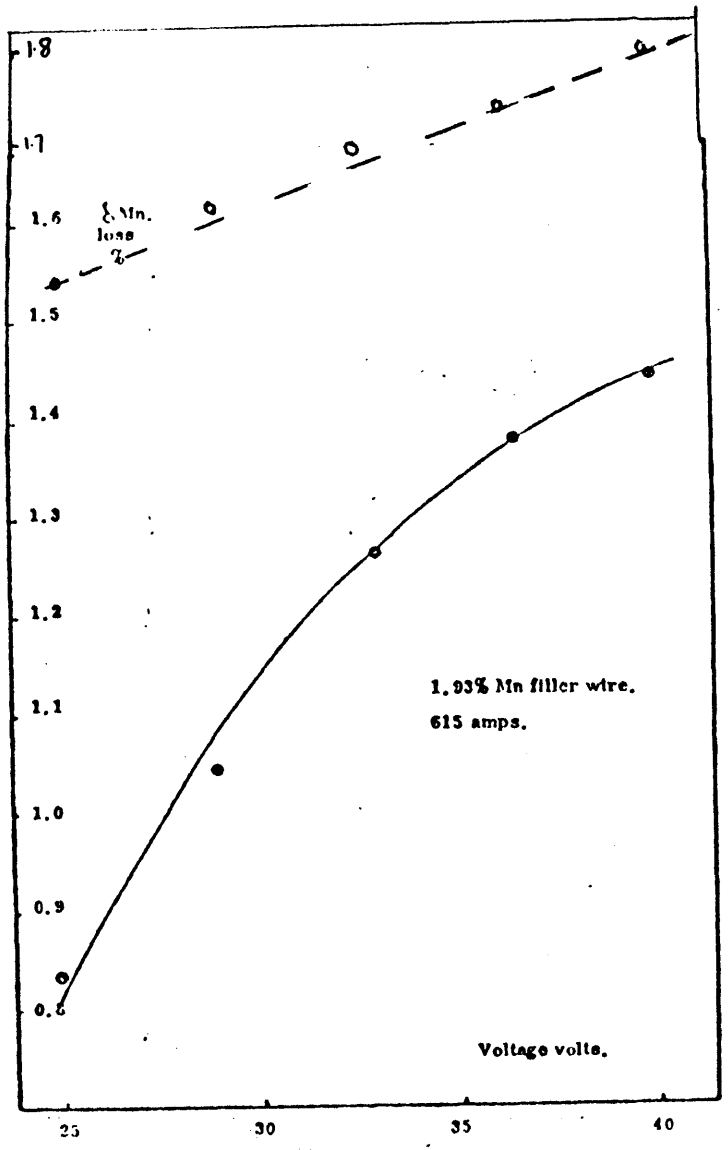

Fig. A(iv): Comparision between manganese lost by droplets and actual amount of manganese lost in welds.

APPENDIX A.2

THERMODYNAMICS OF SLAG-METAL REACTIONS

Welding fluxes usually contain several oxides. During the welding process these oxides can react with the metal either directly through slag metal reactions or indirectly through plasma-slag and plasma metal reactions. A very rough indication of the stability of the oxides present in welding fluxes may be obtained by examining the Ellingham diagram (Figure A.2). This figure also shows that the stability of these oxides decreases with increasing temperature. It should be noted that in this diagram, all constituents (oxides and elements) are assumed to be in their standard state. Figure A.2 gives no indication of the possible interactions between the different oxide constituents, nor does it provide any information on reaction rates or mechanisms. This section very briefly examines the thermodynamics of reactions involving silicon, manganese and oxygen, since these are the principal elements of interest. A more detailed thermodynamic study of slag-metal reactions involving several other elements such as chromium, carbon, sulphur, phosphorus, nickel and molybdenum, in addition to silicon, manganese and oxygen is available in literature [16].

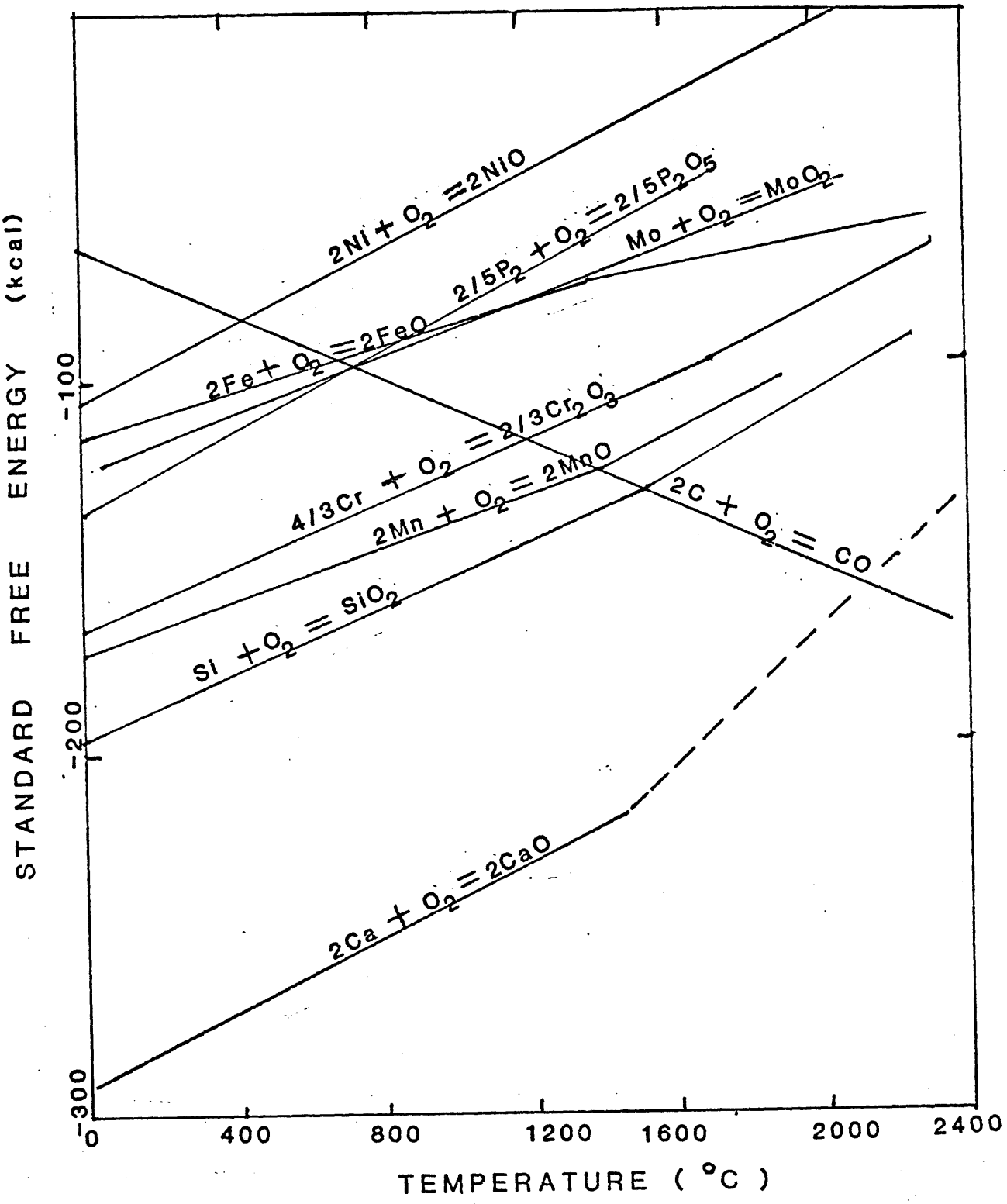

Fig. A2 Ellingham diagram showing the stability of various oxides with changing temperature

Reactions Involving Silicon:

The following reactions may be considered

$$(SiO_2) = SiO(g) + 1/2\ O_2(g) \quad (1)$$

$$SiO(g) = \underline{Si} + \underline{O} \quad (2)$$

$$SiO_2 = \underline{Si} + 2\ \underline{O} \quad (3)$$

The values of the respective equilibrium constants K_1, K_2 and K_3 for these three reactions, at different temperatures; (see Table A.2) indicates that reactions (1) and (3) are strongly temperature dependent. Thus, the high temperatures expected in the zone of droplet reactions would favor reaction (1) to proceed forward. (Note inside the arc cavity both P_{SiO_2} and P_{O_2} <<< 1.) However, the lower temperatures of the zone of cooling and solidifying weld pool would result in reaction (3) proceeding backwards to form silica inclusions in the liquid steel. Davies has claimed that the slag and metal are in equilibrium at an "effective temperature range" of 1600-1650°C. However, thermodynamics clearly rules out this possibility ($K_3 = 2.9 \times 10^{-5}$ at 1600°C), since even if the slag was saturated with silica (at 1600-1650°C) it still cannot account for the high amounts of silicon and oxygen, often observed in weld metals.

Reactions Involving Manganese

The following reactions may be considered

$$MnO = Mn(g) + 1/2\ O_2(g) \quad (4)$$

$$MnO = \underline{Mn} + \underline{O} \quad (5)$$

The values of the equilibrium constants K_4 and K_5 for these reactions (see Table A.2) indicates that reaction (4) is strongly temperature dependent and is very likely to proceed forward at the high temperatures in the zone of droplet reactions. Reaction (5) is also favored at high temperatures, and at the lower temperatures of the cooling weld pool (1600°C) this reaction should also go backwards leading to deoxidation and inclusion formation.

Table A.2: Values of the Equilibrium Constant for Reactions Involving Si, Mn, and O at Different Temperatures. (Approximate values.)

Reaction No.	Equilibrium Constant	T = 1600°C	T = 2000°C	T = 2300°C
1	$K_1 = \frac{(P_{SiO})(P_{O_2})^{1/2}}{a_{SiO_2}}$	10^{-9}	7×10^{-6}	9×10^{-4}
2	$K_2 = \frac{[\%Si][\%O]}{(P_{SiO})}$	9	2.4	1.2
3	$K_3 = \frac{[\%Si][\%O]}{a_{SiO_2}}$	3×10^{-5}	0.4	8.5×10^{4}
4	$K_4 = \frac{[P_{Mn}][P_{O_2}]^{1/2}}{a_{MnO}}$	1.4×10^{-8}	2.1×10^{-5}	1.1×10^{-3}
5	$K_5 = \frac{[\%Mn][\%O]}{a_{MnO}}$	7.4×10^{-2}	1.0	5.3

APPENDIX A.3

MASS BALANCE FOR OXYGEN

Consider a mass balance for oxygen assuming only one step slag metal reactions occur.

$$O_{MB} = \frac{(A.W.)_O}{(M.W.)_{MnO}} [\Delta Mn] + \frac{2(A.W.)_O}{(M.W.)_{SiO_2}} [\Delta Si) + \frac{(A.W.)_O}{(M.W.)_{FeO}} [\Delta Fe] + O_i \qquad (1)$$

where A.W. refers to the atomic weight

M.W. refers to the molecular weight for the elemtn or compound as denoted by the subscripts

ΔMn, ΔSi, and ΔFe refers to the amounts of these elements transferred from the slag to the metal

O_i is the initial metal oxygen content, and

O_{MB} is the oxygen content expected by a mass balance.

Since the amount of iron lost (ΔFe) is not known directly, it can be determined from a mass balance for iron:

$$[\Delta Fe] = -[W_S/W_M] \ (\Delta FeO) \left[\frac{(A.W.)_{Fe}}{(M.W.)_{FeO}}\right] \qquad (2)$$

where (W_S/W_M) is the slag to metal reatio, and (ΔFeO) is the amount of iron oxide gained by the slag. Combining equations (1) and (2), and substituting the values for atomic and molecular weights,

$$O_{MB} = 0.29(\Delta Mn) + 1.14(\Delta Si) - 0.22 * (\Delta FeO) + O_i \qquad (3)$$

Application of equation (3) to the data recorded by Christensen [10] and Belton* [11] shows that the oxygen content of the weld metal as estimated from a mass balance assuming a one step slag metal reaction (O_{MB}) is much lower than the actual weld metal content (O_{weld}). In many cases, O_{MB} is negative. These results, shown in the following table (Table A.3) clearly rules out any possibility of the weld metal oxygen being controlled by a one step slag-metal reaction.

*Belton did not record the slag to metal ratio for his welds so a minimum value of (W_S/W_M) of 0.25 was assumed. A larger value of (W_S/W_M) (as is likely the case) would make O_{MB} even smaller.

Table A.3: Mass Balance of Oxygen

Researcher/Ref/Flux	ΔMn (%)	ΔSi (%)	ΔFeO (%)	O_{MB} (%)	O_{Weld} (%)
Christensen [10] Flux E	0.12	0.11	3.00	-0.044	0.059
	0.04	0.08	3.12	0.007	0.037
	0.17	0.27	2.89	-0.267	0.075
	0.29	0.15	2.99	0.029	0.059
	0.13	0.08	3.22	0.007	0.039
	0.46	0.27	3.01	-0.206	0.070
	0.23	0.06	3.29	-0.129	0.063
	0.10	0.02	3.56	-0.065	0.040
	0.56	0.24	3.33	-0.201	0.072
	0.20	0.02	3.25	-0.093	0.067
	0.44	0.16	3.33	-0.093	0.071
Christensen [10] Flux F	-0.23	0.09	1.36	-0.063	0.026
	-0.13	0.06	1.84	-0.047	0.026
	-0.55	0.25	1.13	-0.132	0.023
	-0.21	0.12	1.25	-0.004	0.023
	-0.06	0.17	1.38	0.031	0.025
	-0.03	0.07	1.81	-0.015	0.021
	-0.35	0.23	1.33	-0.122	0.023
	-0.08	0.12	1.26	0.050	0.026
	-0.04	0.06	1.65	-0.048	0.033
	0.00	0.09	1.92	0.008	0.023
	-0.03	0.20	1.57	-0.073	0.030
	-0.05	0.11	1.48	0.031	0.026
	0.02	0.05	1.66	-0.02	0.030
	0.00	0.07	1.97	-0.019	0.027
	0.05	0.12	1.49	-0.164	0.033
	-0.02	0.09	1.37	-0.007	0.026
Christensen [10] Flux A	-0.51	0.49	3.30	0.083	0.086
	-0.44	0.44	3.64	0.027	0.092
	-0.44	0.35	3.67	0.128	0.084
	-0.36	0.31	3.61	0.005	0.072
	-0.42	0.41	3.45	0.133	0.084
	-0.32	0.29	3.36	0.055	0.071
	-0.26	0.33	3.40	0.105	0.090
	-0.62	0.47	3.30	0.006	0.077
	-0.53	0.45	3.58	0.043	0.068
	-0.55	0.47	3.25	0.072	0.061
	-0.80	0.65	3.10	-0.009	0.075

Table A.3 (cont.)

Researcher/Ref/Flux	ΔMn (%)	ΔSi (%)	ΔFeO (%)	O_{MB} (%)	O_{Weld} (%)
Belton [11] $CaO-SiO_2$ Flux	-0.04	0.07	3.91	-0.09	0.10
	0.00	0.20	3.67	0.05	0.09
	-0.09	0.28	4.06	0.08	0.12
	-0.14	0.33	5.21	0.11	0.13
	0.02	0.28	7.61	-0.06	0.17
	0.04	0.26	9.30	-0.15	0.22

APPENDIX A.4

DETERMINATION OF THE THERMODYNAMIC FACTOR β

$$\beta = m\gamma b$$

where m = the partition coefficient = $\dfrac{\text{N.P.}}{a_{MO_x}}$

γ = the activity coefficient

b = a mass balance factor = $\left(\dfrac{\text{M of wt of } MO_x}{\text{At wt of M}}\right)\left(\dfrac{\text{Wt of Metal}}{\text{Wt of Slag}}\right)$

$$\therefore \beta = \left(\frac{\text{N.P.}}{a_{MO_x}}\right) (\gamma_{MO_x})(b)$$

$$\beta = \frac{\text{N.P.}}{(\gamma_{MO_x})(\%MO_x)} (\gamma_{MO_x})(b)$$

Using typical values of N.P., $\%MO_x$ and b for fluxes F-1 - F-4 (from the experimental results of Chai (ref. 17)), we may estimate β

Flux	$(N.P.)_{Si}$	% SiO_2	% MnO	$(N.P.)_{MnO}$	Average Value of b_{Si}	b_{Mn}	β_{Si}	β_{Mn}
F-1	0.28	42	26	1.8	4.0	2.5	.024	.15
F-2	0.28	40	8	0.5	4.0	2.5	.028	.15
F-3	0.95	50	40	1.2	4.0	2.5	.076	.03
F-4	0.35	36	-	-	4.0	2.5	.04	-

A more general way of determining that β is not very important is by noting that a change of weld metal composition by 1% M changes, slag composition by say 2.1 MO_x. From the figures computed by Chai [17] in the following pages, Figs. A-4(i) to A-4(iii) it can be seen that a 2% change in slag composition has a negligible influence on the neutral point for acid fluxes. For more basic fluxes, there might be some effect. However, the amount of alloying elements transferred in basic fluxes is much lower (see Chapter 5), so the change in slag composition is much smaller (typically less than (%) and consequently again the change in the neutral point is small. Figures A.8(i) and A.8(ii) show that use of equation (33) ($\beta = 0$) and (31) with ($\beta = 0.2$) for flux f of Christensen [10] (basic $CaO-SiO_2$ type with 4.4% Mn) gives little difference in the results. β may be equated to zero for most silicate systems. However, for some other systems such as $MnO-FeO-Al_2O_3$ (although such systems are not normally used for preparing welding fluxes) this need not necessarily be valid (see Figure A.4(v)). Thus before using equation (33), the value of β should be estimated for

such systems, and if β is large, the more rigorous equation (31) should be used instead.

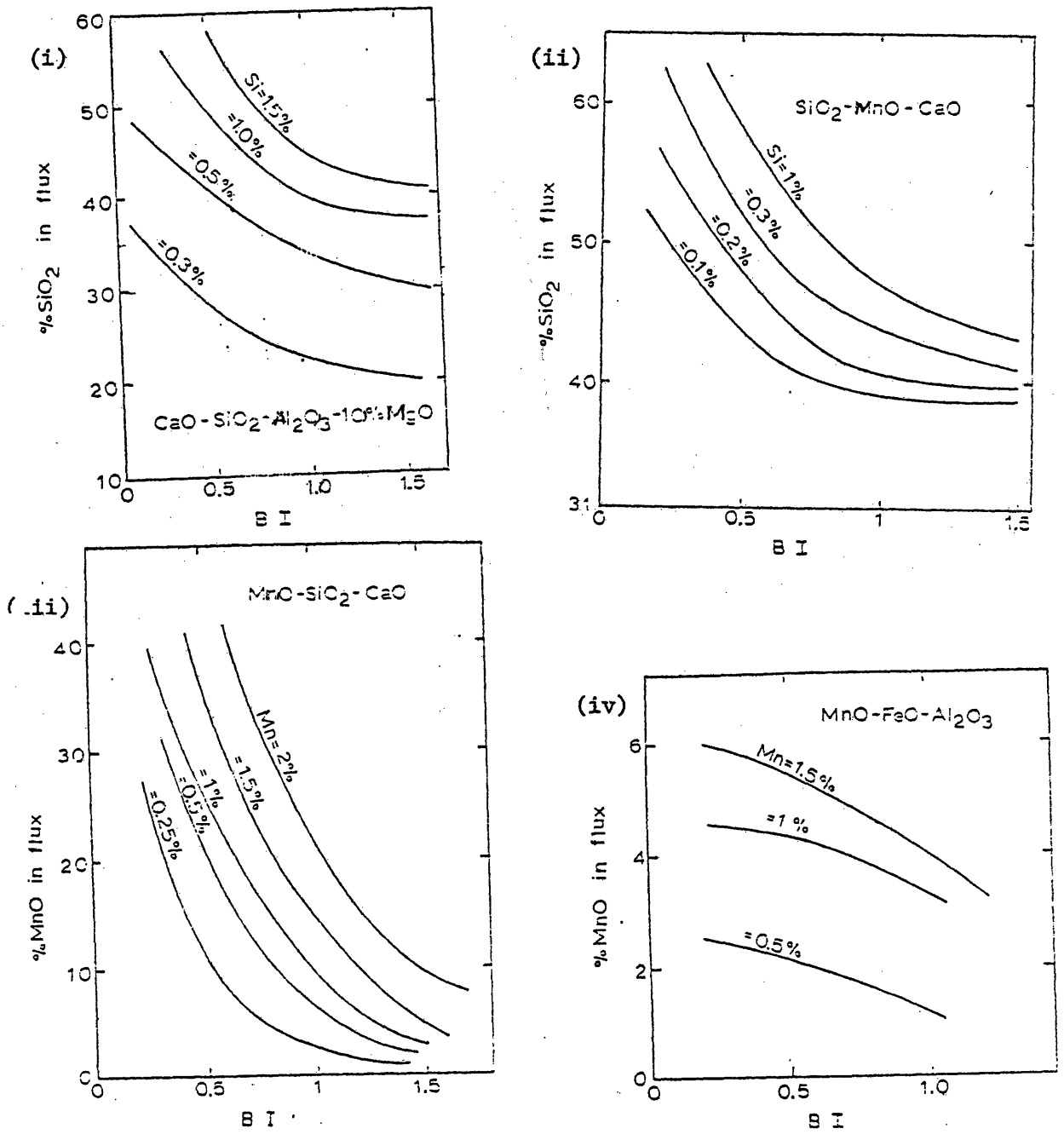

Fig. A.4: Chai's results on the effect of flux composition and basicity index on the neutral point.

APPENDIX A.5

ALLOY TRANSFER IN MULTIPASS WELDING

It was shown that for single pass welding

$$M_f = N.P. - (N.P. - M_i)\exp\left(-\alpha \frac{A_{S/M}}{V_M}\right) \qquad (33)$$

Let

$$F = \exp\left(-\alpha \frac{A_{S/M}}{V_M}\right)$$

Also let $M_i = d\, M_{B.P.} + xM_{e\ell}$ where $x = (1-d)$. Let the final composition of the first layer be M_1, of the second layer M_2 and so on.

$$M_1 = N.P. - [N.P. - (dM_{B.P.} + x\, M_{e\ell})]F$$

$$= N.P.[1 - F] + x\, F\, M_{e\ell} + FdM_{B.P.}$$

$$M_2 = N.P. - [N.P. - (dM_1 + xM_{e\ell})]F$$

$$= N.P. - [N.P. - d\{N.P.(1 - F) + 2FM_{e\ell} + dFM_{B.P.}\} - 2M_{e\ell}]F$$

$$= [N.P.][1 - F][1 + Fd] + xM_{e\ell}F[1 + Fd] + d^2F^2M_{B.P.}$$

$$M_3 = N.P. - [N.P. - (dM_2 + xM_{e\ell})]F$$

$$= N.P. - [N.P. - d\{(N.P.)(1-F)(1+Fd) + 2M_{e\ell}F[1+Fd] + d^2F^2M_{B.P.} + 2M_{e\ell}\}]F$$

$$= [N.P.][1 - F][1 + Fd + (Fd)^2] + 2M_{e\ell}F[1 + Fd + (Fd)^2] + d^3F^3M_{B.P.}$$

$$M_4 = N.P. - [N.P. - (dM_3 - 2M_{e\ell})]F$$

$$= N.P. - [N.P. - d\{(N.P.)(1-F)(1 + Fd + (Fd)^2) + (xM_{e\ell}F)(1 + Fd + (Fd)^2)$$

$$+ d^3F^3M_{B.P.} + xM_{e\ell}\}]F$$

$$= [N.P.][1 - F][1 + (Fd) + (Fd)^2 + (Fd)^3] + [xM_e F][1 + (Fd) + (Fd)^2 + (Fd)^3]$$

$$+ F^4d^4M_{B.P.}$$

The composition of the n^{th} layer is given by

$$M_n = [N.P.][1 - F][1 + (Fd) + (Fd)^2 + \ldots + (Fd)^{n-1}]$$

$$+ [xM_{e\ell}F][1 + (Fd) + (Fd)^2 + \ldots + (Fd)^{n-1}] + (Fd)^n M_{B.P.}$$

Summing the series $[1 + (Fd) + (Fd)^2 + \ldots (Fd)^{n-1}]$, we get

$$M_n = [N.P.][1 - F]\left[\frac{1 - (Fd)^n}{1 - Fd}\right] + [xM_e F]\left[\frac{1 - (Fd)^n}{1 - Fd}\right] + (Fd)^n M_{B.P.}$$

Subsituting back $x = 1 - d$

$$M_n = \left[\frac{[N.P.][1 - F] + (1 - d)\, M_{e\ell}F}{1 - Fd}\right][1 - (Fd)^n] + (Fd)^n M_{B.P.}$$

$$= \left[\frac{[N.P.][1 - F] + M_{e\ell}F - Fd\, M_{e\ell}F + M_{e\ell} - M_{e\ell}}{1 - Fd}\right][1 - (Fd)^n] + (Fd)^n M_{B.P.}$$

$$= \left[\frac{[N.P.][1 - F] - M_{e\ell}[1 - F] + M_{e\ell}[1 - Fd]}{1 - Fd}\right][1 - (Fd)^n] + (Fd)^n M_{B.P.}$$

$$= \left[M_{e\ell} + \frac{(N.P. - M_{e\ell})(1 - F)}{1 - Fd}\right][1 - (Fd)^n] + (Fd)^n M_{B.P.}$$

APPENDIX A.6

RELATIONSHIP BETWEEN THE PARAMETERS (S/a) AND ($\sqrt{B}/a$)

In Section 5.1b, the relationship

$$S/a \approx 3(\sqrt{B}/a)$$

was used, where S is the length of the fusion line

B is the transverse cross-sectional area of fused baseplate

a is the total transverse cross-sectional area of the weld metal (see Figures 20,21).

This relationship may be verified by considering the geometries of different welds (chosen at random) in the following table and comparing the (S/a) ratio to ($\sqrt{3}$ B/a)

Weld No.	S/a	$3\sqrt{B}/a$
25	2.38	2.04
P1	2.00	1.79
P4	3.43	3.21
S1	1.71	1.83
S4	2.10	1.91
800	1.43	1.21

A more general way of examining this relationship is by considering simple geometric figures which can approximate the shape of the fused baseplate metal (Figure A.6), as shown in the following page.

Fig. A.6 : Relationship between (s/a) and ($\sqrt{B}/a$) for simple shapes.

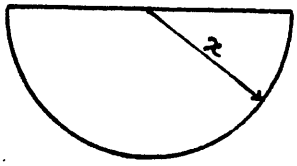

$s = \pi x$
$s = 0.5\pi x^2$
$s/a = 2.5\sqrt{B}/a$

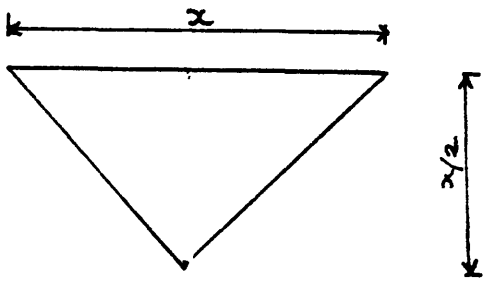

$s = 2x$
$B = x^2/4$
$s/a = 2.8\sqrt{B}/a$

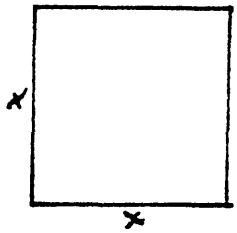

$s = 3x$
$B = x^2$
$s/a = 3\sqrt{B}/a$

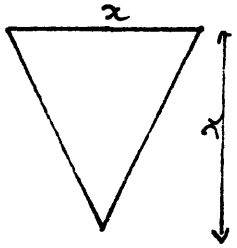

$s = 5x$
$B = 0.5\ x^2$
$s/a = 3.16\sqrt{B}/a$

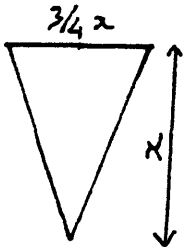

$s = 2.14x$
$B = 0.375x^2$
$s/a = 3.5\sqrt{B}/a$

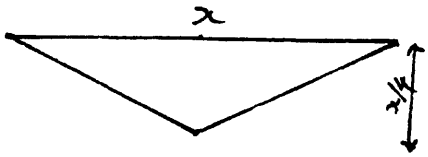

$s = 17x/4$
$B = x^2/8$
$s/a = 2.91\sqrt{B}/a$

APPENDIX A.7

CORRELATION OF THE PARAMETERS (w/a), (ℓ/a) and (W_S/W_M)

The correlation between these parameters may be seen from the data for the following welds

Weld	w/a	ℓ/a	W_S/W_M
S1	1.02	1.85	0.15
S2	1.33	1.83	0.22
S3	2.20	2.43	0.32
S4	1.75	1.94	0.35
S5	2.54	2.56	0.42
S6	1.59	1.61	0.27
S7	4.49	4.87	0.53
S8	1.98	2.36	0.34

Linear correlation coefficient between w/a and ℓ/a: 0.968.

Linear correlation coefficient between w/a and W_S/W_M: 0.927.

Linear correlation coefficient between ℓ/a and W_S/W_M: 0.828.

APPENDIX A.8

This section contains figures comparing the manganese content of the metal as predicted by theory to that obtained experimentally. Data collected in the present investigation and that recorded by other researchers have been used to verify the theory. Only the researchers name, the flux name and the corresponding values of the neutral point (N.P.) and α have been noted. β has been assumed to be zero unless otherwise stated.

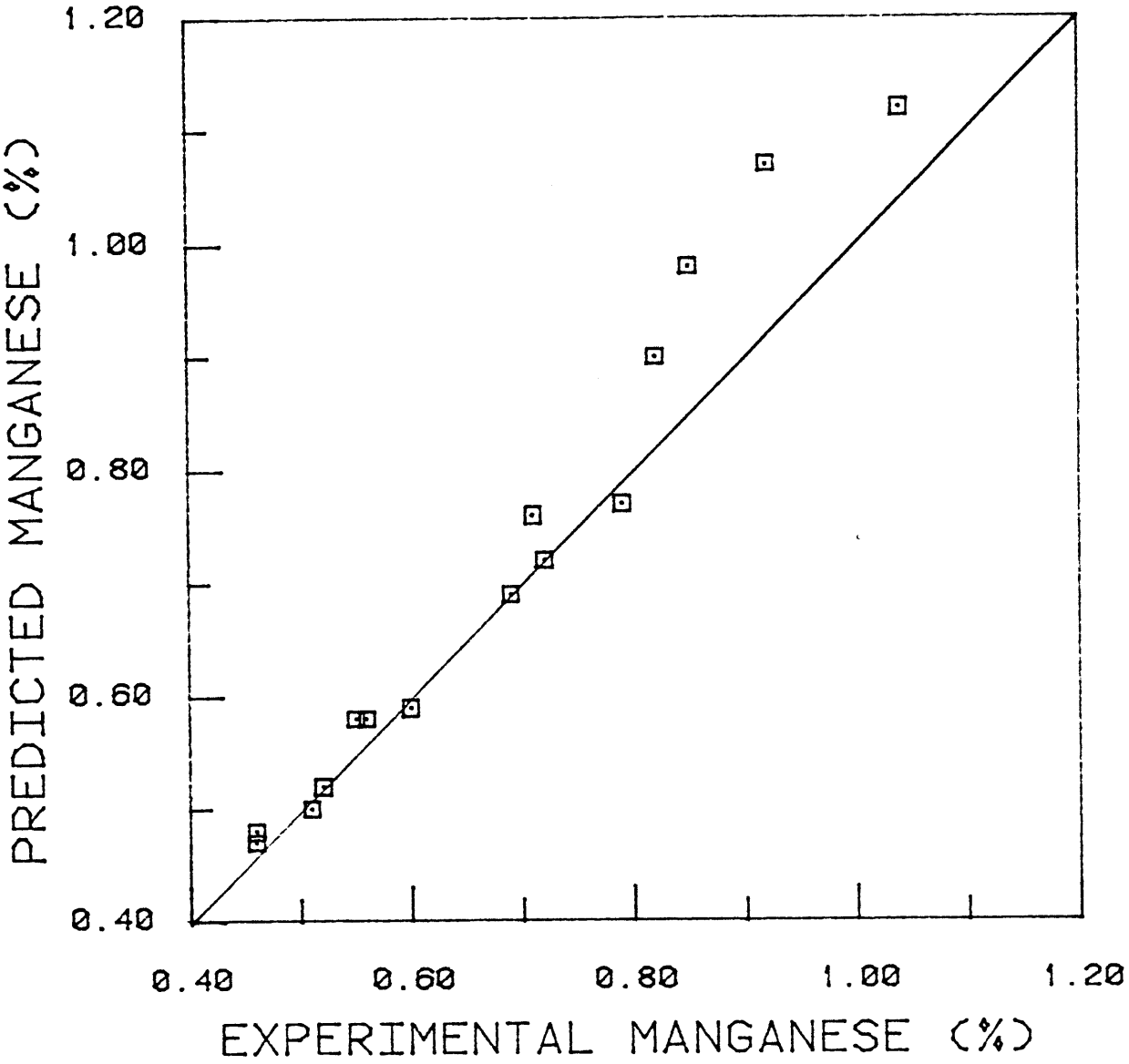

CHRISTENSEN [10], flux f,N.P. 0.55%Mn, α=1.7/3, β=0.00

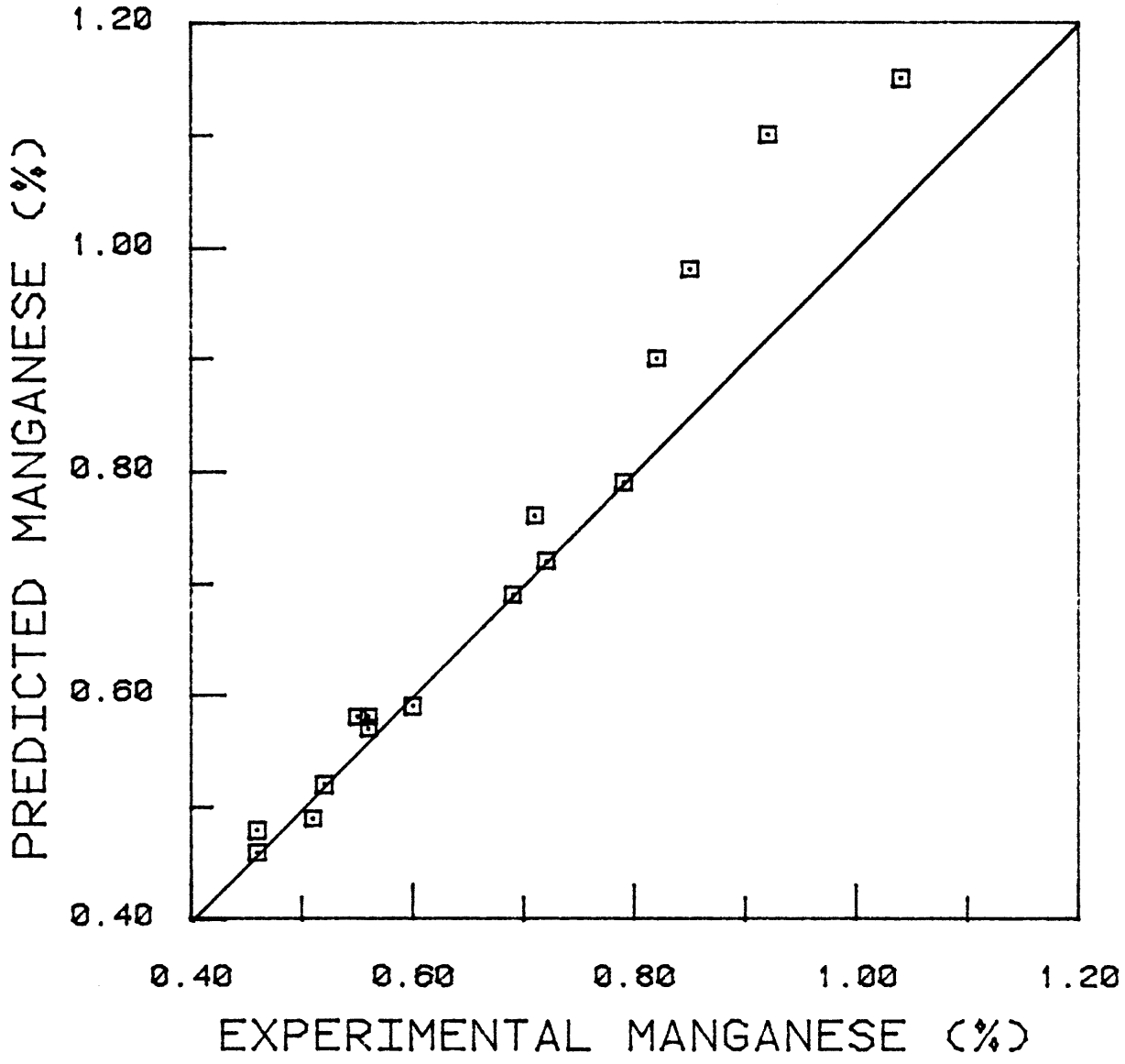

CHRISTENSEN [10],Flux-f,N.P.:0.55%Mn, =1.7/3, β=0.2

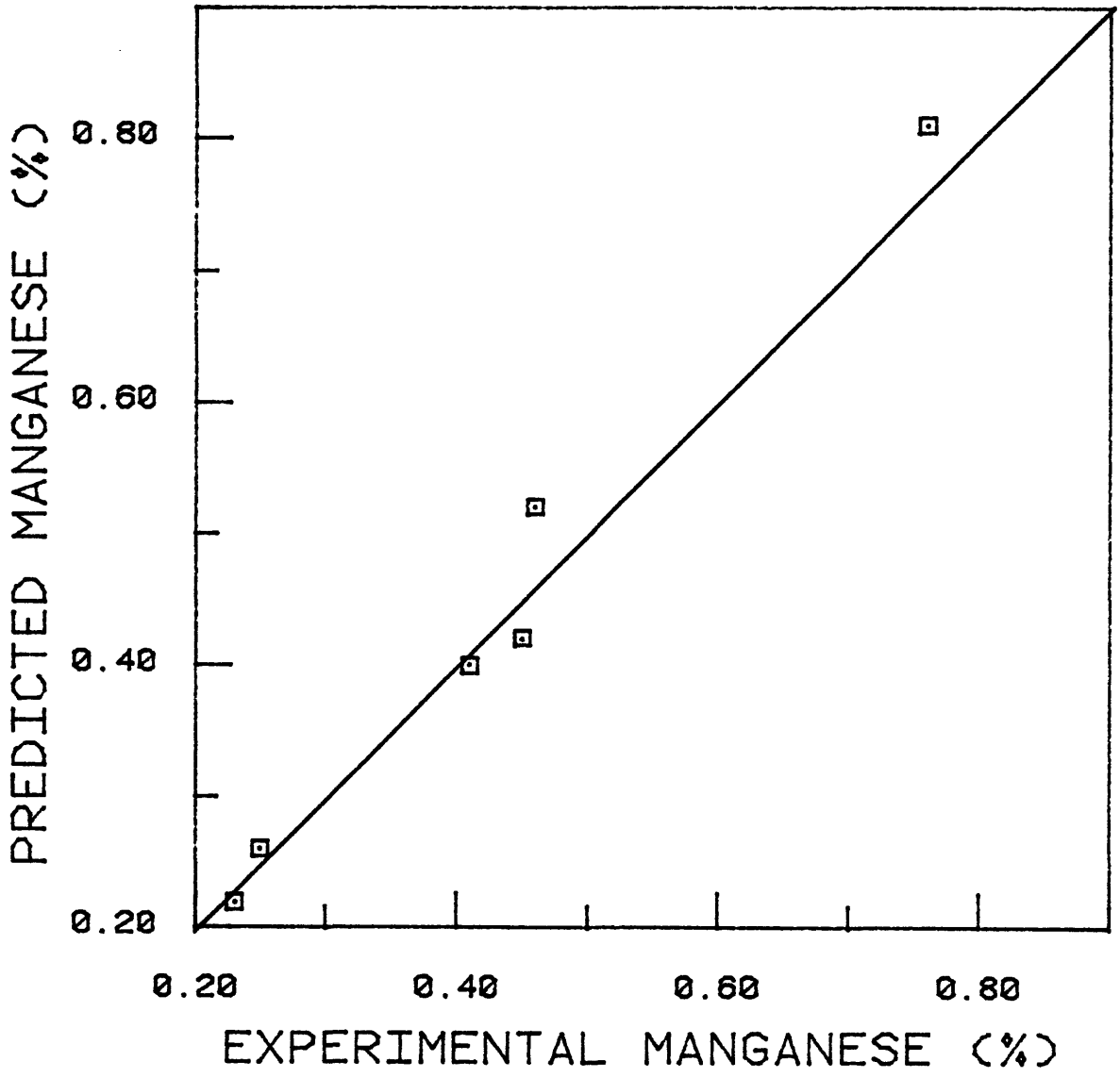

CHRISTENSEN [10], Flux c, N.P.:0.0%Mn, α=1.7

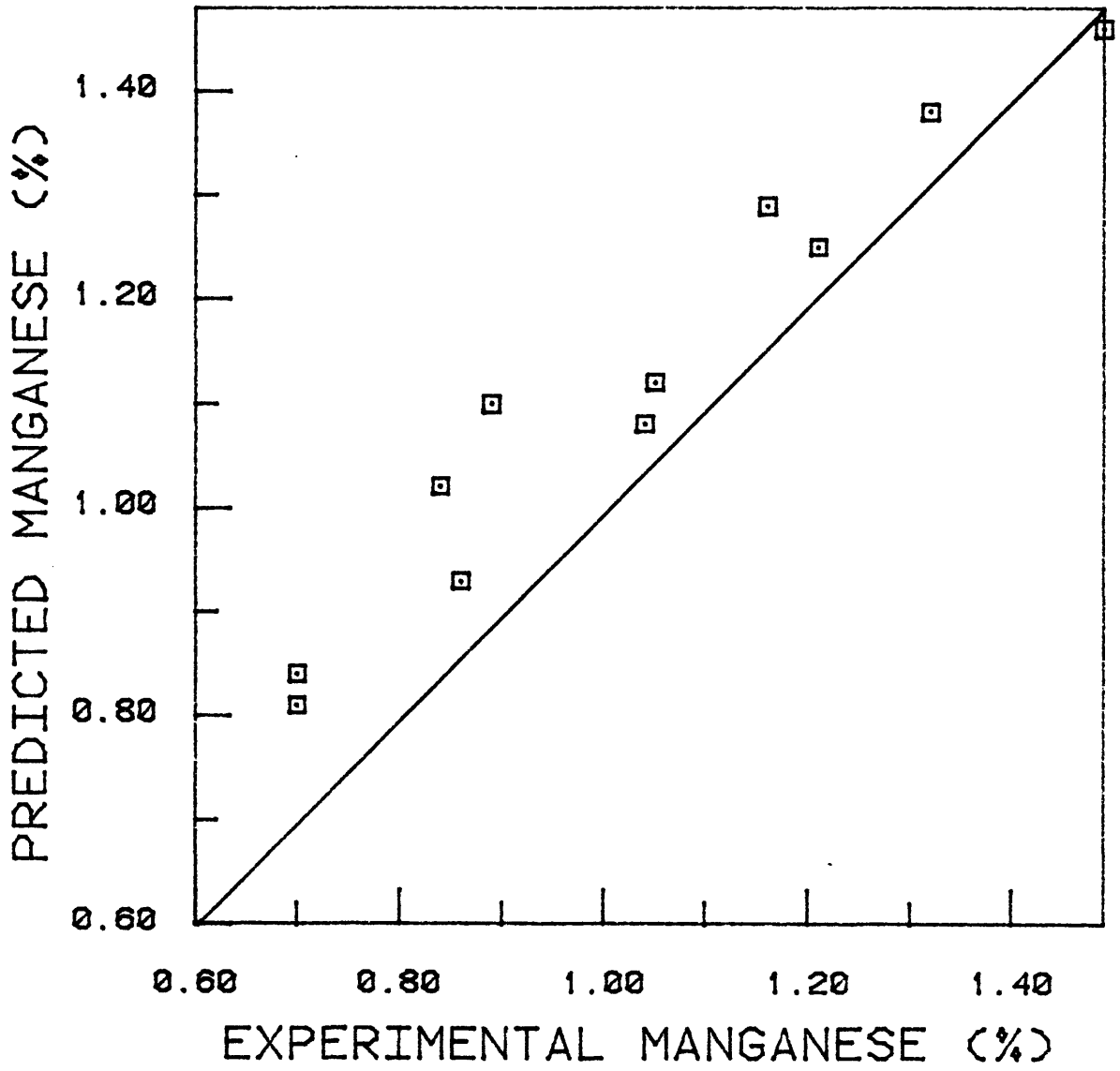

CHRISTENSEN [10], Flux e, N.P. : 1.50%Mn, α = 1.7

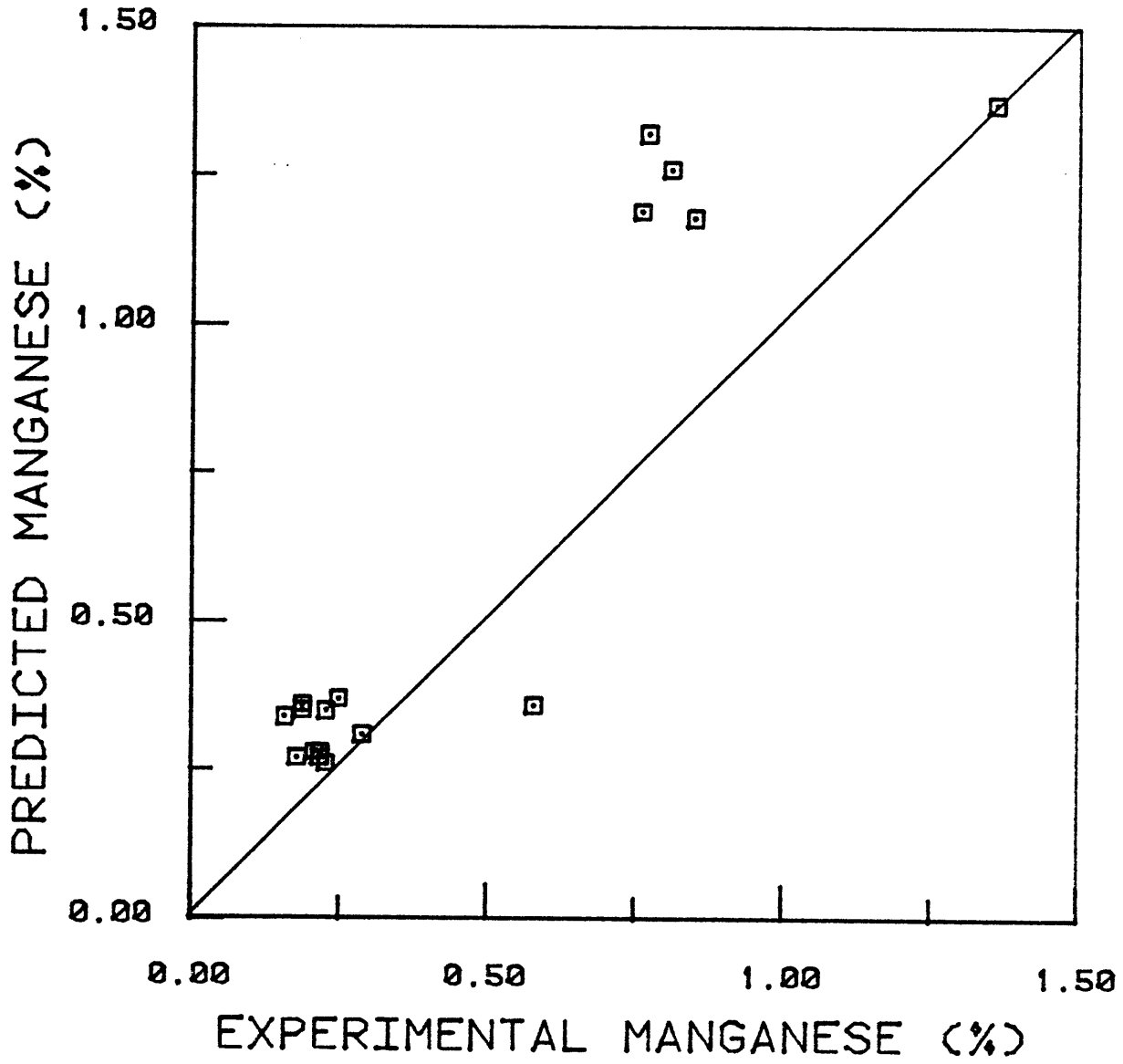

MITRA [16], Fluxes A,B & C, N.P. 0.0%Mn, =1.7/3

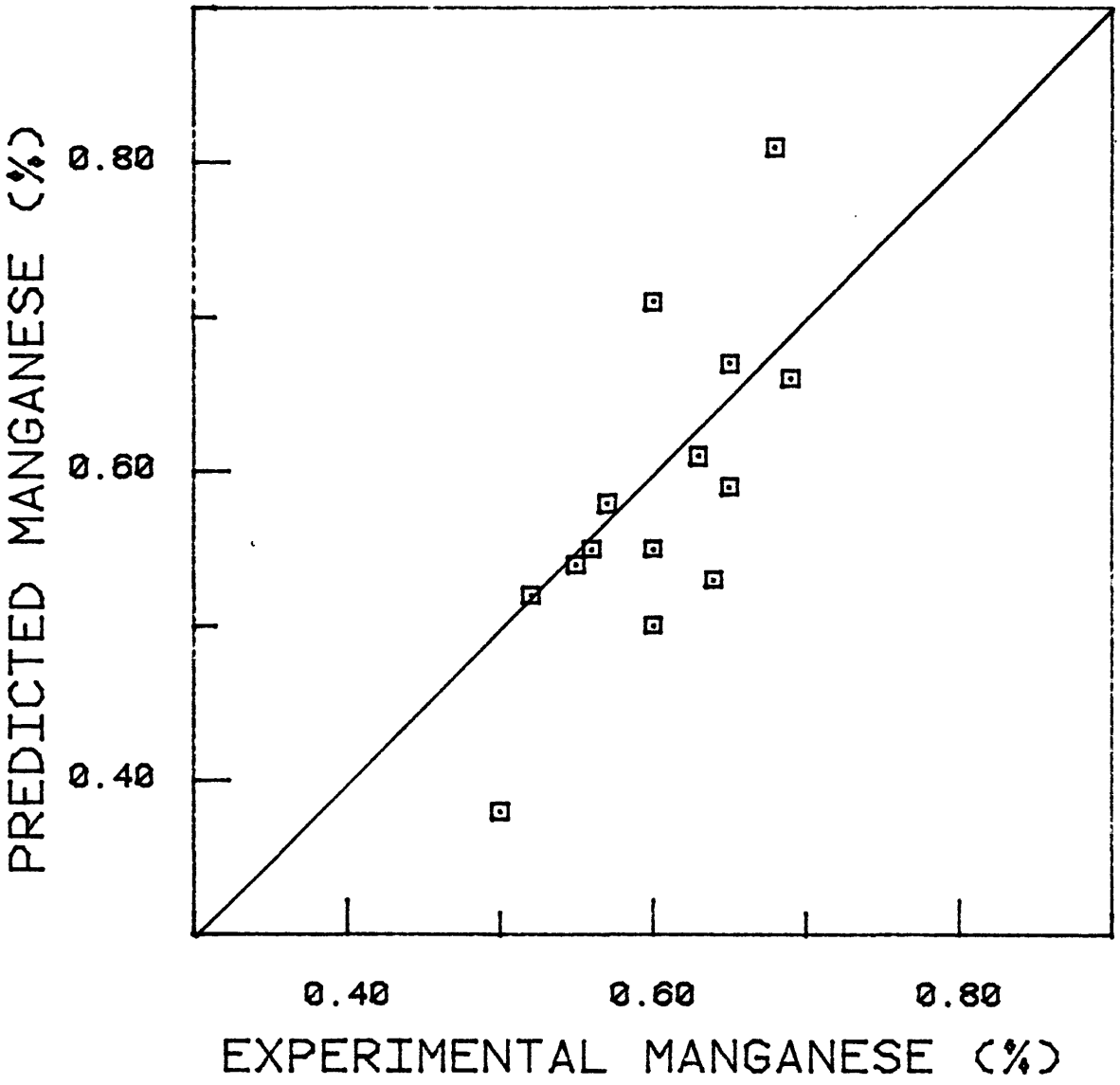

CHRISTENSEN [10], Flux a ,N.P.:0.0%Mn, α=1.7

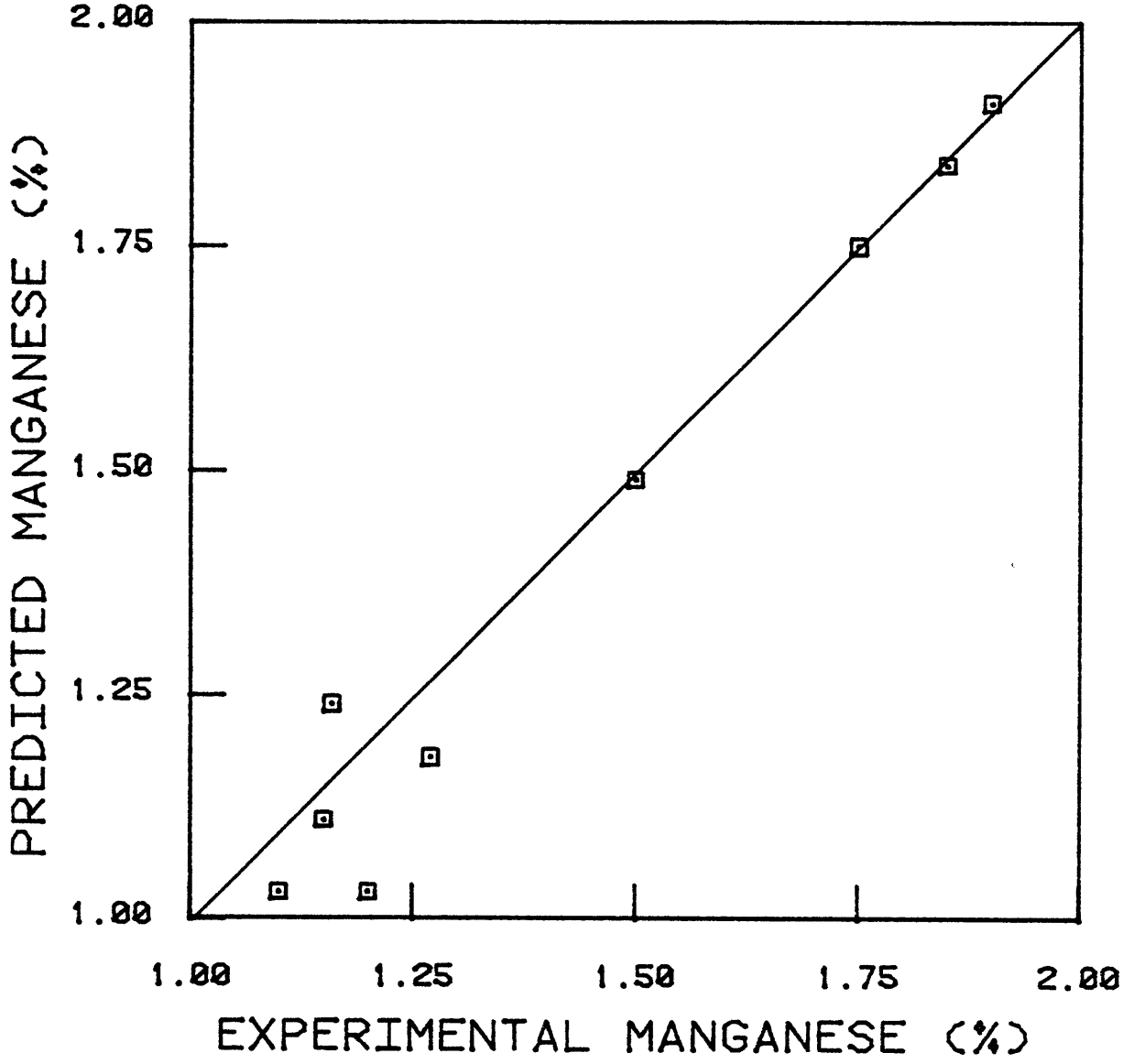

CHAI [17], Flux F-1, N.P. 1.8%Mn, χ= 1.7/3

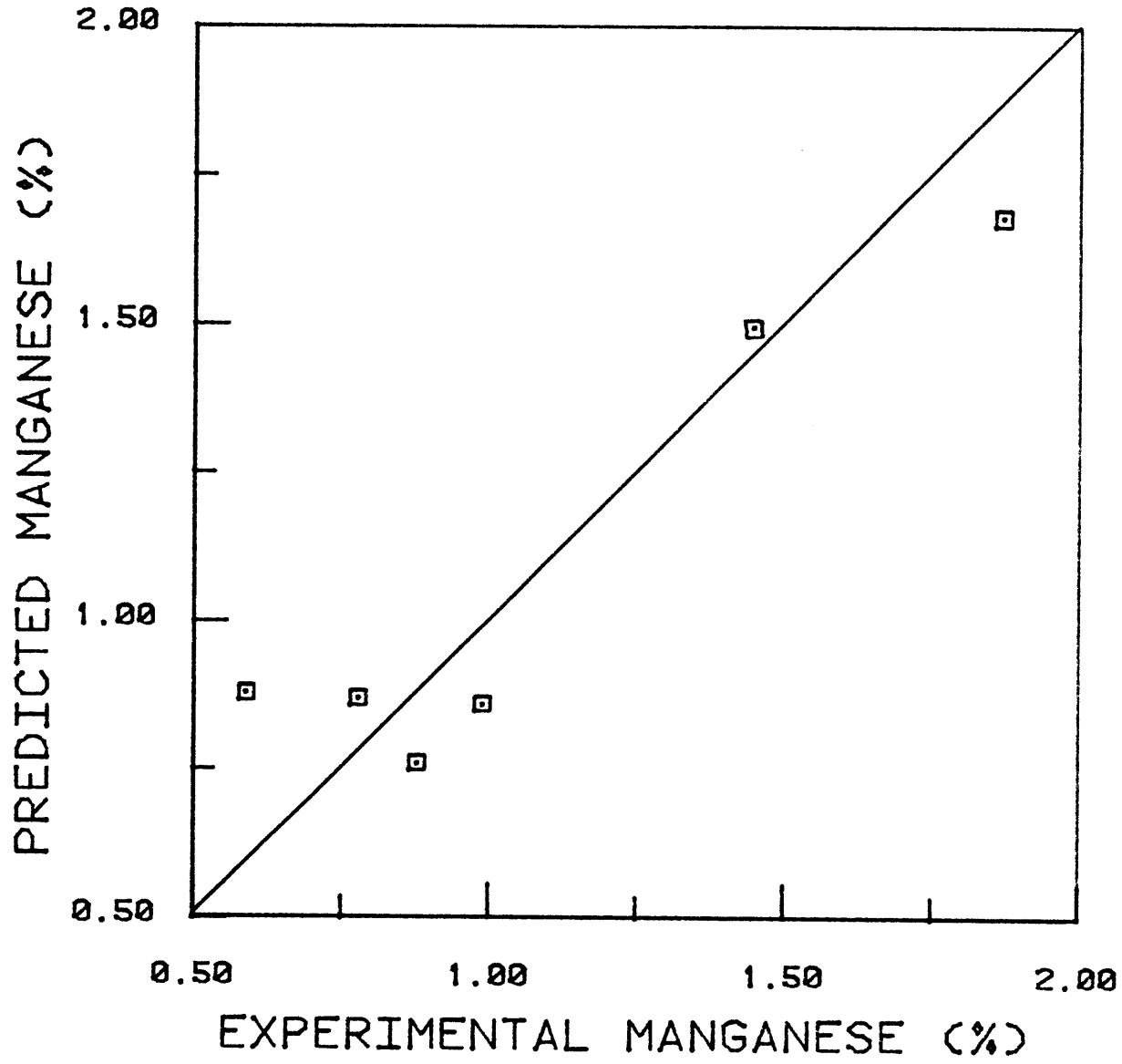

MITRA [16], Flux D, N.P. 1.7%Mn, α = 1.7

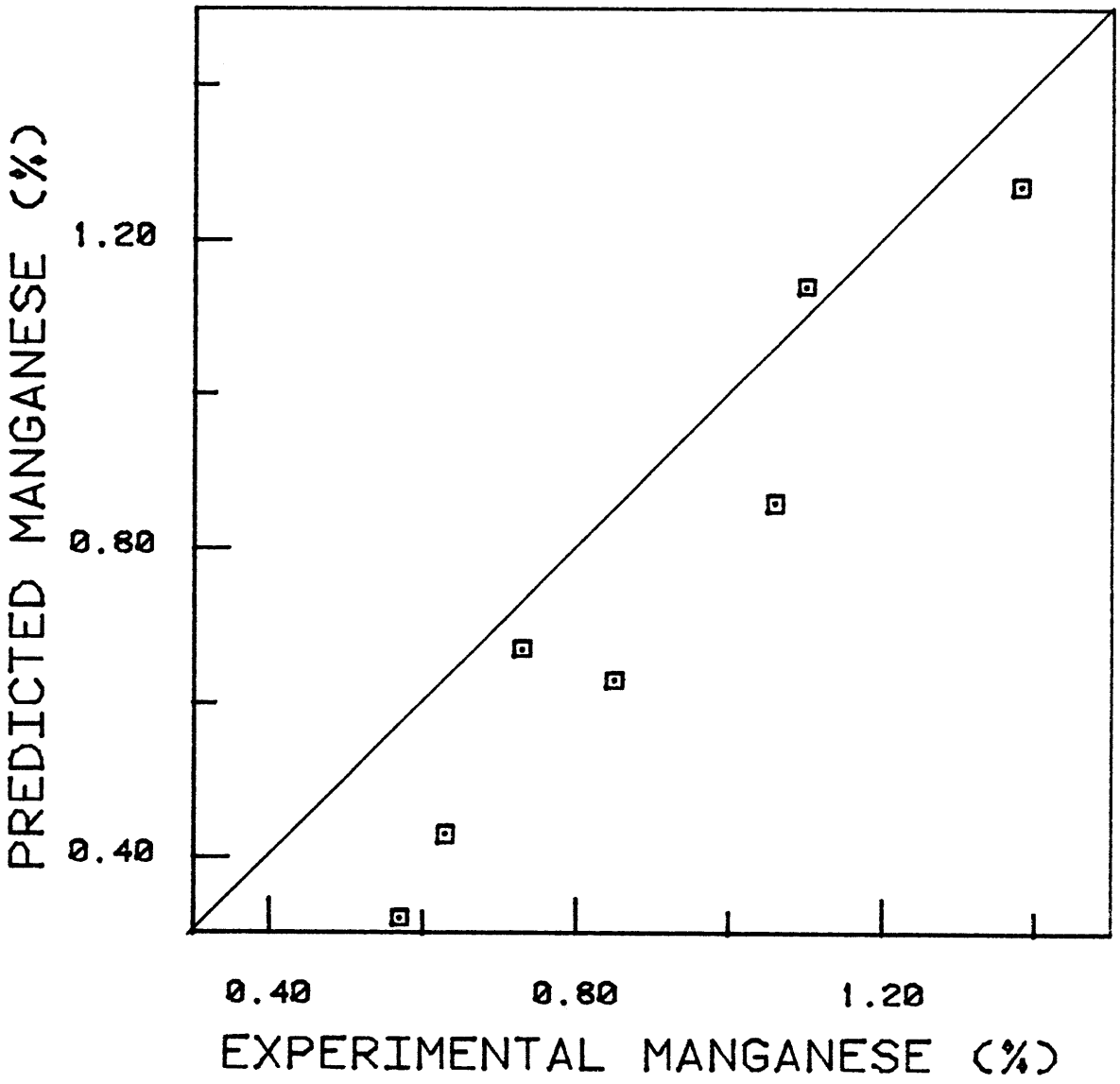

FRUMIN [28], Flux AN-20, N.P.:0.0%MN, α=1.7/3

APPENDIX A.9

EXAMPLE OF CALCULATION OF OVERALL MASS TRANSFER COEFFICIENTS FROM DATA RECORDED BY CHAI [17]*

These calculations assume chemical kinetics have negligible influence

$$J_{Mn} = k_m(\Delta Mn)$$

$$\therefore k_m = \frac{J_{Mn}}{\Delta Mn} \quad (1)$$

For Weld 1-2 (see Table 23)

$$k_m = \frac{2.44 \times 10^{-2}}{0.35} = 0.07$$

From a mass balance

$$J_{MnO} = b\, J_{Mn} \quad (2)$$

$$J_{Mn} = k_s(\Delta a_{MnO})$$

$$\simeq \gamma k_s(\Delta MnO) \quad (3)$$

*All symbols used are same as that used earlier in the main body.

Combining equations (2) and (3)

$$k_s \simeq \frac{J_{MnO}}{b\gamma(\Delta MnO)} \tag{4}$$

also

$$m = \frac{N.P.}{a_{MnO}} = \frac{N.P.}{\gamma[\%MnO]} \tag{5}$$

Dividing equation (4) by (5), we get

$$\frac{m}{k_s} \simeq \frac{[\%MnO][N.P.]}{[\Delta MnO]b}$$

Using Weld 1-2 as an example

$$\frac{m}{k_s} \simeq \frac{16 \times 1.8}{1.54 \times 2.5} = 0.06$$

Overall mass transfer coefficient

$$\frac{1}{k} = \frac{1}{k_m} + \frac{m}{k_s}$$

$$= \frac{1}{.07} + \frac{1}{.06}$$

$$= .032$$

This particular example indicates mixed control of kinetics by mass transport in slag as well as metal phases. However, for some other

welds (1-1, 1-4 and 1-11) mass transport in slag is clearly the dominant factor.

APPENDIX A.10

ESTIMATION OF MANGANESE EVAPORATION DURING FLIGHT OF DROPLETS THROUGH ARC CAVITY

The amount of manganese lost by evaporation inside the arc cavity may be estimated from the equation obtained by Kim and Mclean

$$\ln \frac{[\%Mn]_t}{[\%Mn]_o} = -k(A/v)t \qquad (1)$$

with

$$k = 2.7325\left(-\frac{31870}{1.987\ T}\right) \qquad (2)$$

where $[\%Mn]_o$ and $[\%Mn]_t$ are the initial and final manganese content, (A/v) is the surface to volume ratio (per cm), t the time in seconds and T the absolute temperature. Equation (1) may be used, to give the loss of manganese by evaporation (ΔMn_v)

$$\Delta Mn_v = \%Mn_o - \%Mn_t = \%Mn_o[1 - \exp(-k(A/v)t)] \qquad (3)$$

Lau [28] has suggested that manganese evaporation will increase by enhancement. This factor may be accounted by using the equation

$$k' = E\ k \qquad (4)$$

where E is the enhancement factor, and substituting k' instead of k in equation (3). Thus,

$$\Delta Mn_v = \%Mn_o[1 - \exp(-Ek(A/v)t)] \qquad (5)$$

The time t taken to fall through the arc cavity is about 10 milliseconds [31] and the droplets obtained by Lau had a radius of about 2 mm.

Thus, in equation (5) the following values may be used

$$t = 0.01s$$

$$(A/v) = \frac{4\pi r^2}{\frac{4\pi}{3} r^3} = \frac{3}{r} = 15 \text{ cm}^{-1}$$

Also an initial manganese content $[\%Mn_o] = 1\%$ is assumed. Substituting these values in equation (5), the amount of manganese lost by vaporization (ΔMn_v) at different temperatures, and for different enhnacement factors is estimated in Table A-10. This table clearly shows that the amount lost by vaporization is negligible. Lau's conclusions about manganese vaporization was based on his experimental results. The droplets collected by him in calcium silicate slags lost about 0.2 - 0.3% Mn. However this was probably due to slag-metal reactions at the droplet surface as explained in Appendix A.10.

Table A.10: Amount of Manganese Lost by Vaporization by Droplets and Different Temperatures and Assuming Different Enhancement Factors

Enhancement (E) \ Temperature	2000°C	2200°C	2400°C	2800°C
1	0.0004% Mn	0.0007% Mn	0.0020% Mn	0.003% Mn
20	0.01% Mn	0.02% Mn	0.04% Mn	0.06% Mn
50	0.02% Mn	0.04% Mn	0.10% Mn	0.14% Mn

APPENDIX A.11

ESTIMATION OF SOLIDIFICATION TIME OF DROPLETS COLLECTED BY LAU [28] AND NORTH [18]

The time for solidification of a casting, when heat transfer is interface controlled (as is likely to be the case for the droplets collected by Lau and North) is given by [54]

$$t_s = \frac{\rho_s H}{h(T_m - T_o)} (V/A) \qquad (1)$$

where t_s is the solidification time

ρ_s is the density of the metal (7.8 g/cm^2)

H is the heat of fusion (65 cal/g)

T_m is the melting point of the metal (1500°C)

T_o is the temperature of the mold (25°C)

h is the mold metal heat transfer coefficient (0.1 cal/cm^2°Cs)

(V/A) is the volume to surface ratio of the droplet (.07 cm)

The mold-metal heat transfer coefficient for die castings is typically 0.1 cal/cm^2°Cs, the slag layer on the copper mmold will in fact give even lower values.

Substituting these values in equation (1)

$$t_s = \frac{7.8 \times 65}{0.1 \times (1500-25)} = 0.23 \text{ seconds}$$

This time is enough for slag metal reactions to occur and manganese to diffuse out of the liquid droplets into the slag and give rise to a 0.2 to 0.3% Mn loss as reported by Lau [28]. In the experiments conducted by North [18], droplets were formed on a rotating water cooled copper cylinder beneath a mass of flux. These droplets were 'spun off' the copper cylinder and collected in a water trough. The mold-metal interface heat transfer coefficient for such an arrangement should be substantially lower than that for a stationary mold so the solidification time would be considerable more, leading to considerably more loss of manganese, as reported by North [18]. The observation of North of slag layers, rich in manganese and strongly adherent to the droplet gives further support to this explanation of slag-metal reactions occurring while the droplets were collected.

APPENDIX A.12

This section contains figures comparing the silicon content of the metal as predicted by theory to that obtained experimentally. Data collected in the present investigation and that recorded by other researchers have been used to verify the theory. Only the researchers name, the flux name and the corresponding values of the neutral point (N.P.) and α have been noted. β has been assumed to be zero unless otherwise stated.

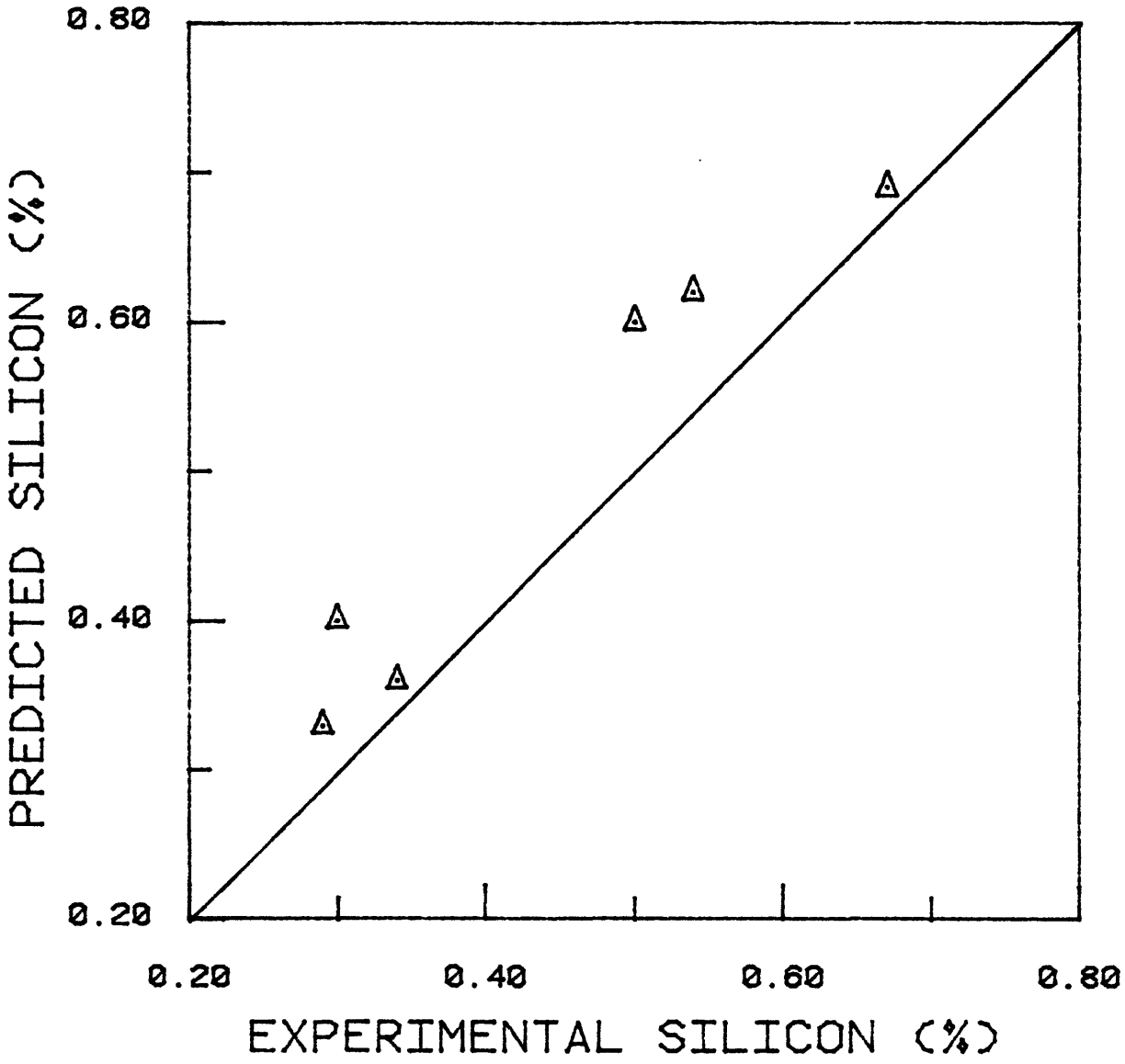

CHRISTENSEN [10],Flux C, N.P.:1.2%Si, α=1.7

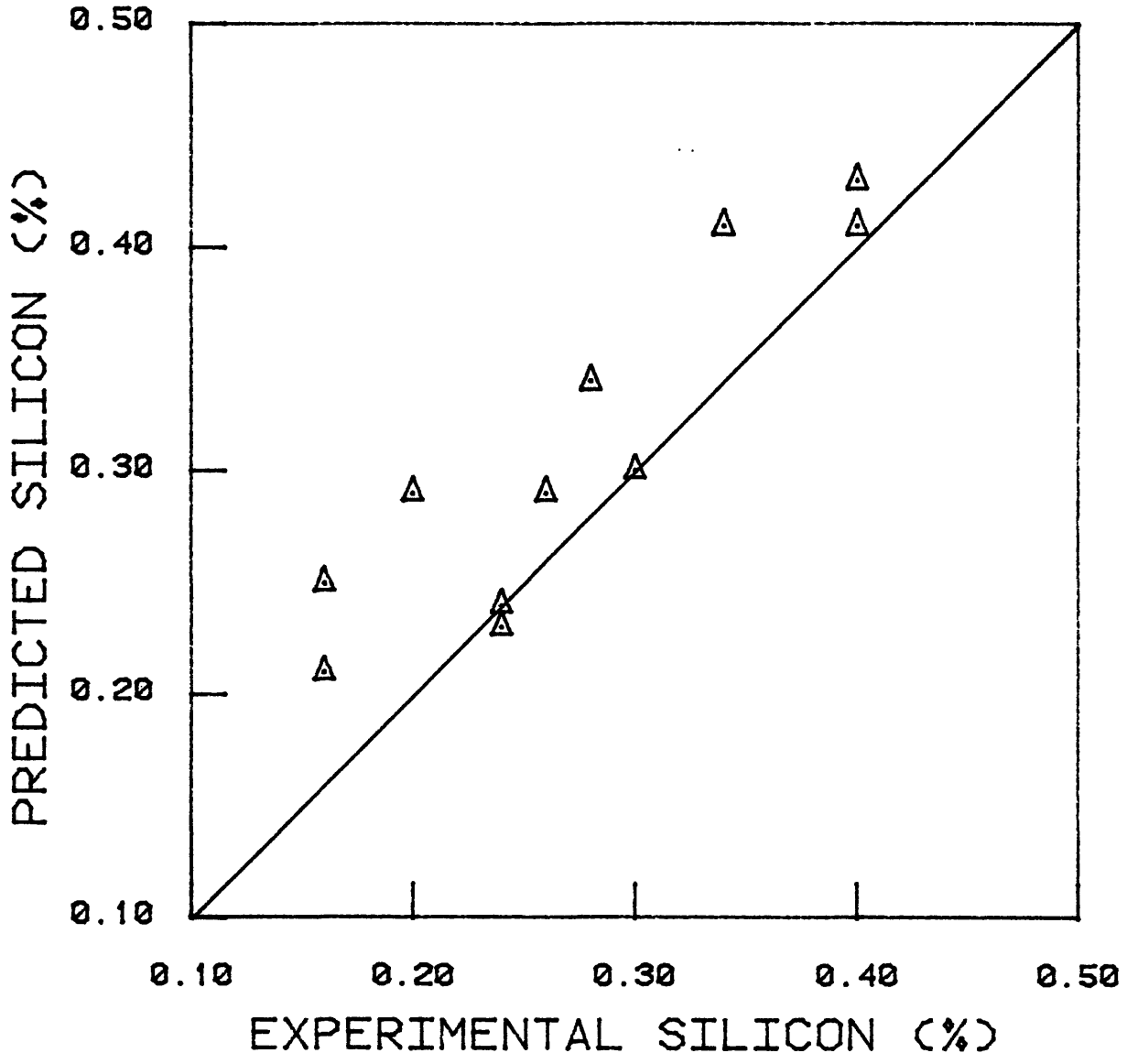

CHRISTENSEN [10], Flux e, N.P.:0.50%Si, α=1.7

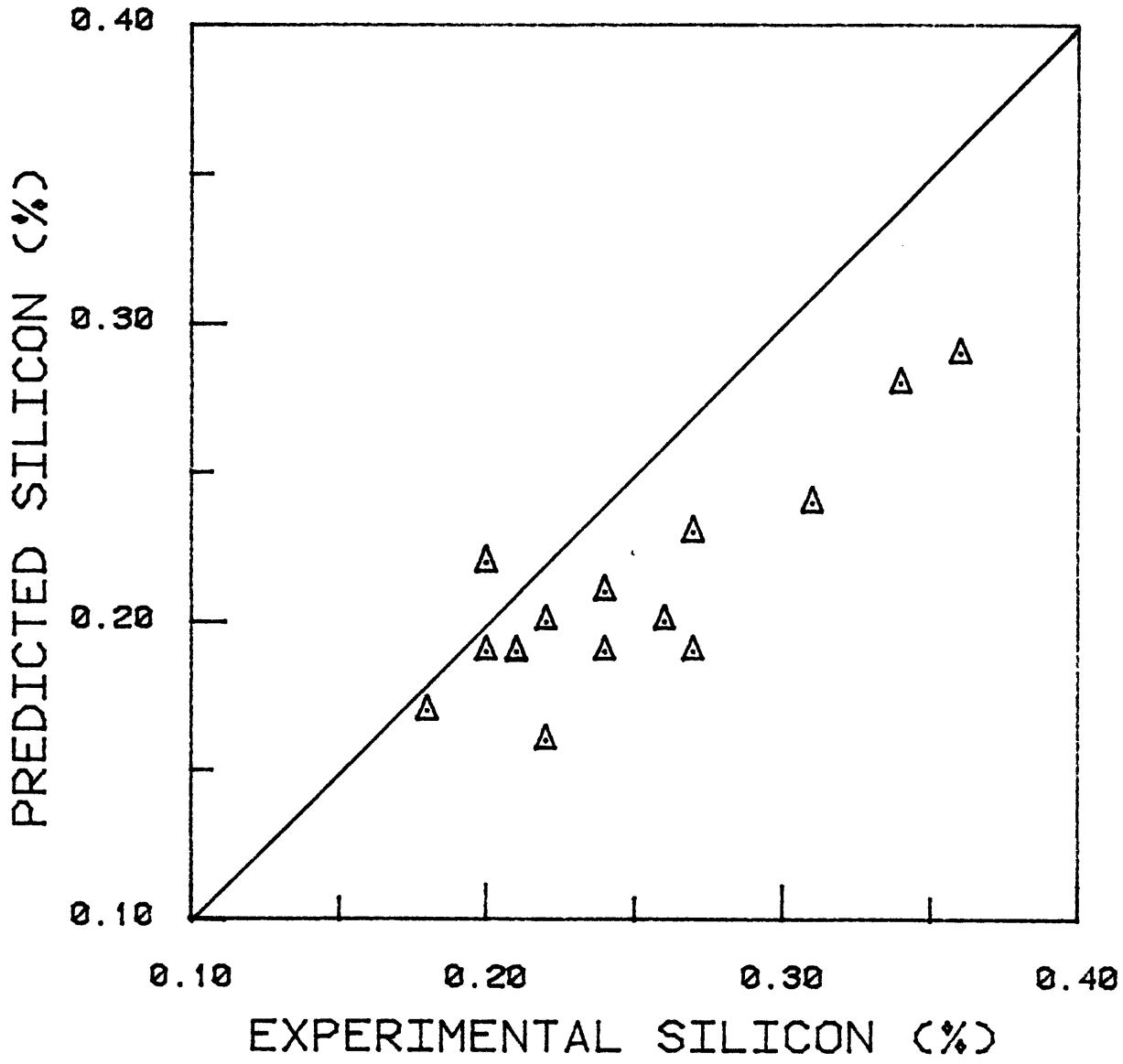

CHRISTENSEN [10], Flux F, N.P.?0.50%Si, α=1.7/3

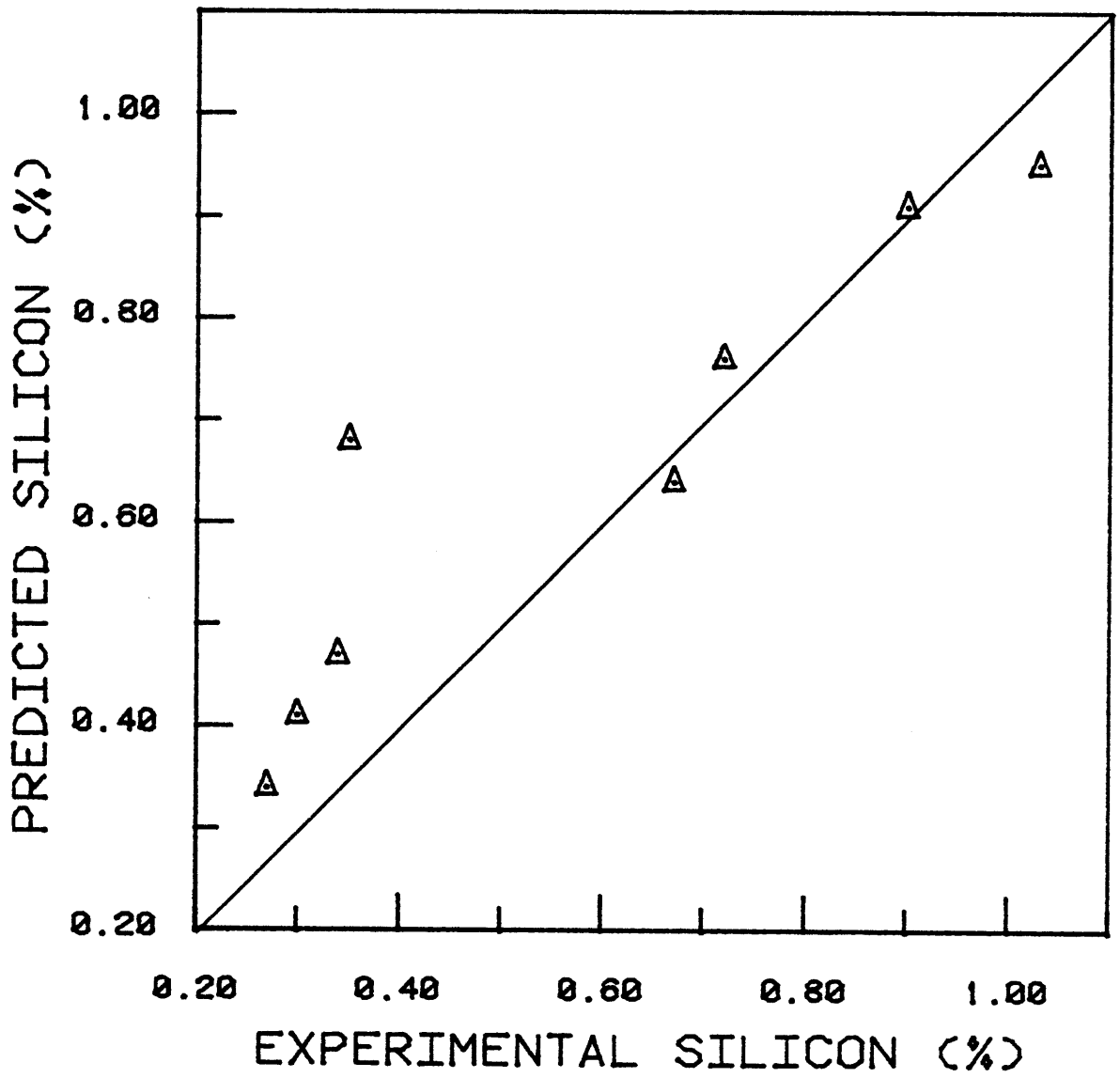

FRUMIN [29], A-348A flux, N.P.1.0%Si, α=1.7

(Multipass Welding)

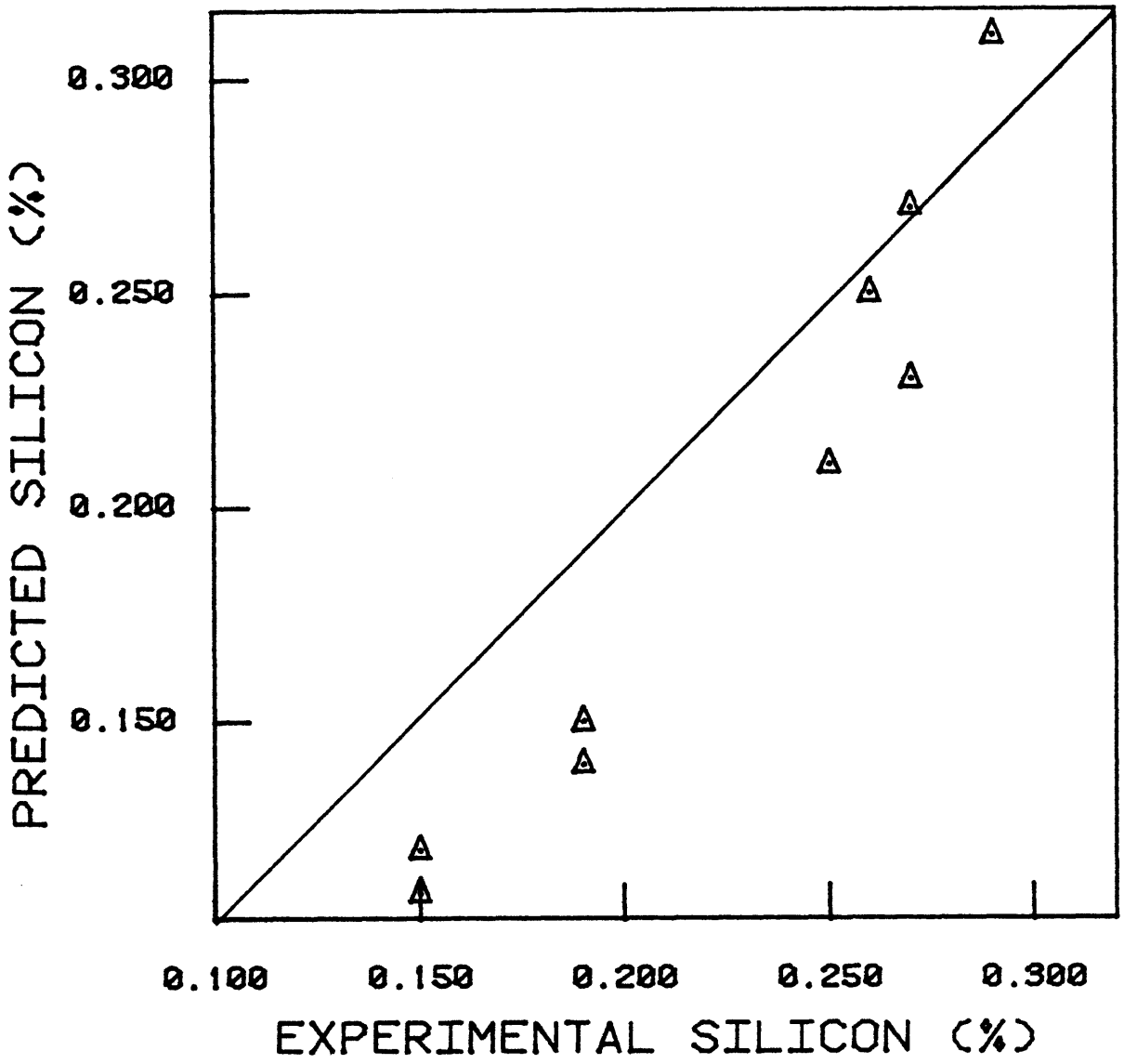

CHAI [10], Flux F-1, N.P.:0.28%Si, α=1.7/3

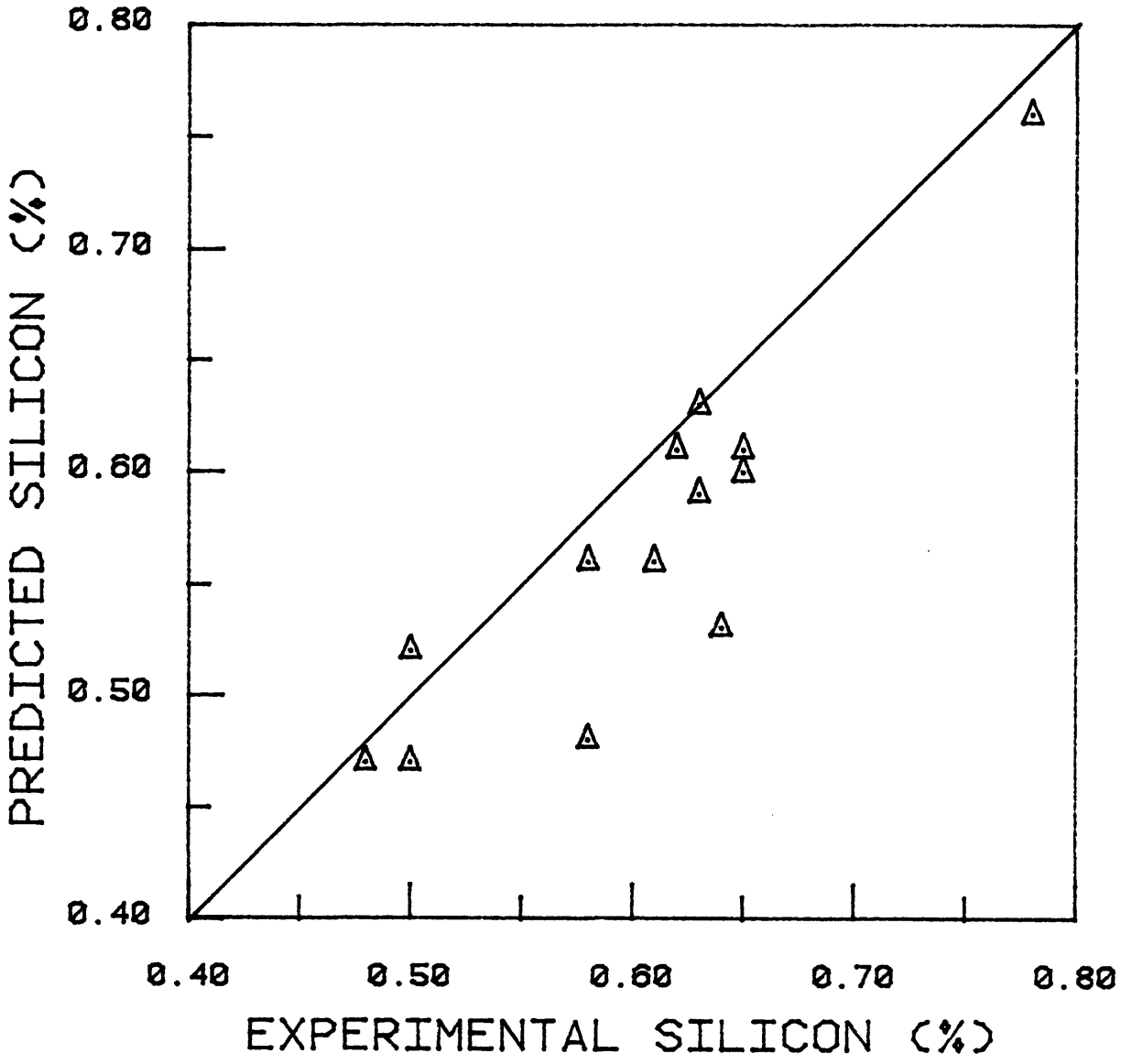

CHRISTENSEN [10], Flux á, N.P. 1.0%Si, α=1.7

APPENDIX A.13

EXAMPLE OF A TEST FOR DETERMINING THE EFFECT OF WELDING CONDITIONS ON WELD METAL CHEMISTRY

The following example (from ref. 85) gives the conditions and results of 'tests' to determine effect of Silicon Content of Flux on Silicon Content of Weld Metal:

Flux type, test 1	Special low-silicon
Flux consumption, test 1	0.15 lb per min
Flux type, test 2	General purpose
Flux consumption, test 2	0.20 lb per min

Welding Conditions for Both Tests

Joint type	Butt
Weld type	U-groove (side 1), V-groove (side 2)
Joint preparation	Machining
Welding position	Flat
Power supply	40-V, 600-amp transformer-rectifier
Preheat and postheat	None
Electrode	3/32-in diam EH14
Electrode stickout	1 in.
Deposition rate	0.5 lb per min per 1000 amp
Number of passes	18

Sequence and conditions of the 18 passes:

Side	Pass No.	Current (dcrp) amp	Voltage	Travel speed ipm
1	1	320	27	20
	2	320	28	18
	3	320	28	18
2	4	350	26	15
	5	330	28	8
	6	330	30	8
	7-10	320	30	8
3	11-18	320	30	8

Chemical Compositions

Base metal	0.20 C.	0.60 Mn.	0.008 Si
Electrode.	0.14 C.	2.00 Mn.	0.024 Si
Weld metal passes 6 and 7:			
Test 1.	0.09 C.	1.00 Mn.	0.014 Si
Test 2.	0.09 C.	0.95 Mn.	0.400 Si

Low-carbon steel (ASTM A285, grade C);
2% Mn steel filler metal (EH14)

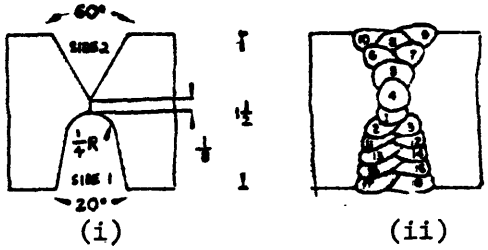

(i) (ii)

Fig. A.13: (i) Joint geometry
(ii) Sequence of Passes

APPENDIX B.1

WELDING CONSUMABLES AND CONDITIONS USED IN PRELIMINARY EXPERIMENTS AND FOR OTHER NORMAL BEAD ON PLATE WELDS

Weld No.	Welding Consumables			Welding Conditions				dil	w/A
	Flux	Electrode	Baseplate	Voltage (volts)	Current (amps)	Speed (cm/min)	Polarity		
1-1	Fx-1	A-7	EZ20	30	400	40	DCEP	-	-
1-2	Fx-1	A-7053	EZ20	30	400	40	DCEP	-	-
1-3	Fx-1	LD-840	1008	30	400	40	DCEP	-	-
1-4	Fx-1	A-7	1008	30	400	40	DCEP	-	-
2-1	Fx-2	A-681	EZ20	30	400	40	DCEP	-	-
2-2	Fx-2	LD-86	LD-86*	30	400	40	DCEP	-	-
3	Fx-1	A-7	EZ20	20	400	40	DCEP	-	-
4	Fx-2	A-7	EZ20	20	400	40	DCEP	-	-
5	Fx-2	LD-44	1008	20	400	40	DCEP	-	-
7	Fx-1	LD-44	1008	20	400	40	DCEP	-	-
8	Fx-2	LD-44	1008	30	400	40	DCEP	-	-
77	Fx-1	LD-44	1008	30	400	40	DCEN	-	-
1777	Fx-2	LD-44	1008	30	400	40	DCEN	-	-
99	Fx-1	A-7	EZ20	30	400	40	DCEN	-	-
1999	Fx-2	A-7	EZ20	30	400	40	DCEN	-	-
M-101	Fx-1	A-7	HiSi	30	300	60	DCEP	-	-
M-103	Fx-1	A-7	HiSi	30	300	60	DCEP	-	-
M-106	Fx-1	A-7	HiSi	30	300	60	DCEP	-	-
M-201	Fx-1	A-681	HiSi	30	300	60	DCEP	-	-
M-203	Fx-1	A-681	HiSi	30	300	60	DCEP	-	-
M-206	Fx-1	A-681	HiSi	30	300	60	DCEP	-	-
M-301	Fx-2	A-681	HiSi	30	300	60	DCEP	-	-
M-303	Fx-2	A-681	HiSi	30	300	60	DCEP	-	-
M-306	Fx-2	A-681	HiSi	30	300	60	DCEP	-	-
M-400	Fx-2	A-7	HiSi	30	300	60	DCEP	-	-
M-403	Fx-2	A-7	HiSi	30	300	60	DCEP	-	-
M-501	Fx-1	A-681	1008	30	300	60	DCEP	-	-
M-503	Fx-1	A-681	1008	30	300	60	DCEP	-	-
M-506	Fx-1	A-681	1008	30	300	60	DCEP	-	-

Weld No.	Welding Consumables			Welding Conditions				dil	w/A
	Flux	Electrode	Baseplate	Voltage (Volts)	Current (amps)	Speed (cm/min)	Polarity		
21	Fx-1	A-7	1008	20	400	40	DCEP	.58	1.68
22	Fx-1	A-7	1008	20	400	60	DCEP	.48	1.56
24	Fx-1	A-7	1008	33	400	40	DCEP	.45	3.21
25	Fx-1	A-7	1008	30	550	80	DCEP	.78	1.88
26	Fx-1	A-7	1008	32	300	40	DCEP	.45	2.15
42	Fx-2	A-7	HiSi	20	400	40	DCEP	.68	1.25
43	Fx-2	A-7	HiSi	30	400	40	DCEP	.66	2.10
44	Fx-2	A-7	HiSi	32	400	40	DCEP	.65	2.50
45	Fx-2	A-7	HiSi	26	400	40	DCEP	.69	1.96
46	Fx-2	A-7	HiSi	30	450	80	DCEP	.79	1.80
S-1	Fx-1	A-7	Stainless	20	400	40	DCEP	.63	1.02
S-2	Fx-1	A-7	Stainless	20	400	40	DCEP	.67	1.30
S-3	Fx-1	A-7	Stainless	30	400	40	DCEP	.61	2.19
S-4	Fx-1	A-7	Stainless	32	500	40	DCEP	.81	1.76
S-5	Fx-1	A-7	Stainless	30	400	80	DCEP	.84	2.54
S-6	Fx-1	A-7	Stainless	26	400	80	DCEP	.84	1.59
S-7	Fx-1	A-7	Stainless	30	250	40	DCEP	.58	4.49
S-8	Fx-1	A-7	Stainless	30	400	80	DCEP	.71	1.98
P1	Fx-2	A-7	EZ20	30	400	40	DCEP	.71	1.60
P2	Fx-2	A-7	EZ20	30	400	40	DCEP	.61	1.71
P3	Fx-2	A-7	EZ20	20	400	40	DCEP	.60	1.71
P4	Fx-2	A-7	EZ20	20	400	80	DCEP	.64	1.84
P5	Fx-2	A-7	EZ20	20	400	40	DCEN	.42	1.46
P6	Fx-2	A-7	EZ20	20	400	80	DCEN	.56	1.65
P7	Fx-2	A-7	EZ20	30	400	40	DCEN	.54	2.43
P8	Fx-2	A-7	EZ20	30	400	40	DCEN	.48	2.34
9A	Fx-1	A-7	1008	28	400	40	DCEP	.59	2.1
9B	Fx-1	LD-40	1008	33	400	40	DCEP	.59	3.2
9C	Fx-1	LD-80	1008	28	540	40	DCEP	.72	1.5
10A	Fx-1	LD-44	1008	32	400	40	DCEP	.60	3.4
10B	Fx-1	L-70	1008	30	400	40	DCEP	.55	2.9
10C	Fx-1	LD-81	1008	28	500	40	DCEP	.64	1.6
14H	Fx-3	Ax-90	HiP	25	250	40	DCEP	0.49	4.63
14N	Fx-3	Ax-90	HiP	22	250	40	DCEP	0.53	4.32
14E	Fx-3	Ax-90	HiP	20	250	40	DCEP	0.50	4.11
16N	Fx-3	Ax-90	HiP	20	250	40	DCEN	0.54	3.31
16X	Fx-3	Ax-90	HiP	24	250	40	DCEN	0.59	3.87
16H	Fx-3	Ax-90	HiP	20	250	40	DCEN	0.61	4.0
16K	Fx-3	Ax-90	HiP	22	250	40	DCEN	0.61	3.42

Weld No.	Welding Consumables			Welding Conditions				dil	w/A
	Flux	Electrode	Baseplate	Voltage (Volts)	Current (amps)	Speed (cm/min)	Polarity		
Si-1	Fx-4	A-7	HiSi	30	400	40	DCEP	0.60	-
Si-3	Fx-4	A-7	HiSi	30	400	30	DCEP	0.55	-
400	Fx-1	A-7	Hy-80	28	400	12	DCEP	-	-
600	Fx-1	A-7	Hy-80	30	600	12	DCEP	-	-
800	Fx-1	A-7	Hy-80	33	800	12	DCEP	-	-
AC2	Fx-1	A-7	Hy-80	30	560	12	AC	-	-
AC3	Fx-1	A-7	Hy-80	34	540	12	AC	-	-
AC4	Fx-1	A-7	Hy-80	32	780	12	AC	-	-

APPENDIX B.2

CHEMICAL COMPOSITION OF SIMPLE BEAD ON PLATE WELDS AND OTHER WELDS MADE DURING PRELIMINARY EXPERIMENTS

(All values in weight percent)

Sample	Elements								
	C	Si	Mn	P	S	Cr	Ni	Mo	O
S-1	.051	.43	1.19	.012	.009	10.3	6.10	.22	-
S-2	.054	.60	1.37	.014	.008	10.8	6.55	.22	.19
S-3	.046	.66	1.27	.019	.009	7.89	5.93	.21	.15
S-4	.049	.71	1.57	.018	.008	13.1	7.86	.26	.19
S-5	.056	.74	1.60	.020	.008	13.3	8.15	.26	.16
S-6	.049	.76	1.63	.019	.007	13.0	8.16	.26	.19
S-7	.047	.83	1.41	.027	.008	5.84	5.62	.20	.15
S-8	.065	.61	1.42	.015	.008	11.4	6.92	.24	.20
P1	.089	.066	.57	.039	.11	.023	.002	.002	.04
P2	.11	.074	.60	.039	.11	.022	.002	.002	.08
P3	.087	.076	.53	.033	.088	.019	.002	.003	.05
P4	.078	.047	.59	.035	.090	.027	.001	.001	.08
P5	.10	.049	.43	.041	.093	.026	.004	.002	.04
P6	.49	.044	.57	.026	.10	.019	.002	.001	.04
P7	.11	.048	.60	.057	.10	.019	.004	.002	.14
P8	.069	.048	.38	.074	.082	.019	.004	.002	.06
42	.021	2.00	.094	.006	.017	.031	.060	.010	.07
43	.022	1.78	.095	.006	.016	.028	.054	.010	-
44	.020	1.74	.074	.008	.015	.031	.064	.011	-
45	.023	2.02	.084	.009	.015	.032	.063	.012	.05
46	.021	2.33	.067	.008	.016	.034	.072	.012	.03
21	.031	.30	.57	.010	.016	.017	.012	.003	-
22	.032	.18	.44	.008	.015	.013	.009	.002	.15
24	.037	.40	.65	.010	.016	.012	.010	.002	.21
25	.027	.34	.61	.014	.015	.011	.013	.004	.20
26	.040	.32	.55	.009	.015	.012	.009	.002	.15
M-601	.048	.35	.58	.013	.016	.014	.013	.004	.17
M-603	.008	.47	.70	.015	.014	.012	.015	.004	.20
M-200	-	2.48	-	-	-	-	-	-	.10

Sample	Elements								
	C	Si	Mn	P	S	Cr	Ni	Mo	O
1-1	.10	.31	.88	.017	.097	.025	.011	.004	-
1-2	.08	.33	1.20	.015	.092	.023	.021	.003	-
1-3	.039	.14	1.15	.015	.012	.051	.029	.24	-
1-4	.037	.40	.65	.010	.016	.012	.010	.002	-
2-1	.032	.70	.99	.016	.012	.030	.034	.005	-
2-2	-	.85	1.41	-	-	-	-	-	-
9A	0.039	0.32	0.62	0.016	0.016	0.019	0.010	0.002	-
9B	0.036	0.54	1.12	0.021	0.015	0.024	0.022	0.23	-
9C	0.040	0.30	0.61	0.012	0.014	0.015	0.020	0.001	-
10A	0.022	0.60	1.20	0.021	0.010	0.044	0.29	0.21	-
10B	0.027	0.47	0.87	0.014	0.015	0.031	0.022	0.18	-
10C	0.049	0.44	0.89	0.006	0.014	0.034	0.010	0.005	-
14H	0.042	0.86	0.83	0.072	0.005	0.023	0.95	0.18	-
14N	0.040	0.86	0.90	0.070	0.005	0.024	1.03	0.19	-
14E	0.065	0.85	1.03	0.038	0.007	0.015	0.53	0.10	-
16N	0.050	0.73	1.04	0.053	0.005	0.024	1.05	0.22	-
16X	0.048	0.75	0.97	0.052	0.005	0.025	1.13	0.23	-
16H	0.061	0.79	0.97	0.049	0.007	0.027	1.18	0.23	-
16K	0.060	0.73	0.97	0.050	0.007	0.026	1.16	0.22	-
3	.096	.18	.76	.012	.089	.023	.009	.004	.04
4	.11	.065	.67	.012	.087	.025	.008	.004	.05
5	.072	.11	1.07	.012	.012	.069	.28	.19	.06
7	.078	.22	1.24	.012	.012	.067	.30	.19	.0
8	.068	.12	.79	.012	.010	.065	.27	.18	.03
77	.039	.55	1.40	.021	.010	.069	.42	.28	-
99	.057	.42	.91	.201	.077	.020	.016	.004	-
M-203	.028	1.86	1.56	.023	.016	.053	.10	.015	.17
M-206	.016	1.51	1.75	.029	.015	.050	.10	.014	.18
M-301	.045	2.33	.50	.016	.015	.058	.10	.016	.02
M-303	.057	1.27	.85	.017	.013	.058	.10	.015	.03
M-306	.074	.90	.96	.023	.013	.058	.091	.015	.03
M-501	.032	.70	.99	.016	.017	.030	.034	.005	.13
M-503	.019	.98	1.54	.025	.017	.037	.060	.006	.18
M-506	.010	1.01	1.64	.028	.017	.038	.072	.007	.20
1777	.096	.10	.86	.012	.010	.05	.33	.22	-
1999	.070	.091	.40	.014	.077	.023	.011	.005	-
Si-1	-	1.61	-	-	-	-	-	-	.10
Si-3	-	1.56	-	-	-	-	-	-	.12

APPENDIX B.3

COMPLETE CHEMICAL COMPOSITION OF WELDS MADE USING A MAGNETIC ARC OSCILLATOR

(i) Welds made with Fx-1 flux, Ax-90 electrode (0.045" dia) and 1008 baseplate. (Welding conditions shown in Table 21.) All values in weight percent.

Sample	C	Si	Mn	P	S	Cr	Ni	Mo	Cu
1B	0.045	0.50	0.91	0.016	0.010	0.028	0.83	0.16	<0.005
2A	0.053	0.55	0.96	0.015	0.010	0.028	0.87	0.17	<0.005
4A	0.053	0.56	0.92	0.012	0.009	0.025	0.71	0.15	<0.005
4B	0.050	0.53	0.87	0.011	0.008	0.022	0.66	0.12	<0.005
5A	0.036	0.55	0.96	0.017	0.009	0.028	0.97	0.19	<0.005
5B	0.027	0.69	1.09	0.023	0.008	0.028	1.15	0.23	<0.005
6A	0.043	0.62	1.03	0.016	0.010	0.026	0.91	0.18	<0.005
6B	0.033	0.55	0.90	0.022	0.011	0.026	0.85	0.17	<0.005
6C	0.036	0.52	0.85	0.017	0.010	0.025	0.76	0.15	<0.005
7A	0.045	0.47	0.82	0.015	0.012	0.026	0.66	0.14	<0.005
7B	0.045	0.51	0.84	0.014	0.011	0.026	0.66	0.13	<0.005
7C	0.042	0.59	1.01	0.011	0.010	0.027	0.82	0.16	<0.005
2B	0.050	0.50	0.99	0.017	0.010	0.032	1.09	0.21	<0.005
3A	0.029	0.56	0.99	0.013	0.008	0.029	0.88	0.17	<0.005
3B	0.032	0.62	1.03	0.012	0.007	0.027	0.84	0.15	<0.005
5C	0.029	0.67	1.05	0.015	0.008	0.029	1.03	0.19	<0.005

(ii) Welds made with Fx-2 flux, Ax-90 electrode (.045" dia) and HiP baseplate. (Welding conditions as shown in Table 22.) All values in weight percent.

Sample	C	Si	Mn	P	S	Cr	Ni	Mo	Cu
12H	0.069	0.35	1.31	0.071	0.004	0.023	0.87	0.16	<0.001
13H	0.061	0.41	1.25	0.053	0.004	0.030	1.22	0.23	<0.001
13N	0.075	0.47	1.17	0.031	0.004	0.029	1.27	0.22	<0.001
11H	0.067	0.40	1.23	0.049	0.004	0.029	1.19	0.22	<0.001
11K	0.063	0.37	1.20	0.053	0.004	0.027	1.04	0.20	<0.001
11E	0.071	0.41	1.07	0.048	0.005	0.031	1.30	0.24	<0.005
11N	0.089	0.37	1.05	0.057	0.006	0.033	1.08	0.21	0.076
13E	0.075	0.42	1.13	0.042	0.006	0.037	1.40	0.27	<0.005
15K	0.078	0.35	0.95	0.038	0.006	0.036	1.56	0.30	<0.005
15N	0.070	0.38	0.98	0.028	0.004	0.033	1.52	0.29	<0.001
15E	0.075	0.40	1.17	0.037	0.004	0.034	1.48	0.28	<0.001

APPENDIX B.4

CHEMICAL COMPOSITION OF WELDS DEPOSITED ON WATER COOLED COPPER MOLD USING A-7 ELECTRODES

(Welding conditions shown in Table 20) All values in weight percent.

Sample	C	Si	Mn	P	S	Cr	Ni	Mo	Cu	O
Cu1	0.033	0.21	0.47	0.004	0.015	0.012	0.005	0.001	0.020	.312
Cu2	0.013	0.25	0.48	0.017	0.012	0.010	0.012	0.009	0.11	.179
Cu3	0.002	0.36	0.66	0.019	0.012	0.010	0.020	0.010	0.28	.164
Cu4	0.019	0.54	0.76	0.012	0.012	0.012	0.012	0.002	0.01	.160

APPENDIX B.5

DATA FROM NORTH'S WORK [18]. DATA IS FOR MULTIPASS WELDS MADE WITH ELECTRODES CONTAINING 1.85-1.95%Mn AND A 65%SiO_2-35%CaO FLUX

Welding Conditions			W_S/W_M	Mn (%)
Current (amps)	Voltage (volts)	Speed (cm/s)		
615	26	.60	.11	1.10
615	29	.71	.20	.89
615	33	.82	.34	.67
615	36	.90	.48	.56
615	40	.99	.54	.49
380	26	.38	.48	.55
380	40	.61	.95	.28
500	26	.50	.23	.77
500	40	.80	.72	.41
700	26	.71	.07	1.18
700	40	1.10	.38	.50
825	26	.83	.05	1.30
825	40	1.32	.29	.58
615	32	.24	.32	.64
615	32	.36	.32	.63
615	32	.52	.32	.66
615	32	.58	.29	.65
615	32	.28	.23	.66
615	32	1.26	.23	.64
615	32	1.69	.23	.64
615	32	2.11	.23	.65
615	32	2.31	.18	.66
615	32	2.54	.18	.66